RESEARCH AND DEVELOPMENT OF Co AND Rh-PROMOTED ALKALI-MODIFIED MOLYBDENUM SULFIDE CATALYSTS FOR HIGHER ALCOHOLS SYNTHESIS FROM SYNTHESIS GAS

A Thesis

Submitted to the College of Graduate Studies and Research

in Partial Fulfillment of the Requirements for the

Degree of Doctor Philosophy (Ph.D.)

in the Department of Chemical Engineering

University of Saskatchewan

Saskatoon

By

Venkateswara Rao Surisetty

PERMISSION TO USE

In presenting this thesis in partial fulfillment of the requirements for a Doctor of Philosophy Degree from the University of Saskatchewan, I agree that the libraries of the University of Saskatchewan may make this thesis freely available for inspection. I further agree that permission for copying of this thesis in any manner, in whole or in part, for scholarly purpose may be granted by Prof. Ajay Kumar Dalai who supervised my thesis work or, in their absence, by the Head of the Department or the Dean of the College of Graduate Research and Studies in which the thesis work was complete. It is understood that any copying or publication or use of this thesis or parts thereof for financial gain shall not be allowed without my written permission. It is also understood that due recognition shall be given to me and to the University of Saskatchewan in any scholarly use which may be made of any material in my thesis.

Requests for permission to copy or to make other use of material in this thesis in whole or parts shall be addressed to:

Head of the Department of Chemical Engineering
University of Saskatchewan
Saskatoon, Saskatchewan
Canada S7N 5A9

ABSTRACT

The demand for mixed alcohols has grown since ether compounds were banned as gasoline octane improvers in North America. Molybdenum-based catalysts in sulfide form are an attractive catalyst system for the conversion of synthesis gas to alcohols, due to their excellent resistance to sulfur poisoning and high activity for the water-gas shift reaction. The higher alcohols activity over these catalysts is low, due to the formation of hydrocarbons and CO_2. Although a number of catalysts have been developed for this purpose, not any are used commercially at this time. The main objective of this Ph.D. research is to develop a catalyst system that is capable of selectively producing higher alcohols, particularly ethyl alcohols from synthesis gas. In the present series of studies, the investigation of an alkali-promoted trimetallic Co-Rh-Mo catalyst system has led to improvements in product stream composition. The effect of different loadings of active metal (Mo), alkali (K) promoter, and metal promoters (Co and Rh) on higher alcohol synthesis from synthesis gas were investigated using commercially available multi-walled carbon nanotubes (MWCNTs) as the catalyst support. The role of support on higher alcohols synthesis was also studied using different supports, such as γ-Al_2O_3, activated carbons with different textural characteristics, and MWCNTs. The catalysts were prepared using the incipient wetness impregnation method and extensively characterized in both oxide and sulfide phases using different techniques. Transmission electron microscopy (TEM) results revealed that the metal particles were uniformly distributed inside and outside of the carbon nanotubes, and that metal dispersions were higher on the alkali-promoted trimetallic catalyst supported on MWCNTs. The existence of promoted and un-promoted MoS_2 sites was confirmed by diffuse reflectance infrared fourier transform spectroscopy (DRIFTS) studies of adsorbed CO over sulfided catalysts. Temperature programmed reduction (TPR) tests showed that the addition of metal promoters improved the reduction behaviour of the catalysts. XRD patterns showed that alkali-promoted catalysts were less crystalline compared to that of the catalyst not promoted with K. The formation of Co (Rh)-Mo-S species was evident in the XANES spectra of bimetallic and trimetallic alkali-promoted MoS_2 catalysts. The activity and selectivity of the catalysts were assessed in a fixed-bed micro-reactor using temperature, pressure, and gas hourly space velocity in the ranges of 275 to 350°C, 800 to 1400 psig (5.52–9.65 Mpa), and

2.4 to 4.2 m^3 (STP)/(kg of cat.)/h, respectively. The Ni-promoted catalyst showed higher activity towards the formation of hydrocarbons over that of alcohols. The total alcohols space time yield (STY) and higher alcohols selectivities are significantly higher over the activated carbon-supported catalysts compared to those supported on alumina. With increased content of K, the formation of alcohols increased and hydrocarbons formation rate was suppressed. The total alcohols STY increased with increased Co content over the Co-promoted MoS_2-K/MWCNTs catalysts, whereas, the maximum ethyl alcohol and higher alcohols selectivities were observed on the catalyst promoted with 4.5 wt % Co. Over the Rh-promoted MoS_2-K/MWCNTs catalysts, the maximum total alcohol yield, ethanol selectivity, and higher alcohols selectivity were observed on the catalyst with 1.5 wt % Rh. The MWCNT-supported alkali-promoted trimetallic catalyst with 9 wt % K, 4.5 wt % Co, 1.5 wt % Rh, and 15 wt % Mo showed the maximum higher alcohols STY and selectivity compared to other catalysts investigated. The textural properties of the support, such as average pore diameter, pore volume and surface area, could significantly influence the extent of reduction, morphology, adsorption and has direct influence on the synthesis of mixed alcohols from synthesis gas. The optimum higher alcohols STY and selectivity were obtained over the Co-Rh-Mo-K/MWCNT catalyst at 330°C, 1320 psi (9.1 Mpa), 3.8 m^3 (STP)/(kg of cat./h) using a H_2 to CO molar ratio value of 1.25. To predict the reaction rate for higher alcohols synthesis, the power law model was used for the reaction between CO and H_2 on the catalyst surface and the data of this study are well fitted by the model. The activation energies of ethanol and higher alcohols obtained over Co-Rh-Mo-K/MWCNTs were low compared to those values reported in the literature. The sulfided alkali-promoted trimetallic Co-Rh-Mo catalyst supported on MWCNTs was stable over a period of 720 h of continuous reaction.

ACKNOWLEDGEMENTS

I would like to express sincere appreciation and gratitude to Professor Ajay Kumar Dalai, an exceptionally devoted professor and supervisor, who through his concern and unlimited enthusiasm for intellectual growth made my learning experience truly rewarding. I am also deeply grateful for his valued guidance and supervision throughout the planning, execution, and communication of my thesis work.

I am also grateful to Professor Janusz Kozinski, Dean of Engineering at the University of Saskatchewan for his invaluable help, guidance, thoughtful suggestions, support, and encouragement. I am most indebted to the members of my advisory committee, Drs. Catherine Niu and Robert Scott (Department of Chemical Engineering, University of Saskatchewan) and Dr. Ranga Ranganathan (Saskatchewan Research Council), for their helpful discussions and suggestions to improve the quality of my research. Sincere appreciation also goes to Dr. Robert Sumner for his guiding role on my advisory committee during the first two years of my research.

I am thankful for scientific discussions with Drs. Eswaramoorthi Iyyamperumal and Ahmad Tavasoli, which improved my knowledge in the area of catalysis and reaction engineering. My special thanks go to Mr. Darren Anweiler at the Saskatchewan Research Council for his help during the initial period of my research and Dr. Yongfeng Hu at the Canadian Light Source for his guidance on XANES analysis. The financial support from Agriculture and Biomass Innovation Network (ABIN), Natural Sciences and Engineering Council of Canada (NSERC), the Saskatchewan Research Council (SRC) and Canada Research Chair (CRC) program are greatly acknowledged.

Technical assistance from Mr. T.B. Wellentiny, Mr. R. Blondin, Mr. P. Rlee, Mr. D. Cekvic, Mr. T. Bonli, and Ms. E. Heli are also highly acknowledged. I would like to acknowledge Mrs. Y. Wilkinson for her help in proof-reading of papers. Additionally, I thank the secretaries of the Department of Chemical Engineering, Mrs. J. Horosko and K. Bader, for creating a friendly and helpful office environment. I also thank my friends and colleagues of the Catalysis and Chemical Reaction Engineering Laboratories in the Department of Chemical Engineering at the University of Saskatchewan, for being so cooperative and understanding.

My profound appreciation and love goes to my mother Mrs. Lakshmamma Surisetty, my daughters Bandhavi Naidu Surisetty and Vaishnavi Naidu Surisetty, my brother Chandra Sekhar Surisetty, and my sisters. Thanks to my father-in-law Babu Rajendra Prasad Thotakura, a special person in my life, for his continuous encouragement. I also want to thank my mother-in-law and sisters-in-law for being such nice people.

Heartful affections and love are acknowledged to Mrs. Lakshmi Prasanna Surisetty, my wife and my friend forever; for all her support, help and understanding, and for being the woman behind my success. I can never thank her enough for all the support I received from her.

DEDICATION

I dedicate my research and this thesis to the loving memory of my late father **Reddemma Surisetty** (1938-1994) for all the sacrifices he made so that I could get a comfortable life. “Dad, you are physically not with me, but not far from me mentally. I wish you were here to see me completing my Doctor of Philosophy degree”.

TABLE OF CONTENTS

CHAPTER 2

CHAPTER 3

CHAPTER 4

CHAPTER 5

CHAPTER 6

CHAPTER 7

CHAPTER 8

CHAPTER 9

CHAPTER 10

CHAPTER 11

CHAPTER 12

APPENDIX A

APPENDIX B

APPENDIX C

APPENDIX D

LIST OF TABLES

LIST OF FIGURES

CHAPTER 1

Introduction and Thesis Outline

Contribution of the Ph.D. Candidate

Literature review and data interpretations were performed by Venkateswara Rao Surisetty. All written text was prepared by Venkateswara Rao Surisetty and discussed with Drs. Dalai and Kozinski.

Contribution of this chapter to overall study

This chapter provides an overview on biomass and its availability in Canada and then discusses various methods of converting biomass to energy. The discussion regarding importance of alcohols as alternative fuels, catalytic conversion of synthesis gas to higher alcohols, various catalyst systems for higher alcohols, catalyst supports and reaction mechanism are presented. In addition, the knowledge gaps, hypothesis, and objectives are discussed along with organization and manuscript content on the thesis.

1.1. Background

In today's modern world, the demand for energy has increased dramatically and is growing rapidly. The worldwide energy consumption in 2008 was estimated as 15 TW (= 1.5 x 10^{13} W) with 86.5% from burning fossil fuels (coal, oil, natural gas, or radioactive elements). About 37% of this energy consumption is utilized by the industrial sector (agriculture, mining, manufacturing, and construction). The second largest consumer is the transportation sector, which is nearly 20% of total energy consumed. Most transportation fuels are derived from fossil fuels. World energy consumption is projected to increase by 60% from 1999 to 2020.[1] The depletion of fossil energy reserves and environmental concerns like climatic changes through greenhouse gas emission shifts the focus to renewable energy resources. Renewable energy uses natural resources such as sunlight, wind, tides, biomass, and geothermal heat that can be replaced without harming the environment. This is also known as "green" energy because it won't run out like energy created from fossil fuels and does not contribute to global warming or the greenhouse effect. Since the latter 20th Century, about 13% of the world's energy consumption comes from renewable sources, with most of it from traditional conversion of biomass to energy.[2]

1.1.1. Biomass

Biomass is a renewable energy resource derived from living and recently dead biological material, including plant or animal matter used for the production of fibers, chemicals, or energy. Biomass mainly consists of cellulose, hemi-cellulose, lignin, and a small amount of other extractives. Biomass is in either solid or liquid form, and usually consists of a complex polymer of carbon, hydrogen, and oxygen with small amounts of nitrogen, sulfur, and inorganic elements.[3] Some biomass sources include forest harvesting residues, wood processors, waste residues from landfill or incineration, wood from fire- and insect-killed forest stands, agricultural crop residues, manure from farm livestock operations, municipal waste diverted from landfills, energy crops, natural rubber products, cellulose-derived casings, canning factory residues, fruit pits, coffee grounds, used cooking oils, and pulping liquors.[4]

1.1.2. Biomass availability in Canada

Canada has vast amounts of biomass from forest resources, agricultural sources, and municipal waste streams that are not utilized effectively today. Canada's forest area is nearly 10% of the world's forest area (3.5 Bha). About 42% of Canada's total land area (998 Mha) is forested, of which 25% (245 Mha) is considered Timber Productive Forest land (TPF), with an estimated standing biomass carbon stock of 15,835 Mt. The energy content from this resource is 566 EJ, which is equivalent to 69 years of Canada's current energy demand met by fossil fuels (8.24 EJ/yr).[5] Around 67.5 M ha of Canada's land is farmland used for the annual production of crops and animals. The total yield of available biomass harvest from farmland is roughly 55 Mt C/yr. Canada's annual biomass from forestry and agricultural sectors is about 143 Mt C/yr, which is equivalent to 5.1 EJ/yr, i.e., about 62% of the energy derived from fossil fuel combustion.[6] Municipal solid waste (MSW) is another source of biomass suitable for energy production. More than 8 Mt C/year is available from disposed and recycled materials, which is equivalent to an energy potential of 0.29 EJ/yr and represents about 3.5% of Canada's current use of fossil fuel energy.[7] Efficient use of MSWs can contribute to Canada's energy needs and reduce greenhouse gas (GHG) emissions from landfills.

Saskatchewan has considerable amounts of wood wastes and surplus straw that are not being effectively utilized. Saskatchewan has wood harvest of about 5.9 million m^3/year i.e., around 2.4 oven dry metric ton/year (ODMT/yr). Also, around 4,600,000 tonnes of biomass in the form of straw is available from agricultural production.[8] Alberta and British Columbia has three and ten times more wood harvest by volume than that of Saskatchewan.

An estimated 60 Mt carbon/yr is available in Canada as residual or waste biomass carbon stream associated with forestry, agricultural, and MSW with energy content ranging between 1.5 EJ/yr and 2.2 EJ/yr that is equivalent to 18% and 27% of the energy demand derived from fossil fuels. The energy content in one ton of biomass is equivalent to that in 111.6 gallon of diesel fuel.[9] Table 1.1 summarizes the biomass available in Canada from different sources and their energy contents.

When fossil fuels such as petroleum are burned, they release carbon dioxide captured by plants billions of years ago, contributing to the build-up of greenhouse gases

that, in turn, contributes to climate change. On the other hand, during their growth plants absorb CO_2 from the air and convert it by photosynthesis into complex biochemical compounds like cellulose and lignin, and release the same amount of CO_2 while burning bio-fuels; hence the energy from biomass is considered CO_2 neutral, provided new plants are grown that are equivalent to the amount of biomass used.[10]

Table 1.1. Summary of the biomass sources in Canada and their energy content[5-7]

Source	Available biomass, Mt C	Energy content EJ
Standing Carbon Stocks from TPF* land	15,835	566
Annual harvest yield from forest	136	3.1
Annual harvest yield from agriculture	88	2.0
Annual Residual or waste biomass	60	1.5

*Timber productive forest

The major components of biomass are carbon, hydrogen and oxygen containing small proportion of nitrogen. The ultimate analysis of a fuel is the elemental analysis of a fuel, presented as C, N, H, O and S together with the ash content. The proximate analysis is presented in terms of moisture, volatiles and fixed carbon. The energy content of biomass is expressed in terms of heating value (HV) or calorific value (CV). HV or CV of a material is the energy released when a material is burnt in air and is presented in terms of energy content per unit mass, or volume. This energy is measured with respect to a reference state as it cannot be measured directly.

Table 1.2 gives the ultimate and proximate analysis for some biomass materials with their corresponding heating values.[11] From the table it is clear that bio fuels when compared to fossil fuels such as coal, have the higher proportion of oxygen and hydrogen, compared to carbon and this reduces the energy value of a fuel because of the lower energy contained in carbon–oxygen and carbon–hydrogen bonds, than in carbon–carbon bonds.

Table 1.2. Analysis of potential biomass gasifier feedstocks[11]

	Ultimate analysis (wt % dry basis)						Proximate analysis (wt % dry basis)			Heating Value (MJ/kg)
	C	H	N	O	S	Ash	Moisture	Volatiles	Fixed Carbon	
Agricultural residues										
Sawdust	50.0	6.3	0.8	43.0	0.03	0.03	7.8	74.0	25.5	19.3
Bagasse	48.0	6.0	--	42.0	--	4.00	1.0	80.0	15.0	17.0
Corn cob	49.0	5.4	0.4	44.6	--	1.00	5.8	76.5	15.0	17.0
Short rotation woody crops										
Beach wood	50.4	7.2	0.3	41.0	--	1.00	19.0	85.0	14.0	18.4
Herbaceous energy crops										
Switch grass	43.0	5.6	0.5	46.0	0.10	4.50	8.4	73.0	13.5	15.4
Straw	43.5	4.2	0.6	40.3	0.20	10.10	7.6	68.8	13.5	17.0
Miscanthus	49.0	4.6	0.4	46.0	0.10	1.90	7.9	79.0	11.5	12.0
Municipal solid waste										
Dry Sewage	20.5	3.2	2.3	17.5	0.60	56.0	4.7	41.6	2.3	8.0
Coals										
Subbituminous	67.8	4.7	0.9	17.2	0.60	8.7	31.0	43.6	47.7	24.6
Bituminous	61.5	4.2	1.2	6.0	5.10	21.9	8.7	36.1	42.0	27.0

Biomass materials have lower carbon and hydrogen percentages and a higher oxygen percentage than fossil fuels (coal, oil, or natural gas), which results in a lower energy content. Figure 1.1 compares the energy content of different energy sources.[12] Compared to other developed countries, Canada has a "green" advantage because it has 0.5% of the world population, 7% of the global land area, and 10% of the world forest.[13] The effective use of Canada's large available waste biomass would improve the nation's ability to reduce toxic air emissions, greenhouse gas build-up, and dependence on imported oil, while supporting agriculture and rural economies.

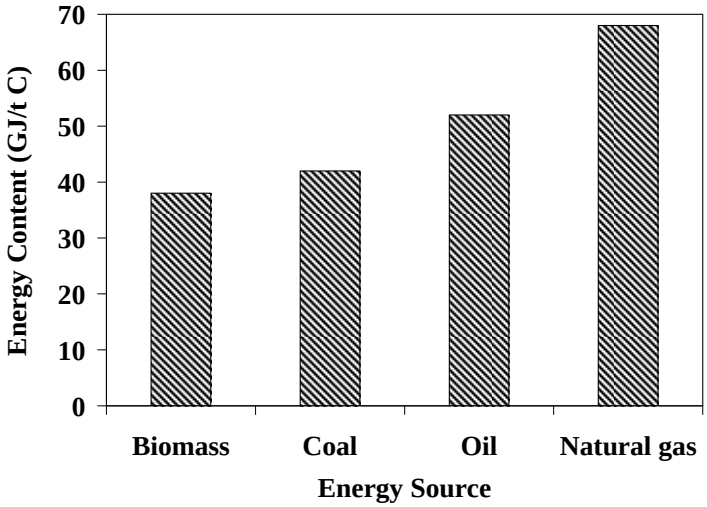

Figure 1.1. Comparison of the energy content of different energy sources[12]

1.2. Biomass conversion to energy

Conversion of biomass to energy can be done using different processes such as thermo-chemical, bio-chemical/biological, and mechanical extraction (with esterification). Factors like type and quantity of biomass feedstock, end-uses of the energy; environmental standards, and economic conditions influence the choice of conversion. Figure 1.2 explains different process involving the thermo-chemical conversion of biomass, intermediate energy carriers, and final energy products.[14] According to the figure the main thermal processes for the conversion of biomass to energy: combustion, gasification, and pyrolysis.

1.2.1. Combustion

Combustion is the first choice for converting biomass to energy. Combustion of biomass using fluidized bed combustion technology at temperatures around 800–1000^{o}C produces hot gases. Any type of biomass can be burned, but in practice only biomass with moisture content less than 50% is feasible, unless the biomass is pre-dried. Wood waste is combusted to produce steam to power an electrical generator feeding into the electric grid that is used for various applications.[15]

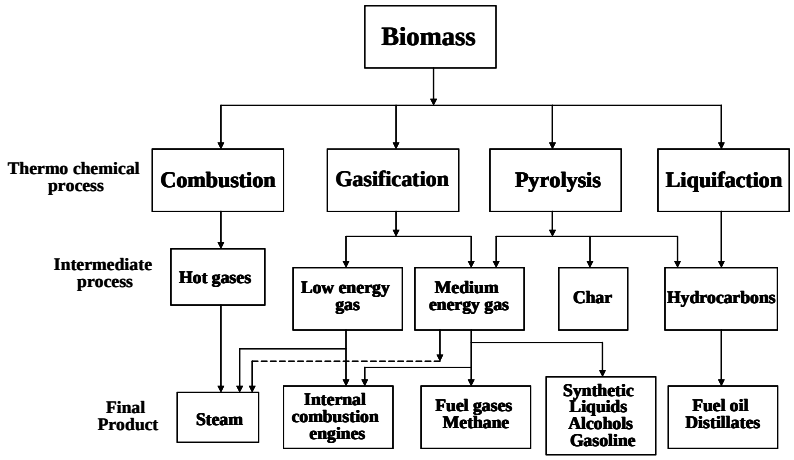

Figure 1.2. Thermo-chemical conversion of biomass into energy[14]

1.2.2. Pyrolysis

Pyrolysis involves the heating biomass at about 500^{o}C in the absence of oxygen to produce a mixture of oils, gases, and solid charcoal. The gaseous products consist of volatile components that are realised through a set of complex reactions. These volatile vapours consist of hydrocarbon gases, hydrogen, carbon monoxide, carbon dioxide, tars, and water vapour. The by-products of pyrolysis that are not vaporized are referred to as char and consist mainly of fixed carbon and ash.[15]

1.2.3. Gasification

Biomass gasification is the thermo-chemical process that uses partial oxidation to convert organically derived, carbonaceous feedstock into a gaseous product known as, synthesis gas. Synthesis gas mainly consists of hydrogen and carbon monoxide, with lesser amounts of carbon dioxide, water, methane, higher hydrocarbons, and nitrogen. The reactions are carried out in a gasification medium such as air, pure oxygen, steam, or

a mixture of these gases at elevated temperatures, 500–1400°C, and atmospheric or elevated pressures up to 33 bar (480 psia).[15] The major reactions involved in the gasification process are as follows:[16]

Partial oxidation: $C + 1/2O_2 \leftrightarrow CO; \quad \Delta H = -111 MJ / kgmole$ (1.1)

Complete oxidation: $C + O_2 \leftrightarrow CO_2; \quad \Delta H = -365 MJ / kgmole$ (1.2)

WGS reaction: $CO + H_2O \leftrightarrow CO_2 + H_2; \Delta H = +131 MJ / kgmole$ (1.3)

Boudouard: $C + CO_2 \leftrightarrow 2CO; \quad \Delta H = +173 MJ / kgmole$ (1.4)

Methane reaction: $C + 2\,H_2 \leftrightarrow CH_4; \quad \Delta H = -75 MJ / kgmole$ (1.5)

Methane reaction: $CO + 3\,H_2 \leftrightarrow CH_4 + H_2O; \Delta H = -206 MJ / kgmole$ (1.6)

All the above reactions may be in equilibrium, which means that the product gas from gasification may consist of a mixture of carbon monoxide, carbon dioxide, methane, hydrogen, and water vapor. WGS reaction represents water-gas-shift reaction

Depending on the process used, gasification produces a low heating or medium heating value gas. Low heating value gas (about 4–6 MJ/N-m^3) can be burned directly for space heating and drying or it can be used as fuel for gas engines and gas turbines. Medium heating value gas can be used as a feed stock to synthesize many liquid fuels such as alcohols and Fischer-Tropsch fuels.[17,18] Table 1.3 shows the three types of product gas with their calorific values and gasifying agents.[19]

Table 1.3. Types of product gases, their calorific values and gasifying agents[19]

Product gases	Calorific value	Gasifying agent
Low CV	4-6 MJ / Nm^3	Using air and steam/air
Medium CV	12–18 MJ / Nm^3	Using oxygen and steam
High CV	40 MJ / Nm^3	Using hydrogen and hydrogenation

1.2.4. Hydro thermal upgrading (HTU) and liquefaction

Hydro thermal upgrading (HTU) and liquefaction processes produce bio-oils from biomass. HTU converts biomass to partly oxygenated hydrocarbon in a wet environment and at high pressure. Liquefaction is the conversion of biomass into a stable liquid hydrocarbon using low temperatures and high hydrogen pressures. This process

does not gain much interest because the reactors and fuel-feeding systems are more complex and more expensive than pyrolysis processes.[14]

1.2.5. Synthesis gas from biomass gasification

The synthesis gas obtained from biomass gasification may contain contaminants as listed in Table 1.4.[20] The removal of contaminants is known as synthesis gas conditioning. These contaminants must be removed to acceptable levels before the gas can be utilized.

Table 1.4. Synthesis gas contaminants and their potential problems[20]

Contaminant	Example	Potential Problem
Particles	Ash, char, fluid bed material	Erosion
Sulfur, Chlorine	H_2S and HCl	Corrosion, emissions, catalyst poisoning
Nitrogen Compounds	NH_3 and HCN	Emissions
Tars	Refractive aromatics	Clogging of filters

The synthesis gas compositions from different biomass gasification technologies are compared in Table 1.5.[21-23] The variation in synthesis gas compositions is due to the influence of different parameters including type of gasifier, feedstock composition, pressure, temperature, and oxidant used.

Table 1.6 shows the typical composition (%v/v) of exit gas obtained estimated after gasification, auto temperature reforming (ATR), and WGS reactions using 85% of dry wood chips with a flow rate of 4 tonne/h with gasification temperature of 950-1000^{o}C, and the pressure of approximately 18 bar inside a circulating fluidized bed.[24] The WGS and ATR are represented by equations 1.6 and 1.8, respectively.

ATR reaction: $$CH_4 + H_2O \leftrightarrow CO + 3H_2; \quad \Delta H = +206 MJ / kgmole \qquad (1.7)$$

Table 1.5. Summary of different gasifier operating conditions and synthesis gas composition[21-22]

Gasifier Type	BFB Range	CFB Range	BCL/FERCO[a]	MTCI[b]	Purox[c]	Shell[d]
Feedstock	Various	Various	Wood	Pulp	MSW	Coal
Inlet conditions						
Throughput (tonne/day)	4.5-181	9-108	24	7	181-195	2155
Pressure (bar)	1-35	1-19	1	1	1	30
Temperature (°C)	650-950	800-1000	600-1000	790-815	1300-1400	1400
Reactant 1	O_2 or Air	Air	Air	--	O_2 or Air	O_2
Input (kg/kg feed)	0.4-2.2	1.25-1.7	0.08	--	--	0.98
Reactant 1	Steam	--	Steam	Steam	--	Steam
Input (kg/kg feed)	0.5-0.64	--	0.31	2.2	--	0
Outlet conditions						
Gas output (m^3/h)	335-8793	1181-12500	800	--	33960	$1.48*10^5$
Exit temperature (°C)	300-800	600-900	820	--	--	240
Heating Value (MJ/m^3)	4-13	4-7.5	18	16.7	7.92	9.51
H_2 to CO ratio	0.2-1.6	0.6-1.0	0.3	4.6	0.6	0.36
Gas composition						
H_2	5-26	7-20	14.9	43.3	23.4	24
CO	13-27	9-22	46.5	9.22	39.1	67
CO_2	12-40	11-16	14.6	28.1	24.4	4
H_2O	<18	10-14	dry	5.57	dry	3
CH_4	3-11	<9	17.8	4.73	5.47	0.02
C_2+	<3	<4	6.2	9.03	4.93	0
Tars	<0.11	<1	--	Scrubbed	--	0
H_2S	~0	~0	--	0.08	0.05	1
O_2	<0.2	0	0	0	--	0
NH_3	0	0	0	0	--	0.04
N_2	13-56	46-52	0	0	--	1

BFB- Bubbling fluidized bed; CFB- Circulating fluidized bed; [a] Indirectly heated CFB with separate combustor; [b] Indirectly heated BFB with separate combustor; [c] Fixed bed; [d] Fluid bed - Entrained Flow (no circulation)

Table 1.6. Calculated compositions (%, v/v) of exit gases from Varnamo plant[24]

Compound	After gasifier (%)	After ATR (%)	After WGS (%)
C_2H_6	0.08	0.00	0.00
C_2H_4	1.53	0.00	0.00
CH_4	8.17	0.80	0.72
CO	11.86	21.48	6.45
CO_2	27.92	20.85	32.09
H_2	11.79	23.36	34.38
H_2O	37.69	33.15	26.01
N_2	0.06	0.05	0.04
Ar	0.06	0.07	0.07
NH_3	0.29	0.23	0.21
H_2S	0.01	0.01	0.01
BTX[a]	0.26	0.01	0.01
Tars	0.27	0.00	0.00

[a] Benzene, Toluene, Xylene

Synthesis gas is an environmentally friendly fuel, especially when the available biomass fuel is cheaper than fossil fuel, and can be used to co-fire existing coal, oil, or natural gas fired boilers. It can be fed to gas turbines in combined cycle systems for electricity generation. The most important use of the synthesis gas is as a chemical feedstock (see Figure 1.3).[25] Synthesis of alcohols from syngas remains an economically attractive method for making fuels and primary materials. Ethyl alcohol synthesis is of particular interest, due to the increasing petroleum prices, environmental concerns, and gasoline additive octane demands.[26] Typically, gasoline blends containing up to 10% ethanol (by volume) are used in Canada. There is great potential to capitalize on ethanol fuel because Canada has the forest resources and cropland needed to support the production of ethanol.

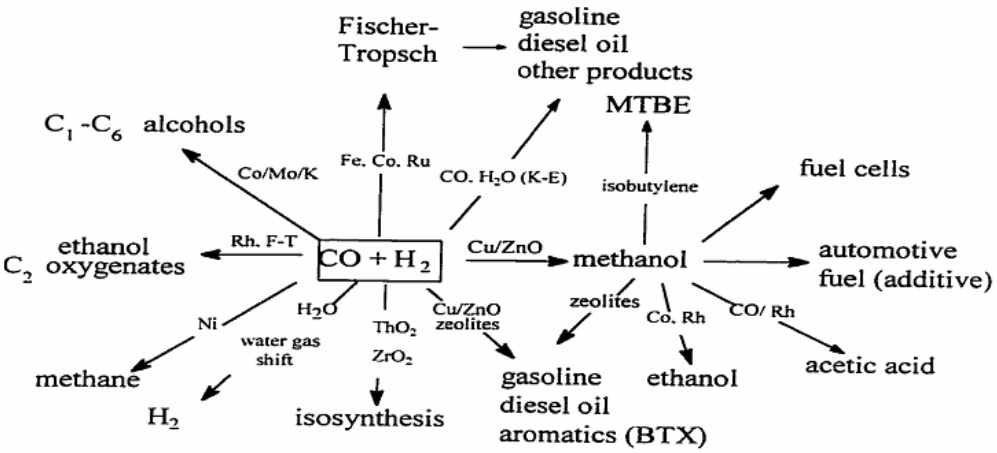

Figure 1.3. Synthesis gas as a potential chemical feed stock[25]

1.3. Alcohols as alternative fuels

Over the past decade, considerable effort by government and industry has been directed towards providing cleaner gasoline for Canadians. Originally, lead was added to gasoline as an octane enhancer. For each gram of lead added to a gallon of gasoline, the octane rating, a measure of the resistance of petrol and other fuels to autoignition in spark-ignition internal combustion engines, goes up about 10 times or more octane numbers.[27] Engines require certain minimum levels of octane rating to run smoothly and resist knocking. Concern about leaded gasoline emissions encouraged the environmental protection agency (EPA) to call for reduced lead in gasoline. As unleaded gasoline became the standard, petroleum refineries looked to other additives to help keep gasoline octane numbers at leaded standards. Aromatics and alcohols have been the most popular choices. Aromatics, such as benzene and toluene, have high octane levels, but the presence of these compounds produces more smoke, smog, as well as benzene, a known carcinogenic compound.[28] The EPA has approved using several alcohols and ethers in unleaded gasoline. Ethanol and methyl tertiary butyl ethers (MTBE) are the two most popular additives. MTBE is not as widely used as ethanol, but refineries use it as an additive because it is not as sensitive to water as other additives and tends not to increase fuel volatility.[29] The fuel properties of gasoline and its contents have a direct impact on

the environment. Table 1.7 gives a brief account of gasoline properties, their desirable impact on engine performance, and their undesirable impact on the environment.[30.]

Table 1.7. Summary of gasoline properties.[30]

Gasoline Property	Desirability	Impact on Environment
Octane Number	Avoid engine knocking; increase fuel-air mix compression ratio, engine power, and efficiency	Octane boosting compounds are not environmentally friendly: – Lead additives are toxic air pollutants and poison catalytic converter catalysts. – Benzene is carcinogenic. – Aromatics produce more smoke and smog. – Olefins form engine fouling gums, more smoke & smog.
Volatility (Reid vapor pressure)	Sufficient light components to give adequate vaporization of fuel air mix for easy engine cold start	– Too many light components result in hydrocarbon loss & result in atmospheric pollution. – Too many heavy components contribute to chamber deposits & spark plug fouling causing release of unburnt hydrocarbons into the atmosphere.
Sulfur Content	Not desirable	– Sulfur compounds are corrosive, foul smelling, and increase sulfur trioxide emissions. – Decreased catalytic converter efficiency. – Adversely affect ignition timing, leading to lower engine efficiency.
Olefins	Desirable for their octane value	– Leads to deposits and gum formation; increased emissions of ozone forming hydrocarbons, and toxic compounds.
Aromatics	Desirable for their octane value	– Increased engine deposits and tailpipe emissions, including carbon dioxide. – Produces carcinogenic benzene in exhaust.
Stability additives	Reduce valve deposits	– Affect carburetors resulting in higher H/C and CO emissions.

Low molecular weight alcohols such as ethanol have replaced other additives as octane boosters in automotive fuels. Alcohols can be promoted as alternative fuels or alternative fuel components in transportation for many reasons, such as:

- Reduction of greenhouse gas emissions
- Reduction of toxic exhaust emissions
- Enhancement of overall energy efficiency
- Reduction of fuel costs
- Societal reasons (e.g., employment in the agricultural sector)

Unlike gasoline and diesel, alcohols contain oxygen. Adding alcohols to petroleum products allows the fuel to combust more completely due to the presence of oxygen, which increases the combustion efficiency and reduces air pollution. Gasoline blended with 10% ethanol becomes mandatory in many nations. An additional factor making ethanol attractive as a fuel extender or substitute is that it is a renewable resource.

Table 1.8 compares the properties of alcohols such as boiling point, latent heat, vapour pressure, solubility in water, etc., with octane and hexadecane.[31] Compared with conventional fuels, alcohols have less combustion energy. However, the lower stoichiometric air to fuel ratio helps alcohol fuels to produce more power inside an engine when they are burned.

Table 1.9 shows the effective blending values of oxygenated fuels as gasoline blends.[32] Research Octane Number (RON) is determined in test engines at a relatively low speed (600 rpm) to simulate city driving speed with frequent acceleration. Motor octane number (MON) is measured at a higher speed (900 rpm), which simulates highway driving.

For most fuel components, RON is greater than MON and the difference between them is used to judge fuel quality. This is known as the sensitivity of the fuel and a maximum value is specified for the gasoline, which typically should be less than 10. Although methanol has the highest percentage of oxygen, its sensitivity is 30 when compared with ethanol, having a sensitivity of 15 and a Reid vapour pressure (RVP) much less than that of methanol. In essence, ethanol is more advantageous when comparing the percent oxygen content, sensitivity, and Reid vapour pressure with other fuels.

Table 1.8. Characteristics of chemically pure fuels.[31]

Fuel	Chemical weight (lb/mole)	Specific gravity	Boiling point (°C)	Latent heat (Btu/lb)	Combustion energy (Btu/lb)	Vapour pressure @100F (psig)	Solubility part in 100 parts H_2O	Stoichiometric air-fuel ratio
Methyl alcohol	32	0.79	65	503	10,260	4.6	infinite	6.5
Ethyl alcohol	46.1	0.79	78	396	13,160	2.2	infinite	9
Butyl alcohol	74.1	0.81	117	186	15,770	0.3	9	11.2
Octane	114	0.70	210	155	20,750	1.72	insoluble	15.2
Hexadecane	240	0.79	287	--	20,320	3.46	insoluble	15

Table 1.9. Effective blending values of the fuels.[32]

Fuel	Density (kg/l)	% of O_2 (wt %)	RON	MON	RVP (kPa)
Methanol	0.796	49.9	130	100	250
Ethanol	0.794	34.7	115	100	130
IPA	0.789	26.6	117	100	70
TBA	0.791	21.6	100	90	65
MTBE	0.744	18.2	110	100	55
ETBE	0.770	15.7	112	100	28

1.3.1. Adverse effects of alcohol fuels

The presence of alcohols in fuel causes corrosion to metallic fuel system components because of increased water content in the fuel and partly because of the organic acids produced in commercial oxygenates. Other major disadvantages of alcohol fuels is vapour lock due to high vapour pressures and low boiling points.[33] The major difference between the alcohols and gasoline is that alcohols are strong solvents and, hence, highly corrosive to some metal parts of the engines. Methanol is more corrosive compared with higher alcohols. There is limited miscibility between methanol and gasoline, because of the presence of minute amounts of water, which causes phase separation. When compared to methanol, ethyl alcohol has low vapour pressure, better solubility with hydrocarbon liquids, improved water tolerance, and higher overall heating value. Other redeeming qualities such as latent heat of vaporization, volatility, and anti-knock values make ethyl alcohol fuels superior than methyl alcohol blended fuels.[33] Phase separation occurs when alcohol and water mix together in an ethanol blended fuel. When the alcohol and water get separated from the gasoline, the resulting mixture settles at the bottom of the tank and becomes corrosive.[35]

Corrosion due to alcohols is of three types: general corrosion, dry corrosion, and wet corrosion. General corrosion causes due to ionic impurities such as chloride ions and acetic acid. Dry corrosion is due to the ethanol molecule and its polarity. The azeotropic formation of ethanol and water causes wet corrosion. If the alcohol/gasoline blend stays for a sufficiently large time inside the tank, it allows the alcohol to absorb moisture from the atmosphere and causes corrosion to the fuel injection system. Non-metallic components such as seals and O-rings in the fuel injection system tend to swell and stiffen due to the presence of alcohols in fuels.[36]

1.3.2. Modifications required for best use of alcohol fuels

In order to best use the alcohols as alternative fuels there are two options, redesign the engine to take full advantage of the alcohol fuel's properties or blend in one or more additives to the ethanol or methanol to improve its characteristics.

Modifications to vehicles

The following modifications are typical for converting conventional vehicles to high-level alcohol blends.[37]

1. Stainless steel fuel tank with stainless flame arrestors in the fill and vent tubes to prevent ignition by an external source.
2. Methanol resistant float level potentiometer with a corrosion protection circuit.
3. Higher flow methanol-tolerant fuel injector and fuel pump to handle higher flow rates.
4. Stainless fuel lines with accompanying Teflon fuel hoses.
5. Anodized aluminium fuel injection rail and modified pressure regulator.

Additives required for improving the fuel properties of alcohols

Alcohols can be used effectively as alternative liquid transportation fuels by modifying their properties by using certain additives, which must be physically and chemically compatible with the base alcohol fuel and have the same or higher specific energy content. Additives must not be readily removable from the fuel, significantly add to exhaust emissions, leave any residue, should not complicate regulatory compliance, and be relatively inexpensive.[38]

Ethanol and methanol are completely miscible with water, but show very poor miscibility with gasoline containing traces of water. So, blending gasoline with ethanol or methanol in the presence of water may lead to a phase separation problem. Additives such as higher alcohols like iso-propanol, 1-butanol, n-decanol, various commercial non-ionic surfactants, and various anionic fatty acid surfactants can be effectively controlled to prevent the phase separation problem. The prevention of phase separation would have definite benefits for overall drivability, as well as in corrosion of water-sensitive components such as aluminium.[39]

Conventional fuel injection systems usually encounter lubrication problems due to the low viscosity of alcohol fuels, which leads to wearing of the engine parts. Higher alcohol additives offer better lubrication and decrease wear in engine parts. During combustion, alcohol blended fuels produce acids that are responsible for wearing of engine parts. Neutralizers such as zinc dialkyldithiophospates and calcium sulfonates are

added in lubricant oil to neutralize these acids and improve lubrication. Shorter lubricant oil change intervals reduce corrosive wear significantly.[40]

1.3.3. Production of industrial ethanol

Ethanol can be manufactured by:

1. Fermentation of sugar derived from grain starches (wheat and corn), sugar beets, or sugar crops using microorganisms;
2. Using surplus wine ethanol; fermentation of the non-sugar lignocellulose fractions of crops (grasses and trees);
3. Synthetically, through direct hydration of ethylene (derived from petroleum);
4. High temperature catalytic conversion of synthesis gas to liquid fuels by the Fischer-Tropsch process to produce a mixture of alcohols.

Fermentation is the primary method for production of beverage alcohol and much of the alcohol used in industry. Fermentation uses a variety of sources including grains such as corn, potato mashes, fruit juices, beet and cane sugar, molasses, and non-sugar lingo-cellulose fractions of crops and grasses. Enzymes such as microscopic yeasts in the absence of oxygen convert carbohydrates to ethanol. The equations for the fermentation of carbohydrates to ethanol in the presence of yeast are:[41]

$$C_{12}H_{22}O_{11} + H_2O \rightarrow 2C_6H_{12}O_6 \quad (1.8)$$

$$C_6H_{12}O_6 \rightarrow 2CH_3CH_2OH + 2CO_2 \quad (1.9)$$

Another method of manufacturing ethanol is reacting ethylene with steam. The catalyst used is solid silicon dioxide coated with phosphoric (V) acid. The reaction is reversible.

$$CH_2 = CH_2 + H_2O \leftrightarrow CH_3CH_2OH \quad (1.10)$$

Only 5% of the ethylene is converted into ethanol at each pass through the reactor. By removing the ethanol from the equilibrium mixture and recycling the ethene, it is possible to achieve an overall 95% conversion. This is a continuous flow process and is much simpler and more efficient than fermentation, producing high purity ethanol. The major disadvantages of this process are that it needs a lot of energy input as the reaction

takes place at high temperature and pressures, and it uses finite resources based on crude oil.[42]

Synthesis of alcohols from synthesis gas remains an economically attractive method for making fuels and primary materials from chemical industries. Synthesis gas can be produced from natural gas reforming, coal gasification, or biomass gasification. Synthesis gas obtained from biomass is advantageous because of the flexibility regarding feedstock, enabling a very wide range of biomass and even residues to be processed, depending on the gasification technology used.[43] Compared to other process, catalytic conversion of synthesis gas to alcohols is advantageous as this uses forest, agricultural surplus, and household waste and does not compete with the feed grains available for human need or use finite resources. Catalytic conversion of synthesis gas to alcohols is a simple and continuous flow process, producing high purity alcohols with comparatively more yields.

1.4. Synthesis of higher alcohols from synthesis gas

The synthesis of higher alcohols from synthesis gas by direct catalysis was recognized in 1923 by Frans Fischer and Hans Tropsch. They reported that a mixture of alcohols, aldehydes, ketones, fatty acids, and esters were formed when the reaction between CO and H_2 was performed at pressures ranging from 10 to 14 MPa and at temperatures of 400 to 500°C in the presence of an alkalized iron oxide catalyst. They named the mixture as synthol and the process as the synthol process.[44] In 1930, Frolich and Cryder reported the formation of alcohols higher than methanol by passing syngas over a Zn:Mn:Cr, 1:1.1:1.03 catalyst. They reported that methanol forms from a formaldehyde intermediate and that the higher alcohols form from the methanol through a stepwise condensation reaction.[45] In the 1940s, Du Pont developed an alkalized Mn-Cr catalyst to synthesize methanol and higher alcohols from syngas for commercial purposes.[46] In the late 1940s, Farbenindustrie et al. introduced the Synol process for the manufacture of alcohols from syngas. This process uses low pressures around 2 MPa with higher productivity of alcohols by modifying the Fischer-Tropsch alkalized iron catalyst.[47] Natta et al. reviewed the synthesis of higher alcohols from CO and H_2, in 1957

and reported that the synthesis of higher alcohols was always related to the presence of strongly basic substances.[48]

1.4.1. Catalyst systems for higher alcohols synthesis

Several authors summarized typical operating conditions, research status, characteristics, and performance of primary groups of catalysts that have been adapted and tested for higher alcohol synthesis (HAS). According to these reviews, there are two major catalyst groups for higher alcohol production:

1. *Modified methanol synthesis catalysts*
    a. Alkali-modified high pressure, high temperature methanol synthesis catalysts.
    b. Alkali-modified low pressure, low temperature methanol synthesis catalysts.
2. *Modified Fischer-Tropsch catalysts*
    a. Fe, Ni, or Co-modified low temperature, low pressure methanol synthesis catalysts.
    b. Supported Rhodium-group catalysts.
    c. Alkali-modified molybdenum-based catalysts.

High pressure, high temperature methanol synthesis catalysts

Natta et al.[49] first studied the synthesis of alcohols from synthesis gas over ZnO/Cr_2O_3 catalysts promoted with alkali metals, which are high pressure and high temperature methanol synthesis catalysts. They reported that Cs, Rb, and K were the most active promoters for production of HAS. The HAS takes place over this catalyst at high temperatures of 400-450^oC and at high pressures of 20.3-25.5 MPa. The addition of alkali metals decreases the hydrocarbon formation and increases the alcohol selectivity.[50,51] When compared with K, incorporation of Cs with Zn/Cr catalysts increased the higher alcohol production rate and selectivity. These catalyst systems represent an improvement in the selectivity towards iso-butanol, but the total product rate of alcohols in the product stream is lower than that of Cu-containing catalysts.[52,53] These catalyst systems require high operating temperatures and pressures, are relatively inactive, and yield branched alcohols, among which iso-butanol is the main product and methanol is the other.[54]

Low pressure, low temperature methanol synthesis catalysts

In 1928, Lewis and Frolich found that high methanol yields are possible by passing a synthesis gas over a $CuO/ZnO/Al_2O_3$ catalyst. Since this discovery, it was found that Cu-based catalysts promoted with alkali resulted higher alcohols from synthesis gas. The presence of Cu in ZnO/Al_2O_3 catalysts enables the alcohol production at lower operating temperature and pressures. Smith et al.[55,56] studied the synthesis of higher alcohols over $Cu/ZnO/Al_2O_3$ catalysts promoted with K_2CO_3 at temperatures of 260-300°C and a pressure of 10 MPa. The alcohols in the product were mostly methanol, with small amounts of higher alcohols. The HAS selectivity enhanced at higher temperatures and lower H_2/CO ratios (approximately 1.0).[57] The low temperatures of 250-300°C and low pressures of 2-10 MPa are used for the synthesis of higher alcohols over these catalysts. These catalyst systems produce mainly branched alcohols, along with methanol. Compared to high temperature, high pressure methanol synthesis catalysts, these catalysts can yield high conversion of alcohols, but with poor selectivity. Long time activation is one advantage of this catalyst system and cannot be used at temperatures greater than 300°C due to sintering of copper.[58,59]

Increasing calcination temperatures from 280-400°C causes a decrease in surface area of the catalyst. The addition of the cesium promoter did not significantly affect the BET area of the base catalyst. The incorporation of cesium resulted in much higher methanol and higher alcohols productivities and by co-feeding a given $C_nH_{2n+1}OH$ alcohol, the $C_{n+1}H_{2n+3}OH$ yield was enhanced. Increasing temperature increases methanol, higher alcohol, and hydrocarbon production rate over a Cs-promoted $Cu/Zno/Cr_2O_3$ catalyst. The addition of water does not affect the methanol synthesis reaction, but inhibits the formation of the C_{2+} oxygenates.[49]

Fe, Ni, or Co-modified low temperature, low pressure methanol synthesis catalysts

In 1934, Taylor modified the hydrogenation action of F-T catalysts by the addition of metal sulfides, borates, phosphates, and/or alkali promoters. In 1952, Anderson et al. proved that alkali-promoted F-T catalysts improved the production of higher alcohol synthesis. Later studies showed that decreased operating temperatures and increased reactant stream contact time reduced the hydrocarbon production and favoured the alcohol formation over Fe- and Co-containing FT catalysts. Typical operating

conditions for these catalysts are 4-10 MPa of pressure, 200-350°C temperature, and 2000-8000 kg/m^3 (STP)/(g of cat.)/h of gas hourly space velocity (GHSV) with a ratio of H_2/CO of 0.5 to 2. The products consist mainly of linear alcohols, with little amount of branched alcohols. Linear alcohol distribution obeys the Schulz-Flory distribution, but the formation of hydrocarbons cannot be reduced to acceptable levels over these catalyst systems. Deactivation causes the destruction of the spinel structures of Cu and Co, Ni or Fe and these cannot be used at temperatures greater than 300°C due to the sintering of Cu.[59] High temperature and pressure could increase carbon deposition from the iron group metals, resulting in catalyst deactivation. The carbon deposition rate of cobalt and nickel catalysts is prohibitively high at temperatures above 250 and 300°C for iron. Hydrogen-rich synthesis gas should be used in order to minimize carbon deposition.[60] F-T catalysts prepared from solutions of various cyanide complexes showed a slightly higher alcohol production than the conventionally prepared bimetallic catalyst.[61]

The selectivity of higher alcohols was increased greatly when nickel and cobalt were added when compared with that of the Cu/Mn/ZrO_2 catalyst. The addition of Fe to the Cu/Mn/ZrO_2 catalyst improved its selectivity for hydrocarbons.[62] The effect of iron was greatly influenced by the method of catalyst preparation. The presence of iron affects the structural properties of the catalyst by increasing the dispersion of copper and by improving the stabilization of the catalyst. The co-precipitation method produced highly dispersed copper species, which favoured the synthesis of methanol and branched alcohols.

The wetness impregnation method gave rise to a highly dispersed copper and copper-iron phase, which showed a good performance for synthesis of straight chain alcohols.[63] Increasing temperature from 270-325°C increased the activity of Cu-Co_2O_3/ZnO/Al_2O_3 catalyst, but decreased the selectivity of C_{2+}OH alcohols. Increasing pressure increased the overall yield, conversion, and selectivity of the alcohols with decreased selectivity of hydrocarbons.[64]

Supported Rhodium-group catalysts

The hydrogenation of carbon monoxide over transition metal catalysts produces a variety of compounds such as hydrocarbons, alcohols, aldehydes, and acids. Over transition metal catalysts, alkali doping inhibits methanol formation and favours the

formation of ethyl alcohol. In 1978, Ichikawa et al. reported that C_2-oxygenated compounds (mainly ethanol) were produced over an Rh-based catalyst during the synthesis of methanol. Among the group VIII metals, Rh is unique in its ability to predominantly catalyze the formation of C_2 oxygenates from syngas. Rhodium is a component of most catalyst studies, usually in combination with promoters to increase its activity or selectivity to ethanol. During the last decade, research has focused on the features of Rh-based catalysts and their function in higher alcohol synthesis. These catalysts are advantageous due to low operating conditions, with typical operating temperatures of 150-250°C and pressures of 0.1-1 MPa.[59]

The addition of transition metals such as Mn, Ti, and Zr in oxide form on Rh/SiO_2 enhances the CO conversion rate by 10 to 50 times compared with Rh/SiO_2, and also improves the selectivity towards C_2-oxygenates. This is due to the oxophilic promoters located at the surface of Rh particles, which enhance the CO dissociation rate and the steady-state coverage of the surface with alkyl groups. The addition of base metals such as Zn and Fe are effective in blocking CO dissociation on the Rh surface and, hence, methanation and C_2- oxygenate formation is substantially suppressed.[65] The addition of Fe and Mo enhance the chain growth properties of the Rh/ZrO_2 catalyst and improve the formation of C_{2+} components. Moderate reaction pressures between 1 and 2.5 MPa and low temperatures between 150-250°C favour the formation of C_{2+} components. The addition of Fe to Rh/ZrO_2 catalysts produces opposing effects: it reduces the number of Rh atoms available for CO and hydrogen adsorption, increases the number of double-bonded CO (Rh-CO-Fe), and favours the formation of oxygenated products. In Rh/ZrO_2 catalysts, iron promotes the activity and selectivity to oxygenated products when present in small quantities (Fe/Rh <1.5), and decreases the activity only when present in larger amounts.[66]

Alkali-modified molybdenum-based catalysts

The sulfides of transition metals have been used in the petroleum industry in hydrodesulfurization, hydrodenigrodenation, and hydrogenation reactions for over 50 years. Molybdenum disulfide (MoS_2) when supported with alkali metals can be used as a catalyst for the production of alcohols from syngas. The commercial Mo-based catalysts to convert synthesis gas to alcohols were first developed by Dow and Union Carbide

companies. The function of the alkali metal is to reduce the hydrogenation ability of alkyl species to produce alkanes and increase the active sites for the formation of alcohols.[67] Alkali-modified molybdenum-based catalysts are more attractive due to their excellent resistance to sulfur poisoning and high activity for the water-gas shift reaction. This saves the cost of ultra-desulfurization for feed gas and separation of water.[68]

The alcohol products over these catalyst systems are linear alcohols, and the mechanism for formation of higher alcohols ($C_{2+}OH$) was via a classical insertion of CO into the corresponding precursor alcohol. The activity and selectivity to $C_{2+}OH$ was low due to A-S-F distribution.[69] The F-T elements such as Ni and Co increase the alcohol yield and selectivity towards higher alcohols of MoS_2 catalysts.[70,71] The presence of Co in alkali-modified MoS_2 catalysts enhanced the $C_1 \rightarrow C_2$ homologation step that led to ethanol as the dominant product.[72] The addition of Ni to K/MoS_2 catalysts leads to methanation.[73] The addition of Mn on $Ni/K/MoS_2$ catalysts inhibits the enrichment of Ni to a certain extent,[74] which restrains the formation of hydrocarbons and carbon chain growth promoted by Ni, leading to improved selectivity of higher alcohols. The typical operating temperature and pressure are in the range of 250-350°C and 5-10 MPa.[59]

Increasing the reactant temperature increases the selectivity of both hydrocarbons and higher alcohols, but decreases the selectivity of methanol. The promoting effect of different alkali metals (K, Rb, and Cs) on MoS_2 catalyst for the formation of higher alcohols depends on the alkali:Mo ratio. The performance of K and Rb are superior to those of Cs at an alkali:Mo ratio of 0.7:1. The performance for Cs-promoted catalysts can be improved by decreasing the ratio from 0.7:1 to 0.22:1.[75] The promotional effect of K was greater than Cs for alcohol synthesis over the $Co\text{-}MoS_2$/clay catalyst.[71,76] The presence of carbon-dioxide in the feed causes greater amounts of water to be produced, but reduces the formation of CO_2. The addition of CO_2 reduces the formation of higher alcohols, while H_2S increases the formation of hydrocarbons.[77] Co-promoted samples increased the alcohol ratios of C_2^+/C_1 in the products relative to that for the un-promoted sample. Co species show a relatively stronger interaction with the Mo component in the form Co-Mo-S structure than in Co-Mo-O structure.[78] Mo species with intermediate valencies (around +3.5) are more active phases for alcohol synthesis

from CO hydrogenation, while those with lower Mo valency are responsible for the production of hydrocarbons.[79]

Depending on the reaction conditions, properties of alkali promoters, and support, Rh-species in catalysts are capable of catalyzing dissociation, insertion, and hydrogenation of CO.[80] The conversion of CO and yield of oxygenates over Mo-Rh/Al_2O_3 catalysts is high when compared to Rh/Al_2O_3 catalysts.[81] The interaction of rhodium with molybdenum affects the oxidation state of the rhodium species, which affects CO adsorption. The formation of alcohols on rhodium catalysts can be catalyzed by the sites that are less electron-rich than those needed for hydrocarbons, and more of these electron-deficient sites can be created by the interaction of rhodium with molybdenum.[82] The incorporation of rhodium into the Mo-K/Al_2O_3 samples increases catalytically active surfaces and is responsible to increase the activity for alcohol synthesis. Due to the co-existence of cationic and metallic rhodium species stabilized by the interaction of rhodium with molybdenum species, the selectivity to the formation of higher alcohols is high.[83,84]

Based on the above reviews, it is clear that alkali-modified molybdenum sulphide catalysts are considered to be more attractive due to their excellent resistance to sulfur poisoning and high activity for the water-gas shift reaction. This saves the cost of ultra-desulfurization for feed gas and separation of water. Addition of Co and/or Rh metal promoters to these catalysts increases the higher alcohol selectivity.

1.4.2. Catalyst supports for higher alcohols synthesis

A catalyst support is the solid material that offers a high surface area of a catalyst by distributing the metal particles over the support. The texture and surface acidity of support can influence metal dispersion, properties of reduction, as well as the interaction between metal and support. The sintering of the active material can be prevented by impregnating the catalyst species on a thermostable support. Typical supports such as, various kinds of carbon, alumina, silica, zirconia, etc. have been used for catalytic conversion of synthesis gas to higher alcohols.[85-87] The supports for higher alcohol synthesis are neutral or basic otherwise can be made neutral or basic by adding alkaline promoters.[88]

The surface acidity of metal oxides, such as Al_2O_3 and ZrO_2 suppress the formation of alcohols and improves the hydrocarbon reaction rate.[88] Activated carbon, as a neutral catalyst support has many advantages for higher alcohols synthesis because of its large surface area, limited interaction between the support and the active material, resistance to acidic or basic media, and stability at high temperatures and pressures.[89] The hydrocarbon selectivity on activated carbon-supported molybdenum catalysts was found to be much less than that of SiO_2, Al_2O_3, and CeO_2.[90] However, the microporous structure (pore size < 2 nm) of activated carbon limits the transportation of the reactants and products through the pores. This results the formation of coke which plugs the pore of the support and finally deactivate the catalyst.[91] Also, activated carbons are impure in nature with l0-15% of ash content, depending on the nature of the precursor used.[92]

Carbon in the form of multi-walled carbon nanotubes (MWCNTs) is drawing attention as a new generation of catalyst support, due to their flexibility as support in tailoring the catalyst properties to specific needs.[93] The use of MWCNTs as catalyst support has been increasing for reactions involving hydrogen as a reactant or product, such as, hydrotreating of crude oil, Fischer-Tropsch, and alcohols synthesis.[94-96] These materials have inert graphitic surfaces and are resistant to acidic or basic media and display unique properties such as meso/macroporous structures that mitigate transport limitations; uniform, and straight pores that allow great metal dispersion; high mechanical strength; and thermal conductivity and can be highly purified.[97-98]

1.4.3. Catalyst preparation and pre-treatment conditions

In a heterogeneous chemical reaction, the activity and selectivity of products also depend on the selection of precursors and method of preparation of the catalyst. The selection of precursors has a direct impact on the cost and availability of the chemicals. The deposition the metals on the support play an important role in such a way that every metal atom is accessible to the reactants.[99] The catalysts for higher alcohols synthesis can be prepared by sequential pore volume impregnation or incipient wetness method. The MoS_2 catalytic species can be prepared from $(NH_4)_2MoS_4$ decomposition or by the reaction of ammonium hepta molybdate tetrahydrate (AHM), with aqueous ammonium sulfide or gaseous hydrogen sulfide.[100] MoS_2 prepared by sulfidation of MoO_3 were

found to be less selective towards the hydrocarbons compared to that made by the decomposition of an ammonium tetrathiomolybdate.[101]

The catalysts, synthesized in the form of a metal oxide, are subjected to a pre-treatment prior to higher alcohols synthesis. The sulfidation and reduction of the catalysts are carried out simultaneously at 450ºC and 3.44 MPa (500 psig) at a heating rate of 2ºC/min and holding for 6 h using gas mixture containing 10 mole% H_2S in H_2 and flow rate of 50 ml/min. The temperature, pressure, heating rate and pre-treatment gas environment can influence the surface area and the activity of the catalyst.[102]

1.4.4. Reaction mechanism for higher alcohol synthesis

Depending on the process conditions and catalyst used, alcohols are synthesized using iso-synthesis (a step-wise CO insertion reaction and a condensation reaction), variants of Fisher-Tropsch synthesis, oxo-synthesis (production of alcohols by the reaction of olefins with one molecule each of CO and H_2 and subsequent hydrogenation of the resulting aldehyde) involving the hydroformylation of olefins, and homologation of methanol and lower molecular weight alcohols to make higher alcohols. The products include primary and secondary alcohols of both normal and branched carbon chains. Other oxygenates such as esters, aldehydes, and ketones are also formed. The following are the chemical reactions involved in the synthesis of higher alcohols from synthesis gas:

$$CO + H_2 \leftrightarrow HCHO \quad (1.11)$$

$$CO + 2H_2 \leftrightarrow CH_3OH \quad (1.12)$$

$$CO + H_2O \leftrightarrow CO_2 + H_2 \quad (1.13)$$

$$CH_3OH + CO + 2H_2 \leftrightarrow CH_3CH_2OH + H_2O \quad (1.14)$$

$$C_nH_{2n+1}OH + CO + 2H_2 \leftrightarrow CH_3(CH_2)_nOH + H_2O \quad (1.15)$$

$$2CH_3OH \leftrightarrow CH_3CH_2OH + H_2O \quad (1.16)$$

$$3CH_3OH \leftrightarrow (CH_3)_2CO + 3H_2O \quad (1.17)$$

$$CH_3OH + CO \leftrightarrow CH_3CHO + H_2O \quad (1.18)$$

$$(CH_3)_2CO + H_2 \leftrightarrow (CH_3)_2CHOH + H_2O \quad (1.19)$$

$$2CH_3CHO \leftrightarrow CH_3COOCH_2CH_3 \quad (1.20)$$

Together with these reactions, undesired side reactions such as hydrocarbon formation may occur, especially that of methane.

$$CO + 3H_2 \leftrightarrow CH_4 + H_2O \quad (1.21)$$

The water gas shift reaction, eq. (1.13), is assumed to be in thermodynamic equilibrium. According to the reaction stoichometry the optimum H_2/CO ratio is 2; however, the simultaneous occurrence of water gas shift reaction means that the optimum ratio is closer to 1. As all the above reactions are exothermic reactions, from a thermodynamic point of view, lower temperatures and higher pressures are advantage for the formation of alcohols.

Santiesteban et al.[103] developed the reaction system for the production of mixed alcohols from syngas over alkali-modified MoS_2 catalysts based on CO insertion mechanism. This reaction scheme can be represented in terms of chain initiation, propagation and termination as follows:

Chain Initiation:

$$CO + s \leftrightarrow CO_S \quad (1.22)$$

$$H_2 + 2s \leftrightarrow 2H_S \quad (1.23)$$

$$CO_S + H_S \leftrightarrow CHO_S + s \quad (1.24)$$

$$CHO_S + H_S \leftrightarrow CH_2O_S + s \quad (1.25)$$

$$CH_2O_S + H_S \leftrightarrow R_1O_S + s \quad (1.26)$$

Chain Propagation:

$$R_iO_S + CO_S \rightarrow R_iCOO_S + s \quad (1.27)$$

$$R_iO_S + 2H_S \rightarrow R_{iS} + H_2O + 2s \quad (1.28)$$

$$R_{iS} + CO_S \rightarrow R_iCO_S + s \quad (1.29)$$

$$R_iCO_S + 2H_S \rightarrow R_{i+1}O_S + 2s \quad (1.30)$$

Chain Termination:

$$R_iO_S + H_S \leftrightarrow R_iOH + 2s \quad (1.31)$$

$$R_iCOO_S + H_S \rightarrow R_iCOOR_{i-1} + 2s \quad (1.32)$$

$$R_{iS} + H_S \rightarrow C_iH_{2i+2} + 2s \quad (1.33)$$

$$R_{iS} \rightarrow C_iH_{2i} + H_S \quad (1.34)$$

where *s* represents the active site of the catalyst.

Reactions represented by eqs. (1.22) to (1.26) are assumed to be in equilibrium. R indicates an alkyl group, i.e., $R_i = C_iH_{2i+1}$. Alcohols are formed by hydrogenation of their precursors R_iO_S, hydrocarbons from R_{iS} and esters from R_iCOO_S by CO insertion and hydrogenation. Together with the above reactions, water gas shift reaction also takes place as given by eq. (1.13).

1.5. Knowledge gap

Based on the literature review, the knowledge gaps in the synthesis of higher alcohols from synthesis gas are identified as follows:

1. There is no open literature on the sulfided trimetallic Co-Rh-Mo catalysts supported on MWCNTs for higher alcohols synthesis from synthesis gas.
2. The promotional effect of alkali on the conversion of synthesis gas over MoS_2 catalysts to produce higher alcohols is not thoroughly understood.
3. The effects of textural properties of the support on the higher alcohols synthesis from CO hydrogenation are not understood.
4. Many researchers have studied the effects of operating conditions as independent variables on the % CO conversion, space time yield (STY) of alcohols, hydrocarbons, and CO_2. However, the interaction effects of operating conditions were not investigated and no model was developed to correlate %CO conversion, STY of products, and selectivity of alcohols with operating conditions in CO hydrogenation reactions.
5. No report is available in literature on the kinetic development of the alkali-modified trimetallic Co-Rh-Mo catalysts in terms of higher alcohols synthesis from synthesis gas.
6. The deactivation behaviour of alkali-promoted MoS_2 catalysts during the induction period in terms of higher alcohols synthesis is not clearly understood.

1.6. Hypothesis

1. Due to a strong interaction of Co species with Mo component, the presence of Co in alkali-modified MoS_2 catalysts enhances the $C_1 \rightarrow C_2$ homologation step that will lead to ethanol as the dominant product.
2. Rhodium species in catalysts are capable of catalyzing dissociation, insertion, and hydrogenation of CO to improve the formation of alcohols depending upon the status of the rhodium species, properties of alkali promoters, and supports as well as reaction conditions.
3. The mesoporous structures of MWCNTs support can mitigate transport limitations and facilitate ease of reduction, as well as uniform metal particle distribution providing high metal dispersion.

1.7. Research objectives

The main objective of the research is to develop a catalyst system that is capable of selectively producing higher alcohols, particularly ethyl alcohol from synthesis gas (containing predominantly carbon monoxide and hydrogen). While a number of catalysts have been developed for this purpose, none are used commercially at this time. The key to development of a commercially attractive higher alcohols production scheme from synthesis gas is to discover a highly efficient catalyst, which must be highly active and stable with suitable reaction conditions during the production period so that high yields of ethyl alcohol can be obtained with high single pass CO conversion. In addition, the catalyst must also be highly selective toward ethyl alcohol to yield a high purity alcohol phase so that separation of unwanted by-products can be avoided.

The main objective was achieved by carefully planning experiments and executing them into different sub-objectives as follows:

1. To study the interaction effect of different group VIII metals (Co, Ni and Rh) with alkali-modified MoS_2 catalysts and to compare the alumina and activated carbon supports for higher alcohol synthesis from CO hydrogenation.

2. To study the effects of active metal (Mo) and alkali promoter (K) and to optimize the Mo and K loadings supported on MWCNTs on the catalytic conversion of synthesis gas to higher alcohols.
3. To study the effect of Co metal promoter on K-Mo/MWCNTs catalysts towards higher alcohols synthesis from synthesis gas.
4. To study the promotional effects of different metal loadings of Rh on K-Mo/MWCNTs catalysts for the formation of higher alcohols from synthesis gas.
5. To study the effect of Co on K-modifed bimetallic Mo and Rh catalysts and to compare the supports, MWCNTs and activated carbon on higher alcohols synthesis reaction.
6. To emphasize the improved performance of molybdenum-sulfided catalysts due to the addition of alkali and metal promoters on modification of surface structure and oxidation states.
7. To study the influence of textural properties of the support on the higher alcohols synthesis using different types of activated carbon-supported K-modified trimetallic Co-Rh-Mo catalysts that are impregnated with best alkali and metal contents. These results are compared with the MWCNT-supported catalyst.
8. To study the interaction effects of operating conditions such as, temperature, pressure, GHSV on higher alcohols synthesis using the best performed catalyst and to develop models to correlate % CO conversion, STY of products, and selectivity of alcohols with operating conditions. It is also aimed to optimize the operating conditions to obtain maximum ethanol STY and selectivity.
9. To develop the intrinsic kinetics of higher alcohol synthesis reaction using best performed catalyst.
10. To study the long term deactivation of the best performed catalyst supported on MWCNTs and activated carbon using the optimum operating conditions.

1.8. Organization of the Thesis

This Ph.D. thesis is organized according to the guidelines for manuscript-based thesis of University of Saskatchewan. This means that in place of presenting raw data and analyzing it for the first time in a uniform manner throughout the thesis, it is presented as a series of journal manuscripts. The bulk of the thesis consists of a series of literary publications of the research that were compiled over the course of the project. These manuscripts were written and submitted for publication as each stage of the Ph.D. project was completed. The manuscripts presented in Chapters 3, 4, 5, 6, and 10 have all been published (or are accepted for publication and in press) in peer-reviewed journals. The manuscripts of the remaining chapters have been submitted for review. In each manuscript-based chapter, two issues are discussed in addition to the manuscript itself. These are the contribution of the Ph.D. candidate and the contribution of the paper to the overall study. Chapters 1 and 12 are original text in this thesis included to introduce the subject matter and discuss the outcome of the project. The relevant literature review and reference list are presented in each chapter, with any useful supplementary material given in the Appendices.

1.9. Manuscript Content of the Thesis

The specific topic of each chapter and the way in which it addresses the overall objectives of the thesis are detailed below. The use of a manuscript-based thesis results in some overlap of material between chapters.

The catalyst activity and selectivity of CO hydrogenation reactions were influenced by type of catalyst, presence of promoter, nature of support, metal loading and dispersion, as well as, preparation method. It has been known that the promotion of group VIII metals, such as Co, Ni and Rh, to alkali-modified MoS_2 catalysts improved the activity and selectivity of higher alcohols synthesis due to the formation of new phases and improving the dispersion of catalytic species. Therefore, in the first part of my research program, various alkali-modified monometallic, bimetallic, trimetallic and tetrametallic catalysts that contain Co, Ni, Rh and Mo metals were prepared using the incipient wetness impregnation method and the catalysts were extensively characterized using various analytical techniques to understand the physico-chemical characteristics.

The catalytic performance of higher alcohol synthesis is carried out under identical experimental conditions using the prepared catalysts. Also, the comparative performance of alumina and activated carbon (AC) as supports to various metals promoted alkali-modified MoS_2 catalysts are evaluated under identical experimental conditions. The results are discussed in Chapter 2 and this work serves as preliminary experimental studies to understand the interaction effect of between the metal promoters (Co, Ni, and Rh) and Mo component as well as, the role of supports, alumina and AC on higher alcohols synthesis.

MWCNTs are new generation of carbon base supports with unique properties such as, inert graphite surface which is capable of hosting hydroxyl and carboxyl functional groups that are necessary for catalyst metal loading. Due to various advantages of MWCNTs as supports compared to other supports, commercially available MWCNT-supported molybdenum based catalysts promoted with potassium were prepared by sequential pore volume impregnation and extensively characterized. The metal (Mo) and promoter (K) contents of the catalysts were optimized for the synthesis of higher alcohols from synthesis gas. The effect of reaction conditions such as temperature and pressure on the catalytic performance was also studied using the best performed catalyst. The details of this study are described in Chapter 3.

The addition of metal promoter, Co to alkali-modified molybdenum sulfide catalysts could enhance the activity and selectivity of higher alcohols, due to their strong abilities of hydrogenation and promotion of carbon chain growth. In Chapter 4, the effect of various loadings of Co on alkali-modified molybdenum-based catalysts supported on MWCNTs was studied towards the higher alcohols synthesis. The best performed Mo and K contents were selected based on the catalytic studies performed in Chapter 3. The best performed catalyst was selected to study the effect of temperature and pressure on the higher alcohols synthesis.

Incorporation of rhodium to the alkali-modified molybdenum-sulfided catalysts significantly modifies the coordination status of the molybdenum atoms in the catalysts and significantly improves the activity and the selectivity towards the formation of oxygenates. Most of the studies reported in the literature are mainly concerned about the oxide form of the Rh-Mo catalysts. It is expected that sulfide form of Mo based catalysts

promoted with Rh metals show better activity and selectivity towards higher alcohols compared to oxide form. Hence, in Chapter 5, a series of Rh promoted alkali-modified molybdenum-based catalysts supported on MWCNTs were prepared by sequential pore volume impregnation. Similar contents of Mo and K as that of Chapter 4 were selected. The prepared catalysts were characterized using different techniques in oxide and sulfide states and the catalytic performance studies were conducted under the similar conditions as that of Chapter 4.

The alkali-modified trimetallic Co-Rh-Mo catalyst system is attractive to reduce Rh content and to increase the activity and selectivity of the catalyst for the formation of higher alcohols, especially ethanol. Chapter 6 aims to study the effect of Co on K-promoted bimetallic Mo and Rh catalysts, the effect of supports, MWCNTs, and AC on higher alcohols synthesis reactions, and the influence of reaction conditions such as temperature and pressure on catalytic performance. The optimum content of Rh was selected based on catalytic performance studies conducted in Chapter 5 and similar contents of Mo and K were used as reported in Chapters 3 to 5.

In Chapters 4 to 6, it was demonstrated that the addition of Co and Rh metal promoters to alkali-modified MoS_2 catalysts supported on MWCNTs display improved catalytic performance towards higher alcohols formation from synthesis gas. The presence of alkali is essential to shift the CO hydrogenation reaction from hydrocarbon formation to higher alcohols, but the promotional effect of alkali on MoS_2 catalysts are not thoroughly understood. The addition of promoters may modify the chemical environment, symmetry, and location of the molybdenum in the supported catalysts. Since these factors exert a strong effect on reactivity, knowledge of the chemical and electronic structure of Mo and S species is important. Chapter 7 aims to emphasize the improved performance of molybdenum-sulfided catalysts due to the addition of alkali and metal promoters on modification of surface structure and oxidation states using the S K-edge and Mo L_3-edge X-ray absorption near-edge structures (XANES).

The textural properties of the support, such as average pore diameter, pore volume and surface area, could significantly influence the extent of reduction, morphology, adsorption and activity/selectivity properties of the active phase, especially in well-dispersed catalysts. The effects of pore size and surface area of activated carbon

support on the catalytic performance of higher alcohols synthesis from synthesis gas have not been elucidated yet. The goal of Chapter 8 is to study the influence of the porous characteristics of commercially available activated carbons on the physico-chemical properties of the catalyst, as well as, the performance of higher alcohols synthesis from synthesis gas using alkali promoted trimetallic Co-Rh-Mo sulfided catalysts supported on activated carbon. The higher alcohols synthesis reaction was also performed under similar reaction conditions using the Co-Rh-Mo-K/MWCNTs catalyst for comparing the MWCNTs support with that of different activated carbons.

The activity and selectivity of the higher alcohols synthesis from catalytic conversion of synthesis gas has a direct effect on the operating conditions such as reaction temperatures, total pressures, GHSV, and H_2 to CO molar feed ratios. The effects of operating conditions as independent variables on the % CO conversion, STY of alcohols, hydrocarbons and CO_2 have been studied[21-23], but their interaction effects have not been investigated and no model has been developed to correlate STY and selectivity of alcohols with operating conditions in CO hydrogenation reactions. Therefore, a part of my Ph.D. research plan was allocated to develop models that correlate the interaction effects of temperature, pressure, and GHSV with that of % CO conversion, STY of alcohols, hydrocarbons and CO_2, as well as selectivity of alcohols in CO hydrogenation reactions using the H_2 to CO molar ratio of 1, using higher alcohols synthesis from synthesis gas over the sulfided K-modified Co-Rh-Mo MWCNT-supported catalyst. The study also aims to optimize the operating conditions to obtain maximum ethanol selectivity. The outcome of this study is discussed in Chapter 9.

It is important to investigate the intrinsic kinetic data in developing a new catalyst system to measure the rate parameters for reactor design based on the catalytic performance using the best performed catalyst. The sulfided alkali-modified trimetallic Co-Rh-Mo catalysts supported on MWCNTs outperformed in terms of higher alcohols activity and selectivity with potential industrial application. Chapter 10 describes the statistical design approach to develop the intrinsic kinetics for higher alcohols synthesis from synthesis gas. The first part of this work deals with the effects of mass transfer diffusions followed by intrinsic kinetic calculations of higher alcohols reactions from synthesis gas.

The key to development of a commercially attractive higher alcohols production scheme from synthesis gas is to discover a highly efficient catalyst that is highly active and stable with suitable reaction conditions during the production period. However, very few publications have focused on the deactivation behaviour of alkali promoted MoS_2 catalysts. In order to understand the decay of activity of the catalyst towards CO hydrogenation and higher alcohols synthesis, it is important to study in detail the contribution of each deactivating feature on the total catalyst deactivation. Chapter 11 investigates the stability of sulfided alkali-modified Co-Rh-Mo catalysts that are supported on MWCNT and activated carbon, during continuous higher alcohols synthesis for 720 h in a fixed-bed micro reactor.

Chapter 12 gives the general discussion and overall conclusions on the catalyst development, different characterization techniques, optimization of process conditions, intrinsic reaction kinetics development and long term deactivation studies of the catalyst for higher alcohols synthesis. Finally, the scope for future work is also discussed in this chapter. The research outcome in the form of publications, conference presentations and patent is given as Appendix A. During the early stage of my Ph.D. studies, a fixed-bed reactor was designed and built. The experimental calibrations of temperature of this reactor and mass flow controllers are given in Appendix B. The example of mass balance data is given as Appendix C and mass transfer calculations are shown as Appendix D. It should be noted that a relevant literature review and reference list are provided at the end of each chapter.

1.10. Error of Experimental Data

It is essential to address the imbedded errors for each analysis as most of the data in the thesis is obtained from experimental results. Table 1.10 shows the error of experimental data together with the number of samples corresponding to each analysis. The errors are calculated in the form of average absolute deviation (± AAD), which are calculated as follows:

If an analysis includes n measurements:

$$X = x_1, x_2, x_3, ...x_N \quad \text{.....(1.35)}$$

$$m(X) = \frac{1}{N}\sum_{i=1}^{N} x_i \quad \text{.....(1.36)}$$

$$AAD = \frac{1}{N}\sum_{i=1}^{N}(x_i - m(X)) \quad \text{.....(1.37)}$$

where, $m(X)$ is the mean value of experimental result, x

N is the total number of samples

Table 1.10. The error of experimental data and number of samples corresponding to each analysis

Analysis	Chapter	Number of sampling	Uncertainty
N_2 adsorption (BET analysis)	2-8 and 11	4	± 5 m^2/g
N_2 adsorption (Pore volume)	2-8 and 11	4	± 0.03 m^3/g
N_2 adsorption (pore diameter)	2-8 and 11	4	± 1 nm
TPR (reduction peak temperature)	2-6 and 11	3	± 4^oC
TEM	2-6, 8, and 11	10 images	± 1 nm
ICP-MS (% Metal content)	2-6, 8, and 11	3	± 0.5
XRD (Particle size)	3-7	2	± 2 nm
Chemisorption (% dispersion)	3-6, 8, and 11	3	± 3
Mass balance for carbon (HAS)	3-7	3	± 2
Mass balance for hydrogen (HAS)	3-7	3	± 4
Mass balance for oxygen (HAS)	2	3	± 4%
Over-all mass balance (HAS)	2	5	± 3%

1.11. Nomenclature

$m(X)$	mean value
N	Total number of samples
x_i	Experimental result

1.12. Abbreviations

AAD	Average absolute deviation
AC	Activated carbon
AHM	Ammonium hepta molybdate
ATR	Auto temperature reforming
BFB	Bubbling fluidized bed
BTX	Benzene, Toluene, Xylene
CFB	Circulating fluidized bed
CV	Calorific value
EPA	Environmental protection agency
GHG	Greenhouse gas
GHSV	Gas hourly space velocity
HAS	Higher alcohol synthesis
HTU	Hydro thermal upgrading
HV	Heating value
MON	Motor Octane Number
MSW	Municipal solid waste
MTBE	Methyl tertiary butyl ethers
MWCNTs	Multi-walled carbon nanotubes
RON	Research Octane Number
RVP	Reid vapour pressure
STY	Space time yield
TPF	Timber Productive Forest
WGS	Water-gas-shift
XANES	X-ray absorption near-edge structures

1.13. References

1. Energy Information Administration, *International Energy Outlook*, 2002, web site www.eia.doe.gov/oiaf/ieo/index.html.
2. Renewable Energy Policy Network for the 21st Century, *Renewables 2007, Global Status Report*, 2008, website www.ren21.net.
3. Boman, C.; Nordin, A.; Boström, D.; Öhman, M. Characterization of inorganic particulate matter from residential combustion of pelletized biomass fuels. *Energ. Fuel* **2004**, *1*, 338–348.
4. Canadian Bioenergy Association, *Biomass sources for bioenergy use in Canada*, 2004, website www.canbio.ca.
5. Wood, S. M.; Layzell, D. B. *A Canadian Biomass Inventory: Feedstocks for a Bio-based Economy*, BIOCAP Canada Foundation, 2003, website http://www.biocap.ca.
6. Bradley, D. *Canada Biomass-Bioenergy Report*, Climate Change Solutions, 2006, website www.climatechangesolutions.net.
7. Müller, A. *A review of the current state of bioenergy development in G8 +5 countries*, Global Bioenergy Partnership, 2007, website www.globalbioenergy.org.
8. Ranganathan, R. *Biomass residue conversion could energize northern economy*, Technology, website www.src.sk.ca/images/Ranganathan_Feb042.pdf.
9. Schumacher, L. Carbon, Greenhouse Gas and Biomass Logistics, website www.ncfap.org/documents/biofuels_aviation/Leon Schumacher - Feedstock Logistics.pdf

10. Jannasch, R. *Report on Bioenergy Research Program*, Resource Efficient Agricultural Production Winter 2001 Newsletter, 2001, website www.reap-canada.com.

11. Ciferno, J. P.; Marano, J. J. *Benchmarking Biomass Gasification Technologies for Fuels, Chemicals and Hydrogen Production*, U.S. Department of Energy, National Energy Technology Laboratory, 2002.

12. Klass, D. L. Biomass for renewable energy and fuels chemicals. *Encyclopedia of Energy* **2004**, *1*, 193-212.

13. Layzell, D. B.; Mitchell, H. *Climate Change and the Biosphere1 Option: Moving to a Sustainable Future*, BIOCAP Canada, (2000), website www.globalcarbonproject.org.

14. McKendry, P. Energy production from biomass (part 2): conversion technologies, *Bioresource Technol.* **2002**, *83*, 47–54.

15. Friends of the earth, *Briefing pyrolysis and gasification*, 2009, web site www.foe.co.uk/resource/briefings/gasification_pyrolysis.pdf.

16. Franco, C.; Pinto, F.; Gulyurtlu, I.; Cabrita, I. The study of reactions influencing the biomass steam gasification process. *Fuel* **2003**, *82*, 835–842.

17. Kuester, J. L. Conversion of guayule residues into fuel energy products. *Bioresource Technol.* **1991**, *35*, 217-222.

18. Sieger, R.; Brady, P. *Thermal Oxidation of Sewage Solids*: *White Paper on Bio-gasification and Other Conversion Technologies*, Water Environment Federation, Residuals and Biosolids Committee, 2003.

19. McKendry, P. Energy production from biomass (part 3): gasification technologies. *Bioresource Technol.* **2002**, *83*, 55–63.

20. Mueller-Langer, F.; Tzimas, E.; Kaltschmitt, M.; Peteves, S. Techno-economic assessment of hydrogen production processes for the hydrogen economy for the short and medium term. *Int. J. Hydrogen Energ.* **2007**, *32*, 3797-3810.

21. Robinson, A. L.; Rhodes, J. S.; Keith, D. W. Assessment of Potential Carbon Dioxide Reductions Due to Biomass−Coal Cofiring in the United States. *Environ. Sci. Technol.* **2003**, *37*, 5081–5089.

22. Ptasinski, K. J.; Prins, M. J.; Pierik, A. Exergetic evaluation of biomass gasification. *Energy* **2007**, *32*, 568-574.

23. Turn, S.Q., Biomass integrated gasifier combined cycle technology: Application in the cane sugar industry. *Int. Sugar Jnl.* **1999**, *101*, 267-272.

24. Energy efficiency and Renewable energy, *Renewable Energy Technology Characterizations*, U. S. Department of Energy, 1997.

25. Bain, R. L. *An Introduction to Biomass Thermo-chemical Conversion*, Biomass and Solar Energy Workshops, National renewable Energy Laboratory, 2004.

26. Agarwal, A. K., Biofuels (alcohols and biodiesel) applications as fuels for internal combustion engines. *Prog. Energ. Combust. Sci.* **2007**, *33*, 233-271.

27. Entenberg, R. D.; Menard, Jr, A. L. Future octane number requirements for future market demand. *J. Marketing*, **1966**, *30*, 28-32.

28. Marin, A.; Kodjak, D. *Relative cancer risk of reformulated gasoline and conventional gasoline sold in the Northeast*, Northeast States for Coordinated Air Use Management, 1998.

29. Grimshaw, P. *Octane Solutions for Older Volvos*, The Gothenburg Bible & Volvo Performance Handbook, 1995.

30. Meyers, R. *A. Green Gasoline, Handbook of Petroleum Refining*, Vol. 3, McGraw Hill: USA, 2003.

31. Smith, J. L.; Workman J. P. *Alcohol for motor fuels*, Farrum and Ranch series no. 5010, 1992.

32. Duncan Seddon & Associates Pty Ltd., Octane enhancing petrol additives/products, 2000, website www.environment.gov.au.

33. Consult, B., *Alcohols/ethers as oxygenates in diesel fuel: Properties of blended fuels and evaluation of practical experiences*, Trans Energy Consulting Ltd., 2005, web site www.iea-amf.vtt.fi.

34. Hansen, A. C; Zhang, Q.; and Peter, W. L. Ethanol–diesel fuel blends — a review. *Bioresource Technol.* **2005**, *96*, 277-285.

35. Sprockett, D. *Alcohol and power equipment - using unleaded gas in lawn mowers*, Flower & Garden Magazine, 1993.

36. Brink, A.; Jordaan, C. F. P.; le Roux, J. H.; Loubser, N. H. Carburetor corrosion: the effect of alcohol–petrol blends. In: *Proceedings of the VII International Symposium on Alcohol Fuels Technology*, Paris, France, 1986.

37. Fisher, M. R. *Vehicle Conversion and Methanol Fuel Program 1980-82*, Bank of America, 1983.

38. Smith, C. H.; Fang, J.; Powders, M.; Aabakken , J., *Issues associated with the use of higher ethanol blends (E17 - E24)*, National Renewable Energy Laboratory, 2002, web site www.nrel.gov.

39. Yüksel, F.; Yüksel, B. The use of ethanol–gasoline blend as a fuel in an SI engine. *Renew. Energ.* **2004**, *29*, 1181-1191.

40. Curtis, T. T.; Lamb, G. D.; Abraham, W. D. *Synthetic diesel engine lubricants containing dispersant-viscosity modifier and functionalized phenol detergent*. U.S. Patent 6,331,510, Dec 18, 2001.

41. Mathewson, S. W. *The Manual for the Home and Farm Production of Alcohol Fuel*, Ten Speed Press, USA, 1980.

42. Lodgsdon, J. E. Ethanol. *Encyclopedia of Chemical Technology* **1994,** *9 (ed. 4)*, 812–860.

43. Kumar, A.; Jones, D. D.; Hanna, M. A. Thermochemical biomass gasification: A review of the current status of the technology. *Energies* **2009**, *2*, 556-581.

44. Anderson, R. B. *The Fischer-Tropsch Synthesis*, Academic Press Inc., Orlando, 1984.

45. Mahdavi, V.; Peyrovi, M. H.; Synthesis of C_1–C_6 alcohols over copper/cobalt catalysts: Investigation of the influence of preparative procedures on the activity and selectivity of Cu–Co_2O_3/ZnO-Al_2O_3 catalyst. *Catal. Commun.* **2006**, *7*, 542-549.

46. McCutchen, M. S. Synthesis of higher alcohols from carbon monoxide and hydrogen in a slurry reaction, Ph.D. Dissertation, North Carolina State University, Raleigh, NC, 1992.

47. Doan, P. T. Characterization of Cu-Co-Cr-K catalysts, M.Sc. Dissertation, Mississippi State University, Starkville, MI, 2001.

48. Iranmahboob, J. Formation of ethanol and higher alcohols from syngas, Ph.D. Dissertation, Mississippi State University, Starkville, MI, 1999.

49. Natta, G.; Colombo, U.; Pasquon, I. *Direct Catalytic Synthesis of Higher Alcohols from Carbon Monoxide and Hydrogen* Catalysis, Vol. 5, (Emmett, P. H. Ed.), Reinhold: New York, 1957, p. 131-174.

50. Campos-Martin, J. M.; Fierro, J. L.; Guerrero-Ruiz. A.; Herman, R. G.; Klier, K. Promoter Effect of Cesium on C–C Bond Formation during Alcohol Synthesis from CO/H_2over $Cu/ZnO/Cr_2O_3$Catalysts. *J. Catal.* **1996**, *163*, 418-428.

51. Hoflund, G. B.; Epling, W. S.; Minahan, D. M. Higher alcohol synthesis reaction study using K-promoted ZnO catalysts. III. *Catal. Letters* **1997**, *45*, 135-138.

52. Minahan, D. M.; Epling, W. S.; and Hoflund, G. B.; Higher-alcohol synthesis reaction study V. Effect of excess ZnO on catalyst performance. *Appl. Catal., A* **1998**, *166*, 375-385.

53. Forzatti, P.; Tronconi, E.; Pasquon, I. Higher Alcohol Synthesis. *Catal. Rev. - Sci. Eng.* **1991**, *33*, 109-168.

54. Tronconi, E.; Ferlazzo, N.; Forzatti, P.; Pasquon, I. Synthesis of alcohols from carbon oxides and hydrogen. 4. Lumped kinetics for the higher alcohol synthesis over a zinc-chromium-potassium oxide catalyst. *Ind. Eng. Chem. Res.* **1987**, *26*, 2122-2129.

55. Smith, K. J.; Anderson, R. B. The higher alcohol synthesis over promoted Cu/ZnO catalysts. *Can. J. Chem. Eng.* **1983**, *61*, 40-45.

56. Smith, K. J.; Anderson, R.B. A chain growth scheme for the higher alcohols synthesis. *J. Catal.* **1983**, *85*, 428-436.

57. Tronconi, E.; Lietti, L.; Forzatti, P.; Pasquon, I. Higher Alcohol Synthesis over Alkali Metal-Promoted High- Temperature Methanol Catalysts. *Appl. Catal.* **1989**, *47*, 317-333.

58. Beretta, A.; Sun, Q.; Herman, R. G.; Klier, K. Production of Methanol and Isobutyl Alcohol Mixtures over Double-Bed Cesium-Promoted Cu/ZnO/Cr_2O_3 and ZnO/Cr_2O_3 Catalysts. *Ind. Eng. Chem. Res.* **1996**, *35*, 1534-1542.

59. Xiaoding, X.; Doesburg, E. B. M.; Scholten, J. J. F. Synthesis of higher alcohols from syngas - recently patented catalysts and tentative ideas on the mechanism. *Catal. Today* **1987**, *2*, 125-170.

60. Fornasari, G.; Huysser, A. D.; Mintchev, L.; Trifiro, F.; Vaccari, A. Cobalt-modified Cu---Zn---Cr catalysts in the synthesis of methanol. *J. Catal.* **1992**, *135*, 386-399.

61. Figueiredoa, R. T.; Granados, M. L.; Fierro, J. L. G.; Vigas, L.; Ramirez de la, P.; Homs, N. Preparation of alumina-supported CuCo catalysts from cyanide complexes and their performance in CO hydrogenation. *Appl. Catal., A* **1998**, *170*, 145-157.

62. Zhao, N.; Xu, R.; Wei, W.; Sun, Y. Cu/Mn/ZrO_2 catalyst for alcohol synthesis by Fischer-Tropsch modified elements. *React. Kinet. Catal. Lett.* **2002**, *75*, 297-304.

63. Xu, R.; Yang, C.; Wei, W.; Li, W.; Sun, Y.; Hu, T. Fe-modified CuMnZrO_2 catalysts for higher alcohols synthesis from syngas. *J. Mol. Catal. A: Chem.* **2004**, *221*, 51-58.

64. Mahdavi, V., Peyrovi, M.H., Islami, M., Yegane J. M., Synthesis of higher alcohols from syngas over Cu-Co_2O_3/ZnO, Al_2O_3 catalyst. *Appl. Catal., A* **2005**, *281*, 259-265.

65. Sachtler, W. M. H.; Ichikawa, M. Catalytic site requirements for elementary steps in syngas conversion to oxygenates over promoted rhodium. *J. Phys. Chem.* **1986**, *90*, 4752-4758.

66. Guglielminotti, E.; Pinna, F.; Rigoni, M.; Strukul, G.; Zanderighi, L. The effect of iron on the activity and the selectivity of Rh/ZrO_2 catalysts in the CO hydrogenation. *J. Mol. Catal. A: Chem.* **1995**, *103*, 105-116.

67. Mills, G. A. *Summary of the Higher Alcohol synthesis workshop*, B. R. Service Corporation, 1992.

68. Tatsumi, T.; Muramatsu, A.; Yokota, K.; Tominga, H. Mechanistic study on the alcohol synthesis over molybdenum catalysts: Addition of probe molecules to CO---H_2. *J. Catal.* **1989**, *115*, 388-398.

69. Woo, H. C.; Park, K. Y.; Kim, Y. G.; Namau, I.-S.; Chung, J. S.; Lee, J. S. Mixed alcohol synthesis from carbon monoxide and dihydrogen over potassium-promoted molybdenum carbide catalysts. *Appl. Catal.* **1991**, *75*, 267-280.

70. Smith, K. J.; Herman R. G.; Klier, K. Kinetic modelling of higher alcohol synthesis over alkali-promoted Cu/ZnO and MoS_2 catalysts. *Chem. Eng. Sci.* **1990**, *45*, 2639-2646.

71. Liu, Z. Y.; Li, X. G.; Close, M. R.; Kugler, E. L.; Petersen, J. L.; Dadyburjor, D. B.; screening of alkali-promoted vapor-phase-synthesized molybdenum sulfide

catalysts for the production of alcohols from synthesis gas. *Ind. Eng. Chem. Res.* **1997**, *36*, 3085-3093.

72. Lu, G.; Zhang, C.F.; Chang, Y.; Zhu, Z.; Ni, Y.; Cheng, L.; Yu, F. Synthesis of mixed alcohols from CO_2 contained syngas on supported molybdenum sulfide catalysts. *Appl. Catal.* **1997**, *150*, 243-252.

73. Santiesteban, J. G.; Bogdan, C. E.; Herman, R. G.; Klier, K. Mechanism of C1-C4 alcohol synthesis over alkali/MoS2 and alkali/Co/MoS2 catalysts. In *Proc. 9th Intern. Congr. Catal.;* Phillips, M. J., Ternan, M., Eds.; The Chemical Institute of Canada: Ottawa, 1988; Vol. 2, p 561.

74. Tatsumi, T.; Muramatsu, A.; Fukunaga, T.; Tominaga, H. Nickel promoted molybdenum catalysts for synthesis of mixed alcohols. In *Proc. 9th Intern. Congr. Catal.*; Phillips, M. J., Ternan, M., Eds.; The Chemical Institute of Canada: Ottawa, 1988; Vol. 2, p 618.

75. Qi, H.; Li, D.; Yang, C.; Ma, Y.; Li, W.; Sun, Y.; Zhong, B. Nickel and manganese co-modified K/MoS2 catalyst: high performance for higher alcohols synthesis from CO hydrogenation. *Catal. Commun.* **2003**, *4*, 339–342.

76. Iranmahboob, J.; Toghiani, H.; Hill, D. O. Dispersion of alkali on the surface of Co-MoS2/clay catalyst: a comparison of K and Cs as a promoter for synthesis of alcohol. *Appl. Catal., A* **2003**, *247*, 207–218.

77. Iranmahboob, J.; Hill, D. O.; Toghiani H. K_2CO_3/Co-MoS_2/clay catalyst for synthesis of alcohol: influence of potassium and cobalt. *Appl. Catal., A* **2003**, *231*, 99-108.

78. Gang, L.; Zhang, C. F.; Chang, Y.; Zhu, Z.; Ni, Y.; Cheng, L.; Yu, F. Synthesis of mixed alcohols from CO2 contained syngas on supported molybdenum sulfide catalysts. *Appl. Catal., A* **1997**, *150*, 243–252.

79. Bian, G.-Z.; Fu, Y.-L.; Ma, Y.-S. Structure of Co–K–Mo/γ-Al_2O_3 catalysts and their catalytic activity for mixed alcohols synthesis. *Catal. Today* **1999**, *51*, 187-193.

80. Li, X.; Feng, L.; Zhang, L.; Dadyburjor, D. B.; Kugler, E. L. Alcohol synthesis over pre-reduced activated carbon-supported molybdenum-based catalysts. *Molecules* **2003**, *8*, 13–30.

81. DeCanio, E. C.; Storm, D. A. Carbon monoxide adsorption by K/Co/Rh/Mo/Al_2O_3 higher alcohols catalysts. *J. Catal.* **1991**, *132*, 375-387.

82. Sudhakar, C.; Bhore, N. A.; Bischoff, K. B.; Manogue, W. H.; Mills, G. A. Molybdena enhanced Rh/Al2O3 catalysts. In *Proc. of the 10th Meeting of the Catalysis Society of North America*, San Diego, CA, 1987.

83. Foley, H. C.; Hong, A. J.; Allard, L. F.; Garratt-Reed, A. J. Bimetallic catalysts comprised of dissimilar metals for the reduction of carbon monoxide with hydrogen. *Appl. Catal.* **1990**, *61*, 351-375.

84. Li, Z.-R.; Fu, Y.-L.; Jiang, M. Structures and performance of Rh-Mo-K/Al_2O_3 catalysts used for mixed alcohol synthesis from synthesis gas. *Appl. Catal., A* **1999**, *187*, 187–198.

85. Kohl, A.; Linsmeier, C.; Taglauer, E.; Knozinger, H. Influence of support and promotor on the catalytic activity of Rh/VO_x/SiO_2 model catalysts. *Phys. Chem. Chem. Phys.* **2001**, *3*, 4639–4643.

86. Wang, Y.; Li, J.; Mi, W. Probing study of Rh catalysts on different supports in CO hydrogenation. *React. Kinet. Catal. Lett.* **2002**, *76*, 141–150.

87. Zurita, M. J. P.; Cifarelli, M.; Cubeiro, M. L.; Goldwasser, J. A. M.;Pietri, E.; Garcia, L.; Aboukais, A.; Lamonier, J.-F. Palladium-based catalysts for the synthesis of alcohols. *J. Mol. Catal. A: Chem.* **2003**, *206*, 339–351.

88. Kim, D. S.; Wachs, I. E.; Segawa, K. Molecular structures and reactivity of supported molybdenum oxide catalysts. *J. Catal.* **1994**, *149*, 268–277.

89. Duchet, J. C.; van Oers, E. M.; de Beer, V. H. J.; Prins, R. Carbon supported sulfide catalysts. *J. Catal.* **1983**, *80*, 386–402.

90. Concha, B. E.; Bartholomew, G. L.; Bartholomew, C. H. CO hydrogenation on supported molybdenum catalysts: Effects of support on specific activities of reduced and sulfided catalysts. *J. Catal.* **1984**, *89*, 536–541.

91. Zaman, M.; Khodadi, A.; Mortazavi, Y. Fischer-Tropsch synthesis over cobalt dispersed on carbon nanotubes-based supports and activated carbon. *Fuel Process. Technol.* **2009**, *90*, 1214–1219.

92. Rodriquez-Reinoso, F. The role of carbon materials in heterogeneous catalysis. *Carbon* **1998**, *36*, 159–175.

93. Pan, X.; Fan, Z.; Chen, W.; Ding, Y.; Luo, H.; Bao, X. Enhanced ethanol production inside carbon-nanotube reactors containing catalytic particles. *Nat. Mater.* **2007**, *6*, 507–511.

94. Sigurdsona, S.; Sundaramurthya, V.; Dalaia, A. K. Adjaye, J. Effect of anodic alumina pore diameter variation on template-initiated synthesis of carbon nanotube catalyst supports. *J. Mol. Catal. A: Chem.* **2009**, *306*, 23-32.

95. Tavasoli, A.; Abbaslou, R. M. M.; Trepanier, M.; Dalai, A. K. Fischer–Tropsch synthesis over cobalt catalyst supported on carbon nanotubes in a slurry reactor. *Appl. Catal., A* **2008**, *345*, 134-142.

96. Ma, X-M.; Lin, G.-D.; Zhang, H.-B. Co-decorated carbon nanotube-supported Co–Mo–K sulfide catalyst for higher alcohol synthesis. *Catal. Letters* **2006**, *111*, 141-151.

97. Eswaramoorthi, I.; Sundaramurthy, V.; Das, N.; Dalai, A. K.; Adjaye, J. Application of multi-walled carbon nanotubes as efficient support to NiMo hydrotreating catalyst. *Appl. Catal., A* **2008**, *339*, 187–195.

98. Xiaoming, M.; Guodong, L.; Hongbin, Z. Co-Mo-K sulfide-based catalyst promoted by multiwalled carbon nanotubes for higher alcohol synthesis from syngas. *Chin. J. Catal.* **2006**, *27*, 1019–1027.

99. Bournonville, J. P.; Franck, J. P.; Martino, G. Preparation of catalysis III. (Poncelet, G; Grange, P.; Eds.) Elsevier Science: USA, 1983, p. 81.

100. Shen, Y. Synthesis of higher alcohols from syngas over MoS_2 based catalysts. M.S. dissertation, Mississippi State University, Mississippi, MI, 1997.

101. Naumann, A. W.; Behan, A. S.; Thorsteinson, E. M. 4th International conference on the chemistry and uses of molybdenum, Golden, Colorado, 1982, p. 313.

102. Gherardi, P.; Ruggeri, O; Trifiro, F; Vaccari, A. Preparation of catalysis III. (Poncelet, G; Grange, P.; Eds.) Elsevier Science: USA, 1983, p. 723.

103. Santiesteban, J. G. Alcohol Synthesis from carbon monoxide and hydrogen over MoS_2-Based catalysts. Ph.D. Dissertation, Lehigh University, Bethlehem, PA, 1989.

CHAPTER 2

Comparative Study of Higher Alcohols Synthesis over Alumina and Activated Carbon-Supported Alkali-Modified MoS_2 Catalysts Promoted with Group VIII Metals

The manuscript provided in this chapter is very similar to the one submitted to the Journal Industrial and Engineering Chemistry Research.

Citation:

Surisetty, V. R.; Eswaramoorthi, I.; Dalai, A. K. Comparative study of higher alcohols synthesis over alumina and activated carbon-supported alkali-modified MoS_2 catalysts promoted with group VIII metals. *Ind. Eng. Chem. Res.* **2010**, Submitted for Review.

Contribution of the Ph.D. Candidate

Fabrication of the fixed-bed reactor, development of the catalysts, characterization and catalytic studies were performed by Venkateswara Rao Surisetty. Data analysis and interpretations were performed by Venkateswara Rao Surisetty with assistance from Drs. Eswaramoorthi Iyyamperumal and Ajay Kumar Dalai. Dr. Eswaramoorthi Iyyamperumal was a Post Doctoral fellow in Catalysis and Chemical Reaction Engineering Laboratories, Department of Chemical Engineering, University of Saskatchewan. All of the writing of the submitted manuscript was done by Venkateswara Rao Surisetty and discussed with Drs. Eswaramoorthi and Dalai. Dr. Dalai provided editorial guidance regarding the style and content of the paper.

Contribution of this chapter to overall study

In order to develop an active catalyst for higher alcohols synthesis, it is necessary to know the role of different metal promoters and supports on alkali modified molybdenum based catalysts. The promotion of group VIII metals to MoS_2 catalysts may increase the reactivity of MoS_2 by modifying the structure of active metal species to

obtain highly dispersed catalysts and shift the product distribution to the formation of oxygenates. The role of catalyst support is well known in a heterogeneous chemical reaction. Catalyst supports such as activated carbon and alumina are mostly used in higher alcohols synthesis. In this research, the main focus is to study the interaction effects of group VIII metal promoters, such as Co, Ni and Rh on Mo component and the role of support on higher alcohols synthesis by analyzing the physico-chemical characteristics of the catalysts using various characterization techniques and performing the higher alcohols synthesis under identical experimental conditions.

2.1. Abstract

Potassium modified molybdenum sulfide catalysts promoted with nickel, cobalt, and rhodium were prepared using alumina or activated carbon as support to obtain highly dispersed MoS_2-based catalysts for higher alcohols synthesis. The N_2 adsorption study indicates a fall in textural characteristics of the catalysts compared to pure supports and this effect is more pronounced in activated carbon-based catalysts. The x-ray diffraction (XRD) phase analysis indicated the existence of promoted and un-promoted MoS_2 phases. The addition of rhodium resulted in an enhanced dispersion of smaller sized MoS_2 particles. The temperature programmed reduction (TPR) studies revealed that the addition of promoters such as, Ni, Co, and Rh improved the reducibility of the catalyst and shifts the reduction temperature of Mo^{+6} to lower temperature. Rh-promoted MoS_2 sites were revealed from diffuse reflectance infrared Fourier transform spectroscopy (DRIFTS) study of adsorbed CO over the Rh-promoted catalysts. Raman spectroscopy revealed the formation of Ni-Mo-S and Co-Mo-S phases in Ni and Co-promoted MoS_2 catalysts. The performance of these catalysts was tested for higher alcohols synthesis under similar conditions at 320^{o}C, 8.3 MPa (1200 psig) and 3.6 m^3 (STP)/(kg of cat.)/h and a H_2 to CO molar ratio of 1. The Ni-promoted catalyst showed activity towards the formation of hydrocarbons over that of alcohols. The addition of Co to the Ni-Mo-K/Al_2O_3 catalyst improved the activity towards the formation of alcohols and hydrocarbons. The activity of Rh-promoted catalysts for higher alcohol synthesis was much higher than that obtained over the rhodium-free catalysts. The total alcohols space time yield and higher alcohols selectivities are significantly higher over the catalysts

supported on activated carbon supported catalysts than the catalysts supported on alumina.

2.2. Introduction

The catalytic conversion of synthesis gas to higher alcohols is a promising route for the production of clean fuels and petrochemical feedstocks from coal, natural gas and hydrocarbon wastes via gasification. The phase out of lead in all gasoline grades and adverse health and environmental effects of Methyl Tertiary Butyl Ether (MTBE), has drawn considerable interest in the synthesis of higher alcohols.[1] Unlike gasoline and diesel, bio-fuels contain oxygen and adding bio-fuels to petroleum products allows the fuel to combust more completely. Bio-fuels reduce toxic air emissions such as, SO_x and NO_x, aromatic hydrocarbons, greenhouse gas build-up, and dependence on imported oil, while supporting agriculture and rural economies. Higher alcohols have low vapor pressure, better solubility with hydrocarbon compounds, improved water tolerance, and higher overall heating values.[2,3] There is much attention on the development of selective catalysts based on modified methanol catalysts and molybdenum sulfide catalysts for higher alcohols synthesis. Modified methanol synthesis catalysts mainly produce branched alcohols, among which iso-butanol is the main product along with the methanol.[4,5] Fe, Ni, or Co-modified low temperature and low pressure methanol synthesis catalyst systems produce linear alcohols, but the production of hydrocarbons cannot be reduced to acceptable levels. Deactivation is the major disadvantage for this catalyst system, due to the destruction of the spinel structures of Cu and Co, Ni or Fe, and the sintering of copper at temperatures greater than 300°C.[6,7]

The sulfides of transition metals have been used in the petroleum industry in hydrodesulfurization, hydrodenitrogenation, and hydrogenation reactions for over 50 years. Molybdenum disulfide (MoS_2) when supported with alkali metals can be used as a catalyst for producing alcohols from synthesis gas. The function of the alkali metal is to reduce the hydrogenation ability of alkyl species to form alkanes and increase the active sites for the formation of alcohols.[8] Alkali-modified molybdenum-based catalysts show a high proportion of higher alcohols at lower pressure and high temperature, and are attractive due to their excellent resistance to sulfur poisoning, high activity for water-gas

shift reaction, and coke-formation tolerance, which saves on the cost of ultra-desulfurization for feed gas and separation of water.[9] The alcohol products over these catalyst systems are linear alcohols, and the mechanism for the formation of higher alcohols ($C_{2+}OH$) is via a classical insertion of CO into the corresponding precursor alcohol. The activity and selectivity to $C_{2+}OH$ was low due to A-S-F distribution.[10]

The Fischer-Tropsch (F-T) elements such as Ni and Co increase the alcohol yield and selectivity towards higher alcohols of MoS_2 catalysts.[11,12] Alkali-modified MoS_2 catalysts promoted with Co show a high activity to alcohols and can produce alcohols with a variable ratio of methanol to higher alcohols by changing the operating conditions.[13] The presence of Co in alkali-modified MoS_2 catalysts enhanced the $C_1 \rightarrow C_2$ homologation step that led to ethanol as the dominant product.[14] The addition of Ni to K/MoS_2 catalysts leads to methanation.[15] The CO hydrogenation studied over $K/Co/Mo/A1_2O_3$ and $K/Co/Mo/SiO_2$ catalysts found that all three elements are necessary for higher activity. Hydrocarbons and alcohols were produced in approximately equal amounts over both catalysts.[16] The promotion of Co to alkali-modified MoS_2 catalysts shrinks the particle size of MoS_2 species, while Co is mainly in the form of Co-Mo-S phase at low Co loading and partly in a Co_9S_8-like structure at high Co loading.[17]

The introduction of noble metals such as Rh and Pt to Mo showed enhanced activity towards higher alcohols. Te et al.[18] compared the CO hydrogenation over Rh/Al_2O_3 and $Rh\text{-}Mo/Al_2O_3$ catalysts and found that higher activity and oxygenate selectivity of $Rh\text{-}Mo/Al_2O_3$ are due to the site isolation effect of molybdenum. Wong et al.[19] investigated the incorporation of Rh into reduced $K/Co/Mo/Al_2O_3$ catalysts and found that the activity and selectivity to the production of alcohols improved significantly due to the strong interaction of the Rh modifier with supported K-Mo-O species. The rate of CO hydrogenation over $Mo\text{-}Rh/Al_2O_3$ increased by a factor of 10 or more and the product distribution shifted to oxygenates in comparison with that over an Rh/Al_2O_3 catalyst.[20]

Most of the studies reported are mainly concerned about the oxide form of the Rh-Mo catalysts. The sulfide form of the Mo catalyst normally shows higher activity compared to the oxide form, with good selectivity towards higher alcohols. It is expected that the sulfide form of Rh-promoted Mo-based catalysts shows better activity and

selectivity towards higher alcohols compared to the oxide form of Rh-Mo catalysts. Hence, this study aims to prepare various alkali-modified monometallic, bimetallic, trimetallic and tetrametallic catalysts that contain Co, Ni, Rh and Mo metals using the incipient wetness impregnation method. Further, it aims to study the interactions between the metal promoters (Rh, Co, and Ni) and Mo component and the role of support by analyzing the physico-chemical characteristics of the catalysts using various characterization techniques. The catalytic performance of higher alcohols synthesis over these catalysts is carried out under identical experimental conditions.

2.3. Experimental

2.3.1. Preparation of modified MoS_2 catalysts

γ-Alumina (Sud Chemie, USA, surface area – 220 m^2/g, pore volume- 0.73 cc/g) and activated carbon (Sigma Aldrich, Canada, surface area-655 m^2/g, pore volume-0.93 cc/g) were used as support for the preparation of MoS_2-based catalysts. Ammonium heptamolybdate (Sigma-Aldrich, Canada), cobalt acetate tetrahydrate (Alfa Aesar, Germany), nickel acetate tetrahydrate (Sigma Aldrich, Canada), rhodium chloride hydrate (Sigma Aldrich, Canada), and potassium carbonate (Sigma Aldrich, Canada) were used as precursors for Mo, Co, Ni, Rh, and K, respectively. All catalysts were prepared following a method reported by Surisetty et al.[21-23] The target compositions of the metal contents over the catalysts are given in Table 2.1. All the catalysts were modified with 6 wt% of K.

2.3.2. Characterization of modified MoS_2 catalysts

Textural characteristics, such as BET surface area and pore volume, of the catalysts were analysed by the N_2 adsorption-desorption method at 77 K on a Micromeritics 2000 ASAP analyser. Before analysis, all samples (0.2 g) were degassed at 200°C for 2-3 h under vacuum and the surface area at liquid N_2 temperature calculated following the BET procedure. The elemental analyses of the calcined catalysts were performed using a PerkinElmer ELAN 5000 inductively coupled plasma mass spectroscopy (ICP-MS) instrument.

The phase and particle size of MoS_2-based metal particles were analyzed by X-ray diffraction (XRD) using a Rigaku X-ray diffractometer with nickel filtrated Cu Kα

radiation, 2θ angles from 10 to 80° at a scanning speed of 0.05°/s. To calculate the average particle size, the Debye-Scherer formula ($d=0.9\lambda/\beta Cos\theta$, where β is full width at half maximum (FWHM), λ – wave length of X-ray, 0.9 – constant) was applied to MoS_2 peak at 2θ value of 26.5°. In this study, the crystal particle size was measured on the basis of maximum length of the particle.

To reveal the reducibility of the metal species in the catalysts, H_2 temperature programmed reduction (TPR) profiles of modified MoS_2 catalysts were performed at atmospheric pressure using a CHEMBET 3000 TPR analyzer, at a linearly programmed rate of 5°C/min up to 800°C, with 3% H_2 in He stream at a flow rate of 30 ml/min.

To study the nature of Mo species, Diffuse Reflectance Infrared Fourier Transform Spectroscopy (DRIFTS) of adsorbed CO was carried out using a Perkin-Elmer Spectrum GX instrument equipped with a DTGS detector using 128 scans and resolution of 4 cm^{-1}. Approximately 20 mg of the powdered sample was placed in the sample cell and cleaned with He flow at 300°C for 2 h. The reduction was carried out under H_2 flow at 400°C for 4 h before CO adsorption. The background spectrum was collected for each sample before admitting CO gas. After cooling to room temperature, pure CO (20 ml/min) was passed over the sample for 30 min and the physisorbed CO removed by purging with He. The spectrum was recorded using 128 scans and a resolution of 4 cm^{-1}. The obtained spectrum is the difference spectrum subtracted from the background spectrum recorded. For comparison, the spectra of all samples were normalized for 20 mg of each sample.

To study the co-ordination environment of Mo species in the catalysts, Raman spectroscopy was used for all Mo-based catalysts using a Renishaw Raman Spectrometer equipped with a Nd:YAG laser source. The octahedral or tetrahedral-coordinated surface oxo-molybdenum species were identified by characteristic bands in the Raman spectrum.

2.3.3. Catalytic studies

The catalytic conversion of synthesis gas to higher alcohols was performed using the feed gas mixture CO (45 mole %), H_2 (45 mole %), and Ar (10 mole %) in a single-pass tubular downflow fixed-bed reactor under the reaction conditions of 320 ^oC, 8.3 MPa (1200 psig), and 3.6 m^3 (STP)/(kg of cat.)/h over a period of 24 h. The high pressure reaction set-up used in this study is as described in our previous work.[21-23] Prior

to the reaction, the catalyst was reduced and sulfided for 6 h at 450°C at a heating rate of 2°C/min using a gas mixture containing 10 mole % H_2S in H_2 and a flow rate of 50 ml/min. The product gas was cooled to 0°C and separated into gas and liquid phases at the reaction pressure. The liquid products were collected at the end of the reaction and analyzed with a Varian 3400 gas chromatograph equipped with a capillary column and a flame ionization detector (FID). The gaseous products were analyzed online on a Shimadzu gas chromatograph through a sampling valve for every 1 h. The experiments were repeated at least twice to check reproducibility and confirm that the results obtained were within the experimental error of ± 2.5%. (An example of the mass balance data is shown in Appendix C).

2.4. Results and Discussion

2.4.1. Characterization of modified MoS_2 catalysts

The typical N_2 adsorption-desorption isotherm of all the catalysts was measured with an aim to measure the total surface area. The typical isotherms for 15 wt % Mo-3 wt % Ni-6 wt % K/Al_2O_3 (Cat 1a) and 15 wt % Mo-6 wt % K/ AC (Cat 2a) are given in Figs. 2.1a and 2.1b, respectively. The alumina-supported catalysts showed Type II isotherm and activated carbon based catalysts showed Type IV isotherm.

The textural characteristics of the prepared catalysts are given in Table 2.1. The total BET surface area, pore volume and average pore diameter values of all the catalysts were much lower compared to those of pure supports. Because of the micro porous nature of activated carbon, a drastic fall in surface area after impregnating with metal species was observed. The measured Rh, Co, Ni and Mo contents of the prepared catalysts are slightly low compared to targeted values. The deviation is more for the alumina-supported catalysts (Cat 1a-1d) than activated carbon-supported catalysts (Cat 2a-2d).

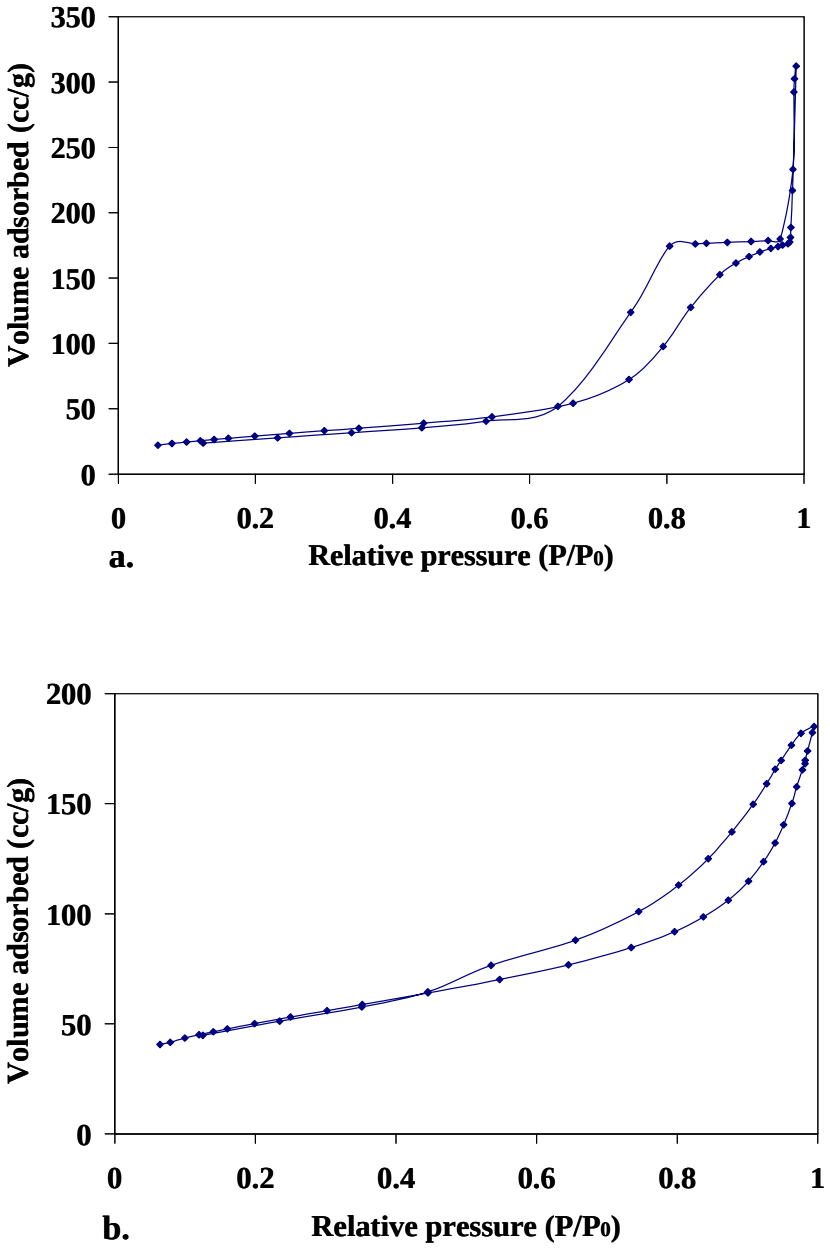

Figure 2.1. N_2 adsorption-desorption isotherms

a. alumina-supported catalyst; b. activated carbon-supported catalyst

Table 2.1. Physico-chemical characteristics of alumina and activated carbon-supported catalysts

Catalyst	Targeted composition (wt%)				Measured composition (wt%)				BET surface area (m^2/g)	Total pore volume (cc/g)	Average pore diameter (nm)	MoS_2* particle size (nm)
	Rh	Co	Ni	Mo	Rh	Co	Ni	Mo				
Cat 1a	0	0	3	15	-	-	2.7	13.5	105	0.28	10.6	36.7
Cat 1b	0	4.5	3	22	-	3.9	2.6	19.9	103	0.30	11.2	31.2
Cat 1c	1	0	0	22	0.4	-	-	17.9	131	0.35	10.7	40.5
Cat 1d	1	4.5	0	15	0.5	3.8	-	12.3	102	0.28	11.2	23.2
Cat 2a	0	0	0	15	-	-	-	14.1	178	0.26	5.9	31.2
Cat 2b	0	4.5	0	22	-	4.1	-	21.2	92	0.15	6.6	36.3
Cat 2c	1	0	3	22	0.7	-	2.8	20.4	80	0.15	8.5	28.2
Cat 2d	1	4.5	-	15	0.8	4.2	-	14.5	98	0.17	7.0	23.4

Cat1a: 15 wt % Mo-3 wt % Ni-6 wt % K/Al_2O_3;
Cat1b: 22 wt % Mo-4.5 wt % Co-3 wt % Ni-6 wt % K/Al_2O_3;
Cat1c: 22 wt % Mo-1.0 wt % Rh-6 wt % K/Al_2O_3;
Cat1d: 15 wt % Mo-4.5 wt % Co-1.0 wt % Rh-6 wt % K/Al_2O_3;
Cat2a: 15 wt % Mo-6 wt % K/ AC;
Cat2b: 22 wt % Mo-4.5 wt % Co-6 wt % K/AC;
Cat2c: 22 wt % Mo-1.0 wt % Rh-3 wt % Ni -6 wt % K/AC;
Cat2d: 15 wt % Mo-4.5 wt % Co- 1.0 wt % Rh-3 wt % Ni -6 wt % K/AC;
* calculated from XRD

The phase and nature of metal species in the catalysts after sulfidation were analysed by XRD. The XRD patterns of alumina-supported catalysts are presented in Fig. 2.2a and those of activated carbon-supported catalysts are in Fig. 2.2b. The Rh free alumina-supported catalysts (Cat 1a and 1b) show expected pattern for the MoS_2 phase.[24,25] When increasing the Mo content from 15 to 22 wt % (Cat 1b and 1c), the intensities of peaks for MoS_2 (at 2θ values 26.5° and 31.5°) are increased significantly confirming the formation of more MoS_2 species. The peak around 2θ value of 13.7° is due to the amorphous MoS_2 species formed over the catalysts.

The introduction of Ni (3 wt %) and Co (4.5 wt %) has little influence on the XRD patterns of the catalysts. The formation of K-Mo-S related species is indicated by peaks at 22.5°, 33.0°, and 46.5°. The intensity of these peaks is dependent on the amount of K. When introducing 1 wt % Rh on K-Mo-based catalysts, the peaks corresponding to K-Mo-S species disappeared, indicating that added Rh inhibits the formation of K-Mo-S species that may be due to the formation of Rh-Mo-S related species. The Rh-Mo bond is much stronger than K-Mo bond, but no evidence for the formation of Rh-Mo-S species is observed in the XRD patterns, which may be because of less added Rh. A low intensity peak at 32.7° observed in Cat 1b and 1d indicates the formation of the Co-Mo-S phase[26,27], but the corresponding Ni-Mo-S phase was not observed in Ni-containing catalysts. This may be due to less added Ni (3 wt %) than Co (4.5 wt %). The intensity for MoS_2 species (2θ=26.5°) is found to be higher in Cat 1b, which is loaded with 22 wt% Mo and 0 wt% Rh. The average particle sizes of Rh free catalysts are comparatively larger than that of Rh containing catalysts (see Table 2.1) indicating the role of Rh in improving the dispersion of MoS_2 particles.

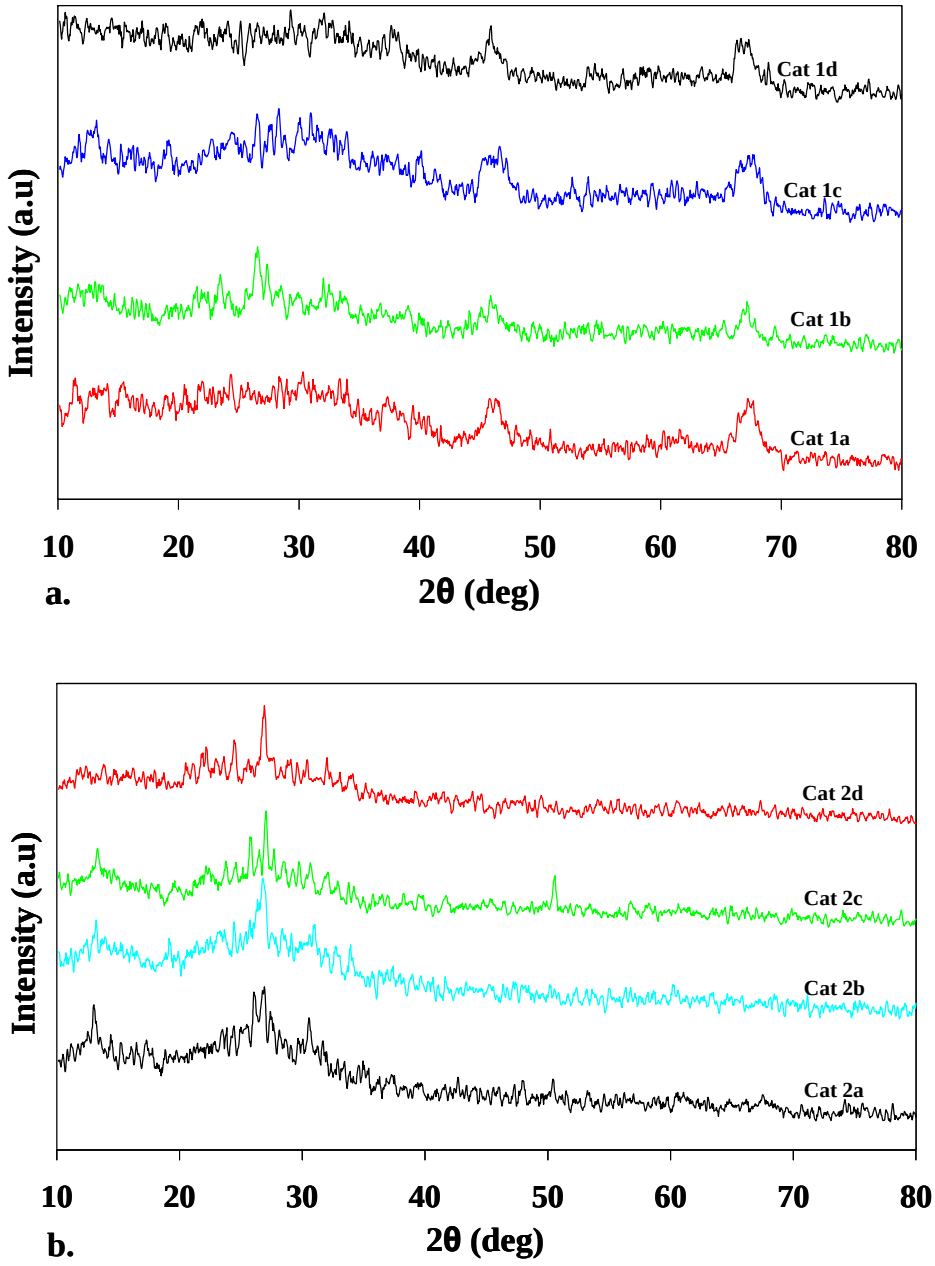

Figure 2.2. XRD patterns: a. alumina-supported catalysts (Cat 1a-1d); b. activated carbon-supported catalysts (Cat 2a-2d)

Cat1a: 15 wt % Mo-3 wt % Ni-6 wt % K/Al_2O_3; Cat1b: 22 wt % Mo-4.5 wt % Co-3 wt % Ni-6 wt % K/Al_2O_3; Cat1c: 22 wt % Mo-1.0 wt % Rh-6 wt % K/Al_2O_3;
Cat1d: 15 wt % Mo-4.5 wt % Co-1.0 wt % Rh-6 wt % K/Al_2O_3; Cat2a: 15 wt % Mo-6 wt % K/ AC;
Cat2b: 22 wt % Mo-4.5 wt % Co-6 wt % K/AC;
Cat2c: 22 wt % Mo-1.0 wt % Rh-3 wt % Ni -6 wt % K/AC;
Cat2d: 15 wt % Mo-4.5 wt % Co- 1.0 wt % Rh-3 wt % Ni -6 wt % K/AC

In the case of activated carbon-supported catalysts (Cat 2a-2d), the intensities of the peaks corresponding to the MoS_2 species are low compared to alumina based catalysts, indicating a higher dispersion of metallic species in former over the later supports. The intensity of peak at $2\theta = 27.3°$, due to K-Mo-S species, is significantly higher in the case of Rh free catalysts. Similar to alumina-based catalysts, there is no significant change due to the Ni and Co additions, indicating the highly dispersed nature of the added species. The peak at $2\theta=13.8°$ due to the characteristic reflection of amorphous MoS_2 species is apparent for all catalysts irrespective of Rh content. Similar to the observation made in Al_2O_3-supported catalysts, the average size of MoS_2 particles is larger in Rh-free catalysts, as given in Table 2.1. Comparatively, the MoS_2 particle sizes are smaller in activated carbon-based catalysts than those over Al_2O_3-supported catalysts.

The reducibility of the added metal species was studied by H_2-TPR and the typical profiles are presented in Figs. 2.3a and 2.3b for alumina (Cat 1a-1d) and activated carbon (Cat 2a-2d) supported catalysts, respectively. All catalysts show the typical hydrogen consumption peak corresponding to the reduction of Mo^{+6} to Mo^{+4} .[28,29] In the case of Cat 1a, which contains Ni, K and Mo, a broad peak around 510°C is seen indicating the major reduction of Mo^{+6} to Mo^{+4}. A shoulder peak in the temperature range 350-370°C is due to the reduction of bulk NiO-related species. When 4.5 wt % Co is introduced on the K-Mo/Al_2O_3 catalyst, the reduction profile moved to a slightly higher temperature. The absence of peak at 350°C, corresponding to the reduction of bulk CoO_3, provides proof for the formation of Co-Mo-O phase[30]. The major peak around 525°C is due to the reduction of Mo^{+6} to Mo^{+4} species.

The high temperature shoulder peak around 600°C is due to the reduction of tetrahedrally coordinated molybdate to lower oxidation state species. When 1 wt % Rh was introduced on K-Mo/Al_2O_3, the reduction temperature of Mo^{+6} to Mo^{+4} was lowered significantly and a small peak is noted at a much lower temperature (150°C). The low temperature peak is due to the reduction of Rh^+ to Rh, and the fall in reduction temperature indicates that the added Rh species enhanced the dispersion of Mo species. The smaller MoS_2 particles due to Rh addition were also confirmed from the average particle size measured from XRD analysis. Upon the addition of Co to Rh-Mo catalysts

(Cat 1d), there was no significant change in the reduction profiles of Rh and Mo. The absence of peak around 350°C for bulk CoO_3 reduction is a good indication of Co-Mo-O phase formation. It can be concluded that the addition of Rh decreases the reduction temperature of Mo significantly by increasing the dispersion.

In the case of activated carbon based catalysts, only Mo and K loaded catalyst (Cat 2a) showed a sharp peak at 530°C due to the reduction of Mo^{+6} to Mo^{+4} in MoS_2 phase. When 4.5 wt % Co is introduced over 22 wt % Mo and 6 wt % K-containing catalyst, the reduction temperature of Mo is slightly increased to 550°C along with a high temperature peak around 650°C due to the reduction of Mo^{+6} to lower oxidation state species. Rh (1 wt %) addition to K-Mo catalyst significantly decreased the reduction temperature similar to that in alumina based catalysts. A broad peak in the temperature range 390-410°C was observed in the TPR profile of Cat 2c. A small peak is noted at 150°C due to the reduction of Rh^{+} to metallic Rh. Rh addition to Co-K-Mo catalyst did not show any significant change in reduction temperature of the Mo^{+4} species, but showed a broad shoulder peak around 630°C due to the reduction of tetrahedrally-coordinated molybdate to lower oxidation state species.

Similar to alumina-supported catalysts, Rh addition leads to the fall in Mo^{+6} reduction temperatures, which may be due to the increased dispersion. Generally, the high temperature reduction peak for tetrahedrally-coordinated molybdate species is clearly visible in catalysts with 22 wt % Mo promoted with either Co or Rh over that of 15 wt % Mo-loaded catalysts. When comparing the alumina and activated carbon-supported catalysts, the reduction temperature of activated carbon-supported catalysts are significantly lower, indicating the higher dispersion of metal particles in the later support, similar to observations from XRD analysis.

The nature of active species in the reduced and sulfided catalysts was studied by DRIFT spectroscopy of CO-adsorbed catalysts. The typical DRIFT bands are shown in Figs. 2.4a and 2.4b for alumina and activated carbon supported catalysts, respectively. In Cat 1a, which contains Ni, Mo and K, a band at 2047 cm^{-1}, due to CO adsorbed on Ni-promoted MoS_2 sites, indicates that added Ni species promoted the active MoS_2 sites. Another band at 2010 cm^{-1} is due to the CO-adsorbed un-promoted MoS_2 sites.

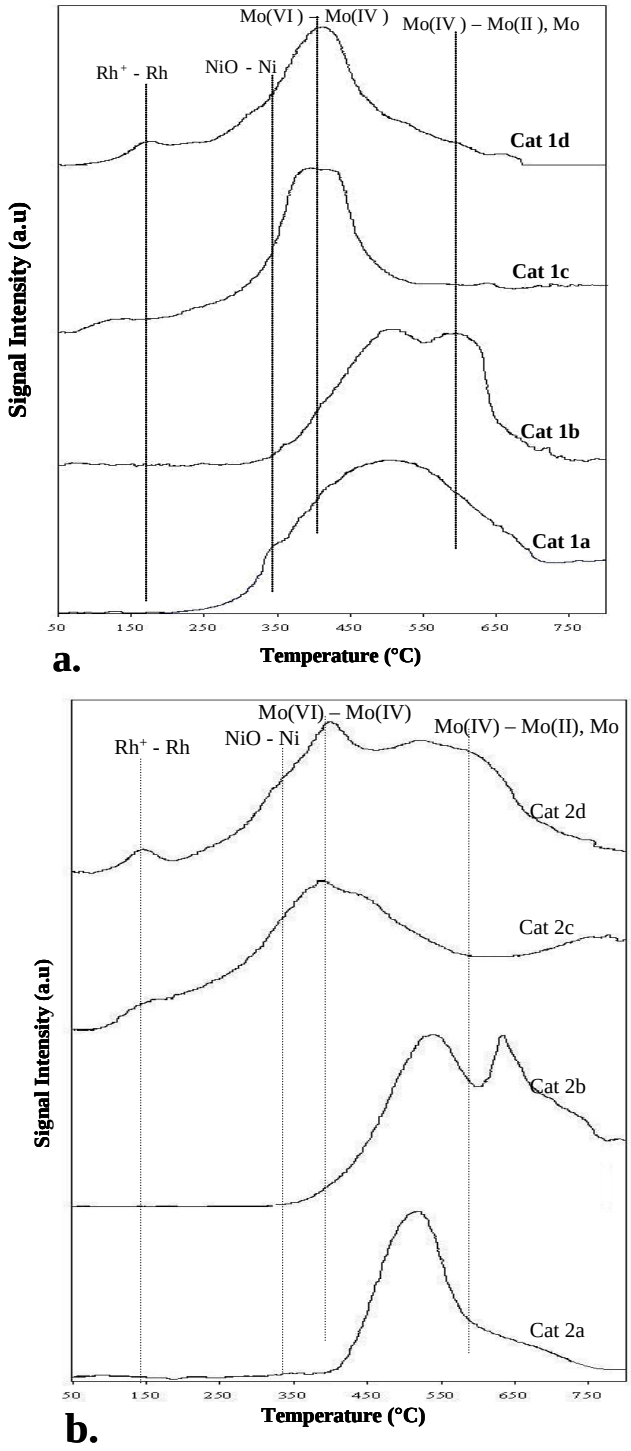

Figure 2.3. TPR profiles a. alumina-supported catalysts (Cat 1a-1d); b. activated carbon-supported catalysts (Cat 2a-2d)

Cat1a: 15 wt % Mo-3 wt % Ni-6 wt % K/Al_2O_3; Cat1b: 22 wt % Mo-4.5 wt % Co-3 wt % Ni-6 wt % K/Al_2O_3;
Cat1c: 22 wt % Mo-1.0 wt % Rh-6 wt % K/Al_2O_3;
Cat1d: 15 wt % Mo-4.5 wt % Co-1.0 wt % Rh-6 wt % K/Al_2O_3; Cat2a: 15 wt % Mo-6 wt % K/ AC;
Cat2b: 22 wt % Mo-4.5 wt % Co-6 wt % K/AC;
Cat2c: 22 wt % Mo-1.0 wt % Rh-3 wt % Ni -6 wt % K/AC; Cat2d: 15 wt % Mo-4.5 wt % Co- 1.0 wt % Rh-3 wt % Ni -6 wt % K/AC

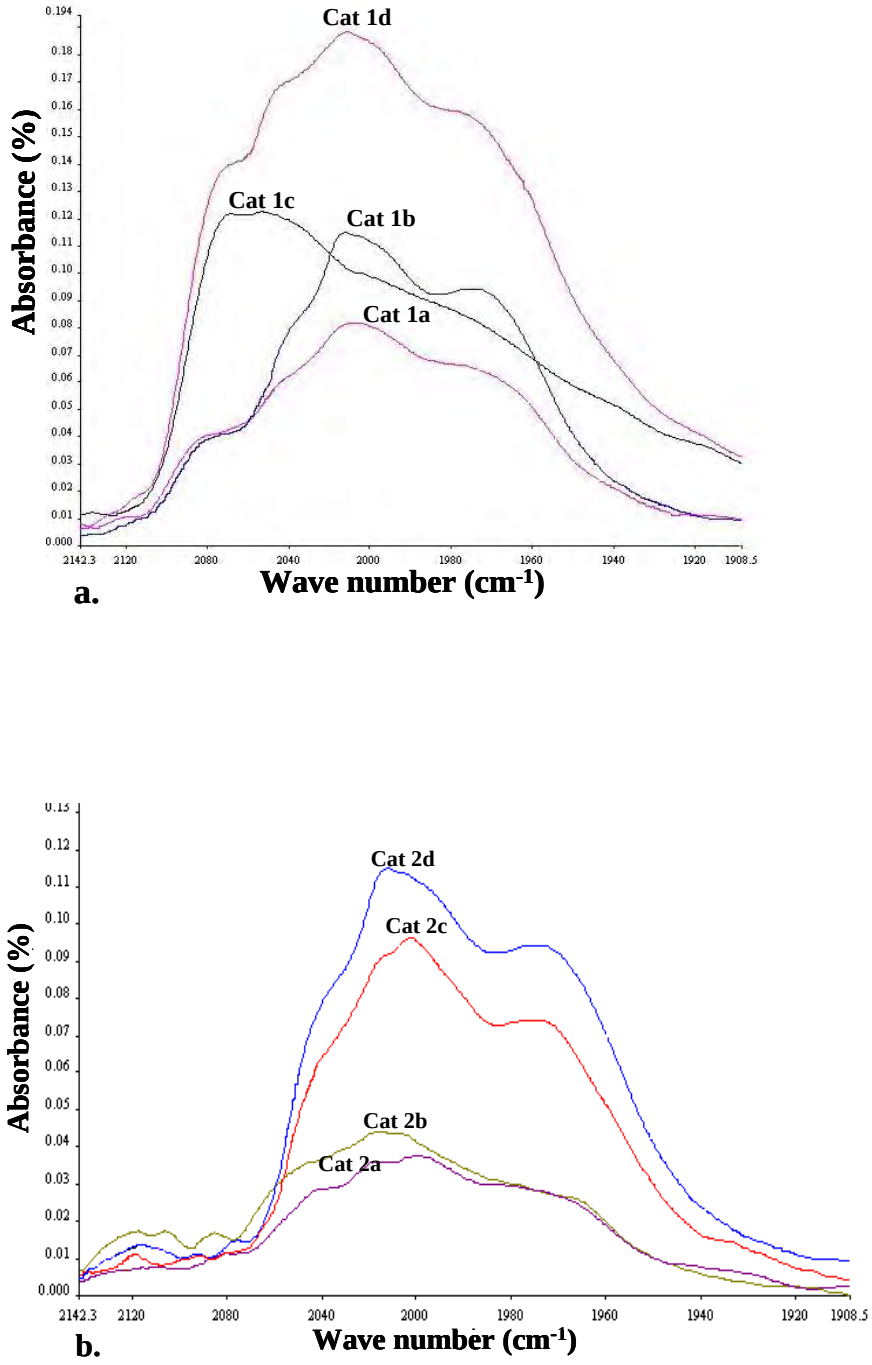

Figure 2.4. DRIFT spectra of adsorbed CO a. alumina-supported catalysts (Cat 1a-1d); b. activated carbon-supported catalysts (Cat 2a-2d)

Cat1a: 15 wt % Mo-3 wt % Ni-6 wt % K/Al_2O_3; Cat1b: 22 wt % Mo-4.5 wt % Co-3 wt % Ni-6 wt % K/Al_2O_3; Cat1c: 22 wt % Mo-1.0 wt % Rh-6 wt % K/Al_2O_3; Cat1d: 15 wt % Mo-4.5 wt % Co-1.0 wt % Rh-6 wt % K/Al_2O_3; Cat2a: 15 wt % Mo-6 wt % K/ AC; Cat2b: 22 wt % Mo-4.5 wt % Co-6 wt % K/AC; Cat2c: 22 wt % Mo-1.0 wt % Rh-3 wt % Ni -6 wt % K/AC; Cat2d: 15 wt % Mo-4.5 wt % Co- 1.0 wt % Rh-3 wt % Ni -6 wt % K/AC

A shoulder band is also noted at lower wave number 1973 cm^{-1}, resulting from CO adsorbed on Mo in the lower oxidation state. The absorption frequencies of all bands are comparatively less with the reported values for pure MoS_2 catalysts, which may be due to the added K species.[21] The charge transfer between K and Mo may create more electron density at Mo, resulting in a shift in absorption frequency to a lower wave number. When 4.5 wt % Co is introduced, significant change in the spectrum is noted. The bands for promoted MoS_2 sites are shifted to lower wave numbers and the intensity of band due to CO from reduced Mo sites are increased significantly, indicating that the Co addition reduces more Mo^{+6} to a lower oxidation state. The introduction of Rh in MoS_2-based catalysts showed a new band at much higher wave number (2087-2093 cm^{-1}) apart from the bands for promoted and un-promoted MoS_2 sites. When increasing the Mo content from 15 to 22 wt %, there is no significant change in the intensity of this band, hence this new band can be accounted for by Rh-promoted MoS_2 sites. Compared to Rh-free catalysts, the absorption frequencies of all the bands are significantly shifted to higher wave numbers. Generally, the intensity of band for promoted, un-promoted and lower oxidation state MoS_2 species are significantly higher for catalysts with 22 wt % Mo than that with 15 wt % Mo. Furthermore, catalysts with more Mo show high intensity bands for CO adsorbed on low oxidation state Mo species.

Activated carbon-supported catalysts show similar patterns for CO adsorbed on the catalysts, but the intensity is comparatively less than alumina-based catalysts. The absorption frequencies of CO adsorbed on various sites are shifted to lower wave numbers when compared to those of alumina based catalysts. There are no clear bands for the catalyst loaded only with Mo and K (Cat 2a). When 4.5 wt % Co introduced, a band around 2045 cm^{-1}, corresponding to Co-promoted MoS_2 sites is clearly visible. The un-promoted MoS_2 sites are represented by a high intensity band at 2010 cm^{1}. The CO adsorbed on lower oxidation state Mo species also shows a band at a much lower wave number (1975 cm^{-1}).

In the case of Rh-containing catalysts (Cat 2c-2d), the band for Rh-promoted MoS_2 sites is noted, but the intensities of the bands are comparatively low. When compared to alumina based catalysts, the bands intensity of the bands is comparatively low. Generally, when compared to alumina-based catalysts, the band intensities for

activated carbon-based catalysts are low, which may be due to the added potassium. Since alumina is acidic, the added K_2CO_3 may be deposited on the surface of the support, leaving the active metal surface free. However, because of activated carbon's neutral nature, the chance for the deposition of K_2CO_3 on the metal surface is greater. In Rh-containing catalysts, the formation of active Rh-Mo-S phase are identified by the new band at a significant high wave number.

The Raman spectra for the sulfided form of the samples that are supported on Al_2O_3 and activated carbon are given in Figs. 2.5a and 2.5b, respectively. The spectrum of the Al_2O_3 support is essentially featureless in the region of 100-1100 cm^{-1} under study. The supported sulfided-molybdenum species and Ni, Co and Rh-promoted MoS_2 species give rise to several bands in this region. The bands around 810 cm^{-1} and 936 cm^{-1} of Ni and Co containing catalysts (Cat 1a-1b) are due to Co or Ni promoted MoS_2 sites, indicating the formation of Co-Mo-S and Ni-Mo-S phases in these catalysts. The low intensity bands at lower wave numbers 365 and 380 cm^{-1} are characteristic of MoS_2 species. For the Rh only containing sample (Cat 1c), an additional sharp band appeared around 1000 cm^{-1}, indicating the formation of $Al_2(MoO_4)_3$ species. The added Mo species reacts with the support available during the calcination, which results in the formation of $Al_2(MoO_4)_3$ species. When both Rh and Co are loaded to K-Mo/Al_2O_3 catalyst (Cat 1d), the intensity of the band responsible for the promoted MoS_2 species increased significantly. No band is observed for $Al_2(MoO_4)_3$ species.

All the catalysts show the presence of MoS_2 species. In the case of activated carbon-supported catalysts (Cat 2a-2d, Fig. 2.5b), the bands due to both un-promoted MoS_2 species and promoted MoS_2 species are observed, similar to that in alumina-supported catalysts. However, the intensities of the bands are significantly lower than on alumina-supported catalysts, which may be due to the mesoporous nature of the activated carbon support compared to alumina. Most of the added metal species are inside the pores of the support, which resulted in a low intensity bands.

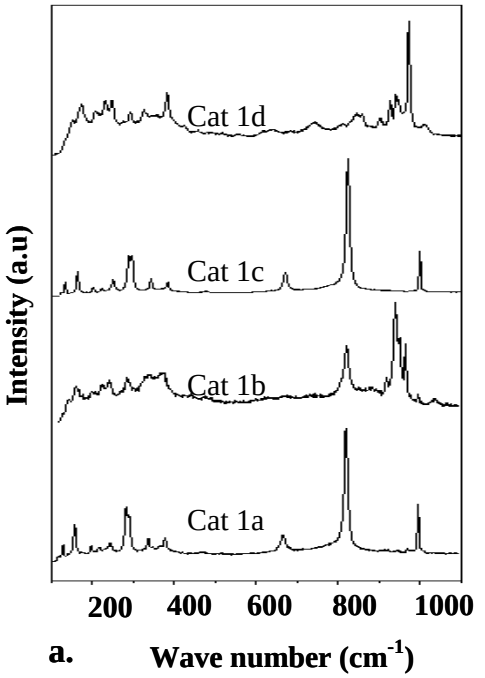

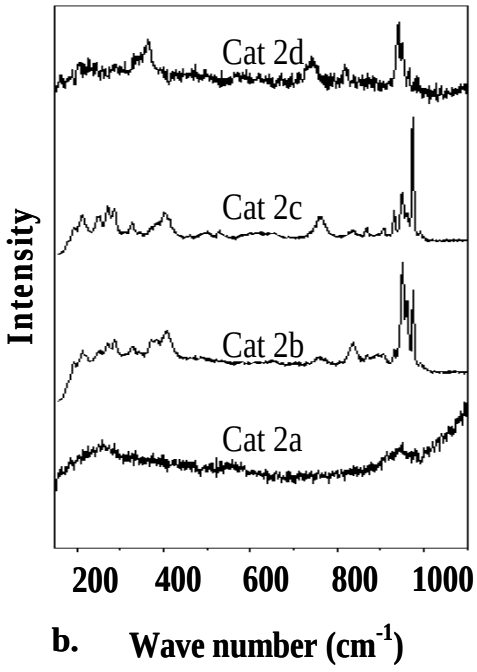

Figure 2.5. Raman spectra a. alumina-supported catalysts (Cat 1a-1d); b. activated carbon-supported catalysts (Cat 2a-2d)

Cat1a: 15 wt % Mo-3 wt % Ni-6 wt % K/Al_2O_3; Cat1b: 22 wt % Mo-4.5 wt % Co-3 wt % Ni-6 wt % K/Al_2O_3;
Cat1c: 22 wt % Mo-1.0 wt % Rh-6 wt % K/Al_2O_3;
Cat1d: 15 wt % Mo-4.5 wt % Co-1.0 wt % Rh-6 wt % K/Al_2O_3; Cat2a: 15 wt % Mo-6 wt % K/ AC;
Cat2b: 22 wt % Mo-4.5 wt % Co-6 wt % K/AC;
Cat2c: 22 wt % Mo-1.0 wt % Rh-3 wt % Ni -6 wt % K/AC; Cat2d: 15 wt % Mo-4.5 wt % Co- 1.0 wt % Rh-3 wt % Ni -6 wt % K/AC

2.4.2. Catalytic activity and selectivity studies

Table 2.2 shows the activity and selectivity results obtained from the CO hydrogenation reaction carried out under similar conditions at 320 ^{o}C, 8.3 MPa (1200 psig), 3.6 m^3 (STP)/(kg of cat.)/h, and H_2 to CO molar ratio of 1 over the sulfided catalysts. The liquid products were collected and the exit gas analyzed to measure the CO conversion. The CO conversion decreased sharply in the first 12 h and then levelled off. The catalytic activity and product selectivity data were calculated after an induction period of 15 h. The analysis of liquid products indicates that methanol and ethanol are the major products, with traces of propanol, iso-propanol, and butanol. The analysis of exit gas indicates that methane is the major component apart from CO, H_2 and CO_2. The results in Table 2.2 show the influence of the different contents of Mo and promoters on the catalytic features for the synthesis of higher alcohols from synthesis gas after an induction period of 15 h. The term higher alcohols in Table 2.2 represents the ethanol and alcohols with a carbon number greater than 2 (C_{2+} alcohols).

The % CO conversion increased with the metal content of the catalyst, suggesting the increased availability of active sites for CO hydrogenation reaction. The CO conversion was high due to the improved CO dissociation and hydrogenation activity over the Ni-promoted alkali-modified MoS_2 catalysts supported on alumina, as well as activated carbon.[31,32] This may be due to the formation of $NiMoS_2$ sites, as evidenced from DRIFT spectroscopy of adsorbed CO. The Al_2O_3-supported alkali-modified MoS_2 catalyst promoted with Ni (Cat 1a) showed activity towards the formation of hydrocarbons over that of alcohols, suggesting the improved methanation ability of the catalysts.[15] Compared to higher alcohols, the methanol selectivity is high over the Ni-promoted catalyst (Cat 1a). The addition of Co to the Ni-Mo-K/Al_2O_3 catalyst improved the activity towards the formation of alcohols and hydrocarbons. The activity of Rh-promoted catalysts for higher alcohol synthesis was much higher than that obtained over the rhodium-free catalysts, which resulted from the generation of the more catalytically active surfaces or sites modified by the rhodium species. Li et al.[33] studied higher alcohols synthesis over Rh-Mo-K/Al_2O_3 catalysts and found that the incorporation of rhodium into the oxidic Mo-K/Al_2O_3 samples leads to a strong interaction of the rhodium with the oxo-molybdenum components which improved the reducibility of the catalysts.

Over the Al_2O_3-supported catalysts, the highest ethanol and higher alcohols selectivities of 11.7% and 14.7% were obtained on the Co-Rh-Mo-K catalyst, indicating that the Co and Rh promoted MoS_2 sites, as shown in DRIFT of adsorbed CO, play an important role in enhancing the growth of carbon chain length in the reaction mechanism.

The catalyst K-Mo/AC showed significantly less CO conversion compared to metal promoted catalysts, indicating that the MoS_2 sites promoted with either Ni, Co, or or Rh are necessary to increase the performance of the catalyst under the experimental conditions studied. Similar to Al_2O_3-supported catalysts, Rh-containing MoS_2 catalysts show higher activity and selectivity towards formation of alcohols, indicating the role of Rh-promoted MoS_2 sites in the reaction mechanism. When comparing the Mo content, catalysts with 15 wt % Mo showed better higher alcohols activity than those with 22 wt % Mo. The total alcohols space time yield and higher alcohols selectivities are significantly higher over the catalysts supported on activated carbon, indicating the role of support in CO hydrogenation reaction. Carbon-supported catalysts have potential advantages such as lower tendencies of carbon deposition and less dehydration over oxide-supported catalysts.[34] The poor higher alcohols selectivities of Al_2O_3-supported catalysts can be accounted by the presence of strong acid sites in the support which may lead to a strong interaction between the added metals and support, favouring the formation of hydrocarbons.

Fig. 2.6 depicts the change in higher alcohols selectivity with % CO conversion obtained over the catalysts supported on alumina (Cat 1a-1d) and activated carbon (Cat 2a-2d). It can be observed from Fig. 2.6 and Table 2.2 that activated carbon supported Ni-Co-Rh-Mo-K catalysts outperformed in terms of CO conversion, total alcohols yield, ethanol selectivity and higher alcohols selectivity, which can be accounted by the formation of MoS_2 sites promoted with Rh, Co and Ni.

Table 2.2. Catalytic performance of sulfided alumina and activated carbon-supported catalysts

(wt. of the cat. = 2 g, P = 8.3 MPa, T = 320°C, GHSV = 3.6 m^3 (STP) /(kg of cat./h), H_2/CO molar ratio = 1)

Catalyst	CO conversion (%)	Product STY (g/(g of cat.)/h)		CO_2 produced (mole %)	Alcohol Selectivity (wt %)		
		Total alcohols	Total Hydrocarbons		Methanol	Ethanol	Higher alcohols
Cat1a	25.2	0.068	0.219	21.4	10.0	4.6	6.6
Cat1b	37.2	0.092	0.291	24.7	6.7	6.0	9.3
Cat1c	31.9	0.098	0.230	26.1	10.4	7.7	9.8
Cat1d	33.6	0.117	0.236	21.3	7.9	11.7	14.7
Cat2a	18.2	0.073	0.123	21.0	16.3	5.4	7.7
Cat2b	32.1	0.118	0.226	20.7	9.0	10.8	14.8
Cat2c	38.3	0.147	0.239	26.8	7.7	16.9	19.7
Cat2d	41.6	0.177	0.250	23.3	3.5	20.4	24.8

Cat1a: 15 wt % Mo-3 wt % Ni-6 wt % K/Al_2O_3; Cat1b: 22 wt % Mo-4.5 wt % Co-3 wt % Ni-6 wt % K/Al_2O_3; Cat1c: 22 wt % Mo-1.0 wt % Rh-6 wt % K/Al_2O_3; Cat1d: 15 wt % Mo-4.5 wt % Co-1.0 wt % Rh-6 wt % K/Al_2O_3; Cat2a: 15 wt % Mo-6 wt % K/ AC; Cat2b: 22 wt % Mo-4.5 wt % Co-6 wt % K/AC; Cat2c: 22 wt % Mo-1.0 wt % Rh-3 wt % Ni -6 wt % K/AC; Cat2d: 15 wt % Mo-4.5 wt % Co- 1.0 wt % Rh-3 wt % Ni -6 wt % K/AC

Table 2.3. Physical characteristics of spent catalysts

Catalyst	BET surface area (m^2/g)	Total pore volume (cc/g)	Average pore diameter (Å)
Cat 1c	105	0.30	99
Cat 1d	78	0.19	103
Cat 2c	72	0.15	83

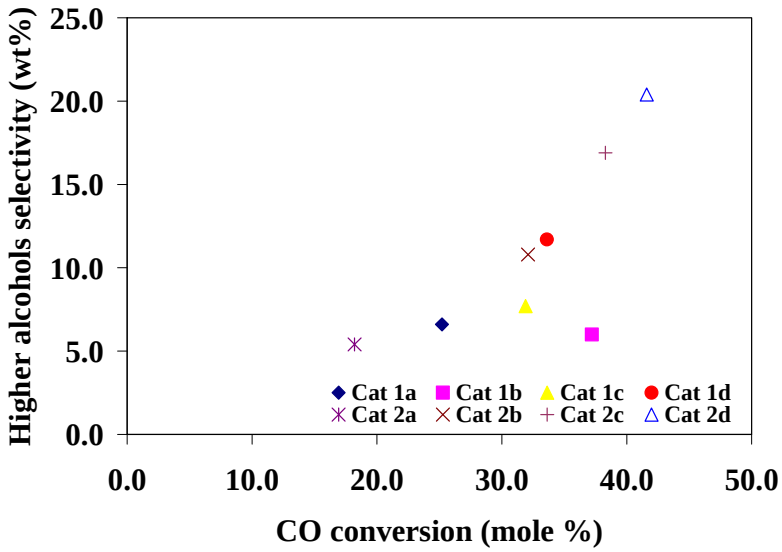

Figure 2.6. Change in higher alcohols selectivity with % CO conversion

(wt. of the cat. = 2 g, P = 8.3 MPa, T = 320°C, GHSV = 3.6 m^3 (STP) /(kg of cat./h), H_2/CO molar ratio = 1)
Cat1a: 15 wt % Mo-3 wt % Ni-6 wt % K/Al_2O_3; Cat1b: 22 wt % Mo-4.5 wt % Co-3 wt % Ni-6 wt % K/Al_2O_3;
Cat1c: 22 wt % Mo-1.0 wt % Rh-6 wt % K/Al_2O_3; Cat1d: 15 wt % Mo-4.5 wt % Co-1.0 wt % Rh-6 wt % K/Al_2O_3;
Cat2a: 15 wt % Mo-6 wt % K/ AC; Cat2b: 22 wt % Mo-4.5 wt % Co-6 wt % K/AC;
Cat2c: 22 wt % Mo-1.0 wt % Rh-3 wt % Ni -6 wt % K/AC; Cat2d: 15 wt % Mo-4.5 wt % Co- 1.0 wt % Rh-3 wt % Ni -6 wt % K/AC

2.4.3. Characterization of spent catalysts

To test the stability of the catalysts after 24 h of reaction, the textural characteristics and phase analysis were carried out for the spent catalysts (Cat 1c, Cat 1d, and Cat 2c). The surface area, pore volume, and average pore diameter values of Cat 1c, Cat 1d and Cat 2c given in Table 2.3 were slightly lower compared to those of their fresh form. No drastic decrease in textural characteristics observed in both Al_2O_3 and activated carbon-supported catalysts, indicating that these are strong and active after 24 h on-stream.

XRD patterns of spent catalysts are shown in Fig. 2.7. Compared to the XRD patterns of fresh Al_2O_3-supported catalysts (Cat 1c and Cat 1d), there is no significant change in the intensities of peaks for MoS_2 and related species. However, there is a significant increase in intensity of peaks for MoS_2 species in activated carbon-supported spent catalyst (Cat 2c), indicating that the particle sizes are increased due to time on stream for 24 h. This may be due to the sintering of metallic particles during the reaction due to the poor interaction between metal particles and the support.

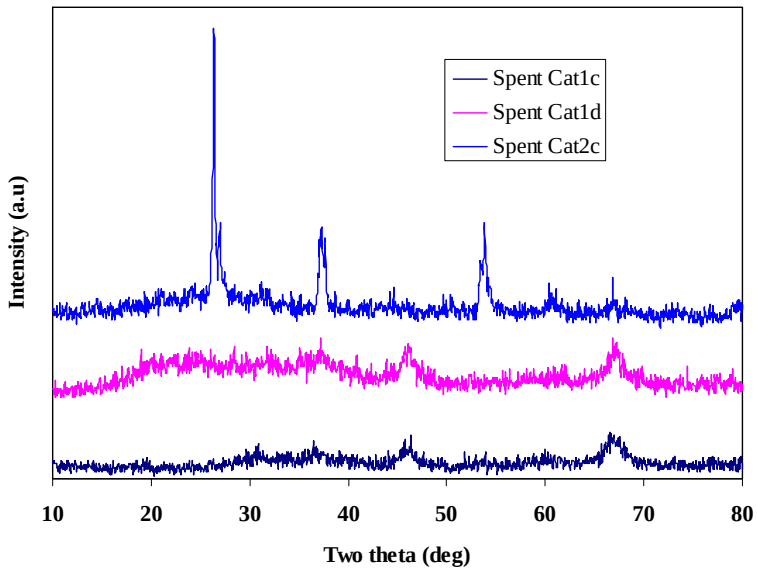

Figure 2.7. XRD patterns of spent catalysts (Cat 1c, Cat 1d and Cat 2c)

Cat1c: 22 wt % Mo-1.0 wt % Rh-6 wt % K/Al_2O_3; Cat1d: 15 wt % Mo-4.5 wt % Co-1.0 wt % Rh-6 wt % K/Al_2O_3; Cat2c: 22 wt % Mo-1.0 wt % Rh-3 wt % Ni -6 wt % K/AC

2.5. Conclusions

Ni, Co and Rh-promoted, K-modified MoS_2 catalysts were prepared using alumina and activated carbon as supports to obtain highly dispersed MoS_2 for higher alcohol synthesis from synthesis gas. A fall in BET surface area, pore volume and pore diameter of the catalysts compared to pure supports indicate the blockage of pores by the added metal particles. The phase analysis by XRD indicated the existence of promoted and unpromoted MoS_2 phases. The addition of Rh resulted in an enhanced dispersion of Mo particles. The TPR studies revealed that the addition of promoters such as, Ni, Co and Rh shifts the reduction temperature of Mo^{+6} to lower temperature. Rh-promoted MoS_2 sites were observed in catalysts with 1 wt % Rh. Raman spectroscopy revealed the formation of Ni-Mo-S and Co-Mo-S phases in Ni and Co promoted MoS_2 catalysts. All the characterization results indicate that added metal particles are better dispersed in activated carbon supported catalysts than alumina based catalysts. The introduction of metal promoters over the K-modified MoS_2 catalysts significantly increased the CO conversion. The Al_2O_3-supported alkali-modified MoS_2 catalyst promoted with Ni showed activity towards the formation of hydrocarbons over that of alcohols. The addition of Co to the Ni-Mo-K/Al_2O_3 catalyst improved the activity towards the

formation of alcohols and hydrocarbons. The activity of Rh-promoted catalysts for higher alcohol synthesis was much higher than that obtained over the rhodium-free catalysts. The total alcohols space time yield and higher alcohols selectivities are significantly higher over the activated carbon supported catalysts compared to those supported on alumina.

2.6. Abbreviations

AC	Activated carbon
DRIFTS	Diffuse reflectance infrared Fourier transform spectroscopy
GHSV	Gas hourly space velocity
ICP-MS	Inductively coupled plasma – mass spectroscopy
STY	Space time yield
TPR	Temperature programmed reduction
XRD	X-ray diffraction

2.7. References

1. Verkerk, K. A. N.; Jaeger, B.; Finkeldei, C.; Keim, W. Recent developments in isobutanol synthesis from synthesis gas. *Appl. Catal., A* **1999**, *186*, 407–431.
2. Smith J. L.; Workman, J. P. Alcohol for motor fuels. Farrum and Ranch series no. 5010, 1992.
3. Brusstar, M. Research in Alcohol-Fueled Engines. EPA NVFEL NEVC Annual Meeting, U. S. Environmental Protection Agency, 2003.
4. Campos-Martin, J. M.; Fierro, J. L. G.; Guerrero-Ruiz, A.; Herman, R. G.; Klier, K. Promoter effect of cesium on C–C bond formation during alcohol synthesis from CO/H_2 over $Cu/ZnO/Cr_2O_3$ catalysts. *J.Catal.* **1996**, *163*, 418–428.
5. Beretta, A.; Sun, Q.; Herman, R. G.; Klier, K. Production of methanol and isobutyl alcohol mixtures over double-bed cesium-promoted $Cu/ZnO/Cr_2O_3$ and ZnO/Cr_2O_3 catalysts. *Ind. Eng. Chem. Res.* **1996**, *35*, 1534–1542.
6. Xu, R.; Yang, C.; Wei, W.; Li, W.-H.; Sun, Y.-H; Hu, T.-D. Fe-modified $CuMnZrO_2$ catalysts for higher alcohols synthesis from syngas. *J. Mol. Catal. A: Chem.* **2004**, *221*, 51–58.

7. Mahdavi, V.; Peyrovi, M. H.; Islami, M.; Mehr, J. Y. Synthesis of higher alcohols from syngas over Cu-Co_2O_3/ZnO, Al_2O_3 catalyst. *Appl. Catal., A* **2005**, *281*, 259–265.

8. Woo, H. C.; Park, K. Y. Mixed alcohols synthesis from carbon monoxide and dihydrogen over potassium-promoted molybdenum carbide catalysts. *Appl. Catal., A* **1991**, *75*, 267–280.

9. Feng, L.; Li, X.; Dadyburjor, D. B.; Kugler, E. L. A temperature-programmed-reduction study on alkali-promoted, carbon-supported molybdenum catalysts. *J. Catal.* **2000**, *190*, 1–13.

10. Smith, K. J.; Herman, R. G.; Klier, K. Kinetic modelling of higher alcohol synthesis over alkali-promoted Cu/ZnO and MoS_2 catalysts. *Chem. Eng. Sci.* **1990**, *45*, 2639–2646.

11. Liu, Z. Y.; Li, X. G.; Close, M. R.; Kugler, E. L.; Petersen, J. L.; Dadyburjor, D. B. Screening of alkali-promoted vapor-phase-synthesized molybdenum sulfide catalysts for the production of alcohols from synthesis gas. *Ind. Eng. Chem. Res.* **1997**, *36*, 3085–3093.

12. Lu, G.; Zhang, C. F.; Chang, Y.; Zhu, Z.; Ni, Y.; Cheng, L.; Yu, F. Synthesis of mixed alcohols from CO_2 contained syngas on supported molybdenum sulfide catalysts. *Appl. Catal., A* **1997**, *150*, 243–252.

13. Murchison, C. B.; Conway, M. N.; Steven, R. R.; Quarderer, G. J. Mixed alcohols from syngas over molybdenum catalysts. In In *Proc. 9th Intern. Congr. Catal.*; 1998; Vol. 2, p 626.

14. Wei, J.; Iglesia, E.; Isotopic and kinetic assessment of the mechanism of reactions of CH_4 with CO_2 or H_2O to form synthesis gas and carbon on nickel catalysts. *J. Catal.* **2004**, *224*, 370–383.

15. Tatsumi, T.; Muramatsu, A.; Fukunaga, T.; Tominaga, H. Nickel promoted molybdenum catalysts for synthesis of mixed alcohols. In *Proc. 9th Intern. Congr. Catal.*; Phillips, M. J., Ternan, M., Eds.; The Chemical Institute of Canada: Ottawa, 1988; Vol. 2, p 618.

16. Fujumoto, A.; Oba, T. Synthesis of C_1-C_7 alcohols from synthesis gas with supported cobalt catalysts. *Appl. Catal., A* **1985**, *13*, 289–319.

17. Surisetty, V. R.; Dalai, A. K.; Kozinski, J. Synthesis of higher alcohols from synthesis gas over Co-promoted alkali modified-MoS_2 catalysts supported on MWCNTs. *Appl. Catal., A* **2010**, in press.

18. Te, M.; Lowenthal, E. E.; Foley, H. C. Comparative study of Rh/Al_2O_3 and $Rh-Mo/Al_2O_3$ catalysts. *Chem. Eng. Sci.* **1994**, *49*, 4851–4859.

19. Wong, S. F.; Stromville, N. Y.; Storm, D. A.; Montvale, N. J.; Patel, M. S. *Catalyst and method for producing lower aliphatic alcohols*. US Patents 4,983,638, Jan 8, 1991.

20. Sudhakar, C.; Bhore, N. A.; Bischoff, K. B.; Manogue, W. H.; Mills, G. A. Molybdena enhanced Rh/Al2O3 catalysts. In *Proc. of the 10th Meeting of the Catalysis Society of North America*, San Diego, CA, 1987.

21. Surisetty, V. R.; Tavasoli, A.; Dalai, A. K. Synthesis of higher alcohols from syngas over alkali promoted MoS_2 catalysts supported on multi-walled carbon nanotubes. *Appl. Catal. A* **2009**, *365*, 243–251.

22. Surisetty, V. R.; Dalai, A. K.; Kozinski, J. Effect of Rh promoter on MWCNT-supported alkali-modified MoS_2 catalysts for higher alcohols synthesis from CO hydrogenation. *Appl. Catal. A*, **2010**, *381*, 282–288.

23. Surisetty, V. R.; Dalai, A. K.; Kozinski, J. Alkali-promoted trimetallic Co-Rh-Mo sulfide catalysts for higher alcohols synthesis from synthesis gas: Comparison of MWCNT and activated carbon supports. *Ind. Eng. Chem. Res.* **2010**, *49*, 6956-6963.

24. Rueda, N.; Bacaud, R.; Vrinat, M. Highly Dispersed, Nonsupported Molybdenum Sulfides. *J. Catal.* **1997**, *169*, 404–406.

25. Iranmahboob, J.; Hill, D. O.; Toghiani, H. Characterization of $K_2CO_3/Co–MoS_2$ catalyst by XRD, XPS, SEM, and EDS. *Appl. Surf. Sci.* **2001**, *185*, 72–78.

26. Arco, M. D.; Carrazan, S. R. G.; Rives, V.; Lambias, F. L. G.; Malet, P. Surface species formed upon supporting molybdena on alumina by mechanically mixing both oxides. *J. Catal.* **1993**, *141*, 48–57.

27. Rajagopal, S.; Marini, H. J.; Marzari, J. A.; Miranda, R. Silica-alumina-supported acidic molybdenum catalysts - TPR and XRD characterization. *J. Catal.* **1994**, *147*, 417–428.

28. Noronha, F. B.; Baldanza, M. A. S.; Schmal, M. CO and NO adsorption on alumina–Pd–Mo catalysts: effect of the precursor salts. *J. Catal.* **1999**,*188*, 270–280.

29. Arnoldy, P.; Moulijn, J. A. Temperature-programmed reduction of CoO/AI_2O_3 catalysts. *J. Catal.* **1985**, *93*, 38–54.

30. Travert, A.; Dujardin, C.; Mauge, F.; Veilly, E.; Cristol, S.; Paul, J.-F.; Payen, E. CO adsorption on CoMo and NiMo sulfide catalysts: A combined IR and DFT study. *J. Phys. Chem. B* **2006**, *110*, 1261–1270.

31. Hedrick, S. A.; Chuang, S. S. C.; Pant, A.; Dastidar, A. G. Activity and selectivity of group VIII, alkali-promoted Mn-Ni, and Mo-based catalysts for C_{2+} oxygenate synthesis from the CO hydrogenation and $CO/H_2/C_2H_4$ reactions. *Catal. Today* **2000**, *55*, 247–257.

32. Qi, H.; Li, D.; Yang, C.; Ma, Y.; Li, W.; Sun, Y.; Zhong, B. Nickel and manganese co-modified K/MoS_2 catalyst: high performance for higher alcohols synthesis from CO hydrogenation. *Catal. Commun.* **2003**, *4*, 339–342.

33. Li, Z.; Fu, Y.; Jiang, M.; Hu, T.; Liu, T.; Xie, Y. Active carbon supported Mo-K catalysts used for alcohol synthesis. *J. Catal.* **2001**, *199*, 155–161.

34. Duchet, J. C.; van Oers, E. M.; de Beer, V. H. J.; Prins, R. Carbon-supported sulfide catalysts. *J. Catal*. **1983**, *80*, 386–402.

CHAPTER 3

Synthesis of Higher Alcohols from Synthesis Gas over Alkali-Promoted MoS_2 Catalysts Supported on Multi-Walled Carbon Nanotubes

The manuscript provided in this chapter is very similar to the one published in the journal Applied Catalysis A: General.

Citation:

Surisetty, V. R.; Tavasoli, A.; Dalai, A. K. Synthesis of higher alcohols from syngas over alkali-promoted MoS_2 catalysts supported on multi-walled carbon nanotubes. *Appl. Catal., A* **2009**, *365*, 243–251.

Contribution of the Ph.D. Candidate

Experimental design and experiments were performed by Venkateswara Rao Surisetty. Drs. Ajay Kumar Dalai and Ahmad Tavasoli provided consultation regarding the experiments, data analysis and interpretations. Dr. Ahmad Tavasoli was a visiting researcher for a period of one year. All written text was prepared by Venkateswara Rao Surisetty and discussed with Drs. Tavasoli and Dalai. Dr. Dalai provided editorial guidance regarding the style and content of the paper.

Contribution to Overall Study

In chapter 2 the performance of Co, Rh and Ni- promoted alkali-modified MoS_2 catalysts were studied using the conventional supports such as alumina and activated carbon. The group-VIII metal promotion, especially Co and Rh to alkali-modified molybdenum sulfide catalysts showed improved activity and selectivity towards the formation of higher alcohols. Activated carbon is found to be a better support compared to alumina for higher alcohols synthesis. However, activated carbon supported catalysts have a microporous structure that may result in transport limitation in the reaction. This can be avoided by using novel support such as, multiwalled carbon nanotubes (MWCNTs) which has meso/macroporous structures that may mitigate transport limitations. Also, their uniform, and

straight pores may allow great metal dispersion, high mechanical strength, and thermal conductivity.

The first step in developing a catalyst system that is highly active and selective for higher alcohols formation from CO hydrogenation is to determine the effective loadings of active metal, Mo and alkali promoter, K. The primary focus of this paper is to study the effects of various Mo and K contents on the catalytic performance of higher alcohols synthesis. The commercially available multi-walled carbon nanotubes (MWCNTs) were used as catalyst support. The effects of operating conditions such as temperature and pressure on higher alcohols reaction were also studied.

3.1. Abstract

An extensive study of higher alcohol synthesis from synthesis gas using potassium (K) promoted molybdenum sulfide supported on multi-walled carbon nanotubes (MWCNTs) catalysts is reported. Up to 20 wt % of Mo and 9 wt % of K are added to the MWCNTs by incipient wetness impregnation method. The catalysts are extensively characterized by different methods and the activity and selectivity of the catalysts are assessed in a fixed-bed micro-reactor. Increasing the amount of K from 3 to 9 wt % increased K–Mo–O interactions, decreased the Mo particle sizes from 20.6 to 12.2 nm and increased the percentage dispersion from 20.2 % to 30.9 %. Most of the metal particles (~80%) were homogeneously distributed inside the tubes and the rest on the outer surface of the MWCNTs. Temperature programmed reduction (TPR) tests showed that increasing the amount of Mo increased the first and second TPR peak temperatures from 516 and 765 to 530 and 835°C, respectively. However, addition of K decreased the peak temperatures from 534 and 825 to 519 and 787°C, respectively. DRIFT spectroscopy of absorbed CO was used to study the nature of active species in the sulfided form of catalysts. Addition of K increased the formation of alcohols and suppressed the formation of hydrocarbons. Catalyst 15 wt % Mo and 9 wt % K supported on MWCNTs showed the highest yield (0.11 g of total alcohol/(g of cat./h)) and selectivity (25.6%) towards alcohols. The optimum conditions for producing the higher alcohols from synthesis gas (mole ratio of H_2 and CO is equal to 2) using gas hourly space velocity (GHSV) of 3.6 m^3 (STP)/(kg of cat./h) are determined to be 320°C and 9.65 MPa (1400 psig).

3.2. Introduction

Synthesis of alcohols from synthesis gas remains an economically attractive method for making fuels and chemicals. Higher alcohol synthesis is of interest due to the increasing petroleum prices, environmental concerns, and gasoline octane additive demands.[1] Many researchers have developed several catalytic systems for higher alcohol synthesis through CO hydrogenation. Based on their research, the catalysts for higher alcohol synthesis are categorized into two groups:[2–8] one is to produce methanol and branched alcohols, such as modified methanol synthesis catalysts; the other is to form straight-chain alcohols, such as molybdenum sulfide catalysts and Co/Cu-based catalysts. Among them molybdenum based catalysts are more attractive due to their excellent resistance to sulfur poisoning and high activity for the water–gas shift reaction.[9]

Molybdenum disulfide (MoS_2) catalysts produce mainly hydrocarbons but, when promoted with alkali can produce alcohols from synthesis gas. The function of alkali is to reduce the hydrogenation ability of alkyl species to form alkanes, and increase the active sites for the formation of alcohols.[10] Jiang et al.[11] and Lee et al.[12] studied the effect of potassium promoter on alcohol synthesis over alkali modified molybdenum based catalysts. Iranmahboob et al.[13] studied the effects of K and Cs for synthesis of alcohols and found that the promotional effect of K was greater than Cs over Co-MoS_2/clay catalyst. The commercial alkali modified molybdenum based catalysts were first developed by Dow and Union Carbide companies to convert synthesis gas to alcohols.[14] The alcohol products over these catalyst systems are linear alcohols, and the mechanism for formation of higher alcohols ($C_{2+}OH$) was probably via a classical insertion of CO into the corresponding precursor alcohol. The activity and selectivity of these catalysts to $C_{2+}OH$ formation was low as the alcohols obtained over these catalysts follow Anderson–Schulz–Flory distribution.[15]

Supported metal catalysts are mainly of the interest for the reactions involving hydrogen as reactance or product. The use of multi-walled carbon nanotubes (MWCNTs) has been drawing attention, due to their flexibility as support in tailoring the catalyst properties to specific needs.[16,17] Carbon nanotubes possess similar properties to activated carbon such as resistant to acidic or basic media and stable at high temperatures in an inert atmosphere. Moreover, they have several unique features, such as, highly graphitized tube-walls, nanosized channels and sp^2-C-constructed surfaces. They also display exceptionally high

mechanical strength, high thermal and electrical conductivity, and medium to high specific surface areas, which render this kind of nano-structured carbon material full of promise as a novel catalyst/support.[18,19] Activated carbon has a microporous structure which may lead to transport limitations in the reaction. This can be minimized by using mesoporous structured carbon nanotubes.[20]

It is expected that the catalytic performance depends to a certain extent on the support used. Due to various advantages of MWCNTs as supports compared to catalysts supported on activated carbon, five different MWCNT-supported molybdenum based catalysts promoted with potassium by sequential pore volume impregnation (Mo loading varies from 10 to 20 wt % and K varies from 3 to 9 wt %) were prepared. These catalysts were then used as catalysts for the synthesis of mixed alcohols. The effects of active metal (Mo) and promoter (K) and reaction conditions such as temperature and pressure on the catalytic performance were studied as described below.

3.3. Experimental

3.3.1. Preparation of Mo-K/MWCNTs catalysts

MWCNTs (purity > 95%) obtained from M. K. Nano, Canada was used as a support for the preparation of the catalysts. Prior to impregnation the support was treated with 30% HNO_3 reflux at 100°C overnight, washed with distilled water several times and dried at 120 °C for 6 h. All the catalysts were prepared by the incipient wetness impregnation with aqueous solutions of $(NH_4)_6Mo_7O_{24}.4H_2O$ and K_2CO_3. First, the support was impregnated with an aqueous solution of K_2CO_3, followed by drying at 120°C for 2 h and stabilizing in an argon flow of 50 ml/min for 4 h at 300°C at a heating rate of 10°C/min. Then it was impregnated with Mo precursor, dried at 120°C for 2 h and stabilized in an argon flow of 50 ml/min for 12 h at 450°C at a heating rate of 10 °C/min. Five catalysts were prepared with three different levels of Mo (10, 15, and 20 wt %), fixing K at 6 wt % and three different levels of K (3, 6, and 9 wt %) with a fixed Mo at 15 wt %.

3.3.2. Characterization of Mo-K/MWCNTs catalysts

The molybdenum loadings of the stabilized catalysts were performed using PerkinElmer ELAN 5000 inductively coupled plasma-mass spectroscopy (ICP-MS) instrument.

A PerkinElmer TG/DTA thermo gravimetric differential thermal analyzer was used to measure weight changes of the sample when heated under a flow of argon (flow rate of 40 ml/min) at a constant heating rate of 10°C/min.

Surface area, pore volume and average pore diameter of catalysts and support were measured using an ASAP 2000 Micromeritics system. All the samples were degassed at 200°C for 2 h under 50 m torr vacuum and their BET area, pore volume, and pore diameter was determined.

The phases and particle sizes of the crystals present in support and all the catalysts were analyzed by XRD using a Rigaku X-ray diffractometer with a nickel filtered Cu Ka radiation, 2θ angles from 10° to 80° at a scanning speed of 0.05 °/s. The Debye–Scherer formula (d = 0.9l/bcosu, where b is FWHM, λ – wave length of X-ray, 0.9 – constant) was applied to MoO_3 at 2θ = 41.2°, in order to calculate the average particle size.

The morphology of the MWCNTs support and catalysts was characterized by transmission electron microscopy (TEM). Sample specimens for TEM studies were prepared by ultrasonic dispersion of the catalysts in ethanol, and the suspensions were dropped onto a carbon-coated copper grid. TEM investigations were carried out using a Philips CM20 (100 kV) transmission electron microscope equipped with a NARON energy-dispersive spectrometer with a germanium detector.

The H_2-TPR profiles of the catalysts were performed in order to study the reducibility of the metal species in the catalysts. The stabilized catalyst sample (0.2 g) was first purged in a flow of argon at 170°C to remove traces of water, and then cooled to 40 °C. Then the TPR of each sample was performed using 3.1% H_2 in He stream at a flow rate of 30 ml/min at atmospheric pressure using CHEMBET 3000 TPD-TPR analyzer equipped with a thermal conductivity detector, heating at a linearly programmed rate of 10 °C/min up to 850°C.

The amount of chemisorbed hydrogen was measured using the CHEMBET 3000 TPD-TPR analyzer system. The stabilized catalyst sample (0.2 g) was first purged in a flow of argon at 170°C to remove traces of water. The temperature was then raised to 500°C at a linearly programmed rate of 10°C/min and catalyst was reduced for 12 h under hydrogen flow and then cooled to 100°C. Then the flow of hydrogen was switched to argon for 30 min in order to remove the weakly adsorbed hydrogen. Afterwards the temperature programmed

desorption (TPD) of the samples was performed by increasing the temperature of the samples, with a ramp rate of 10 °C/min, to 500°C under the argon flow. The TPD spectrum was used to determine the molybdenum dispersion and its surface average crystallite size. The system was initially calibrated with Ag_2O. The area under the peak which is proportional to the H_2 consumption is used to determine the number of Mo atoms on the surface. The % dispersion of Mo can be calculated from eq. (3.1) as given below.[21] If the % dispersion is less than 20%, eq. (3.2) is used to calculate particle diameter (d_p). eq. (3.3) is used if the % dispersion is in between 20% and 92%.[22]

$$\% \, Dispersion = \frac{No. \, of \, Mo \, atoms \, on \, surface}{No. \, of \, Mo \, atoms \, in \, sample} * 100 \qquad (3.1)$$

$$d_p = \frac{5.01}{(dispersion)} \qquad for \; dispersion < 0.2 \qquad (3.2)$$

$$d_p = \frac{3.32}{(dispersion)^{1.23}} \qquad for \; 0.2 < dispersion < 0.92 \qquad (3.3)$$

Diffuse reflectance infrared Fourier transform spectroscopy (DRIFTS) of carbon monoxide adsorption experiments were performed using a PerkinElmer Spectrum GX instrument equipped with DTGS detector and a KBr beam splitter. Approximately 10 mg of powdered catalyst was placed in the sample cup inside a Spectrotech diffuse reflectance in situ cell equipped with ZnSe windows and a thermocouple which allows the direct measurement of the sample surface temperature. Spectra for each experiment were averaged over 128 scans in the region 3000–1000 cm^{-1} with a nominal 4 cm^{-1} resolution. Prior to the CO adsorption, the catalyst was in situ sulfided using 10% (v/v) H_2S/H_2 (30 ml/min) at 400°C for 4 h. After sulfidation, the flow was switched to He (30 ml/min), the temperature was decreased to 35°C and then the background spectrum was recorded. The CO adsorption process was carried out at 35°C by introducing pure CO (30 ml/min) into the sample cell for 30 min for saturation of adsorption. After adsorption, the system was subsequently purged with He (30 ml/min) for 30 min to remove the physically adsorbed CO molecules. Then the spectra were collected under He flow and the background spectrum was subtracted from the post-adsorption spectra.

3.3.3. Catalytic studies

Higher alcohol synthesis (HAS) were performed in a tubular down flow, fixed-bed reactor system. The reactor was made up of inconel tube of 450-mm length and 22-mm inside diameter. The reactor was packed with 2 g of catalyst diluted with 90 mesh size silicon carbide and housed in an electric furnace controlled by a temperature controller. The reactor was pressurized to 3.44 MPa (500 psig) with He and the sulfidation as well as the reduction was carried out for 6 h at 450°C at a heating rate of 2 °C/min using gas mixture containing 10 mole % H_2S in H_2 and flow rate of 50 ml/min. The temperature was then lowered to the reaction temperature, and the system was then pressurized to the reaction condition. The feed gas mixture (CO (30 mole %), H_2 (60 mole %), and Ar (10 mole %)) was passed through mass flow controllers and the HAS reaction was carried out at steady state under the reaction conditions of 290–340°C, 4.143–9.65 MPa (600–1400 psig), and gas hourly space velocity of 3.6 m^3 (STP)/(kg of cat.)/h over a period of 24 h. The product gas was cooled to 0°C and separated into gas and liquid phases at the reaction pressure. The CO conversion and other gaseous products were monitored with a time interval of 1 h. The liquid products were collected after completion of the run and analyzed with a Varian 3400 gas chromatograph equipped with

capillary column and FID. The volume and weight of liquid products were measured to check the mass balance. The gaseous products were analyzed online on a Shimadzu chromatograph through a sampling valve. Using Ar as internal standard, the CO conversion was calculated and the overall mass balance of the reaction was calculated. The error of the total mass balance and carbon mass balance around the reactor was within ± 2.5%.

3.4. Results and Discussion

3.4.1. Characterization of Mo-K/MWCNTs catalysts

The elemental compositions of calcined Mo-K/MWCNTs catalysts measured by ICP-MS are given in Table 3.1 along with the targeted compositions. The measured Mo contents of the prepared catalysts are found to be slightly lower compared to targeted values. The discrepancies may be due to incomplete impregnation of Mo from the solution to the support, because of the hygroscopic nature of the Mo precursor (ammonium hepta molybdate tetrahydrate).

Table 3.1. The chemical compositions and textural properties of MWCNT-supported Mo-K catalysts

Catalyst	Targeted composition (wt %)		Measured composition (wt %)	BET surface area (m^2/g)	Total pore volume (cc/g)	Average pore diameter (Å)
	K	Mo	Mo			
Fresh CNT	--	--	--	178	0.54	122
30% HNO_3 Treated CNT	--	--	--	220	0.66	109
10Mo6KCNT	6	10	9.4	117	0.47	152
15Mo6KCNT	6	15	14.1	98	0.40	159
20Mo6KCNT	6	20	18.4	95	0.36	167
15Mo3kCNT	3	15	14.1	106	0.44	157
15Mo9KCNT	9	15	14.1	96	0.37	163

The typical N_2 adsorption–desorption isotherm of all the catalysts were measured with an aim to measure the total surface area. The typical isotherms for catalysts 10Mo6KCNT and 15Mo6KCNT are given in Figs. 3.1a and 3.1b, respectively. All the catalysts showed Type IV isotherm, which is characteristic of mesoporous adsorbents with strong affinity. The textural characteristics of the prepared catalysts are given in Table 3.1. The total BET surface area and pore volume values of all the catalysts are found to be much lower compared to those of pure support. A drastic decrease in surface area after impregnating with metal species is observed, which is likely due to pore blockage of the support.

The TGA technique was used to find the stabilization temperature of the impregnated catalysts. Figs. 3.2a and 3.2b shows the results of TGA for 6 wt % K on MWCNTs and 10 wt % Mo 6 wt % K on MWCNTs supports, respectively. It is clear from Fig. 3.2a, that the rapid weight loss for K loaded MWCNTs starts below 200°C and continued up to a temperature of 300°C. So, the stabilization temperature of the dried K loaded MWCNTs catalysts was determined as 300°C to remove the displaceable water and counter ions present in the catalyst. From Fig. 3.2b, the stabilization temperature of the dried Mo loaded K/MWCNTs catalysts was determined as 500°C.

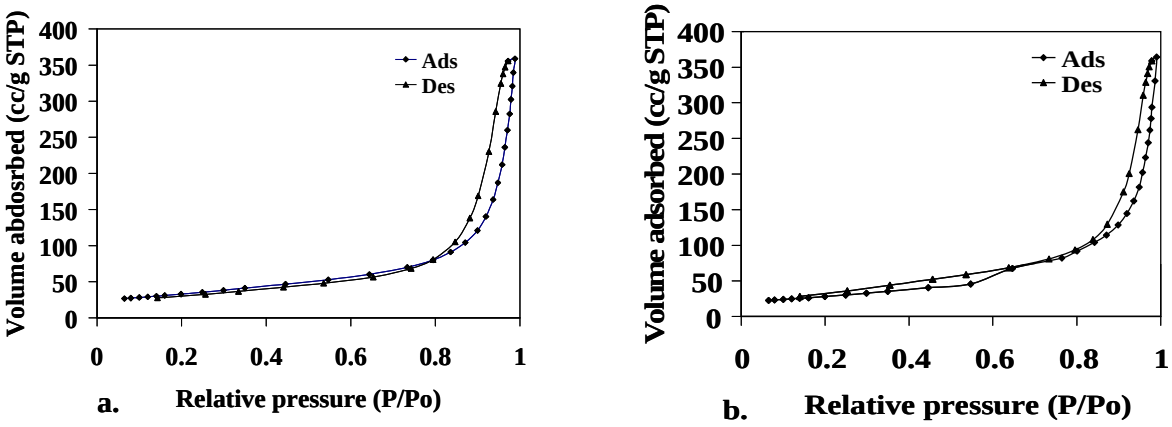

Figure 3.1. N_2 adsorption-desorption isotherms of catalyst a. 10Mo6KCNT; and b. 15Mo6KCNT

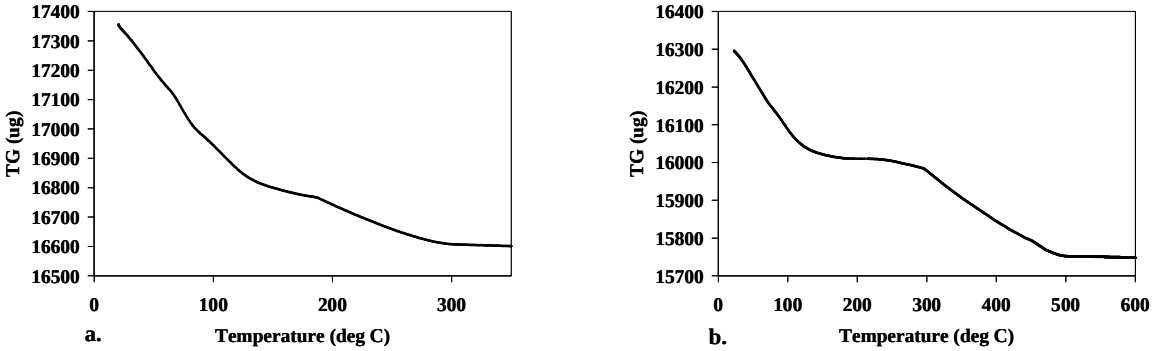

Figure 3.2. Thermogravimetric analysis of catalysts a. 6KCNT; and b. 10Mo6KCNT

The XRD patterns of the acid treated MWCNTs support and the stabilized catalysts supported on MWCNTs containing 6 wt % K with varying Mo loadings and 15 wt % Mo with varying K loadings are compared in Figs. 3.3a and 3.3b, respectively. The peaks marked as 1, 2 and 3 in Figs. 3.3a and 3.3b correspond to the crystalline structure of graphitic carbon, MoO_3, and mixed K–Mo oxide species representing $K_2Mo_2O_7$. These generated peaks are matched with the corresponding peaks using the JCPDS chemical spectra data bank.[23,24] When Mo loading increases from 10 to 20 wt %, the corresponding MoO_3 peaks (2θ = 41.3°, 60.2°) appear more significantly, indicating the grown particle size of the MoO_3 at higher metal loadings.

At a fixed Mo loading of 15 wt %, the intensities of peaks for MoO_3 decreased significantly when K loading increased from 3 to 9 wt %. This indicates the fact that Mo dispersion increases with the addition of K species, leading to smaller particles resulting a decrease in intensity of XRD peaks for MoO_3 species. The peaks (2θ = 20.6°, 25.7°, 31.2°) with weak intensities corresponding to $K_2Mo_2O_7$ species are observed for the sample with a K loading of 3 wt % and when K loading is increased to 9 wt %, the intensities of these peaks are very significant. This implies that with increased K loading, the chemical interactions between K–Mo–O species are increased, enhancing the conditions for the formation of alcohols.[25]

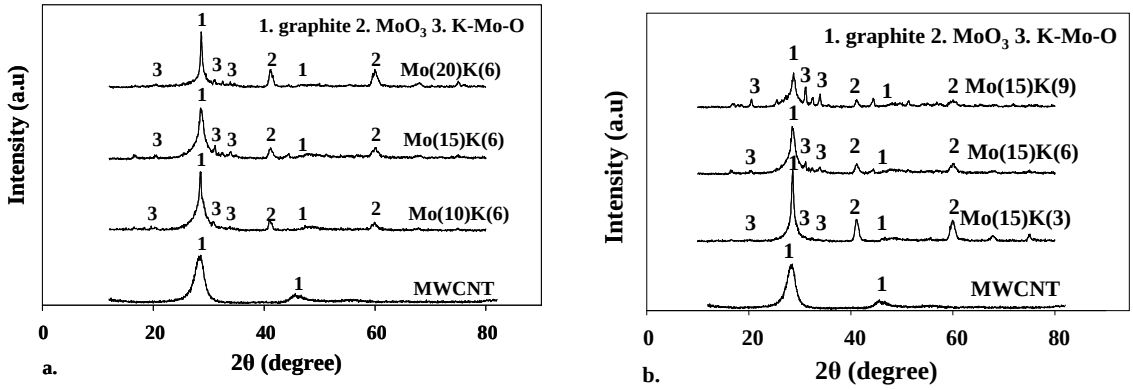

Figure 3.3. XRD patterns of support and catalysts with varying a. Mo content; and b. K content

Table 3.2 shows the average MoO_3 particle size and the full width at half maximum values (FWHM) of all the catalysts calculated from the XRD spectrum, using the Debye–Scherer formula at 2θ = 41.3°. It is clear that with increase in Mo loading from 10 to 20 wt % on MWCNT-supported catalysts with 6 wt % K the FWHM values decreased from 0.838 to 0.488 whereas the crystal diameter of MoO_3 increased from 10.1 to 26.5 nm. Increased K loading from 3 to 9 wt % on catalysts with 15 wt % Mo supported on MWCNTs increased the FWHM values from 0.418 to 0.688 and decreased the crystal diameter of MoO_3 from 20.6 to 12.2 nm, which confirms the increased dispersion with an increased K loading.

Table 3.2. Crystallite sizes of Mo based on H_2 temperatures programmed desorption and XRD data

Catalyst	μ mole H_2 desorbed/ (g of cat.)	% Dispersion	D_P (nm) (H_2 - TPD)	D_P (nm) (XRD)	FWHM (XRD)
10Mo6KCNT	49.0	34.5	12.3	10.1	0.83^o
15Mo6KCNT	58.6	23.3	19.9	17.4	0.48^o
20Mo6KCNT	50.7	16.6	30.2	26.5	0.32^o
15Mo3kCNT	47.9	20.2	23.7	20.6	0.41^o
15Mo9KCNT	63.9	30.9	14.1	12.2	0.68^o

Fig. 3.4a represents the sample of the purified MWCNTs material analyzed by TEM. The purified product is comprised of an interwoven matrix of MWCNTs. The TEM image of 10 wt % Mo, 6 wt % K supported on MWCNTs catalyst is shown is Fig. 3.4b. Most of the Mo particles (~80%) are well distributed inside the tubes and remaining (20%) on the outside of the tube-walls. The particles inside the tubes are fairly uniform and the most abundant ones are 6–10 nm in size in accordance with the average inner diameter of the CNTs, whereas those on the outer surface are about 10–30 nm.

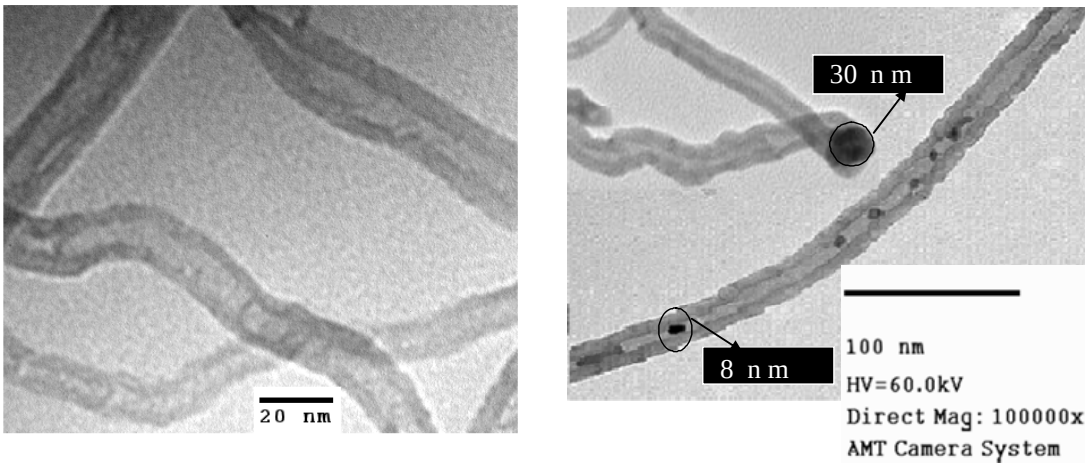

Figure 3.4. TEM image a. Purified MWCNTs; and b. 10Mo6KCNT

The stabilized catalysts were characterized by TPR in order to obtain the reduction behavior of oxidized phases. Figs. 3.5a and b shows the H_2 consumption profiles of the MWCNTs supported catalysts containing (1) varying Mo loadings on 6 wt % K and (2) 15 wt % of Mo with varying loadings of K as a function of temperature.

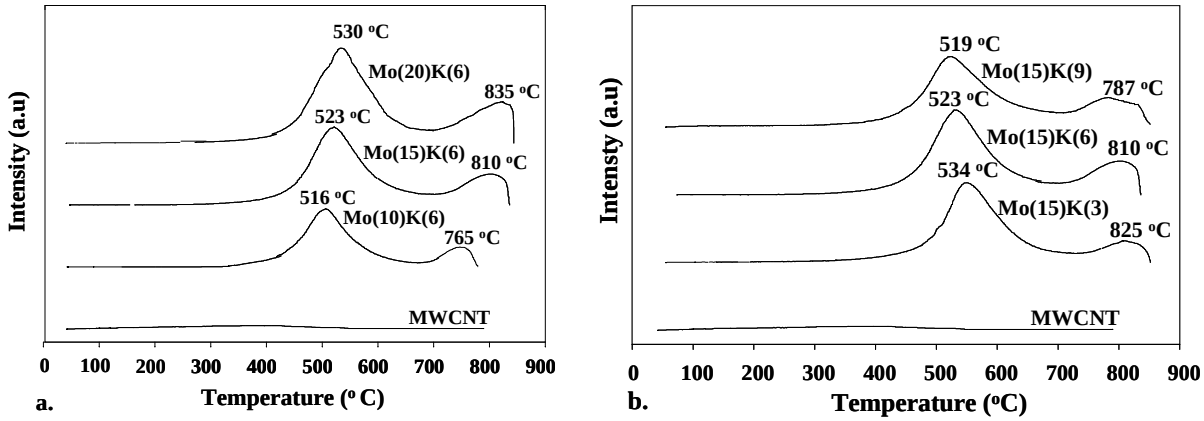

Figure 3.5. H_2-TPR profiles of support and catalysts with varying a. Mo content; and b. K content

The TPR profiles showed typical patterns for the reduction of Mo species from Mo^{6+} to Mo^{4+} in the first step (in the temperature range of 450–650°C) and Mo^{4+} lower oxidation state (Mo^0) in the second step (>700°C), as explained in the literature.[26-28] When Mo loading was varied from 10 to 20 wt %, the position of the peak corresponding to the first step reduction shifted from 516 to 530°C, whereas the broad peak corresponding to reduction of lower oxidation state at higher temperature shifted from 765 to 835°C, indicating that increased Mo addition inhibited the reduction of catalysts supported on MWCNTs in dilute hydrogen.[29]

With increased K loading from 3 to 9 wt %, the maximum temperature for the reduction of Mo^{6+} to Mo^{4+} was found to shift to lower temperature. This is due to the fact that increased K loading promoted the formation of Mo species that are reducible at lower temperatures. That indicates that increased K loadings lead to ease reduction of Mo in the catalyst to Mo species with intermediate valence value by preventing the further reduction of Mo. This reduction behavior with increased loading of K catalyst may be due to change in interaction between the active Mo components and the support.[30]

All the stabilized catalysts were characterized for hydrogen chemisorption tests and the results are given in Table 3.2. Increased Mo loading from 10 to 15 wt % increased the hydrogen uptake and decreased when the Mo loading is further increased to 20 wt %. This shows that some of the pores are blocked by increasing the Mo content form 15 to 20 wt %.

It is clear from the results that increasing Mo loading decreased the % dispersion, while increased the particle diameter, which is in agreement with the results from other characterization techniques. The dispersion of the Mo crystallites increased and the average Mo cluster size decreased when K loading increased from 3 to 9 wt %, which is due to interaction of Mo and K and production of mixed oxides of Mo-K. This mixed oxide formation can decrease the MoO_3 particle size. Higher dispersion and small molybdenum cluster size will increase the number of sites available for alcohol synthesis reaction in MWCNT supported catalysts. Since the catalyst with 15 wt % Mo and 9 wt % K has higher H_2 uptake, it is expected that this catalysts will have more activity.

The nature of catalyst species in the sulfided form of catalysts was studied by DRIFT spectroscopy of CO adsorbed catalysts. The typical DRIFT bands for all the catalysts are shown in Fig. 3.6.

The 15 wt % Mo catalyst is prepared in order to distinguish by spectra from the MoS_2 bands with K promoted Mo catalysts. CO adsorption on the sulfided 15 wt % Mo supported on MWCNTs catalyst yields two bands one at 2095 and other at 2058 cm^{-1} due to the adsorption of CO on the MoS_2-like species. The band at 2095 cm^{-1} corresponds to CO adsorption on partly reduced Mo centers that have Mo^{5+} atoms. The band at 2058 cm^{-1} is due to much reduced Mo atoms, like Mo^{4+} atoms.[45] All the catalysts that are promoted with K showed little absorbance compared to un-promoted Mo catalyst. This may be due to the fact that K atoms occupied MoS_2 species thus preventing CO adsorption.

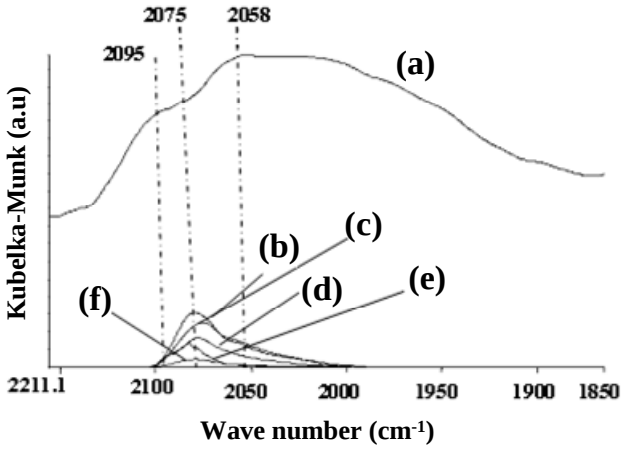

Figure 3.6. DRIFT spectra of adsorbed CO on sulfided catalysts

a.15MoCNT; b. 15Mo3KCNT; c. 20Mo6KCNT; d. 15Mo6KCNT; e. 10Mo6KCNT; f. 15Mo9KCNT

3.4.2. Catalytic studies for higher alcohol synthesis

The higher alcohol synthesis reaction was carried out after reduction and sulfidation in a fixed-bed reactor at 310 °C under the pressure of 6.89 MPa (1000 psig), 3.6 m^3 (STP)/ (kg of cat.)/h to understand the effects of active metal (Mo) and alkali promoter (K). The liquid products were collected at 0 °C and the exit gas was analyzed to measure the CO conversion.

The analysis of liquid products indicates that the alcohols likely followed the CO-insertion mechanism, forming linear alcohols. Methanol, ethanol, and n-propanol are the major products together with small amounts of n-butanol and other higher alcohols. The analysis of exit gas indicates that methane is the major component apart from CO, H_2 and CO_2. All the experiments were repeated two times to check the reproducibility and confirmed that the results obtained are within the experimental error of ± 2.5%.

Fig. 3.7 represents the CO conversion as time-on-stream during higher alcohol synthesis using catalyst 15 wt % Mo and 9 wt % K supported on MWCNTs at 320 °C and 9.65 MPa. It is seen that during 24 h of alcohol synthesis, the CO conversion sharply reduced in the first 12 h, and then levels off. This indicates that the catalyst is quite stable over 12–24 h of time-on-stream.

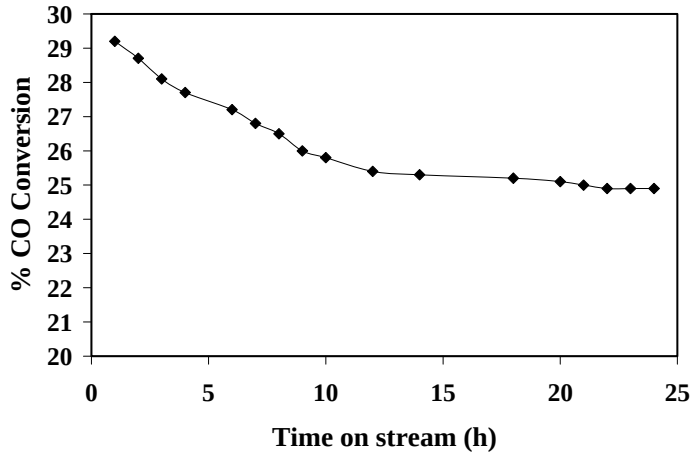

Figure 3.7. % CO Conversion with time-on-stream

(Cat. - 15Mo9KCNT = 2 g, T = 320 °C P = 1400 psig, GHSV = 3.6 m^3 (STP)/(kg of cat.)/h, H_2 to CO molar ratio = 2)

Effects of active metal

% CO conversions, activity and selectivity of the catalysts towards products, with increasing Mo loadings on the catalysts containing 6 wt % supported on MWCNTs are presented in Figs. 3.8a, 3.8b and 3.8c, respectively. The CO conversion increased monotonically with increase in Mo loading and the catalyst with 20 wt % Mo and 6 wt % K showed the highest CO conversion of 25.7%. This is due to improved activity for hydrogenation reaction with increase in Mo wt % in the catalyst.[31] When compared to the catalysts containing 6 wt % K, the catalyst with 15 wt % Mo showed higher activity and selectivity towards alcohol synthesis. On increasing Mo content from 10 to 15 wt %, the total alcohol space time yield (STY) is increased from 0.042 to 0.088 g of total alcohol/(g of cat.)/h and slightly decreased to a value of 0.08 g/(g of cat.)/h upon increasing Mo loading to 20 wt %.

It is clear from H_2 chemisorption studies that the catalyst with 20 wt % Mo has a larger MoO_3 crystal diameter compared to other catalysts causing the pore blockage of the support. The STY and selectivity of hydrocarbons monotonically increased; where as the selectivity towards water–gas shift reaction is decreased monotonically with increase in Mo loading, confirming the methanation ability of Mo-based catalysts.[32] Fig. 3.8d shows the selectivity trends of individual alcohols with increased Mo loadings. The maximum higher

alcohol selectivity of 9% is observed over the catalyst with 15 wt % Mo content. The reason may be better explained from the XRD and TPD characterizations with varying Mo content. It is clear from XRD and TPD that the catalyst with 20 wt % Mo showed large MoO_3 particle size, which is responsible for poor activity of the catalyst towards the formation of higher alcohols.

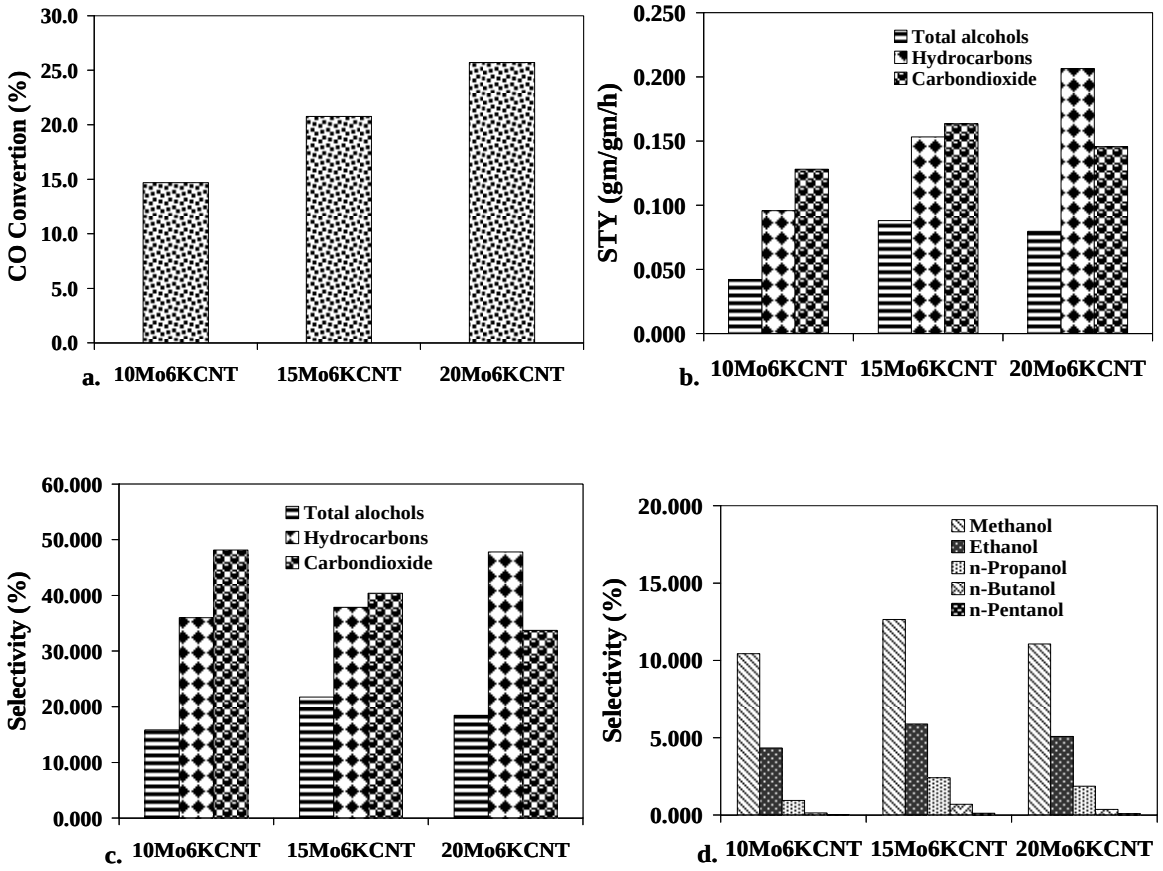

Figure 3.8. Catalytic performance of sulfided Mo-K/MWCNT catalysts with varying Mo content

a. % CO converted; b. Space time yield of products; c. Selectivity of products; and d. Selectivity of alcohols

(Catalyst = 2 g, P = 1000 psig, T = 310 °C, GHSV = 3.6 m^3 (STP)/(kg of cat.)/h H_2 to CO molar ratio = 2)

Effect of alkali

The promotional effect of alkali is studied over the catalysts with Mo loading of 15 wt % supported on MWCNTs. Fig. 3.9a, 3.9b, 3.9c, and 3.9d shows the influence of K loadings on % CO conversion, activity of products, selectivity of products and selectivity of methanol and higher alcohols, respectively. The % CO conversion decreased slightly from 21.6 to 20.4% when wt % of K is increased from 3 to 9, which is due to decreased availability of MoS_2 sites that are responsible for H_2 activation.[33] The total alcohol production rate increased from 0.059 to 0.1 g of total alcohol/(g of cat.)/h. The water–gas shift reaction rate increased slightly, whereas the total hydrocarbons production rate decreased from 0.189 to 0.137 g of total hydrocarbon/(g of cat.)/h, when K content in the catalyst is raised from 3 to 9 wt%. The selectivity of total alcohols increased from 15.2 to 24.2% with increase in K content. It is clear from the XRD results that increased K loading increased the intensity of the peaks corresponding to K–Mo–O interactions and decreased the intensity of the peaks corresponding to molybdenum oxides.

Santiesteban et al.[34] suggested the detailed mechanism for synthesis of higher alcohol over MoS_2 catalysts. This reaction scheme can be simplified as shown below:

$$CO + 2H_2 \leftrightarrow CH_3OH \quad (3.4)$$

$$CH_3OH + H_2 \rightarrow CH_4 + H_2O \quad (3.5)$$

$$CH_3OH + CO + 2H_2 \rightarrow C_2H_5OH + H_2O \quad (3.6)$$

$$C_2H_5OH + CO + 2H_2 \rightarrow C_3H_7OH + H_2O \quad (3.7)$$

$$CO + H_2O \leftrightarrow CO_2 + H_2 \quad (3.8)$$

In this reaction scheme the reactions representing with eqs. (3.4) and (3.8) are reversible. All subsequent reactions proceed mainly via a CO-insertion mechanism and are assumed to be irreversible. Reaction (3.8), the water–gas shift reaction is assumed to be in thermodynamic equilibrium. Methane is the main hydrocarbon obtained in the products and all the alcohols obtained are mainly linear alcohols. According to Xie et al.[35], the interactions between the surface species, $Mo^{6+,}$ K^+, S_2^{-2}, and O^{2-} are responsible for increasing the alcohol formation rate over the alkali modified MoS_2 catalysts. It has been confirmed from XRD results that increased K loading from 3 to 9 wt % clearly increased K–Mo interactions and these interactions are responsible for the formation of ethanol, propanol and other higher alcohols via a CO-insertion mechanism (reactions (3.6) and (3.7)). From these results, we can

say that formation of alcohols are greatly promoted by K doping, which can be due to increased amounts of the sulfided K–Mo interaction species resulting from the precursor of oxidic K–Mo interaction species.[11] The decrease in hydrocarbon formation rate is observed with increased K content, which may be due to decreased availability of hydrogenation active centers, i.e., MoS_2 species.[36]

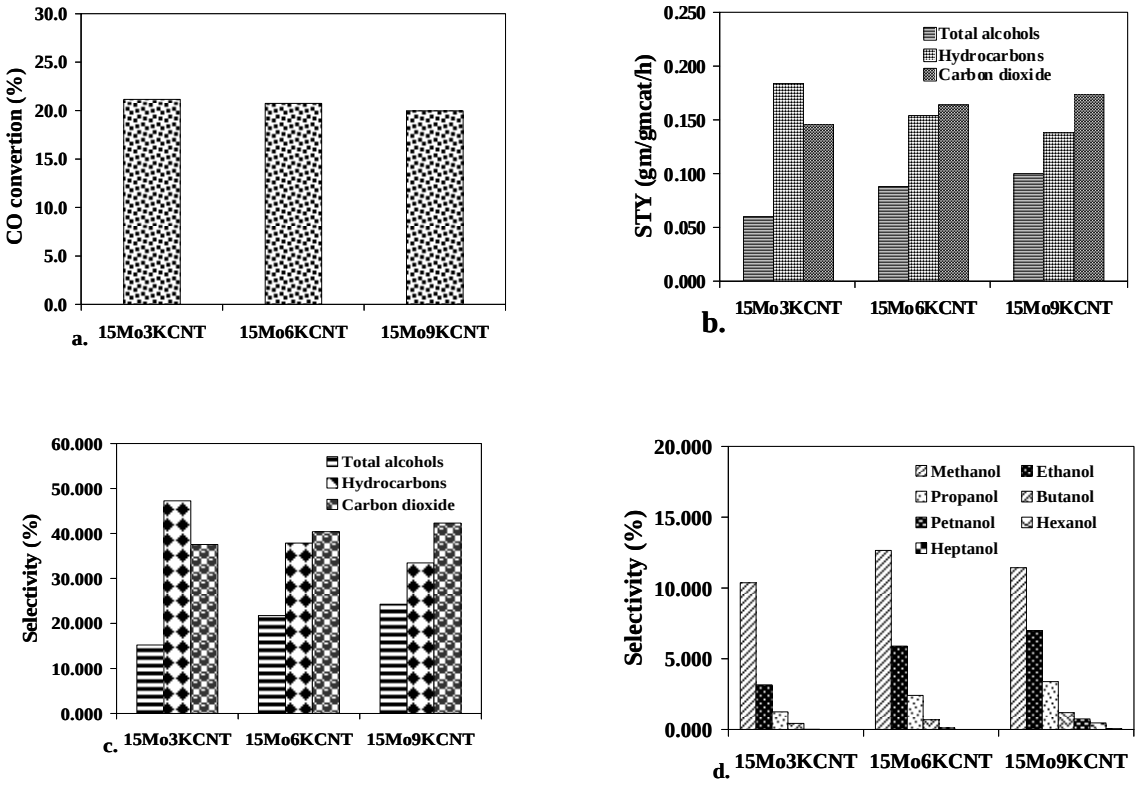

Figure 3.9. Catalytic performance of sulfided Mo-K/MWCNT catalysts with varying K content

a. % CO converted; b. Space time yield of products; c. Selectivity of products; and d. Selectivity of alcohols

(Cat. = 2 g, P = 1000 psig, T = 310 ^oC, GHSV = 3.6 m^3 (STP)/(kg of cat.)/h H_2 to CO molar ratio = 2)

There is a controversy in the available literature about the influence of alkali on CO_2 selectivity over reduced alkali modified Mo-based catalysts for alcohol synthesis. Tatsumi et al.[37] reported that CO_2 selectivity decreases with an increasing K/Mo molar ratio, where as, Liu et al.[38] claimed that CO_2 molar selectivity increases with increasing K/Mo molar ratio. The CO_2 selectivity from our results indicated that there is slight increase from

37 to 42%, when the K loading is increased from 3 to 9 wt % over sulfided Mo catalysts supported on MWCNTs. From Fig. 3.9d, it is clear that increasing K doping promotes the formation of higher alcohols, especially ethanol and propanol due to increasing the number of CO activating centers. A maximum in the selectivity of methanol is observed with increasing K loading. Also, the selectivity of higher alcohols increased from 4.8 to 12.3% when K content is increased from 3 to 9 wt %. Butanol is the highest carbon number alcohol observed over the catalyst with 3 wt % K content, whereas, higher alcohols, such as hexanol and heptanol are also observed along with other alcohols when K content is increased to 9 wt %. This confirms that the added alkali-metal promoters acted to increase the chain-growth probability as well as to promote the formation of oxygenates.

The change in higher alcohols selectivity (wt %) with CO conversion obtained over different K-modified MoS_2 catalysts are represented as Fig 3.10. It is observed from this figure that the catalyst with 15 wt % Mo showed the higher alcohols selectivity even though the % CO conversion is less compared to that of the catalyst with 20 wt % Mo. With increased K content, the selectivity of higher alcohols increased at almost constant CO conversion.

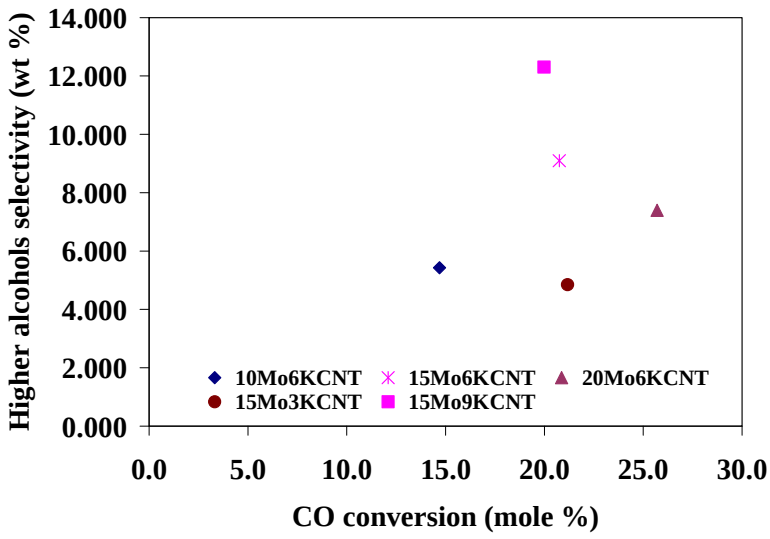

Figure 3.10. Change in higher alcohols selectivity with % CO conversion

(Cat. = 2 g, P = 1000 psig, T = 310 °C, GHSV = 3.6 m^3 (STP)/(kg of cat.)/h H_2 to CO molar ratio = 2)

Effect of temperature

The catalyst with 15 wt % Mo 9 wt % K supported on MWCNTs is used to study the temperature effect from 290 to 340°C on higher alcohol synthesis and the reactions were performed using the pressure and GHSV as 1000 psig and 3.6 m^3 (STP)/(kg of cat.)/h, respectively. It can be observed from Fig. 3.11a, that CO conversion and hydrocarbon space time yield increased monotonically with temperature. The rate of formation of alcohols was more favorable when temperature was increased from 290 to 320°C. When the temperature was raised beyond 320°C, the maximum yield of alcohol was not consistent with CO conversion due to the high selectivity to hydrocarbon.

From Fig. 3.11b, it is clear that, the hydrocarbon selectivity decreased monotonically, whereas selectivity towards water–gas shift reaction increased with increasing temperature. The total alcohols and higher alcohols selectivity displayed pronounced increases, reaching maximum of about 25.6 and 14.3% respectively, at the expense of the selectivity to hydrocarbons. The molar ratio of higher alcohols to methanol increases significantly with increasing temperature, confirming the increased promotional ability of alkali towards selective formation of higher alcohols at higher temperatures.[38]

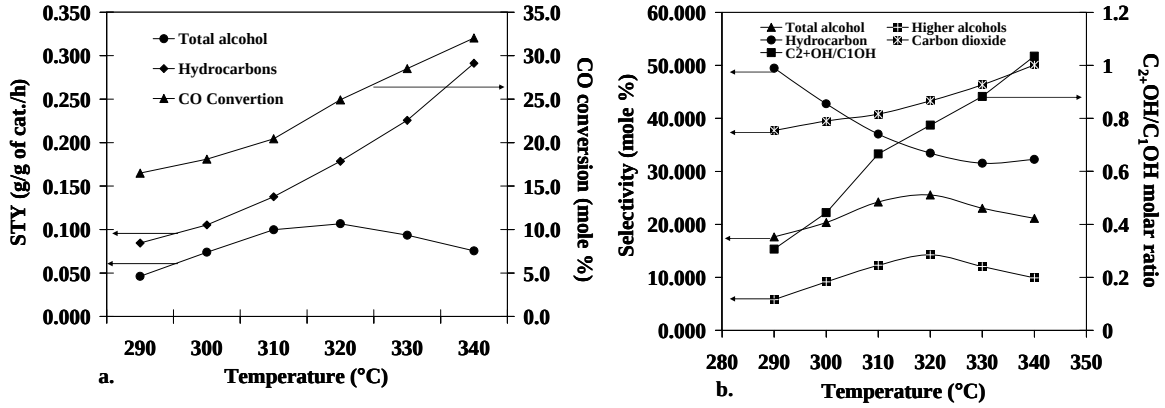

Figure 3.11. Catalytic performance of sulfided Mo-K/MWCNT catalysts with temperature

(Cat. - 15Mo9KCNT = 2 g, P =1000 psig, GHSV = 3.6 m^3 (STP)/(kg of cat.)/h H_2 to CO molar ratio = 2)

Effect of pressure

In order to study the effect of pressure, the performances of CO hydrogenation to higher alcohols synthesis reaction were investigated within the pressure range of 4.14–9.65 MPa (600–1400 psig) over 15 wt % Mo 9 wt % K supported on MWCNTs, using a temperature of 310°C and GHSV of 3.6 m^3 (STP) /(kg of cat.)/h From Fig. 3.12a and 3.12b, it is observed that increased pressure monotonically increased the % CO conversion, total alcohol formation rate, and hydrocarbon formation rate. It is also noted that as pressure increased the selectivity of higher alcohols increased, whereas selectivity of hydrocarbons and carbon dioxide decreased and the molar ratio of $C_{2+}OH/C_1OH$ increased. Based on the reaction mechanism discussed in the last sections and Le-Chatelier's principal increasing the pressure will shift the reaction (3.4) to the right hand side. This will in turn increase the formation of methanol as well as the higher alcohols. Our results are in agreement with the literature indicating that increasing the pressure at constant temperature favors the formation of higher alcohols.[39,40]

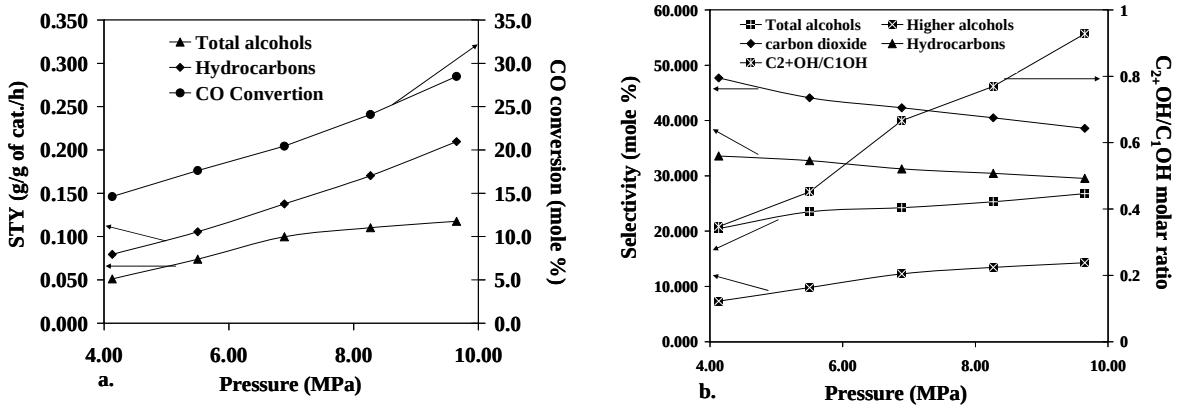

Figure 3.12. Catalytic performance of sulfided Mo-K/MWCNT catalysts with pressure

(Cat.- 15Mo9KCNT = 2 g, T = 310 °C, GHSV = 3.6 m^3 (STP)/(kg of cat.)/h H_2 to CO molar ratio = 2)

3.4.3. Comparison of the activities of sulfided Mo-K catalysts

Table 3.3 compares the activities of sulfided 15 wt % Mo 9 wt % K (catalyst E) supported on MWCNTs with those of similar catalysts available in the literature. The catalysts with highest activity from each work were selected for comparison purpose. The authors (Woo et al.[41]) have indicated that the catalyst A, which is unsupported sulfided Mo-K, showed negligible activity. Catalyst E is 18 times more active than catalyst B which is supported on SiO_2. Catalyst C, prepared using ultra sonic technology and Cat E showed similar activity. This data indicate that the sulfided Mo-K catalysts supported on MWCNTs perform well compared to those in the literature.

Table 3.3. Comparison of the activities of sulfided Mo-K catalysts

Sample	A	B	C	D	E
Catalyst	Mo-K	Mo-K/SiO_2	Mo-K/AC**	Mo-K/AC	Mo-K/MWCNTs
Temp. (K)	300	773	573	593	593
H_2/CO molar ratio	1.0	1.0	2.0	1.0	2.0
Pressure (MPa)	1.5	1.6	8.0	8.0	9.65
CO conversion (%)	12.6	8.2	11.43	22.49	32.9
STY of alc. (g/(g of cat./h))	90 %*	0.006	0.11	0.12***	0.11

* Activity was normalized for an initial activity of 100%; ** Ultrasonic preparation of the catalyst; *** The units of STY is g of alc./(ml of cat./h) (A) Woo et al.[41]; (B) Muramatsu et al.[42]; (C) Li et al.[43]; (D)Li et al.[44]; (E) Sulfided 15 wt % Mo 9 wt % K/MWCNTs.

3.5. Conclusions

Potassium promoted molybdenum sulfide supported on multi-wall carbon nanotubes catalysts is used to produce higher alcohols from synthesis gas. From several TEM results it was found that around 80% of the Mo particles were uniformly distributed inside the tubes and the rest were on the outside of the tubes. Addition of K to the Mo/MWCNT catalyst increases K–Mo–O interactions, decreases the Mo particle sizes and increases the percentage dispersion. Increasing the amount of Mo shifts the TPR peak to higher temperatures while addition of K promoted the reducibility of the catalysts. DRIFT spectroscopy of absorbed CO is used to study the nature of active species in the sulfided form of catalysts. The catalysts that are promoted with K showed little adsorption compared to the un-promoted Mo catalyst. Catalyst 15 wt % Mo and 9 wt % K supported on MWCNTs showed the highest yield (0.11 g of total alcohol/(g of cat.)/h) and selectivity (25.6%)

towards alcohols. The optimum conditions for producing the higher alcohols from synthesis gas (mole ratio of H_2 and CO is equal to 2) using gas hourly space velocity of 3.6 m^3 (STP)/(kg of cat.)/h were determined as 320°C and 9.65 MPa (1400 psig).

3.6. Abbreviations

GHSV	Gas hourly space velocity
HAS	Higher alcohol synthesis
ICP-MS	Inductively coupled plasma – mass spectroscopy
MWCNTs	Multi-walled carbon nanotubes
STY	Space time yield
TEM	Transmission electron microscopy
TGA	Thermo gravimetric analysis
TPD	Temperature programmed desorption
TPR	Temperature programmed reduction
XRD	X-ray diffraction

3.7. References

1. Herman, R. *Studies in Surface and Catalyst*, 7th Chapter, Elsevier: Amsterdam, 1990.
2. Forzatti, P.; Tronconi, E.; Pasquon, I. Higher Alcohol Synthesis. Catal. *Rev. Sci. Eng.* **1991**, *33*, 109–168.
3. Dalmon, J. A.; Chaumette, P.; Mirodatos, C. Higher alcohols synthesis on cobalt based model catalysts. *Catal. Today* **1992**, *15*, 101–127.
4. Smith, K. J.; Anderson, R. B. A chain growth scheme for the higher alcohols synthesis. *J. Catal.* **1984**, *85*, 428–436.
5. Camposmartin, J. M.; Guerreroruiz, A.; Fierro, J. L. G. Structural and surface properties of CuO-ZnO-Cr_2O_3 catalysts and their relationship with selectivity to higher alcohol synthesis. *J. Catal.* **1995**, *156*, 208–218.
6. Boz, I.; Sahibzada, M.; Metcalfe, I. S. Kinetics of the higher alcohol synthesis over a K-promoted CuO/ZnO/Al2O3 catalyst. *Ind. Eng. Chem. Res.* **1994**, *33*, 2021–2028.

7. Xu, X.; Doesburg, E. B. M.; Scholten, J. J. F. Synthesis of higher alcohols from syngas - recently patented catalysts and tentative ideas on the mechanism. *Catal. Today* **1987**, *2*, 125–170.
8. Sheffer, G. R.; Jacobson, R. A.; King, T. S. Chemical nature of alkali-promoted copper-cobalt-chromium oxide higher alcohol catalysts. *J. Catal.* **1989**, *116*, 95–107.
9. Woo, H. C.; Park, K. Y. Mixed alcohols synthesis from carbon monoxide and dihydrogen over potassium-promoted molybdenum carbide catalysts. *Appl. Catal., A* **1991**, *75*, 267–280.
10. Tatsumi, T.; Muramatsu, A.; Yokota, K.; Tominga, H. Mechanistic study on the alcohol synthesis over molybdenum catalysts : Addition of probe molecules to CO---H_2. *J. Catal.* 1989, *115*, 388–398.
11. Jiang, M.; Bian, G.-Z.; Fu, Y.-L. Effect of the K---Mo interaction in K---MoO_3/γ-Al_2O_3 catalysts on the properties for alcohol synthesis from syngas. *J. Catal.* **1994**, *146*, 144–154.
12. Lee, J. S.; Kim, S.; Lee, K. H.; Nam, I.-S.; Chung, J. S.; Kim, Y. G.; Woo, H. C. Role of alkali promoters in K/MoS_2 catalysts for CO-H_2 reactions. *Appl. Catal., A* **1994**, *110*, 11–25.
13. Iranmahboob, J.; Toghiani, H.; Hill, D. O. Dispersion of alkali on the surface of Co-MoS_2/clay catalyst: a comparison of K and Cs as a promoter for synthesis of alcohol. *Appl. Catal., A: Gen.* **2003**, *247*, 207–218.
14. Mills, G. A. *Summary of the Higher Alcohol Synthesis Workshop*, B.R. Service Corporation, 1992.
15. Smith, K. J.; Herman, R. G.; Klier, K. Kinetic modelling of higher alcohol synthesis over alkali-promoted Cu/ZnO and MoS_2 catalysts. *Chem. Eng. Sci.* **1990**, *45*, 2639–2646.
16. Jong, K. P. D.; Geus, J. W. Carbon Nanofibers: Catalytic synthesis and applications. *Catal. Rev. Sci. Eng.* **2000**, *42*, 481–510.
17. Serp, P.; Corrias, M.; Kalck, P. Carbon nanotubes and nanofibers in catalysis. *Appl. Catal., A* **2003**, *253*, 337–358.
18. Marsh, H.; Heintz, E. A.; Rodriquez-Reinoso, F. *Introduction to Carbon Technologies,* University of Alicante, 1997.

19. Rodriquez-Reinoso, F. The role of carbon materials in heterogeneous catalysis. *Carbon* **1998**, *36*, 159–175.
20. van Steen, E.; Prinsloo, F. F. Comparison of preparation methods for carbon nanotubes supported iron Fischer–Tropsch catalysts. *Catal. Today* **2002**, *71*, 327–334.
21. Jacobs, G.; Das, T.; Zhang, Y.; Li, J.; Racoillet, G.; Davis, B. H. Fischer–Tropsch synthesis: support, loading, and promoter effects on the reducibility of cobalt catalysts. *Appl. Catal., A* **2002**, *233*, 263–281.
22. Borodzinski, A.; Bonarowska, M. Relation between crystallite size and dispersion on supported metal catalysts. *Langmuir* **1997**, *13*, 5613–5620.
23. Eswaramoorthi, I.; Sundaramurthy, V.; Das, N.; Dalai, A. K.; Adjaye, J. Application of multi-walled carbon nanotubes as efficient support to NiMo hydrotreating catalyst. *Appl. Catal., A* **2008**, *339*, 187–195.
24. Calafata, A.; Vivas, F.; Brito, J. L. Effects of phase composition and of potassium promotion on cobalt molybdate catalysts for the synthesis of alcohols from CO_2 and H_2. *Appl. Catal., A* **1998**, *172*, 217–224.
25. Bao, J.; Fu, Y.-L.; Bian, G.-Z. Sol–gel Preparation of K–Co–Mo catalyst and its application in mixed alcohol synthesis from CO hydrogenation. *Catal. Lett.* **2008**, *121*, 151–157.
26. Feng, L.; Li, X.; Dadyburjor, D. B.; Kugler, E. L. A temperature-programmed-reduction study on alkali-promoted, carbon-supported molybdenum catalysts. *J. Catal.* **2000**, *190*, 1–13.
27. Noronha, F. B.; Baldanza, M. A. S.; Schmal, M. CO and NO adsorption on alumina–Pd–Mo catalysts: Effect of the precursor salts. *J. Catal.* **1999**, *188*, 270–280.
28. Venezia, A. M.; Parola, V. L.; Deganello, G.; Cauzzi, D.; Leonardi, G.; Predieri, G. Influence of the preparation method on the thiophene HDS activity of silica supported CoMo catalysts. *Appl. Catal., A* **2002**, *229*, 261–271.
29. Qina, S.; Zhang, C.; Xu, J.; Wu, B.; Xiang, H.; Li, Y. Effect of Mo addition on precipitated Fe catalysts for Fischer–Tropsch synthesis. *J. Mol. Catal. A: Chem.* **2009**, *304*, 128–134.

30. Li, X.; Feng, L.; Zhang, L.; Dadyburjor, D. B.; Kugler, E. L. Alcohol synthesis over pre-reduced activated carbon-supported molybdenum-based catalysts. *Molecules* **2003**, *8*, 13–30.

31. Kim, H.-G.; Lee, K. H.; Lee, H.-G.J. S. Carbon monoxide hydrogenation over molybdenum carbide catalysts. *Res. Chem. Intermed.* **2000**, *26*, 427–444.

32. Scholz, G. A.; Morrison, S. R. Methanation on exfoliated and supported MoS_2. *Can. J. Chem.* **1989**, *67*, 862–866.

33. Klier, K.; Herman, R. G.; Nunan, J. G.; Smith, K. J.; Bogdan, C. E.; Young, C. W.; Santiesteban, J.G.; *Methane Conversion*. Bibby, D. M., Chang, C. D., Howe, R. F., Yurchak, S.Y., Eds.; Elsevier: Amsterdam, 1988, p. 109.

34. Santiesteban, J. G.; Bogdan, C. E.; Herman, R. G.; Klier, K. Mechanism of C_1-C_4 alcohol synthesis over alkali/MoS_2 and alkali/Co/MoS_2 catalysts. In *Proc. 9th Intern. Congr. Catal.;* Phillips, M. J., Ternan, M., Eds.; The Chemical Institute of Canada: Ottawa, 1988; Vol. 2, p 561.

35. Youchang, X.; Naasz, B. N.; Somorjai, G. A. Alcohol synthesis from Co and H_2 over molybdenum sulfide. The effect of pressure and promotion by potassium carbonate. *Appl. Catal.* **1986**, *27*, 233–241.

36. Li, X.; Feng, L.; Liu, Z.; Zhong, B.; Dadyburjor, D. B.; Kugler, E. L. Higher alcohols from synthesis gas using carbon-supported doped molybdenum-based catalysts. *Ind. Eng. Chem. Res.* **1998**, *37*, 3853–3863.

37. Tatsumi, T.; Muramatsu, A.; Tominaga, H.; Sekiyu, G. Molybdenum catalysts for synthesis of mixed alcohols from synthesis gas. *J. Jpn. Petrol. Inst.* **1992**, *35*, 233–243.

38. Liu, Z.; Li, X.; Close, M. R.; Kugler, E. L.; Petersen, J. L.; Dadyburjor, D. B. Screening of alkali-promoted vapor-phase-synthesized molybdenum sulfide catalysts for the production of alcohols from synthesis gas. *Ind. Eng. Chem.Res.* **1997**, *36*, 3085–3093.

39. Iranmahboob, J.; Hill, D. O. Alcohol synthesis from syngas over K_2CO_3/CoS/MoS_2 on activated carbon. *Catal. Lett.* **2002**, *78*, 49–55.

40. Quarderer, G. J.; Cochran, G. A. *Catalytic process for producing mixed alcohols from hydrogen and carbon monoxide*. Eur. Patent No. 119,609, Mar 16, 1984.

41. Woo, H. C.; Nam, I.-S.; Lee, J. S.; Chung, J. S.; Kim, Y. G. Structure and distribution of alkali promoter in K/MoS_2 catalysts and their effects on alcohol synthesis from syngas. *J. Catal.* **1993**, *142*, 672–690.

42. Muramatsu, A.; Tatstmi, T.; Tominaga, H. Active species of molybdenum for alcohol synthesis from carbon monoxide-hydrogen. *J. Phys. Chem.* **1992**, *96*, 1334–1340.

43. Li, D.; Zhao, N.; Qi, H.; Li, W.; Sun, Y. H.; Zhong, B. Ultrasonic preparation of Ni modified K_2CO_3/MoS_2 catalyst for higher alcohols synthesis. *Catal. Commun.* **2005**, *6*, 674–678.

44. Li, D.; Zhao, N.; Qi, H.; Li, W.; Sun, Y. H.; Zhong, B. Higher alcohol synthesis over a La promoted $Ni/K_2CO_3/MoS_2$ catalyst. *Catal. Commun.* **2004**, *5*, 605–609.

45. Peri, J. B. Computerized infrared studies of molybdenum/alumina and molybdenum/silica catalysts. *J. Phys. Chem.* **1982**, *86*, 1615–1622.

CHAPTER 4

Synthesis of Higher Alcohols from Synthesis Gas over Co-Promoted Alkali-Modified MoS_2 Catalysts Supported on MWCNTs

The manuscript provided in this chapter is very similar to the one accepted for publication in the journal Applied Catalysis A: General.

Citation:

Surisetty, V. R.; Dalai, A. K.; Kozinski, J. Synthesis of higher alcohols from synthesis gas over Co-promoted alkali modified-MoS_2 catalysts supported on MWCNTs. *Appl. Catal., A* **2010**, in press.

Contribution of the Ph.D. Candidate

Experiments were planned and performed by Venkateswara Rao Surisetty. Drs. Ajay Kumar Dalai and Janusz Kozinski provided guidance in planning the experiment. The submitted manuscript was written by Venkateswara Rao Surisetty, while Dr. Ajay Kumar Dalai provided comments and suggestions regarding the style and content of the paper.

Contribution to Overall Study

In Chapter 3, it was shown that the catalyst with Mo and K loadings of 15 and 9 wt %, respectively, outperformed in terms of activity and selectivity towards higher alcohols over the investigated range. The addition of Co to alkali-modified MoS_2 catalysts strongly promotes the carbon chain growth, especially for the stage of methanol to ethanol. The main objective of this research is to study the higher alcohols synthesis from synthesis gas using various contents of Co-promoted catalysts with15 wt % Mo and 9 wt % K that are supported on multi-walled carbon nanotubes (MWCNTs). It is also aimed to study the influence of temperature and pressure on higher alcohols reaction from CO hydrogenation.

4.1. Abstract

A series of Co (0 to 6 wt %) promoted 15 wt % Mo and 9 wt % K catalysts were prepared using multi-walled carbon nanotubes (MWCNTs) as support. These catalysts were extensively characterized in oxide and sulfide phases and tested for higher alcohol synthesis reaction from CO hydrogenation (molar ratio of H_2 to CO is equal to 1). The diffraction peaks that represent the characteristic K-Mo-S phase were observed in the x-ray diffraction (XRD) patterns of sulfided Co-promoted Mo-K/MWCNTs catalysts. Diffuse reflectance infrared Fourier transform spectroscopy (DRIFTS) of adsorbed CO revealed that Co addition to Mo-K/MWCNTs catalyst not only increases the number of surface Mo sites, but also promotes the reducibility of Mo. The total alcohol space time yield (STY) reached a maximum at 0.207 g/(g of cat.)/h on the catalyst promoted with 6 wt % Co, whereas the catalyst with 4.5 wt % Co exhibited selectivities of 14% and 23% towards ethyl alcohol and higher alcohols, respectively, at 320°C and 8.27 MPa. The best conditions for producing higher alcohols from synthesis gas (mole ratio of H_2 and CO is equal to 1) using gas hourly space velocity of 3.6 m^3 (STP)/(kg of cat.)/h are determined as 330°C and 9.65 MPa.

4.2. Introduction

Higher alcohols synthesis from hydrogenation of carbon monoxide has been of interest in recent years due to the increasing concerns for environmental protection and resources utilization. The addition of higher alcohols (C_{2+} alcohols) to gasoline increases the octane number of the fuel, thereby decreasing toxic exhaust gases, such as CO and NO_x.[1,2] Of the several catalytic systems developed for alcohol synthesis,[3-8] alkali-promoted molybdenum sulfide catalysts are more attractive because of their high catalytic activity and excellent resistance to deactivation pathways, such as sulfur poisoning and coking.[9,10] These catalytic systems display a high proportion of methanol to C_{2+} alcohols.[11,12] Previous research shows that the addition of 3d transition metal components improves the activity and selectivity of C_{2+} alcohols by modifying the structural effects of the alkali-modified molybdenum sulfide catalysts to obtain highly dispersed catalysts.[13-15] Storm[16] and Fujimoto et al.[17] reported that the incorporation of cobalt to the alkali-modified MoS_2 catalysts increased the space time yield (STY) of

higher alcohols on Al_2O_3 and SiO_2 supports, respectively. Murchison et al.[18] found that Co-promoted alkali-modified molybdenum sulfide catalysts showed better activity and selectivity towards the formation of higher alcohols, compared to that of Ni. Santiesteban et al.[19] and Bian et al.[20] reported that additions of Co and K to supported Mo catalysts increased both the activity and selectivity of higher alcohols. Xiang et al.[21] tested the catalysts K-Co-β-Mo_2C for higher alcohols synthesis and concluded that the Co strongly promoted carbon chain growth, especially for the stage of methanol to ethanol.

Activated carbon-supported catalysts hold several advantages, including resistance to acidic or basic media, stability at high temperatures, and an inert graphitic surface.[22,23] Carbon in the form of multi-walled carbon nanotubes (MWCNTs) is drawing attention as a catalyst support.[24] Similar to activated carbon, MWCNTs provide a relatively inert support and high temperature stability.[25] Their unique characteristics such as, appropriate pore-size distribution favoring maximum metallic dispersion, highly graphitized tube walls, and nano-sized channels make them quite suitable as catalytic supports.[26-28] Eswaramoorthi et al.[29] proved the application of multi-walled carbon nanotubes as efficient support to NiMo catalyst for hydrodesulfurization (HDS) and hydrodenitrogenation reactions. Tavasoli et al.[30] compared the Co/MWCNTs with Co/Al_2O_3 for Fischer–Tropsch synthesis and concluded that the CO hydrogenation as well as Fischer–Tropsch synthesis rate were greatly improved on MWCNT-supported catalysts because of the uniform dispersion of metal clusters on the support. Ma et al.[31] claimed that the Co-decorated MWCNT-promoted the enhancement of activity of CO hydrogenation and the improvement of the selectivity of higher alcohol synthesis.

In our previous work, the catalyst with Mo loading of 15 wt % Mo and K loading of 9 wt % supported on MWCNTs showed the highest yields and selectivity towards alcohols, compared to the catalysts with 10 and 20 wt % Mo and 3 and 6 wt % K.[32] The addition of 3d transition metals, such as Co, to the MWCNT-supported Mo-K catalysts could enhance the activity and selectivity of higher alcohols, due to their strong abilities of hydrogenation and promotion of carbon chain growth. In the present study, we prepared a series of Co (3, 4.5, and 6 wt %)-promoted alkali-modified molybdenum-based catalysts (9 wt % K and 15 wt % Mo) supported on MWCNTs by sequential pore volume impregnation. These catalysts were characterized using different techniques in

oxidized and sulfided states. The MWCNT-supported catalyst with 15 wt % Mo and 9 wt % K (Mo-K/MWCNT) is used as a reference catalyst to distinguish the effects of Co promoter. The effects of reaction conditions, such as temperature and pressure, on the catalytic performance for higher alcohols synthesis were also studied.

4.3. Experimental

4.3.1. Preparation of Co-promoted Mo-K/MWCNTs catalysts

MWCNTs (purity > 95%) obtained from M. K. Nano, Canada was used as a support for the preparation of the catalysts. Prior to impregnation, the support was treated with 30% HNO_3 reflux at 100°C overnight, washed with distilled water several times, and dried at 120°C for 6 h. The oxide samples were prepared by the incipient wetness impregnation method using ammonium heptamolybdate tetrahydrate (Sigma-Aldrich), potassium carbonate (Aldrich), and cobalt acetate tetrahydrate (Alfa-Aesar) as precursors for Mo, K, and Co, respectively. At the first step, the support was impregnated with an aqueous solution of K_2CO_3, followed by drying at 120°C for 2 h, and stabilized in an argon flow of 50 ml/min at 300°C at a heating rate of 10°C/min for 4 h. It was further impregnated with aqueous solutions containing the required amount of $(NH_4)_6Mo_7O_{24}$, and $Co(CH_3COO)_2$ followed by drying at 120°C for 2 h and stabilized in an argon flow of 50 ml/min at 450°C at a heating rate of 10°C/min for 12 h. The sulfide samples were obtained by heat-treating the oxide precursors in a flow of 10 mole % H_2S in H_2 gas at 450°C at a heating rate of 2°C/min for 4 h.

4.3.2. Characterization of Co-promoted Mo-K/MWCNTs catalysts

The contents of Mo, and Co of the oxide precursor catalysts were determined using a Perkin-Elmer ELAN 5000 inductively coupled plasma-mass spectroscopy (ICP-MS) instrument.

The surface area, pore volume, and average pore diameter of oxide samples were measured by N_2-physisorption at 77 K using a Micromeritics ASAP 2000. Approximately 0.2 g of sample was used for each analysis. The moisture and other adsorbed gases present in the sample were removed before analysis by degassing the

sample at 200°C for 2 h under 66.7 Pa (500 mm Hg). The sample was then evacuated at 2.67 Pa (20 μm Hg) before N_2 adsorption.

A Perkin-Elmer thermogravimetric (TG) differential thermal analyzer (DTA) was used to measure weight changes of the sample when heated under a flow of argon (flow rate of 40 ml/min) at a constant heating rate of 10°C/min.

Powder X-ray diffraction (XRD) analysis patterns of oxide and sulfide forms of samples were recorded on a Rigaku X-ray diffraction instrument with nickel filtered Cu Kα radiation (λ = 0.1541 nm). Each sample was scanned at a rate of 0.05°/s, with 2θ varying from 10° to 80°. In order to obtain the XRD patterns in sulfided form, the catalysts were first sulfided for 6 h at 450°C at a heating rate of 2°C/min, using a gaseous mixture containing 10 mole % H_2S in H_2 at a flow rate of 50 ml/min. After sulfidation, the catalysts were cooled to room temperature in a flow of He and the sample was transferred to sample holders under protection of He.

The morphology of the oxide samples was characterized by transmission electron microscopy (TEM). TEM investigations were carried out using a Philips CM20 (100 kV) transmission electron microscope equipped with a NARON energy-dispersive spectrometer with a germanium detector. The inner diameters, wall thicknesses, and length of carbon nanotubes, as well as the sizes of the catalyst particles, were measured by digital micrograph software (version 3.6.5, Gatan Inc.).

The oxide samples were characterized by scanning electron microscopy (SEM) using a Phillips SEM-505 scanning electron microscope operating at 300 kV in SE display mode. The outer diameter of the nano-tubes was measured using Digital micrograph software (version 3.6.5, Gatan Inc.).

The temperature programmed reduction (TPR) profiles of the catalysts were performed in order to study the reducibility of the metal oxides in the catalysts. For each analysis, approximately 0.2 g of sample was used, which was first purged in a flow of argon at 170°C to remove traces of water and then cooled to 40°C. The TPR of each sample was performed using a 3.1 mole% H_2 in He stream at a flow rate of 30 ml/min at atmospheric pressure, using a CHEMBET 3000 TPD-TPR analyzer equipped with a thermal conductivity detector, heating at a linearly programmed rate of 10 °C/min up to 800°C.

Carbon monoxide is used as a probe molecule in order to determine the number of accessible surface metal atoms present on sulfided catalysts. The CO uptake (μmole/g of cat.) measured from CO chemisorption is equivalent to the number of active metal atoms that are accessible to the reactant molecules. The stoichiometric coefficient (CO to metal ratio) of 1 was used and the extent of reduction was assumed to be 100% in metal dispersion calculations. The carbon monoxide uptake on sulfided catalysts was measured using the Micromeritics ASAP 2000 instrument. Prior to the CO chemisorption measurement, 0.2 g of sample was sulfided in situ using 10 mole % H_2S in H_2 at 400°C for 4 h. The sample was then evacuated at 120°C until the static pressure remained less than 6.6 x 10^{-4} Pa. Chemisorption was performed by passing pulses of CO over the sample to measure the total gas uptake at 35°C.

Diffuse reflectance infrared Fourier transform spectroscopy (DRIFTS) of adsorbed CO is an efficient tool to monitor the changes of Mo-related active species due to Co addition. The sulfided catalysts were subjected to DRIFTS of adsorbed CO in a Perkin-Elmer Spectrum GX instrument equipped with DTGS detector and a KBr beam splitter. Approximately 10 mg of powdered oxide sample was placed in the sample cup inside a Spectrotech diffuse reflectance in situ cell equipped with ZnSe windows and a thermocouple which allows the direct measurement of the sample surface temperature. Spectra for each experiment were averaged over 64 scans in the region 3000-1000 cm^{-1} with a nominal 4 cm^{-1} resolution. Prior to CO adsorption, the catalyst was sulfided using 10 mole % H_2S in H_2 (50 ml/min) at 375°C for 4 h. After sulfidation, the flow was switched to He (50 ml/min) and the temperature was decreased to 30°C and a background spectrum was recorded. CO adsorption was carried out at 30°C by introducing pure CO (30 ml/min) into the sample cell for 30 min. After adsorption, the system was purged with He (50 ml/min) for 30 min to remove the physisorbed CO molecules. Then the spectra were collected under He flow.

X-ray absorption near edge spectra (XANES) at the sulfur L-edge were measured using the variable line spacing plane grating monochromator (VLS PGM) beamline (5.5-250 eV) on the 2.9 GeV synchrotron light source energy of the Canadian light source (CLS) at the University of Saskatchewan, Saskatoon, SK Canada. The powder samples were pressed on a stainless steel sample holder using a piece of carbon

conducting tape and the spectra were recorded. A bright and high monochromatic photon beam is provided by the VLS PGM beam line, which employs three diffraction gratings. The light is directed from the 185 mm planar undulator using two horizontal deflecting mirrors and one vertical focusing mirror through the entrance slit and onto the selected grating.

4.3.3. Catalytic performance for higher alcohols synthesis

A single-pass tubular downflow, fixed-bed reactor of 450-mm length and 22-mm inside diameter made of inconel tube was used to perform higher alcohol synthesis reactions (HAS). The reactor was packed with 2 g of catalyst diluted with 12 ml of 90 mesh size silicon carbide and housed in an electric furnace controlled by a temperature controller. The reactor was pressurized to 3.44 MPa (500 psig) with He and the sulfidation together with the reduction was carried out for 6 h at 450°C at a heating rate of 2°C/min using a gas mixture containing 10 mole % H_2S in H_2 and flow rate of 50 ml/min. The temperature was then lowered to the reaction temperature, and the system was then pressurized to the reaction conditions. The feed gas mixture CO (45 mole %), H_2 (45 mole %), and Ar (10 mole %) was passed through mass flow controllers. The HAS reaction was carried out at steady state under the reaction conditions of 300 to 340°C, 5.51 (800 psig) to 9.65 MPa (1400 psig), and a gas hourly space velocity (GHSV) of m^3 (STP)/(kg of cat.)/h over a period of 24 h. The product gas was cooled to 0°C and separated into gas and liquid phases at the reaction pressure. The CO conversion and other gaseous products were monitored with a time interval of 1 h. The liquid products were collected at the end of the reaction and analyzed with a Varian 3400 gas chromatograph equipped with a capillary column and a flame ionization detector (FID). The volume and weight of liquid products were measured to check the mass balance. The gaseous products were analyzed online on a Shimadzu gas chromatograph through a sampling valve. Using Ar as an internal standard, the CO conversion was calculated and the overall mass balance of the reaction was determined. The experiments were repeated at least twice to check reproducibility and to confirm that the results obtained were within the experimental error of ± 2.5%.

Mass balance calculations, similar to those proposed by Bahome et al.[33],were used to calculate the % CO conversion, % CO_2 produced, product STY, and alcohol selectivity (wt %), and are given as follows:

$$CO\ conversion\ (mole\ \%) = \frac{Moles\ (CO_{in}\text{-}CO_{out}) * gas\ contraction}{Moles\ (CO_{in})} * 100 \quad 4.1$$

where the gas contraction was determined from the Ar_{in}/Ar_{out} calibration.

$$CO_2\ produced\ (mole\ \%) = \frac{Moles\ of\ CO_2\ produced}{Moles\ of\ CO\ converted} * 100 \quad 4.2$$

$$Product\ STY\ (g/g\ of\ cat./h) = \frac{Wt.\ of\ the\ product\ produced}{Wt.\ of\ the\ catalyst\ used * time\ of\ reaction} \quad 4.3$$

$$Alcohol\ selectivity\ (wt\ \%) = \frac{Wt.\ of\ the\ alcohol\ produced}{Total\ Wt.\ of\ the\ alcohol\ produce} \quad 4.4$$

4.4. Results and Discussion

4.4.1. Characterization of Co-promoted Mo-K/MWCNT catalysts

The physico-chemical properties of all the catalysts are displayed in Table 4.1. Elemental chemical analysis indicates that most of the Mo, and Co precursors are deposited on the support during the incipient wetness impregnation. The measured compositions are slightly lower compared to targeted compositions, which may result from the hygroscopic nature of precursors. The BET surface area and pore volume of all the catalysts were much lower than the pure support. The BET surface area of Mo-K/MWCNT catalyst was found to be 96 m^2/g. With the incorporation of 3 wt % Co, the surface area decreased to 83 m^2/g. When the Co loading was increased to 6 wt %, the BET surface area further decreased to 72 m^2/g. This apparently is due to pore blockage of MWCNTs by the Co, Mo and K.

Table 4.1. Physico-Chemical properties of MWCNT-supported catalysts

Catalyst	Targeted composition (wt %)			Measured composition (wt %)		BET surface area (m^2/g)	Total pore volume (cc/g)	Average pore diameter (nm)	CO uptake (µmole/ g of cat.)	Dispersion of metals (%)
	K	Mo	Co	Mo	Co					
Acid treated MWCNT	--	--	--	--	--	220	0.66	10.9	--	--
Mo-K/MWCNT	9	15	--	14.1	--	96	0.37	16.3	94	30.0
3 wt % Co-Mo-K/MWCNT	9	15	3	14.3	2.6	83	0.35	16.8	145	34.9
4.5 wt % Co-Mo-K/MWCNT	9	15	4.5	14.3	4.3	78	0.33	17.2	182	38.5
6 wt % Co-Mo-K/MWCNT	9	15	6	14.4	5.7	72	0.31	17.5	190	36.8

Table 4.1 gives the results of CO uptake (µmole/g of cat.), and % dispersion of metals measured from CO chemisorption of the sulfided catalysts. The CO uptake increased by 54% with the addition of 3 wt % Co on the catalyst with 15 wt % Mo and 9 wt % K supported on the MWCNTs and, hence, it is expected that the addition of promoters will enhance the CO hydrogenation capability of the MWCNTs-supported Mo-K catalysts. The CO uptake value increased from 145 to 190 (µmole/g of cat.) with increased Co loading from 3 to 6 wt %. The metal dispersion is high for the catalysts with 4.5 wt % Co content. Low dispersion at high Co content of Co-Mo catalysts supported on natural and aluminum-pillared clays was also observed by Moronta et al.[34] using cobalt chloride as a catalytic precursor for Co. This is attributed to the formation of large particles at higher Co loadings.

The thermogravimetric technique was used to find the stabilization temperature of the impregnated catalysts. As shown in Fig. 4.1, all the catalysts exhibited identical profiles for weight loss versus system temperature. The weight loss around 100°C probably resulted from evaporation of moisture. The figure clearly shows that rapid weight loss started below 330°C and continued to a temperature of 500°C; therefore, the stabilization temperature of the dried Co- promoted Mo-K/MWCNTs catalysts was determined to be 500°C.

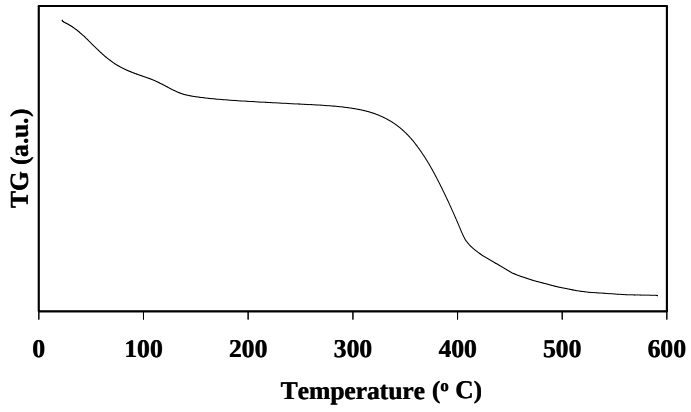

Figure 4.1. Sample TGA profile exhibited by 6 wt % Co-Mo-K/MWCNT catalyst

The XRD patterns of the catalysts in oxidized and sulfided form were measured and shown in Fig. 4.2 and Fig. 4.3, respectively. The most probable phases in the samples were detected using the JCPDS chemical spectra data bank.

The results of the possible crystal phases with their corresponding reflection planes are given in Table 4.2. The strong intensity peak at 2θ value of 26.6° and the small asymmetric peak at 43.2° are due to the reflections of graphite phase present in the support.[29] The characteristic reflections correspond to the crystalline structure of MoO_3 are observed at 2θ value of 40.2°, and 64.5°.[35] Several kinds of K-Mo-O mixed phases exist in oxidized form of catalysts. The peaks at 2θ values of 19.4°, 28.5°, 29.8°, and 30.9° correspond to the characteristic reflections of $K_2Mo_2O_7$ phase.[36] Other K-Mo-O phases, such as K_2MoO_4 (2θ = 16.0°), $K_2Mo_7O_{20}$ (2θ = 23.6°), KMo_4O_6 (2θ = 37.1°, and 46.1°), and $K_{0.33}MoO_3$ (2θ = 44.6°) may also exist.[37,38] No peaks related to the Co species are detected from the XRD spectra of the catalysts in the oxide form, indicating good dispersion of those species on the catalyst.

The various diffraction peaks observed in the XRD patterns of oxide samples are completely removed after sulfidation, and the new diffraction peaks with less diffraction intensity representing different sulfide species appeared. This confirmed that newly formed active phases during the sulfidation step are well dispersed on the MWCNTs support. The reflections of MoS_2 crystallites are observed at 2θ values of 14.6°, 33.4°, 40.9°, and 58.9°.[39] The peaks at 2θ values 30.1°, and 31.5° are due to the characteristic reflections of K-Mo-S species, which represent K_2MoS_4.[40] These peaks are related to active sites for higher alcohol synthesis.[41`] The peaks at 2θ values of 47.9° and 52.4° are due to the different reflecting planes characteristic of bulk Co_9S_8 particles.[42] The intensities of these peaks increase at higher Co content (4.5 and 6 wt %).

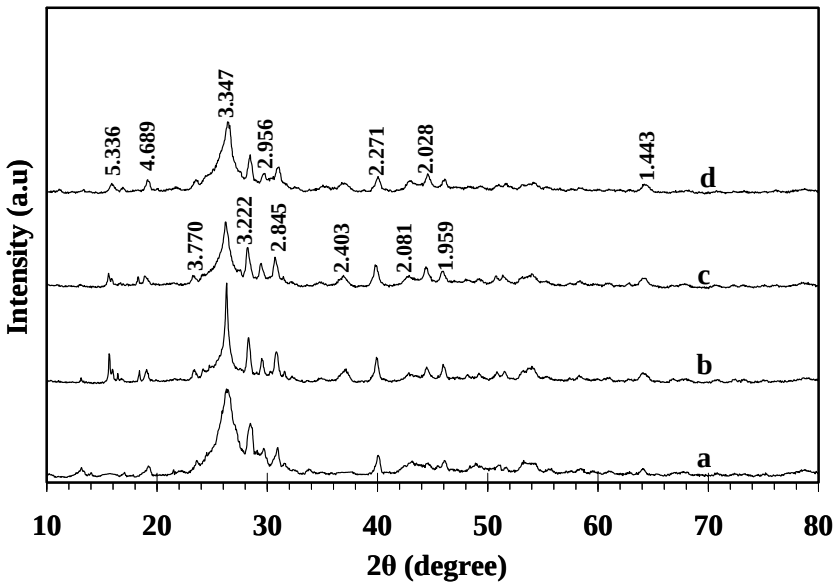

Figure 4.2. XRD patterns of the catalysts in oxidized form a. Mo-K/MWCNT; b. 3 wt % Co-Mo-K/MWCNT; c. 4.5 wt % Co-Mo-K/MWCNT; d. 6 wt % Co-Mo-K/MWCNT

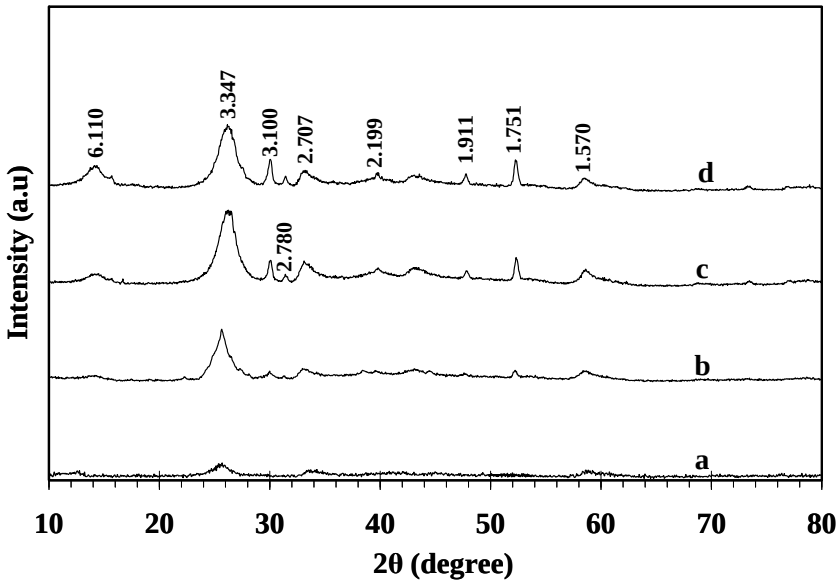

Figure 4.3. XRD patterns of catalysts in sulfided form a. Mo-K/MWCNT; b. 3 wt % Co-Mo-K/MWCNT; c. 4.5 wt % Co-Mo-K/MWCNT; d. 6 wt % Co-Mo-K/MWCNT

Table 4.2. Crystal phases and reflection planes from XRD analysis

Crystal phase	2θ	d-spacing	Reflection plane h k l
Oxidized form of catalysts:			
Graphite (C)	26.6°	3.347	1 1 1
Graphite (C)	43.2°	2.081	0 1 0
MoO_3	40.2°	2.271	1 5 0
MoO_3	64.5°	1.443	0 6 2
K_2MoO_4	16.0°	5.336	1 1 0
$K_2Mo_2O_7$	19.4°	4.689	1 1 0
$K_2Mo_7O_{20}$	23.6°	3.770	1 0 2
$K_2Mo_2O_7$	28.5°	3.222	0 0 2
$K_2Mo_2O_7$	29.8°	2.956	0 1 2
$K_2Mo_2O_7$	30.9°	2.845	2 1 0
KMo_4O_6	37.1°	2.403	4 0 0
$K_{0.33}MoO_3$	44.6°	2.028	6 2 0
KMo_4O_6	46.3°	1.959	3 2 1
Sulfided form of catalysts:			
MoS_2	14.6°	6.110	0 0 3
MoS_2	33.4°	2.707	1 0 1
MoS_2	40.9°	2.199	0 1 5
MoS_2	58.9°	1.570	1 1 0
K_2MoS_4	30.1°	3.020	3 0 1
K_2MoS_4	31.5°	2.780	3 0 2
Co_9S_8	47.9°	1.911	5 1 1
Co_9S_8	52.4°	1.751	4 4 0

Scanning electron microscopy is used to identify the growth of MWCNTs. Fig. 4.4 shows the surface morphology of the grown carbon nanotubes in bundles. The nanotubes are found to be tangled and are clustered with impregnated metal particles. The outside diameter of the MWCNTs clearly shows that the nanotubes are multi-walled and have a structure with several walls of graphitic carbons in concentric circles.

The TEM images of Co- promoted Mo-K/MWCNT catalysts were recorded and the representative image is shown in Fig. 4.5. The TEM images of the catalysts revealed that the catalyst particles are well dispersed inside the tubes and also on the outside of the tube walls. Most of the nano-tube caps are found to be open, resulting from the acid treatment prior to impregnation. After acid treatment, the BET surface area of the MWCNTs increased from 178 to 220 m^2/g and the pore volume increased from 0.54 to 0.66 cc/g. MWCNTs diameters range from 5 to 12 nm, while wall thicknesses range from 3 to 8 nm, and tube lengths are between 200 and 400 nm. The particle sizes of the metal species that are inside and outside of the tubes are in the range of 3 to 4 nm.

The TPR studies of K-promoted Mo-based catalysts reveal two main reduction peaks. The low temperature reduction peak appearing around 500°C is attributed to the reduction of octahedral coordinated Mo (Mo^{+6}) species to tetrahedral coordinated Mo (Mo^{+4}) species, and the high temperature peak around 800°C is due to the reduction of Mo^{+4} species to lower oxidation state.[43,44] The effect of different loadings of Co (3 to 6 wt %) on the reducibility of the MWCNT-supported 15 wt % Mo and 9 wt % K catalyst are shown in Fig. 4.6.

The TPR profiles of the Co-promoted catalysts display similar reduction patterns as that of un-promoted Mo-K catalysts. The first H_2 consumption peak is most likely due to the overlap of multiple peaks corresponding to the reduction of MoO_3 and Co_3O_4 species, as these species have the same reduction temperature; the high temperature reduction peak corresponding to the reduction of MoO_2 species.[45] Increasing Co content from 3 to 6 wt % shifted the low temperature reduction peak from 540 to 525°C and the high temperature reduction peak from 729 to 716°C, suggesting that the Co promoter facilitates the reduction of Mo species.

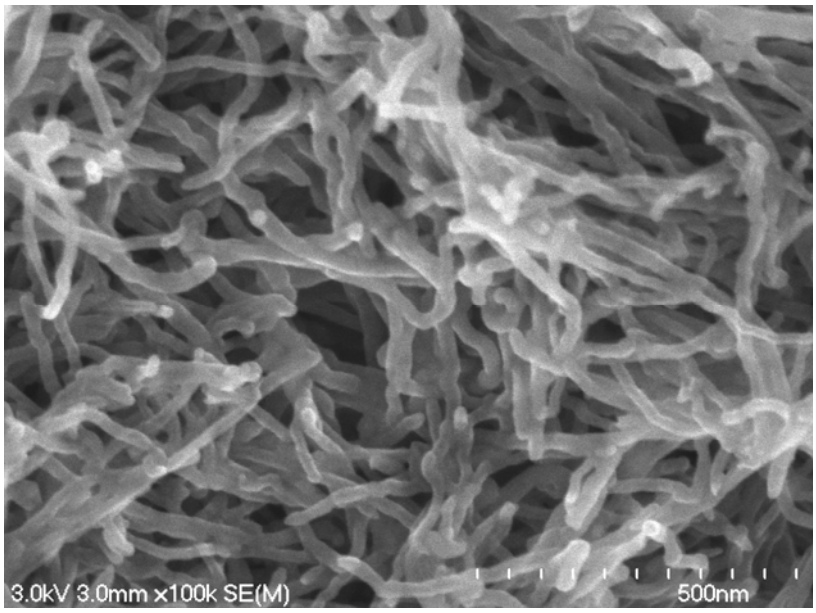

Figure 4.4. SEM image of 4.5 wt % Co-Mo-K/MWCNT

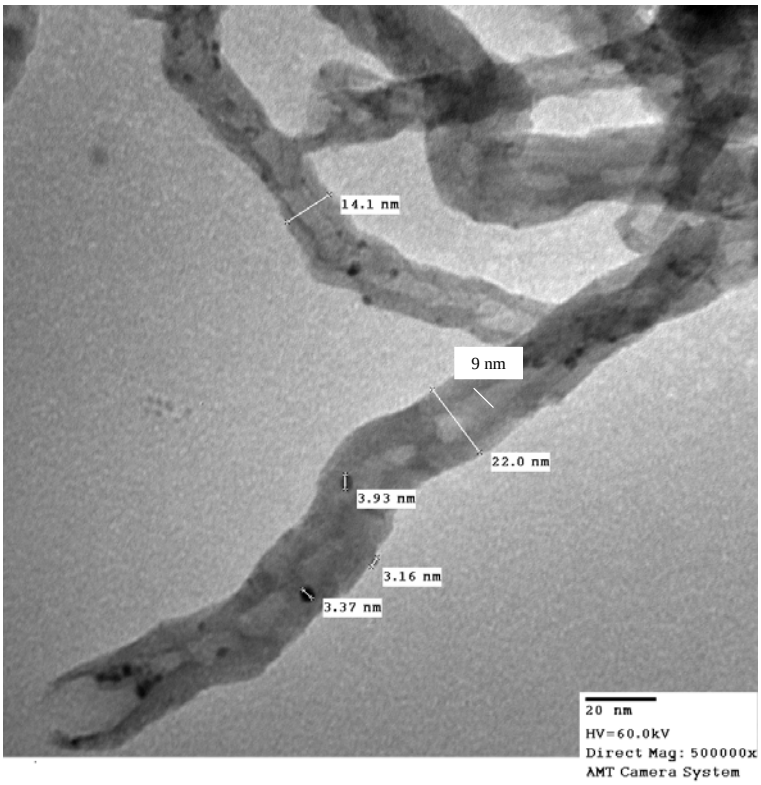

Figure 4.5. TEM image of 4.5 wt % Co-Mo-K/MWCNT

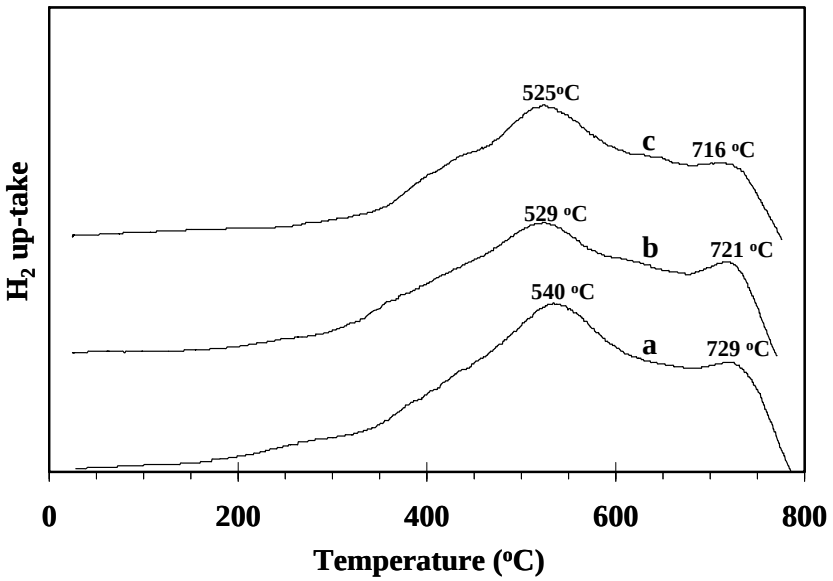

Figure 4.6. H_2-TPR profiles a. 3 wt % Co-Mo-K/MWCNT; b. 4.5 wt % Co-Mo-K/MWCNT; c. 6 wt % Co-Mo-K/MWCNT

DRIFT spectroscopy of CO adsorbed catalysts was used to study the active species in the sulfide form of the catalysts. The typical CO adsorption DRIFT bands for Co-promoted catalysts with 15 wt % Mo and 9 wt % K supported on MWCNTs is shown in Fig. 4.7. Topsoe et al.[46] concluded that Co or Ni promotion on Mo-based catalysts increased the CO adsorption. From Fig. 4.7, it was observed that CO adsorption on sulfided Co-promoted catalysts yield different bands, representing promoted and un-promoted MoS_2 species. The bands in the range of 1980 to 1950 cm^{-1} are due to CO adsorbed on four or five co-ordinated Mo sites.[47] The intensity of these bands is relatively strong on the Mo-K/MWCNTs catalyst that was promoted with 3 wt % Co. The 3 wt % Co-promoted catalyst exhibits another main band at 2078 cm^{-1}, which can be assigned to a v(CO) band characteristic of linear stretching of CO adsorbed on Mo^{+2} species.[48] The characteristic bands representing un-promoted partially reduced Mo^{+5} species are observed in the range of 2100 to 2090 cm^{-1} on all the Co-promoted catalysts.[49] The weak CO adsorption bands at around 2057 and 2038 cm^{-1} are observed on the catalyst with 3 wt % Co, due to the adsorption of CO on Co-promoted MoS_2 sites.[47]

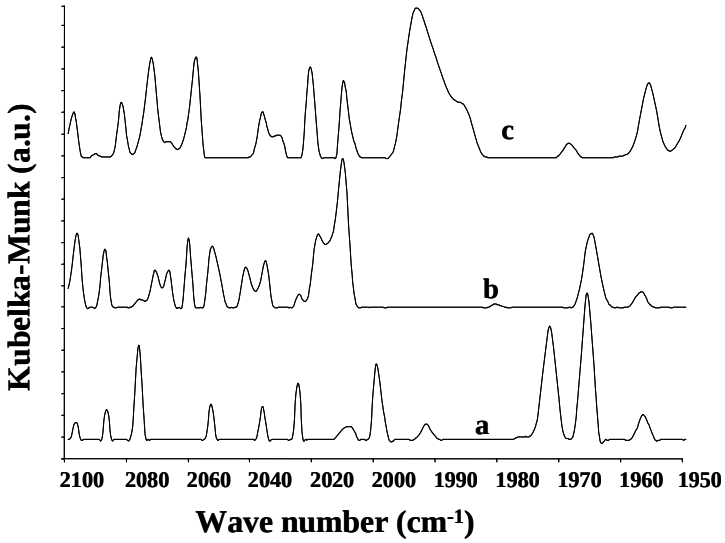

Figure 4.7. DRIFTS of adsorbed CO on sulfided catalysts a. 3 wt % Co-Mo-K/MWCNT; b. 4.5 wt % Co-Mo-K/MWCNT; c. 6 wt % Co-Mo-K/MWCNT

When Co loading was increased to 4.5 wt % Co, the intensity of bands on the Co-promoted Mo sites increased significantly, and the bands for the promoted MoS_2 sites shifted to lower wave numbers. This indicates that Co addition reduces more Mo^{+6} to a lower oxidation state. The strong CO adsorption band at 2015 cm^{-1} was observed along with shoulder bands at 2020 and 2030 cm^{-1}, corresponding to the Mo^{+1} species observed on the Mo-K/MWCNTs catalyst that was promoted with 4.5 wt % Co.[50] When Co loading was increased to 6 wt %, a strong CO adsorption band was observed at around 1995 cm^{-1}, representing more reduced Mo sites (Mo^0) along with Mo^{+1} species.[51]

The sulfur L-edge spectra were recorded by total electron yield (TEY) and fluorescence modes as a function of photon energy using synchrotron radiation, and the spectra were normalized for the X-ray fluctuation of the synchrotron ring, I_o. The spectra recorded in these two modes were found to be very similar, and only the TEY/I_o spectra of the catalysts together with the reference substance (CaS) are presented. Fig. 4.8 compares the XANES spectra of the CaS with Mo-K/MWCNTs, and 4.5 wt % Co-Mo-K/MWCNTs catalysts in sulfided form. XANES spectra of all the sulfided catalysts were in comparison with that of the reference material, CaS confirming that sulfidation of catalysts leads to the formation of a metallic sulfide phase.

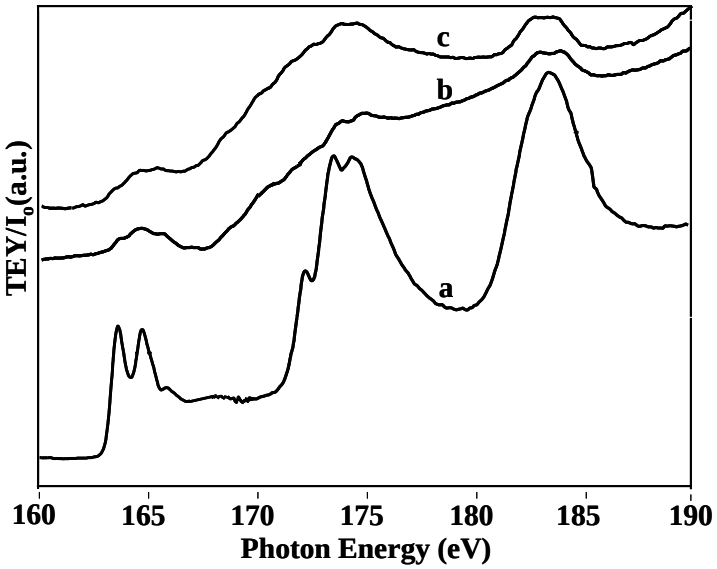

Figure 4.8. XANES analysis: a. CaS; b. Sulfided Mo-K/MWCNTs; c. Sulfided 4.5 wt % Co-Mo-K/MWCNTs

4.4.2. Catalytic performance for higher alcohols synthesis

The catalyst activity studies towards higher alcohol synthesis reaction were carried out under similar conditions at 320 °C, 8.27 MPa (1200 psig), m^3 (STP)/(kg of cat.)/h and H_2 to CO molar ratio of 1. The catalyst particle size in the range of 147-210 μm was selected to eliminate the mass transfer resistances. Fig. 4.9 gives the results of the % CO conversion as time-on-stream during higher alcohol synthesis reaction over the un-promoted MWCNT-supported catalysts with 15 wt % Mo and 9 wt % K, and catalysts with varying loadings of Co (3, 4.5, and 6 wt %). Baghalha et al.[52] suggested that the deactivation in sulfided Co-Mo catalysts is due to the loss of sulfur and coke deposition. The presence of a Co-Mo-S phase on the Co-promoted MoS_2 catalysts has the ability for better hydrogenation of CO, reducing the deposition of coke. The formation of Co_9S_8 species decreases the surface area of the active Co-Mo-S species, which results in the higher deactivation behavior during the early stage of reaction.[13] These results, coupled with previous XRD results are consistent with the development of Co_9S_8 particles. The Co-containing catalysts are quite stable after the first 15 h. The catalytic activity and product selectivity data were calculated after an induction period of 15 h.

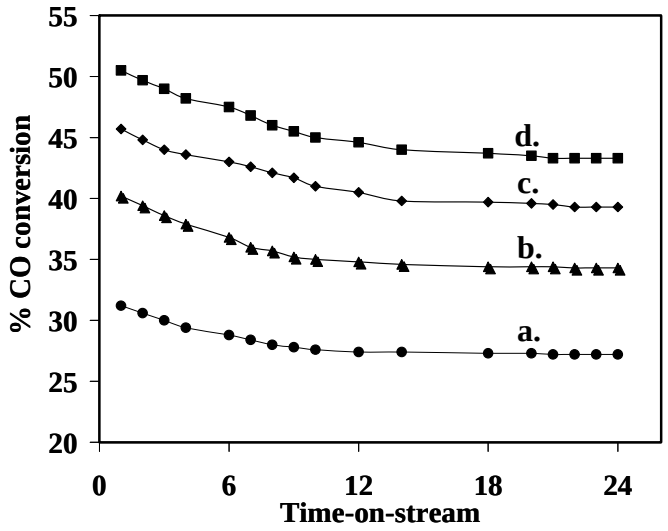

Figure 4.9. % CO conversion with time on stream

a. Mo-K/MWCNT; b. 3 wt % Co-Mo-K/MWCNT;
c. 4.5 wt % Co-Mo-K/MWCNT; d. 6 wt % Co-Mo-K/MWCNT

(wt. of the cat. = 2 g, P = 8.3 MPa, T = 320°C, GHSV = 3.6 m^3(STP)/(kg of cat.)/h, H_2/CO molar ratio = 1)

The results in Table 4.3 show the influence of adding different Co loadings to the Mo-K/MWCNTs sample on the catalytic features for the synthesis of higher alcohols from synthesis gas after an induction period of 15 h. In the case of catalysts without Co, the % CO conversion increased from 27% to 35% with the addition of 3 wt % Co on the MWCNT-supported 15 wt % Mo and 9 wt % K catalysts. At the same time, incorporation of a cobalt promoter remarkably increased the STY of total alcohols from 0.131 to 0.176 g/(g of cat.)/h. Sun et al.[53] explained that one molybdenum atom of every two is substituted by cobalt and the Co atoms located at edge surfaces generate partially promoted Co-Mo-S surface species. The incorporation of Co on edge surfaces on MoS_2 increases the number of active sites, thus significantly increasing the activity of the catalyst.[54]

Table 4.3. Catalytic performance of sulfided MWCNT-supported catalysts

(wt. of the cat. = 2 g, P = 8.3 MPa, T = 320°C, GHSV = 3.6 m^3(STP)/(kg of cat.)/h, H_2 to CO molar ratio = 1)

Catalyst	CO conversion (%)	Product STY (g/(g of cat.)/h)		CO_2 produced (%)	Alcohol Selectivity (wt %)			
		Total alcohols	Total Hydrocarbons		Methanol	Ethanol	Higher alcohols	Total alcohols
Mo-K/MWCNT	27.4	0.131	0.299	21.1	11.9	5.0	9.2	21.1
3 wt.% Co-Mo-K/MWCNT	34.6	0.176	0.348	26.8	7.9	12.1	19.1	27.0
4.5 wt.% Co-Mo-K/MWCNT	39.7	0.198	0.373	31.6	7.0	14.1	23.2	30.2
6 wt.% Co-Mo-K/MWCNT	43.5	0.207	0.412	30.2	5.6	13.1	22.8	28.4

The % CO conversion increased to 40% and 44% and the total alcohols STY of 0.198 and 0.207 g/(g of cat.)/h were observed on catalysts with a Co content of 4.5 and 6 wt %, respectively. This can be explained from the results obtained from CO chemisorption on sulfided Co-contained catalysts, in which the activity of the catalysts for alcohol formation is in accordance with the increased amount of hydrogen uptake at higher Co loadings. By increasing the Co loadings from 3 to 6 wt % on the MWCNT-supported Mo-K catalyst, the hydrocarbon (HC) formation rate, especially that of methane, increased monotonically from 0.348 to 0.412 g/(g of cat.)/h. This is due to the increased availability of metallic sulfide sites, such as MoS_2 and Co_9S_8 that improve the activity for the hydrogenation reaction.[13,55]

Carbon dioxide obtained from the water gas shift (WGS) reaction is another major product during the higher alcohol synthesis reaction from synthesis gas. Hou et al.[56] explained that the oxy-sulfide form of partially reduced Mo^{+5} species are the active sites for the formation of CO_2 over sulfided molybdenum-based catalysts. They suggested that the WGS reaction occurs by the oxy-sulfide redox mechanism as explained in Fig. 4.10. According to the mechanism, the sulfided form of Mo^{+5} species reacts with water molecules to form oxy-sulfided Mo^{+5} species. These species react with CO to produce CO_2 and reduce to Mo^{+4} species with a vacancy and coordinated oxygen, which in turn re-oxidize to Mo^{+5} upon reaction with H_2O to form H_2. The DRIFTS of adsorbed CO spectra are consistent with partially reduced Mo^{+5} species.

It was observed from DRIFTS spectroscopy of sulfided catalysts and TPR studies of oxide catalysts that the addition of Co improves the reducibility of Mo-K/MWCNT catalysts, which in turn improves the WGS reaction rate. The amount of CO_2 produced (32%) on the Co-promoted catalysts was observed to be higher on the catalyst containing 4.5 wt % Co. which can be better explained from the XRD results. The intensity of the peaks Co-S species increased when the Co loading was increased from 4.5 to 6 wt %, favoring the formation of hydrocarbons at higher Co loadings.

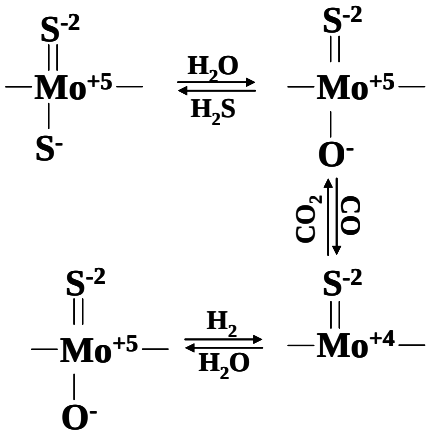

Overall reaction: $CO + H_2O \rightleftharpoons CO_2 + H_2$

Figure 4.10. Reaction scheme for the water gas shift reaction using the oxy-sulfide redox mechanism

The molar ratio of higher alcohols ($C_{2+}OH$) to methanol (C_1OH) is obtained as a function of wt. of Co on the MWCNT-supported Mo-K catalyst after sulfidation and the molar ratio increased linearly as a function of wt % of Co. From Fig. 4.11, the following simulated linear equations were obtained for (4.5) the % CO conversion and (4.6) the molar ratio of higher alcohols to methanol as a function of wt % of Co:

$$Y_1 = 2.712\ X + 27.146;\ R^2 = 0.996 \quad \text{(4.5)}$$

$$Y_2 = 0.344\ X + 0.444;\ R^2 = 0.999 \quad \text{(4.6)}$$

where, X is wt % of Co, Y_1 - CO conversion (%), and Y_2 is molar ratio of $C_{2+}OH/C_1OH$.

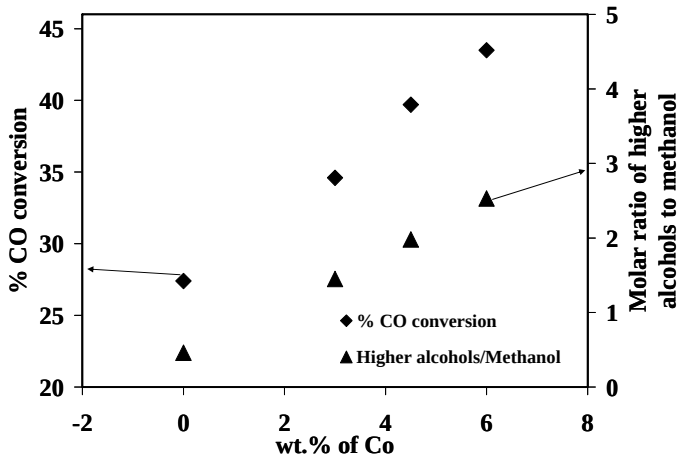

Figure 4.11. % CO conversion and molar ratio of higher alcohols to methanol as a function of wt % of Co (wt. of the cat. = 2 g, P = 8.3 MPa, T = 320°C, GHSV = 3.6 m^3(STP)/(kg of cat.)/h, H_2/CO molar ratio = 1)

Fig. 4.12 represents the change in higher alcohols selectivity (wt %) with CO conversion obtained over different Co-promoted 9 wt % K-modified 15 wt % Mo sulfided catalysts supported on MWCNT. It is observed from this figure that the catalyst with increased content of Co on Mo-K/MWCNT catalysts, the % CO conversion and higher alcohols selectivity increased almost linearly from 0 to 4.5 wt % of Co, and then CO conversion further increased, but the higher alcohol selectivity was levelled off with further Co content up to 6 wt %.

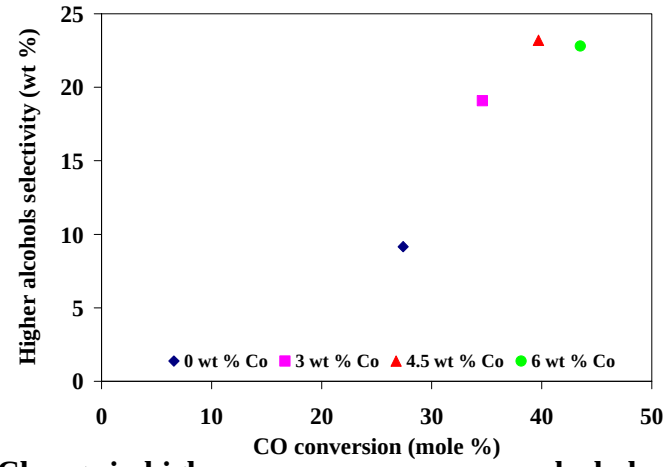

Figure 4.12. Change in higher alcohols selectivity with % CO conversion over Co-promoted Mo-K/MWCNT (wt. of the cat. = 2 g, P = 8.3 MPa, T = 320°C, GHSV = 3.6 m^3(STP)/(kg of cat.)/h, H_2/CO molar ratio = 1)

The individual distributions of alcohols over the Mo-K/MWCNT, and 4.5 wt % Co-promoted Mo-K/MWCNT catalysts are depicted in Fig. 4.13, and 4.14, as an Anderson-Schulz-Flory (ASF) plot. The ASF distribution can quantitatively be written as follows: $Y_n = P^{n-1} * (1-P)$, where Y_n is the mole fraction of the alcohol with a carbon number of n and P is the chain growth probability factor.[34] The ASF distribution obtained over the un-promoted Mo-K/MWCNT catalyst was linear with a chain growth probability of 0.33. The 4.5 wt % Co promoted catalyst showed large deviations from the ideal ASF distribution for methanol, which deviated lower, and ethanol, which deviated higher. The chain growth probability was calculated to be 0.47 over 4.5 wt % Co promoted Mo-K/MWCNT catalyst, assuming a linear distribution of alcohols. This confirms that the addition of Co promoter to alkali-modified MoS_2 catalysts increases the reaction rate towards the formation of higher alcohols, with ethanol as a dominant product, by accelerating the CO insertion mechanism during the C_1-C_2 homologation step.

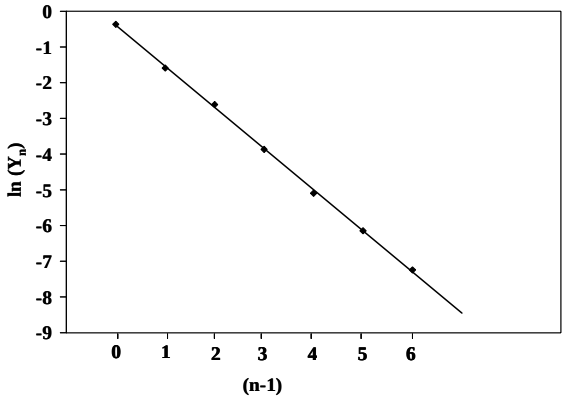

Figure 4.13. ASF plots of distributions of alcohols over the Mo-K/MWCNT

(wt. of the cat. = 2 g, P = 8.3 MPa, T = 320°C, GHSV = 3.6 m^3(STP)/(kg of cat.)/h, H_2/CO molar ratio = 1)

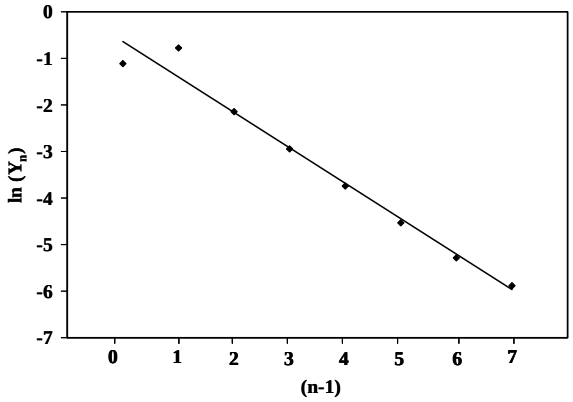

Figure 4.14. ASF plots of distributions of alcohols over the 4.5 wt % Co-Mo-K /MWCNT (wt. of the cat. = 2 g, P = 8.3 MPa, T = 320°C, GHSV = 3.6 m^3 (STP)/(kg of cat.)/h, H_2 to CO molar ratio = 1)

Fig. 4.15 represents the molar percentage distribution of alcohols on un-promoted and 4.5 wt % Co-promoted Mo-K/MWCNT-supported 15 wt % Mo and 9 wt % K catalysts. Methanol (56%), ethanol (24%), propanol (11%), and butanol (6%) are the major products observed over the un-promoted catalyst. When the catalyst was promoted with Co, the methanol molar percentage decreased to 23%, whereas, ethanol molar percentage increased to 47%. Alcohols up to octanol with some traces of nonanol and decanol were detected over Co promoted Mo-K catalysts. Thus, Co not only promotes the activity and selectivity toward higher alcohols (particularly ethyl alcohol), but also propagates the chain growth mechanism leading to the formation of higher alcohols up to heptanol, with some traces of octanol.

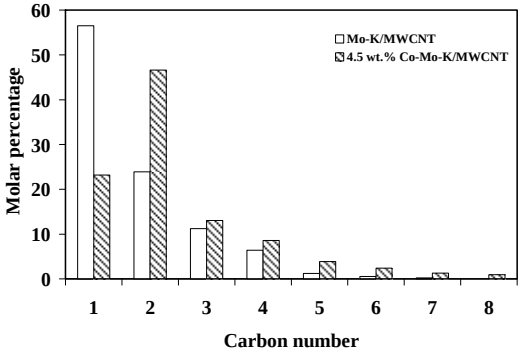

Figure 4.15. Molar percentage of alcohols over the catalysts Mo-K/MWCNT and 4.5 wt % Co-Mo-K/MWCNT

(wt. of the cat. = 2 g, P = 8.3 MPa, T = 320°C, GHSV = 3.6 m^3(STP)/(kg of cat.)/h, H_2/CO molar ratio = 1)

The 4.5 wt % Co-promoted Mo-K/MWCNT catalyst was used to study temperature effects in the range of 300 to 340°C on higher alcohols synthesis. The reactions were performed under similar conditions at 8.27 MPa (1200 psig) and 3.6 m^3 (STP)/(kg of cat.)/h and the results are given in Tables 4.4. The percentage CO conversion and hydrocarbon STY increased monotonically with increasing temperature. Maximum total alcohol space time yields of 0.236 g/(g of cat.)/h was observed at 330 °C over the 4.5 wt % Co-promoted Mo-K/MWCNT catalyst. When the temperature was raised beyond 330°C, the maximum yield of alcohol was not consistent with CO conversion due to the high selectivities to hydrocarbon production and WGS reaction. The total alcohols and higher alcohols selectivities increased, reaching maxima of about 34% and 28% at 330°C, at the expense of hydrocarbons selectivity. The methanol selectivity decreased monotonically with increasing temperature. The molar ratio of higher alcohols to methanol increased significantly with increases in temperature, confirming the increased promotional ability of Co towards selective formation of higher alcohols at higher temperatures.[57]

To investigate pressure effects, reaction pressures were varied in the range of 5.52 to 9.65 MPa (800 to 1400 psig) over 4.5 wt % Co catalyst at 320 °C and m^3 (STP)/(kg of cat.)/h. Table 4.5 shows that increasing the pressure results in a monotonic increase in CO conversion, total alcohol formation rate, hydrocarbon formation rate, and WGS reaction rate. The 4.5 wt % Co-promoted catalysts exhibit maximum total alcohol STY of 0.219 g/(g of cat.)/h at 9.65 MPa. In addition, increasing the pressure increases the selectivity of methanol, higher alcohols, and the molar ratio of higher alcohol to methanol.

Table 4.4. Performance of 4.5 wt % Co-Mo-K/MWCNTs at different temperatures

(wt. of the cat. = 2 g, P = 8.3 MPa, GHSV = 3.6 m^3(STP)/(kg of cat.)/h, H_2 to CO molar ratio = 1)

Temperature (^oC)	CO conversion (%)	Product STY (g/(g of cat.)/h)		CO_2 produced (%)	Alcohol Selectivity (wt %)			Higher alcohols/ methanol (moles/moles)
		Total alcohols	Total Hydrocarbons		Methanol	Ethanol	Higher alcohols	
300	31.6	0.139	0.296	24.9	9.7	10.7	16.0	0.99
310	35.7	0.165	0.347	28.3	8.3	12.6	19.6	1.42
320	39.7	0.198	0.373	31.6	7.0	14.1	23.2	1.98
330	44.5	0.236	0.395	34.5	5.7	16.7	28.4	2.63
340	47.2	0.225	0.423	40.4	5.0	15.6	27.2	3.01

Table 4.5. Performance of 4.5 wt % Co-Mo-K/MWCNTs at different pressures

(wt. of the cat. = 2 g, T = 320^{o}C, GHSV = 3.6 m^3(STP)/(kg of cat.)/h, H_2 to CO molar ratio = 1)

Pressure (psig)	CO conversion (%)	Product STY (g/(g of cat.)/h)		CO_2 produced (%)	Alcohol Selectivity (wt %)			Higher alcohols/ methanol (moles/moles)
		Total alcohols	Total Hydrocarbons		Methanol	Ethanol	Higher alcohols	
800	29.8	0.121	0.302	23.4	5.1	11.3	15.2	0.93
1000	33.6	0.159	0.345	27.7	6.2	12.9	19.4	1.45
1200	39.7	0.198	0.377	31.6	7.0	14.1	23.2	1.98
1400	43.9	0.219	0.398	36.8	7.7	15.2	24.7	2.47

Table 4.6 compares the activities of sulfided 4.5 wt % Co-promoted, 15 wt % Mo, and 9 wt % K (catalyst D) supported on MWCNT with those of similar catalysts available in the literature. The catalysts with highest activity from each work were selected for comparison purpose. This data indicate that the sulfided Mo–K catalysts supported on MWCNT perform well compared to those in the literature. Co promotion to alkali-modified MoS_2 catalysts improved the activity and selectivity of higher alcohols, especially ethanol due to the enhanced $C_1 \rightarrow C_2$ homologation step of CO insertion mechanism.[58] The presence of alkali reduces the formation of metal sulfide species that are responsible for the hydrogenation ability of alkyl species to form alkanes and increase the active sites for the formation of alcohols.[59] MWCNT support plays an important role in attaining higher dispersions due to their well-defined hollow interiors and appropriate pore-size distribution that facilitates the uniform distribution of metal species and having limited interactions with the metal species.[60]

Table 4.6. Comparison of the activities of sulfided Co-promoted Mo-K catalysts

Sample	**A**	**B**	**C**	**D**
Catalyst	**Co-Mo-K /Al_2O_3**	**Co-Mo-K /AC**	**Co-Mo-K/Co decorated MWCNTs**	**Co-Mo-K /MWCNTs**
Temperature (^oC)	350	330	340	330
H_2/CO molar ratio	1.67	2.0	1.0	1.0
Pressure (MPa)	5.0	5.0	5.0	8.3
CO conversion (%)	6.8	14.3	12.6	44.5
STY of alcohols (g/ (g of cat.)/ h)	0.029*	0.199**	0.154	0.236

*The units of STY is ml/(g of cat./ h); ** The units of STY is g/(ml of cat.)/h. (A) Bian et al.[20];
(B) Li et al.[13]; (C) Ma et al.[31]; (D) sulfided 4.5 wt.% Co, 15 wt. % Mo 9 wt.% K supported on MWCNT.

4.5. Conclusions

Metal dispersion of 39% was observed on the MWCNT-supported 15 wt % Mo and 9 wt % K catalysts that are promoted with 4.5 wt % Co. From the TEM images, it was found that metal species were uniformly distributed inside and outside of the tubes, with particle sizes in the range of 3 to 4 nm. Temperature programmed reduction (TPR) tests showed that increasing the amount of Co from 3 to 6 wt % decreased the first and second TPR peak temperatures from 540 and 729 to 525 and 716°C, respectively. The highest total alcohol space time yield of 0.207 g/(g of cat.)/h was observed on the catalyst promoted with 6 wt % Co, whereas the catalyst with 4.5 wt % Co exhibited maximum selectivities of 14% and 23% towards ethyl alcohol and higher alcohols, respectively, at 320°C and 8.3 MPa. The molar ratio of higher alcohols to methanol increased significantly with increases in temperature and pressure over the investigate range of 300 to 340°C and 5.52 to 9.65 MPa, respectively.

4.6. Abbreviations

CLS	Canadian Light Source
DRIFTS	Diffuse reflectance infrared Fourier transform spectroscopy
GHSV	Gas hourly space velocity
ICP-MS	Inductively coupled plasma – mass spectroscopy
MWCNTs	Multi-walled carbon nanotubes
STY	Space time yield
TEM	Transmission electron microscopy
TEY	Total electron yield
TGA	Thermo gravimetric analysis
TPR	Temperature programmed reduction
VLS PGM	Variable line spacing plane grating monochromator
XANES	X-ray absorption near edge spectra
XRD	X-ray diffraction

4.7. References

1. Mahdavia, V.; Peyrovia, M. H.; Islamib, M.; Mehrb, J. Y. Synthesis of higher alcohols from syngas over Cu-Co_2O_3/ZnO, Al_2O_3 catalyst. *Appl. Catal., A* **2005**, *281*, 259-265.
2. Kulawska, M.; Skrzypek, J. Kinetics of the synthesis of higher aliphatic alcohols from syngas over a modified methanol synthesis catalyst. *Chem. Eng. Process*. **2001**, *40*, 33-40.
3. Forzatti, P.; Tronconi, E.; Pasquon, I. Higher alcohol synthesis. *Catal. Rev.: Sci. Eng*. **1991**, *33*, 109-168.
4. Dalmon, J. A.; Chaumette, P.; Mirodatos, C. Higher alcohols synthesis on cobalt based model catalysts. *Catal. Today* **1992**, *15*, 101-127.
5. Smith, K. J.; Anderson, R. B. A chain growth scheme for the higher alcohols synthesis. *J. Catal.* **1984,** *85*, 428-436.
6. Camposmartin, J. M.; Guerreroruiz, A.; Fierro, J. L. G. Structural and surface properties of CuO-ZnO-Cr_2O_3 catalysts and their relationship with selectivity to higher alcohol synthesis. *J. Catal*. **1995,** *156*, 208-218.
7. Boz, I.; Sahibzada, M.; Metcalfe, I. S. Kinetics of the higher alcohol synthesis over a K-promoted CuO/ZnO/Al_2O_3 catalyst. *Ind. Eng. Chem. Res*. **1994,** *33*, 2021-2028.
8. Xu, X.; Doesburg, E. B. M.; Scholten, J. J. F. Synthesis of higher alcohols from syngas - recently patented catalysts and tentative ideas on the mechanism. *Catal. Today* **1987**, *2*, 125-170.
9. Woo, H. C.; Park, K. Y.; Kim, Y. G. ; Nam, I.; Chung, J. S.; Lee, J. S. Mixed alcohol synthesis from carbon monoxide and dihydrogen over potassium-promoted molybdenum carbide catalysts. *Appl. Catal.* **1991**, *75*, 267-280.
10. Bao, J.; Fu, Y-L.; Bian, G-Z. Sol–gel preparation of K–Co–Mo catalyst and its application in mixed alcohol synthesis from CO hydrogenation. *Catal. Lett.* **2008**, *121*, 151-157.
11. Iranmahboob, J.; Hill, D. O. Alcohol synthesis from syngas over K_2CO_3/CoS/MoS_2 on activated carbon. *Catal. Lett*. **2002**, *78*, 49-55.

12. Lee, J. S.; Kim, S.; Lee, K. H.; Nam, I. S.; Chung, J. S ; Kim, Y. G.; Woo, H. C. Role of alkali promoters in K/MoS_2 catalysts for CO-H_2 reactions. *Appl. Catal., A* 1994, *110*, 11-25.

13. Li, Z.; Fu, Y.; Bao, J.; Jiang, M.; Hu, T.;Liu, T.; Xie, Y-N. Effect of cobalt promoter on Co–Mo–K/C catalysts used for mixed alcohol synthesis. *Appl. Catal., A* **2001,** *220*, 21-30.

14. Shen, J. Y.; Matsuzaki, T.; Hanaoka, T.; Takeuchi, K.; Sugi, Y. The promoter function of molybdenum in Rh/Mo/SiO_2 catalysts for CO hydrogenation. *Catal. Lett*. **1994,** *28*, 329-336.

15. Li, D.; Yang, C.; Li, W.; Sun, Y.; Zhong, B. Ni/ADM: a high activity and selectivity to C_{2+}OH catalyst for catalytic conversion of synthesis gas to C_1-C_5 mixed alcohols. *Top. Catal*. **2005,** *32*, 233-240.

16. Storm, D. A. The production of higher alcohols from syngas using potassium promoted Co/Mo/$A1_2O_3$ and Rh/Co/Mo/$A1_2O_3$. *Top. Catal*. **1995,** *2*, 91-101.

17. Fujimoto, A.; Oba, T. Synthesis of C_1-C_7 alcohols from synthesis gas with supported cobalt catalysts. *Appl. Catal.* **1985**, *13*, 289-319.

18. Murchison, C. B.; Murdick, D. A. *Process for producing olefins from carbon monoxide and hydrogen*. U.S. Patent 4,199,522, Apr 22, 1980.

19. Santiesteban, J. G.; Bogdan, C. E.; Herman, R. G.; Klier, K. Mechanism of C_1-C_4 alcohol synthesis over alkali/MoS_2 and alkali/Co/MoS_2 catalysts. In *Proc. 9th Intern. Congr. Catal.;* Phillips, M. J., Ternan, M., Eds.; The Chemical Institute of Canada: Ottawa, 1988; Vol. 2, p 561.

20. Bian, G. Z.; Fu, Y. L.; Ma, Y.-S. Structure of Co–K–Mo/γ-Al_2O_3 catalysts and their catalytic activity for mixed alcohols synthesis. *Catal. Today* **1999**, *51*, 187-193.

21. Xiang, M.; Li, D.; Li, W.; Zhong, B.; Sun, Y. Synthesis of higher alcohols from syngas over K/Co/β-Mo_2C catalysts. *Catal. Commun*. **2007,** *8*, 503-507.

22. Duchet, J. C.; van Oers, E. M.; de Beer, V. H. J.; Prins, R. Carbon-supported sulfide catalysts. *J. Catal.* **1983**, *80*, 386-402.

23. Moene, R.; Tazelaar, F. W.; Makkee, M.; Moulijn, J. A. Nickel-catalyzed conversion of activated carbon extrudates into high surface area silicon carbide by reactive chemical vapour deposition. *J. Catal.* **1997**, *170*, 311-324.

24. Pan, X.; Fan, Z.; Chen, W.; Ding, Y.; Luo, H.; Bao, X. Enhanced ethanol production inside carbon-nanotube reactors containing catalytic particles. *Nat. Mater.* **2007**, *6*, 507–511.

25. van Berge, P. J.; van de Loosdrecht, J.; Barradas, S.; van der Kraan, A. M. Oxidation of cobalt based Fischer–Tropsch catalysts as a deactivation mechanism. *Catal. Today.* **2000,** *58*, 321-334.

26. Xiaoming, M.; Guodong, L.; Hongbin, Z. Co-Mo-K sulfide-based catalyst promoted by multiwalled carbon nanotubes for higher alcohol synthesis from syngas. *Chin. J. Catal.* **2006**, *27*, 1019–1027.

27. Serp, P.; Corrias, M.; Kalck, P. Carbon nanotubes and nanofibers in catalysis. *Appl. Catal., A* **2003**, *253*, 337-358.

28. Sigurdson, S.; Sundaramurthy, V.; Dalai, A. K.; Adjaye, J. Effect of anodic alumina pore diameter variation on template-initiated synthesis of carbon nanotube catalyst supports. *J. Mol. Catal. A*: Chem. **2009**, *306*, 23-32.

29. Eswaramoorthi, I.; Sundaramurthy, V.; Das, N.; Dalai, A. K.; Adjaye, J. Application of multi-walled carbon nanotubes as efficient support to NiMo hydrotreating catalyst. *Appl. Catal., A* **2008**, *339*, 187–195.

30. Tavasoli, A.; Abbaslou, R. M. M.; Trepanier, M.; Dalai, A. K. Fischer–Tropsch synthesis over cobalt catalyst supported on carbon nanotubes in a slurry reactor. *Appl. Catal., A* **2008**, *345*, 134-142.

31. Ma, X-M.; Lin, G.-D.; Zhang, H.-B. Co-decorated carbon nanotube-supported Co–Mo–K sulfide catalyst for higher alcohol synthesis. *Catal. Letters* **2006**, *111*, 141-151.

32. Surisetty, V. R.; Tavasoli, A.; Dalai, A. K. Synthesis of higher alcohols from syngas over alkali promoted MoS_2 catalysts supported on multi-walled carbon nanotubes. *Appl. Catal. A* **2009**, *365*, 243–251.

33. Bahome, M. C.; Jewell, L. L.; Hildebrandt, D.; Glasser, D.; Coville, N. J. Fischer–Tropsch synthesis over iron catalysts supported on carbon nanotubes. *Appl. Catal., A* **2005,** *287*, 60-67.

34. Moronta, A.; Troconis, M.E.; Gonzalez, E.; Moran, C.; Sanchez, J.; Gonzalez, A.; Quinonez, J. Dehydrogenation of ethylbenzene to styrene catalyzed by Co, Mo and CoMo catalysts supported on natural and aluminum-pillared clays: Effect of the metal reduction. *Appl. Catal., A* **2006**, *310*, 199-204.

35. Li, Z.; Fu, Y.; Jiang, M.; Hu, T.; Liu, T.; Xie, Y. Active carbon supported Mo-K catalysts used for alcohol synthesis. *J. Catal.* **2001**, *199*, 155–161.

36. Jiang, M.; Bian, G.-Z.; Fu, Y.-L. Effect of the K---Mo interaction in K---MoO3/γ-Al2O3 catalysts on the properties for alcohol synthesis from syngas. *J. Catal.* **1994**, *146*, 144–154.

37. Calafata, A.; Vivas, F.; Brito, J. L. Effects of phase composition and of potassium promotion on cobalt molybdate catalysts for the synthesis of alcohols from CO2 and H2. *Appl. Catal., A* **1998**, *172*, 217–224.

38. Fu, Y.-L.; Fujimoto, K.; Lin, P.; Omata, K.; Yu, Y. Effect of calcination conditions of the oxidized precursor on the structure of a sulfided K-Mo/γ-Al2O3 catalyst for mixed alcohol synthesis. *Appl. Catal., A* **1995**, *126*, 273–285.

39. Li, D.; Zhao, N.; Qi, H.; Li, W.; Sun, Y. H.; Zhong, B. Higher alcohol synthesis over a La promoted Ni/K_2CO_3/MoS_2 catalyst. *Catal. Commun.* **2004**, *5*, 605–609.

40. Qi, H.; Li, D.; Yang, C.; Ma, Y.; Li, W.; Sun, Y.; Zhong, B. Nickel and manganese co-modified K/MoS2 catalyst: high performance for higher alcohols synthesis from CO hydrogenation. *Catal. Commun.* **2003**, *4*, 339–342.

41. Harris, S.; Chianelli, R. R. Catalysis by transition metal sulfides: A theoretical and experimental study of the relation between the synergic systems and the binary transition metal sulfides. *J. Catal.* **1986**, *98*, 17–31.

42. Delmon, B. *in: Proc. 3rd International Conference on the chemistry and uses of Molybdenum*, 1979; p.17.

43. Feng, L.; Li, X.; Dadyburjor, D. B.; Kugler, E. L. A temperature-programmed-reduction study on alkali-promoted, carbon-supported molybdenum catalysts. *J. Catal.* **2000**, *190*, 1–13.

44. Noronha, F. B.; Baldanza, M. A. S.; Schmal, M. CO and NO adsorption on alumina-Pd-Mo catalysts: Effect of the precursor salts. *J.Catal.* **1999**, *188*, 270–280.

45. Kurhinen, M.; Pakkanen, T. A. CoMo/alumina prepared from carbonyl precursors: DRIFT, TPR and HDS studies. *Appl. Catal., A* **2000**, *192*, 97-103.

46. Topsoe, N.Y.; Topsoe, H. Characterization of the structures and active sites in sulfided Co---Mo/Al_2O_3 and Ni---Mo/Al_2O_3 catalysts by NO chemisorption. *J. Catal*. **1983**, *84*, 386-401.

47. Eswaramoorthi, I.; Dalai, A. K. DRIFT studies of adsorbed CO over sulfided K–Rh–Mo/Al_2O_3 catalysts: Detection of Rh–Mo–S phase. *Catal. Lett.* **2009**, *131*, 203-212.

48. Aegerter, P. A.; Quigley, W. W. C.; Simpson, G. J.; Ziegler, D. D.; Logan, J. W.; McCrea, K. R.; Glazier, S.; Bussell, M. E. Thiophene hydrodesulfurization over alumina-supported molybdenum carbide and nitride catalysts: Adsorption sites, catalytic activities, and nature of the active surface. *J. Catal*. **1996**, *164*, 109-121.

49. Sundaramurthy, V.; Eswaramoorthi, I.; Dalai, A. K.; Adjaye, J. Hydrotreating of gas oil on SBA-15 supported NiMo catalysts. *Micropor. Mesopor. Mat.*, **2008**, *111*, 560-568.

50. Wu, W.; Wu, Z.; Liang, C.; Chen, X.; Ying, P.; Li, C. In Situ FT-IR spectroscopic studies of CO sdsorption on fresh Mo_2C/Al_2O_3 catalyst. J. Phys. *Chem. B* **2003**, *107*, 7088-7094.

51. Wu, Z.; Sun, F.; Wu, W.; Feng, Z.; Liang, C.; Wei, Z.; Li, C. On the surface sites of MoP/SiO_2 catalyst under sulfiding conditions: IR spectroscopy and catalytic reactivity studies. *J. Catal*. **2004**, *222*, 41-52.

52. Baghalha, M.; Hoseini, S. M. Long-Term Deactivation of a commercial CoMo/γ-Al_2O_3 catalyst in hydrodesulfurization of a naphtha stream. *Ind. Eng. Chem. Res*. **2009,** 48, 3331-3340.

53. Sun, M.; Nelsona, A. E.; Adjaye, J. On the incorporation of nickel and cobalt into MoS_2-edge structures. *J. Catal*. **2004,** *226*, 32-40.

54. Topsøe, H.; Clausen, B. S.; Massoth, F. E. *Hydrotreating Catalysis, Science and Technology*, Vol. 11, Springer: Berlin, 1996.

55. Kim, H.-G.; Lee, K. H.; Lee, H.-G.J. S. Carbon monoxide hydrogenation over molybdenum carbide catalysts. *Res. Chem. Intermed.* **2000**, *26*, 427–444.

56. Hou, P.; Meeker, D.; Wise, H. Kinetic studies with a sulfur-tolerant water gas shift catalyst. *J. Catal.* **1983,** *80*, 280-285.

57. Liu, Z.; Li, X.; Close, M. l R.; Kugler, E. L.; Petersen, J. L.; and Dadyburjor, D. B.; Screening of alkali-promoted vapor-phase-synthesized molybdenum sulfide catalysts for the production of alcohols from synthesis gas. *Ind. Eng. Chem. Res.* **1997,** 36, 3085-3093.

58. Surisetty, V. R.; Dalai, A. K.; Kozinski, J. Effect of Rh promoter on MWCNT-supported alkali-modified MoS_2 catalysts for higher alcohols synthesis from CO hydrogenation. *Appl. Catal., A* **2010,** *381*, 282-288.

59. Tatsumi, T.; Muramatsu, A.; Yokota, K.; Tominga, H. Mechanistic study on the alcohol synthesis over molybdenum catalysts : Addition of probe molecules to CO---H_2. *J. Catal.* 1989, *115*, 388–398.

60. Surisetty, V. R.; Dalai, A.K.; Kozinski, J. Alkali-promoted trimetallic Co-Rh-Mo sulfide catalysts for higher alcohols synthesis from synthesis gas: Comparison of MWCNT and activated carbon supports. *Ind. Eng. Chem. Res.* **2010**, *49*, 6956-6963.

CHAPTER 5

Effect of Rh Promoter on MWCNT-Supported Alkali-Modified MoS_2 Catalysts for Higher Alcohols Synthesis from CO Hydrogenation

The manuscript provided in this chapter is very similar to the one published in the journal Applied Catalysis A: General.

Citation:

Surisetty, V. R.; Dalai, A. K.; Kozinski, J. Effect of Rh promoter on MWCNT-supported alkali-modified MoS_2 catalysts for higher alcohols synthesis from CO hydrogenation. *Appl. Catal., A* **2010**, *381*, 282–288.

Contribution of the Ph.D. Candidate

Experiments were designed and performed by Venkateswara Rao Surisetty. Drs. Ajay Kumar Dalai and Janusz Kozinski provided consultation regarding the experimental program. Data analysis and interpretations were performed by Venkateswara Rao Surisetty. All of the writing of the submitted manuscript was written by Venkateswara Rao Surisetty with Dr. Dalai providing editorial guidance regarding the style and content of the paper.

Contribution to Overall Study

In this Chapter the effects of different Rh loadings on the catalyst with 15 wt % Mo and 9 wt % K for higher alcohols synthesis from CO hydrogenation were studied. It is aimed to study the interaction effects of Rh metal with alkali-modified molybdenum-based catalysts and hence a catalyst was prepared using 1.5 wt % of Rh supported on MWCNTs. The effects of temperature and pressure, on the catalytic performance for higher alcohols synthesis were also studied.

5.1. Abstract

The promotional effects of Rh (0 to 2 wt %) on Mo-K/MWCNTs catalysts for higher alcohol synthesis from synthesis gas (molar ratio of H_2 to Co is equal to 1) were examined. Diffraction peaks representing the characteristic K-Mo-S phase were observed in the X-ray diffraction (XRD) patterns of the sulfided form of the Rh-promoted Mo-K/MWCNTs catalysts. When 1 wt % Rh was introduced on the multi-walled carbon nanotube (MWCNT)-supported 15 wt % Mo and 9 wt % K catalysts, the reduction temperature of Mo(VI) to Mo(IV) was significantly decreased to 394°C. Metal dispersions were increased from 30% to 42%, with an increase in Rh content from 0 to 2 wt %. The existence of promoted and un-promoted MoS_2 sites was confirmed by a diffuse reflectance infrared Fourier transform spectroscopy (DRIFTS) study of adsorbed CO over sulfided catalysts. The maximum total alcohol yield of 0.211 g/(g of cat.)/h, ethanol selectivity of 16%, and higher alcohols selectivity of 25% were observed on the catalyst with 1.5 wt % Rh at 320°C and 8.3 MPa. The best conditions for producing higher alcohols from synthesis gas (mole ratio of H_2 and CO is equal to 1) using gas hourly space velocity (GHSV) of 3.6m^3 (STP)/(kg of cat.) /h are determined as 330°C and 9.65 MPa (1400 psig).

5.2. Introduction

Higher alcohols is an alternative fuel to improve the octane number of gasoline and is recognized as a promising route for the production of clean fuels and petrochemical feed stocks from coal, natural gas, and hydrocarbon wastes via gasification.[1,2] Alkali modified molybdenum catalysts in oxide and sulfide forms can be used for the synthesis of higher alcohols.[3] The sulfide form of these catalysts are more promising because of their excellent resistance to sulfur poisoning and high activity for water–gas shift reaction, as well as high tolerance to coke build up. This saves the cost of ultra-desulfurization for feed gas and water separation.[4,5] The control of product selectivity is of major interest because an Anderson–Schulz–Flory polymerisation process describes the product distribution over these catalysts.[6] For higher alcohols synthesis, CO should be activated both dissociatively and non-dissociatively on the catalyst sites.[7] Depending on the reaction conditions, the status of the rhodium species,

and the properties of alkali promoters and supports, the rhodium species in catalysts is capable of catalyzing dissociation, insertion, and hydrogenation of CO.[8,9] The high cost of Rh and its low reactivity towards the formation of higher alcohols hinder its commercial utilization. Suitable supports and promoters enhance the reactivity of Rh towards the higher alcohol synthesis reaction.[10,11]

Luo et al.[12] and Ojeda et al.[13] concluded that Rh-based catalysts favor high selectivity towards C_2-oxygenates. Sudhakar et al.[14] reported that the CO hydrogenation rate and the formation of oxygenates increased by incorporating molybdenum in Rh/Al_2O_3. Li et al.[15] reported that rhodium incorporation into the $Mo\text{-}K/Al_2O_3$ catalysts increased the selectivity to the formation of C_{2+} alcohols, due to the co-existence of cationic and metallic rhodium species stabilized by the interaction of rhodium with the molybdenum species. This may be due to the addition of rhodium to the alkali-promoted molybdenum-sulfided catalysts, which significantly modified the coordination status of the molybdenum atoms in the catalysts.[16] Matsumoto et al.[17] tested the effect of Rh addition on the $Ir\text{-}Mo/SiO_2$ catalysts and found that incorporating Rh increases both the activity and the selectivity towards the formation of oxygenates.

Multi-walled carbon nanotubes (MWCNTs) have well-defined hollow interiors and display exceptionally high mechanical strength, thermal stability, and electrical conductivity.[18,19] Their unique characteristics, such as resistance to acidic or basic media, inert graphitic surface, appropriate pore-size distribution, and nano-sized channels make them a promising support for various catalytic applications.[20,21] Yin et al.[22] showed that the Ru catalyst supported on MWCNTs exhibits the highest conversion of NH_3 for the generation of CO_x-free H_2 compared to those supported on various oxides and activated carbon. Tavasoli et al.[23] found that CO conversion and Fischer–Tropsch synthesis rate were higher on Co catalysts supported on MWCNTs than that supported on alumina as MWCNTs aided the uniform dispersion of Co metal clusters on the support.

The 15 wt % Mo and 9 wt % K MWCNT-supported catalyst outperformed in terms of higher alcohols yield and selectivity over the investigative range of Mo (10–20 wt %) and K (3–9 wt %).[24] In the present study, a series of Rh (0, 1, 1.5, and 2 wt %)-promoted alkali-modified molybdenum-based catalysts (15 wt % Mo and 9 wt % K) supported on MWCNTs were prepared by sequential pore volume impregnation. The

prepared catalysts were characterized using different techniques in oxide and sulfide states. The effects of reaction conditions, such as temperature and pressure, on the catalytic performance for higher alcohols synthesis were studied. In order to study the interaction effects of Rh metal with alkali-modified molybdenum-based catalysts, a catalyst is prepared using 1.5 wt % of Rh on MWCNTs support.

5.3. Experimental

5.3.1. Preparation of MWCNT-supported catalysts

Rh promoted Mo-K/MWCNT

MWCNTs (purity > 95%) obtained from M.K. Nano, Canada were used as supports for the preparation of the catalysts. Prior to impregnation, the supports were treated with 30% HNO_3 reflux at 100°C overnight, washed with distilled water several times, and dried at 120°C for 6 h. The oxide samples were prepared by the incipient wetness impregnation method using ammonium heptamolybdate tetrahydrate (Sigma–Aldrich), potassium carbonate (Aldrich), and rhodium chloride hydrate (Aldrich) as precursors for Mo, K, and Rh, respectively. At the first step, the supports were impregnated with an aqueous solution of K_2CO_3, followed by drying at 120°C for 2 h, and stabilized in an argon flow of 50 ml/min at 300°C at a heating rate of 10°C /min for 4 h. It was further impregnated with aqueous solutions containing the required amount of $(NH_4)_6Mo_7O_{24}$ and $RhCl_3$, followed by drying at 120°C for 2 h and stabilized in an argon flow of 50 ml/min at 450°C at a heating rate of 10°C /min for 12 h. The sulfide samples were obtained by heat treating the oxide precursors in a flow of 10 mole % H_2S in H_2 gas at 450°C at a heating rate of 2°C /min for 4 h.

Rh/MWCNT

The MWCNT support was impregnated with an aqueous solution of $RhCl_3$. It was dried at 120°C for 2 h and stabilized in an argon flow of 50 ml/min at 450°C at a heating rate of 10°C/min for 12 h.

5.3.2. Characterization of Rh-promoted Mo-K/MWCNT catalysts

The contents of Mo and Rh of the oxide catalysts were determined using a Perkin-Elmer ELAN 5000 inductively coupled plasma-mass spectroscopy (ICP-MS) instrument.

The surface area, pore volume, and average pore diameter of oxide samples were measured by N_2-physisorption at 77 K using a Micromeritics ASAP 2000. Approximately 0.2 g of sample was used for each analysis. The moisture and other adsorbed gases present in the sample were removed before analysis by degassing the sample at 200°C for 2 h under 66.7 Pa (500mmHg). The sample was then evacuated at 2.67 Pa (20μm Hg) before N_2 adsorption.

A Perkin-Elmer thermogravimetric (TG) differential thermal analyzer (DTA) was used to measure weight changes of the sample when heated under a flow of argon (flow rate of 40 ml/min) at a constant heating rate of 10°C/min.

Powder X-ray diffraction (XRD) analysis patterns of oxide and sulfide forms of samples were recorded on a Rigaku Xray diffraction instrument with nickel filtered Cu Kα radiation (λ = 0.1541 nm). Each sample was scanned at a rate of 0.05 °/s, with 2θ varying from 10 to 80°. In order to obtain the XRD patterns in sulfided form, the catalysts were first sulfided for 6 h at 450°C at a heating rate of 2°C/min, using a gaseous mixture containing 10 mole % H_2S in H_2 at a flow rate of 50 ml/min. After sulfidation, the catalysts were cooled to room temperature in a flow of He and the sample was transferred to sample holders under protection of He.

The morphology of the oxide samples was characterized by transmission electron microscopy (TEM). TEM investigations were carried out using a Philips CM20 (100 kV) transmission electron microscope equipped with a NARON energy-dispersive spectrometer with a germanium detector. The inner diameters, wall thicknesses, and length of carbon nanotubes, as well as the sizes of the catalyst particles, were measured by digital micrograph software (version 3.6.5, Gatan Inc.).

Temperature programmed reduction (TPR) profiles of the catalysts were performed to study the reducibility of the metal oxides in the catalysts. For each analysis, approximately 0.2 g of sample was used, which was first purged in a flow of argon at 170°C to remove traces of water and then cooled to 40°C. The TPR of each sample was performed using a 3.1 mole % H_2 in He stream at a flow rate of 30 ml/min at atmospheric pressure, using a CHEMBET 3000 TPD-TPR analyzer equipped with a thermal conductivity detector, heating at a linearly programmed rate of 10°C/min up to 800°C.

Carbon monoxide is used as a probe molecule in order to determine the number of accessible surface metal atoms present on sulfided catalysts. The CO uptake (μmole/g of cat.) measured from CO chemisorption is equivalent to the number of active metal atoms that are accessible to the reactant molecules. Metal dispersion is defined as the ratio of CO uptake to the theoretical number of Rh and Mo metal atoms ((μmole/g of cat.) present in the sample. The stoichiometric coefficient (CO to metal ratio) of 1 was used and the extent of reduction was assumed to be 100% in metal dispersion calculations. The carbon monoxide uptake on the sulfided catalysts was measured using the Micromeritics ASAP 2000 instrument. Prior to the CO chemisorption measurement, 0.2 g of sample was sulfided in situ using 10 mole % H_2S in H_2 at 400°C for 4 h. The sample was then evacuated at 120°C until the static pressure remained less than 6.6 x 10^{-4} Pa. Chemisorption was performed by passing pulses of CO over the sample to measure the total gas uptake at 35°C.

Diffuse reflectance infrared Fourier transform spectroscopy (DRIFTS) of adsorbed CO is an efficient tool to monitor the changes of Mo-related active species, due to Rh addition. The sulfided catalysts were subjected to DRIFT spectroscopy of adsorbed CO in a Perkin-Elmer Spectrum GX instrument equipped with a DTGS detector and a KBr beam splitter. Approximately 10 mg of powdered oxide sample was placed in the sample cup inside a Spectrotech diffuse reflectance in situ cell, equipped with ZnSe windows and a thermocouple, allowing direct measurement of the sample surface temperature. Spectra for each experiment were averaged over 64 scans in the region 3000–1000 cm^{-1} with a nominal 4 cm^{-1} resolution. Prior to CO adsorption, the catalyst was sulfided using 10 mole % H_2S in H_2 (50 ml/min) at 375°C for 4 h. After sulfidation, the flow was switched to He (50 ml/min) and the temperature was decreased to 30°C, and a background spectrum was recorded. CO adsorption was carried out at 30°C by introducing pure CO (30 ml/min) into the sample cell for 30 min. After adsorption, the system was purged with He (50 ml/min) for 30 min to remove the physisorbed CO molecules, and the spectra were collected under He flow.

5.3.3. Catalytic studies

A single-pass tubular downflow fixed-bed reactor of 450-mm length and 22-mm inside diameter made of inconel tube, was used to perform higher alcohol synthesis reactions (HAS). The reactor was packed with 2 g of catalyst diluted with 12 ml of 90

mesh size silicon carbide and housed in an electric furnace controlled by a temperature controller. The reactor was pressurized to 3.44 MPa (500 psig) with He. The Mo-K/MWCNT catalysts with or without Rh promoters were sulfided and reduced in-situ for 6 h at 450°C at a heating rate of 2°C/min, using a gas mixture containing 10 mole % H_2S in H_2 and flow rate of 50 ml/min. The Rh/MWCNT catalyst was reduced with pure H_2 for 6 h at 450°C at a heating rate of 2°C/min and flow rate of 50 ml/min. The temperature was then lowered to the reaction temperature and the system was pressurized to the reaction conditions. The feed gas mixture CO (45 mole %), H_2 (45 mole %), and Ar (10 mole %) was passed through mass flow controllers. The HAS reaction was carried out at steady-state under the reaction conditions of 300 to 340°C, 5.51 (800 psig) to 9.65 MPa (1400 psig), and a gas hourly space velocity (GHSV) of 3.6 m^3 (STP) /(kg of cat.)/h over a period of 24 h. The product gas was cooled to 0°C and separated into gas and liquid phases at the reaction pressure. The CO conversion and other gaseous products were monitored with a time interval of 1 h. The liquid products were collected at the end of the reaction and analyzed with a Varian 3400 gas chromatograph equipped with a capillary column and a flame ionization detector (FID). The volume and weight of liquid products were measured to check the mass balance. The gaseous products were analyzed online on a Shimadzu gas chromatograph through a sampling valve. Using Ar as an internal standard, the CO conversion was calculated and the overall mass balance of the reaction was determined. The experiments were repeated at least twice to check reproducibility and to confirm that the results obtained were within the experimental error of ± 2.5%.

5.4. Results and Discussion

5.4.1. Characterization of Rh-promoted Mo-K/MWCNT catalysts

The elemental compositions of stabilized catalysts are given in Table 5.1, along with the targeted compositions. These results indicate that most of the precursors are deposited on the support during the incipient wetness impregnation. The measured compositions are slightly below the corresponding targeted values, which may result from the hygroscopic nature of precursors.

Table 5.1 shows the textural characteristics of all the stabilized catalysts. The surface area and pore volume of all the catalysts were much lower than the pure support.

The BET surface area of the Mo-K/MWCNT catalyst was 96 m^2/g. When Rh loading on the MWCNT-supported 15 wt % Mo, 9 wt % K catalyst was increased from 1 to 2 wt %, a decrease in BET surface area from 80 to 69 m^2/g was observed, confirming that the pore blockage increased with Rh loadings.

Table 5.1 gives the results of CO uptake (μmole/g of cat.), and % dispersion of metals measured from CO chemisorption of the sulfided catalysts. The CO uptake increased by 24.5% when the catalyst with 15 wt % Mo and 9 wt % K supported on the MWCNTs was promoted with 1wt % Rh. With the addition of Rh, the active sites on the support that adsorb CO were increased, which is indicated by large CO uptake. Hence it is expected that the Rh promotion enhanced the CO hydrogenation capability of the MWCNT-supported Mo-K catalysts. The metal dispersion increased from 35.2% to 41.8% when the Rh metal content on the Mo-K/MWCNT catalyst was increased from 1 to 2 wt %, resulting in the formation of more active sites for higher alcohols synthesis reaction at higher Rh loadings.

The XRD patterns of the catalysts in oxidized and sulfided form were measured and are shown as Figs. 5.1 and 5.2, respectively. The most probable phases in the samples were detected using the JCPDS chemical spectra data bank. The results of the possible crystal phases for the oxidized and sulfided samples with their corresponding reflection planes are given in Table 5.2.

The peak at 2θ value of 26.6° is due to the reflection of graphite phase of MWCNT.[25] The characteristic reflections corresponding to the crystalline structure of MoO_3 are observed at a 2θ value of 40.2°.[26] Several kinds of K-Mo-O mixed phases exist in oxidized form of catalysts. The peaks at 2θ values of 19.4°, 28.5°, 29.8°, and 30.9° correspond to the characteristic reflections of the $K_2Mo_2O_7$ phase.[27]. Other K-Mo-O phases, such as KMo_4O_6 (2θ = 37.1°) and $K_2Mo_7O_{20}$ (2θ = 53.8°) also exist. For the Rh species, no peaks are detected from the XRD spectra of the catalysts in the oxide form, indicating good dispersion of those species on the catalyst.

Table 5.1. Elemental compositions, textural properties and chemisorption measurement results

Catalyst	Targeted composition (wt %)			Measured composition (wt %)		BET surface area (m^2/g)	Total pore volume (cc/g)	Average pore diameter (nm)	CO uptake (μmole/g of cat.)	Dispersion of metals (%)
	K	Mo	Rh	Mo	Rh					
Acid treated MWCNT	--	--	--	--	--	220	0.66	10.9	--	--
MoS_2-K/MWCNT	9	15	--	14.1	--	96	0.37	16.3	94	30.0
1 wt % Rh-Mo-K/MWCNT	9	15	1	14.2	0.7	80	0.32	17.3	117	35.2
1.5 wt % Rh-Mo-K/MWCNT	9	15	1.5	14.4	1.3	74	0.30	17.7	135	39.5
2 wt % Rh-Mo-K/MWCNT	9	15	2	14.3	1.8	69	0.27	18.2	147	41.8

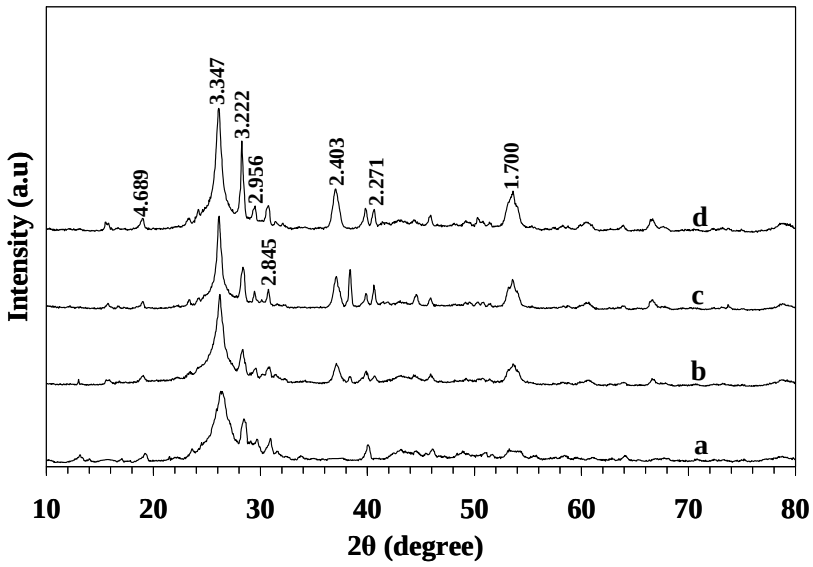

Figure 5.1. XRD patterns of the catalysts in oxidized form
a. Mo-K/MWCNT; b. 1 wt % Rh-Mo-K/MWCNT;
c. 1.5 wt % Rh-Mo-K/MWCNT; d. 2 wt % Rh-Mo-K/MWCNT

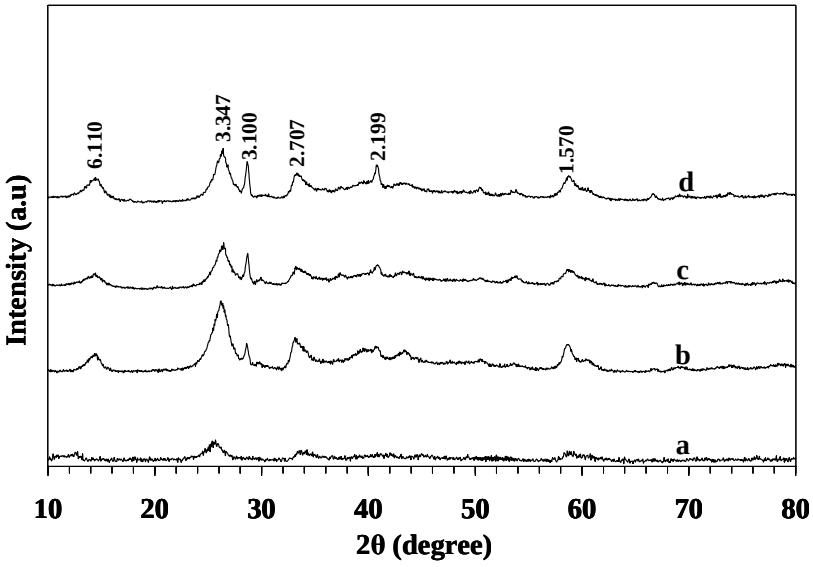

Figure 5.2. XRD patterns of catalysts in sulfided form
a. Mo-K/MWCNT; b. 1 wt % Rh-Mo-K/MWCNT;
c. 1.5 wt % Rh-Mo-K/MWCNT; d. 2 wt % Rh-Mo-K/MWCNT

Table 5.2. Crystal phases and reflection planes from XRD

Crystal phase	2θ	d-spacing	Reflection plane h k l
Oxidized form of catalysts:			
Graphite (C)	26.6°	3.347	1 1 1
MoO_3	40.2°	2.271	1 5 0
$K_2Mo_2O_7$	19.4°	4.689	1 1 0
$K_2Mo_2O_7$	28.5°	3.222	0 0 2
$K_2Mo_2O_7$	29.8°	2.956	0 1 2
$K_2Mo_2O_7$	30.9°	2.845	2 1 0
KMo_4O_6	37.1°	2.403	4 0 0
$K_2Mo_7O_{20}$	53.8°	1.700	0 10 4
Sulfided form of catalysts:			
MoS_2	14.6°	6.110	0 0 3
MoS_2	33.4°	2.707	1 0 1
MoS_2	40.9°	2.199	0 1 5
MoS_2	58.9°	1.570	1 1 0
KMo_3S_3	28.7°	3.100	1 1 1

The various diffraction peaks observed in the XRD patterns of oxide samples are completely removed after sulfidation, and the new diffraction peaks with less diffraction intensity representing different sulfide species appeared. This confirmed that newly formed active phases during the sulfidation step are well dispersed on the MWCNT support. The reflections of MoS_2 crystallites are observed at 2θ values of 14.6°, 33.4°, 40.9° and 58.9°.[28] The peaks at 2θ values 28.7° are due to the characteristic reflections of the K-Mo-S species, which represents KMo_3S_3.[29]

The TEM images of 1.5 wt % Rh-promoted Mo-K/MWCNT catalysts were recorded, and the representative image as shown in Fig. 5. 3 was selected from several micrographs. No amorphous carbon or other impurities in and around the tubes are observed claiming its advantage to be used as catalyst support. The walls are well structured, with thickness ranges from 3 to 8 nm, indicating that MWCNT are multi-walled in nature and the length of the tubes are between 200 and 400 nm. Most of the nanotube caps are found to be open and the pore diameter ranges from 5 to 10 nm. The metal particles are well dispersed inside and outside of the tube walls and the particle sizes are in the range of 3–4 nm.

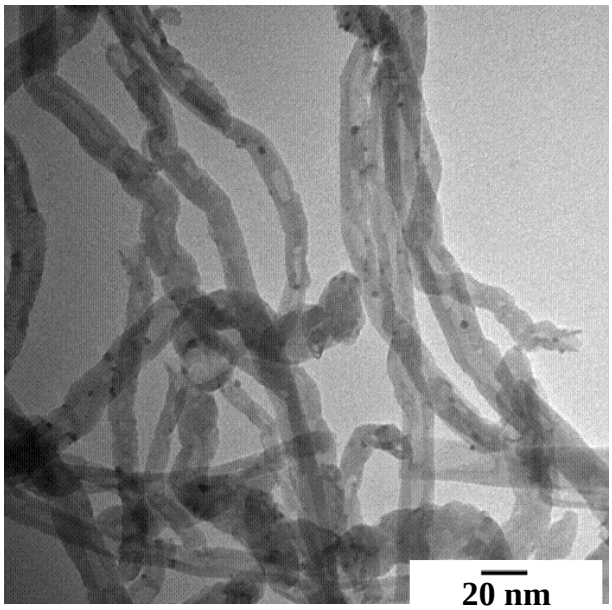

Figure 5.3. TEM image of 1.5 wt % Rh-Mo-K/MWCNT

Two main reduction peaks are observed in the TPR studies of the K-promoted Mo-based catalysts, the low temperature reduction peak appearing around 519°C and the high temperature peak around 787°C. The reduction of octahedral-coordinated Mo (Mo^{6+}) species takes place at low temperatures, followed by the reduction of tetrahedral-coordinated Mo (Mo^{4+}) species to a lower oxidation state.[30]

The TPR profiles of the Rh-promoted Mo-K/MWCNT catalysts are represented in Fig. 5.4. When 1 wt % Rh was introduced on the MWCNT-supported 15 wt% Mo and 9 wt % K catalyst, the low temperature reduction peak significantly shifted from 519 to 392°C, whereas, the high temperature reduction peak shifted from 787 to 733°C. This explains that the reduction behavior of alkali-modified Mo catalysts was greatly improved by Rh promotion due to the possible interaction between Rh and Mo metal species.[31] A small peak was noted on the Rh-promoted catalyst at a lower temperature in the range of 150–225°C due to the reduction of rhodium species.[15] However, with increased Rh content from 1 to 2 wt %, the low temperature reduction peak shifted from 392 to 408°C and the peak intensity was increased due to increased H_2 consumption. It can be interfered from the results that the dispersion of Rh and Mo metals species were improved at higher Rh content favoring the formation of smaller particles, resulted due to strong interaction between Rh and Mo.

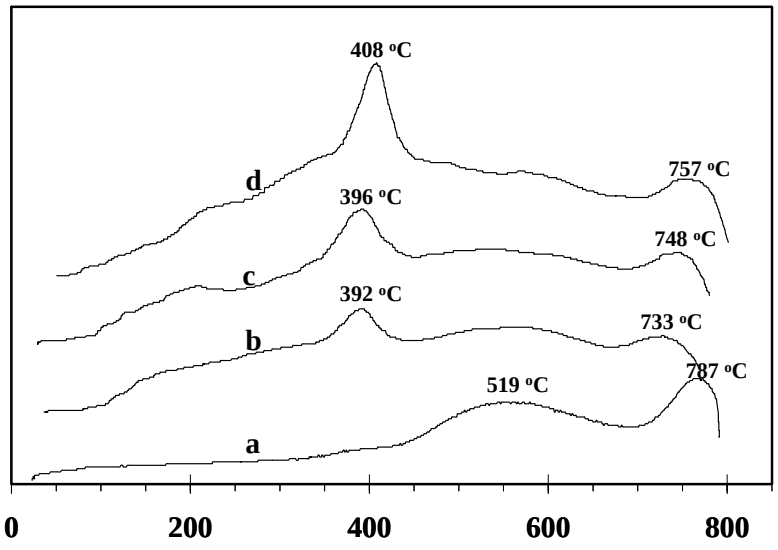

Figure 5.4. H_2-TPR profiles :

a. Mo-K/MWCNT; b. 1 wt % Rh-Mo-K/MWCNT;
c. 1.5 wt % Rh-Mo-K/MWCNT; d. 2 wt % Rh-Mo-K/MWCNT

The effect of wt % of Rh on the metal interactions between Rh and Mo over sulfided Mo-K/MWCNTs catalysts was studied using DRIFTS after CO adsorption (Fig. 5.5). The intensity of the peaks were observed to be weak on the catalyst with 15 wt % Mo and 9 wt % K supported on the MWCNTs compared to those with Rh promoted catalysts. The sample promoted with 1 wt% Rh on Mo-K/MWCNTs showed relatively weak bands in the range of 2195–2130 cm^{-1}, strong bands with maxima at 2110, 2095, and 2065 cm^{-1}, a band with maxima around 2045, 2025, and 2010 cm^{-1}, and a weak broad band at around 1980 cm^{-1}. The characteristic bands in the range of 2195–2130 cm^{-1} are assigned to the adsorption of CO on Rh^{n+} sites, resulting from chloride precursors. Zafeiratos et al.[32] observed the formation of cationic Pt^{n+} sites in the range of 2184–2120 cm^{-1} over the Pt-Mo catalyst supported on titania. The intensity of these bands increased with an increase in wt % of Rh. The CO adsorption bands of un-promoted partially reduced Mo^{5+} species are observed in the range of 2110–2065 cm^{-1} on all the Rh-promoted catalysts.[33] The characteristic bands due to the linear adsorption of CO at Rh^0 sites on the catalyst with 1 wt % Rh were observed at around 2045, 2025, and 2010 cm^{-1}. The broad band at around 1980 cm^{-1} on the catalyst with 1 wt % Rh represents the formation of partially reduced Mo species.

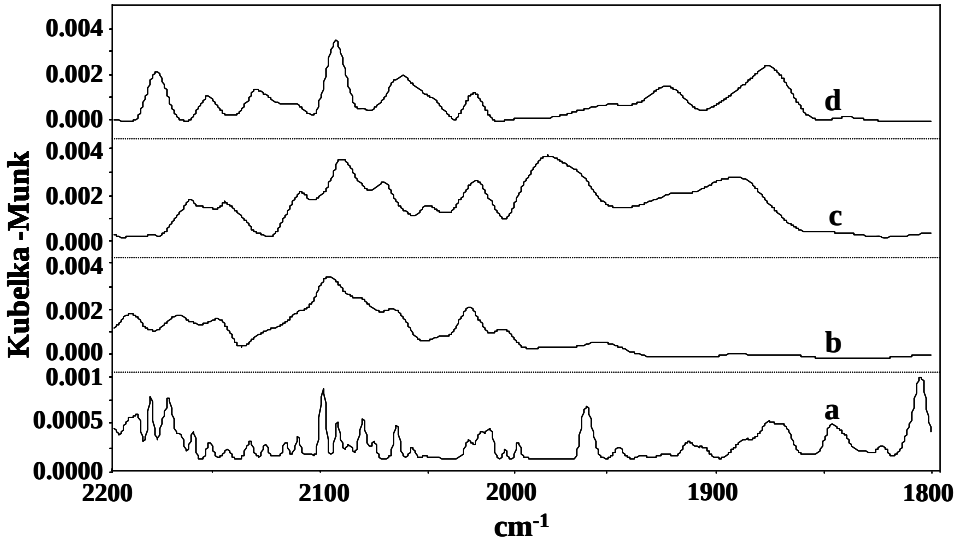

Figure 5.5. DRIFT spectra of adsorbed CO on sulfided catalysts

a. Mo-K/MWCNT; b. 1 wt % Rh-Mo-K/MWCNT;
c. 1.5 wt % Rh-Mo-K/MWCNT; d. 2 wt % Rh-Mo-K/MWCNT

An increase in intensity of these peaks and a shift to lower wave numbers were observed on the catalyst with 1.5 wt % Rh. These results combined with H_2-TPR and CO chemisorption results indicates that a strong electronic interaction occurs between Rh and Mo, leading to the formation of a Rh-Mo mixed phase on the MWCNT-supported catalyst with 15 wt % Mo and 9 wt % K, promoted with 1.5 wt% Rh. The new peak at around 1845 cm^{-1}, due to bridging carbonyls strongly perturbed by potassium, was observed on the catalyst with 2 wt % Rh.[34] These bands may correspond to the formation of isolated sites and are not very coverage dependent.[35]

5.4.2. Catalytic studies

The catalyst activity studies towards higher alcohols synthesis reaction were carried out under similar conditions at 320°C, 8.27 MPa (1200 psig), 3.6m^3 (STP) /(kg of cat.)/h, and H_2 to CO molar ratio of 1. Fig. 5.6 gives the results of the % CO conversion as time-on-stream during the higher alcohols synthesis reaction over MWCNT-supported catalysts with 15 wt % Mo and 9 wt % K, promoted with varying loadings of Rh (0, 1, 1.5, and 2 wt %). The Rh-promoted MoS_2-K/MWCNT catalysts are quite stable after the first 9 h of time on stream. The Rh/MWCNT exhibited the % CO conversion of 6.4% and the catalyst is quiet stable during the 24 h reaction time. The catalytic activity and product selectivity data were calculated after an induction period of 15 h.

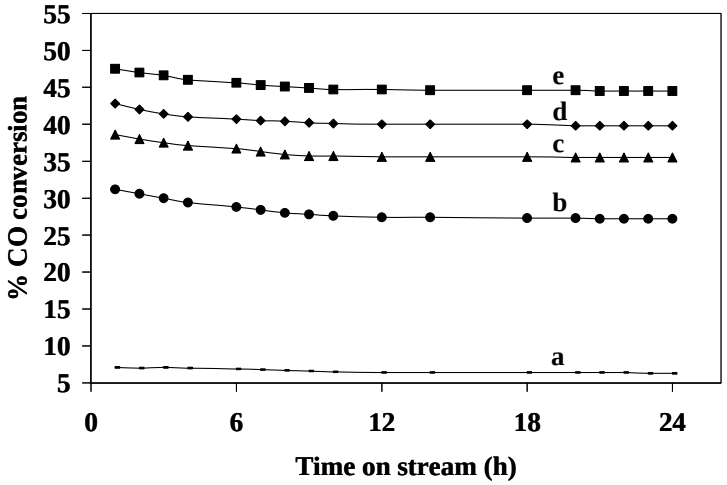

Figure 5.6. % CO conversion with time on stream :
a. Rh/MWCNT; b. Mo-K/MWCNT; c. 1 wt % Rh-Mo-K/MWCNT; d. 1.5 wt % Rh-Mo-K/MWCNT; e. 2 wt % Rh-Mo-K/MWCNT

(wt. of the cat. = 2 g, P = 8.3 MPa, T = 320°C, GHSV = 3.6 m^3(STP)/(kg of cat.)/h, H_2/CO molar ratio = 1)

Table 5.3 gives the activity and selectivity of the catalysts towards higher alcohols synthesis reactions. CO conversion increased linearly as a function of Rh loading on MoS_2-K/MWCNT, from 27% for the un-promoted catalyst to 45% for the catalyst having 2 wt % Rh. The total alcohols STY of 0.131 g/(g of cat.)/h was observed on the 15 wt % Mo and 9 wt % K catalyst supported on MWCNTs. With the incorporation of 1 wt % Rh, the total alcohols STY increases to 0.181 g/(g of cat.)/h. This might be due to the synergic interaction of the rhodium with the molybdenum species that improves the formation of the catalytically active surfaces or sites.[15] The activity of the catalysts for the formation of alcohols reached a maximum value of 0.211 g/(g of cat.)/h on the catalyst with 1.5 wt % and decreased to 0.205 g/(g of cat.)/h, over the catalyst with 2 wt % Rh content. The hydrocarbon formation rate increased monotonically from 0.316 to 0.354 g/(g of cat./h) and the percentage of CO_2 produced varied from 31 to 37%, with an increase in Rh content from 1 to 2 wt %.

The methanol selectivity decreased monotonically from 12 to 4%, with an increase in Rh content from 0 to 2 wt %. Of the Rh loadings investigated, the catalyst with 1.5 wt % Rh on the MWCNT-supported 15 wt % Mo and 9 wt % K resulted in maximum selectivities of 30%, 16%, and 25% towards total alcohols, ethanol, and higher alcohols, respectively. Defining the structural property relationships by linking the results of characterization with catalytic testing, Rh promotion facilitates the interaction between Rh and K-modified Mo species after sulfidation and reduction, leading to a decrease in the size of the molybdenum species by increasing the percentage dispersion of particles.

The Rh/MWCNT catalyst showed very little activity compared to the Rh promoted MoS_2-K/MWCNT (see Table 5.3). The liquid products consisted of ethanol as major alcohol together with methanol, n-propanol and traces of n-butanol. Other C_2-oxygenates such as acetaldehyde and acetic acid are also observed in the liquid products obtained over this catalyst. The total alcohols and hydrocarbons space time yield of 0.011 and 0.027 g/(g of cat.)/h was obtained with this catalyst. From these results, it can be concluded that the activity of promoted Rh-Mo-K catalysts supported on MWCNTs is due to the synergistic effect of Rh and Mo, leading to the formation of Rh-Mo mixed phase.[31]

Table 5.3. Catalytic performance of MWCNT supported catalysts

(wt. of the cat. = 2 g, P = 8.3 MPa, T = 320°C, GHSV = 3.6 m^3 (STP)/(kg of cat.)/h, H_2/CO molar ratio = 1)

Catalyst	CO conversion (%)	Product STY (g/(g of cat.)/h)		CO_2 produced (mole%)	Alcohol Selectivity (wt.%)		
		Total alcohols	Total Hydrocarbons		Methanol	Ethanol	Higher alcohols
1.5 Rh/MWCNT	6.4	0.011	0.027	10.4	2.3	14.9	15.5
MoS_2-K/MWCNT	27.4	0.131	0.299	21.1	11.9	5.0	9.2
1 wt % Rh- MoS_2-K/MWCNT	35.7	0.181	0.316	30.7	6.4	13.2	19.9
1.5 wt % Rh- MoS_2-K/MWCNT	40.1	0.211	0.332	34.6	5.4	16.0	24.6
2 wt % Rh- MoS_2-K/MWCNT	44.7	0.205	0.354	37.4	4.0	16.4	24.4

As seen in Fig. 5.7, the molar ratio of higher alcohols to methanol increases linearly as a function of wt % of Rh. The following linear equations were simulated for (1) the % CO conversion and (2) the molar ratio of higher alcohols to methanol as a function of wt % of Rh:

$$Y = 8.6229\,X + 27.274;\ R^2 = 0.99 \quad (5.1)$$

$$Y = 1.6286\,X + 0.3929;\ R^2 = 0.995 \quad (5.2)$$

where, X is the wt % of Rh on the MWCNT-supported 15 wt % Mo and 9 wt % K catalysts after sulfidation, and Y is the molar ratio of $C_{2+}OH/C_1OH$.

The change in higher alcohols selectivity (wt %) with CO conversion obtained over different Rh-promoted 9 wt % K-modified 15 wt % Mo sulfided catalysts supported on MWCNT are presented in Fig 5.8. It is observed from this figure that the catalyst with increased content of Rh on Mo-K/MWCNT catalysts, the % CO conversion and higher alcohols selectivity increased almost linearly from 0 to 1.5 wt % of Rh, whereas, a decreased higher alcohols selectivity decreased with % CO conversion with further increase in Rh content from 1.5 to 2 wt %.

The individual distribution of alcohols over the 1.5 wt% Rh-promoted Mo-K/MWCNT catalyst is depicted in Fig. 5.9 as an Anderson–Schulz–Flory (ASF) plot. A large deviation from the ideal ASF distribution for methanol, which deviated lower and ethanol, which deviated higher, is observed. The chain growth probability is calculated to be 0.46, assuming a linear distribution of alcohols. This confirms that the addition of Rh promoters to alkali-modified MoS_2 catalysts increases the reaction rate towards the formation of higher alcohols, with ethanol as a dominant product, by accelerating the CO insertion mechanism during the C_1 to C_2 homologation step.[36]

Fig. 5.10 represents the molar percentage distribution of alcohols obtained over the 1.5 wt % Rh-promoted Mo-K/MWCNT catalyst. The methanol and ethanol molar percentages of 18 and 53%, respectively, were observed for the Rh-promoted catalyst. Alcohols up to octanol, with some traces of nonanol and decanol, were obtained over this catalyst. This confirms that Rh not only promotes the activity and selectivity toward higher alcohols (particularly ethyl alcohol), but also propagates the chain growth mechanism leading to the formation of higher alcohols.

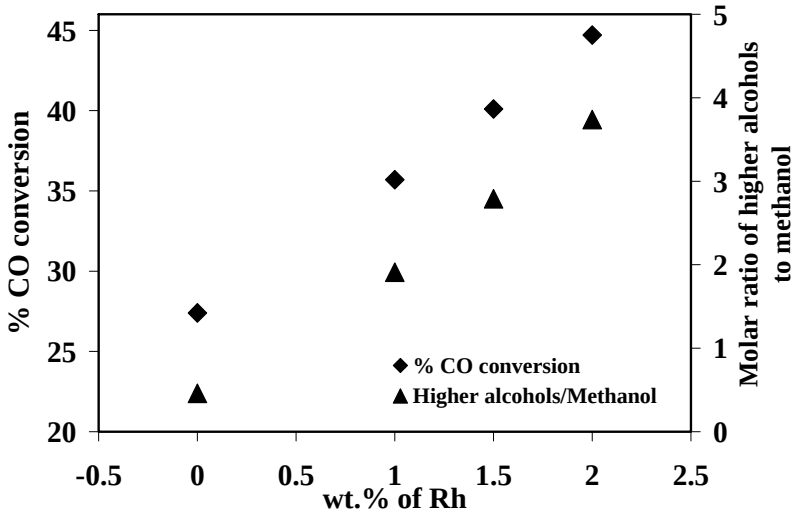

Figure 5.7. % CO conversion and molar ratio of higher alcohols to methanol as a function of wt % of Rh

(wt. of the cat. = 2 g, P = 8.3 MPa, T = 320°C, GHSV = 3.6 m^3 (STP)/(kg of cat.)/h, H_2/CO molar ratio = 1)

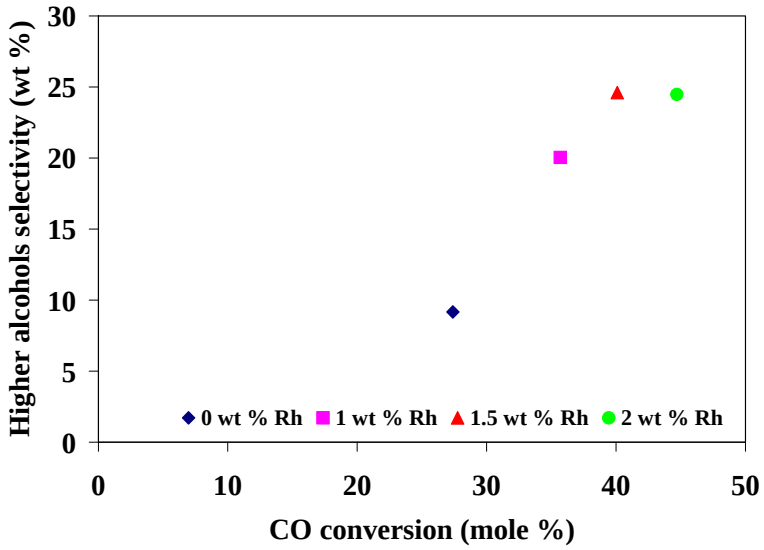

Figure 5.8. Change in higher alcohols selectivity with % CO conversion over Rh-promoted Mo-K/MWCNT

(wt. of the cat. = 2 g, P = 8.3 MPa, T = 320°C, GHSV = 3.6 m^3(STP)/(kg of cat.)/h, H_2/CO molar ratio = 1)

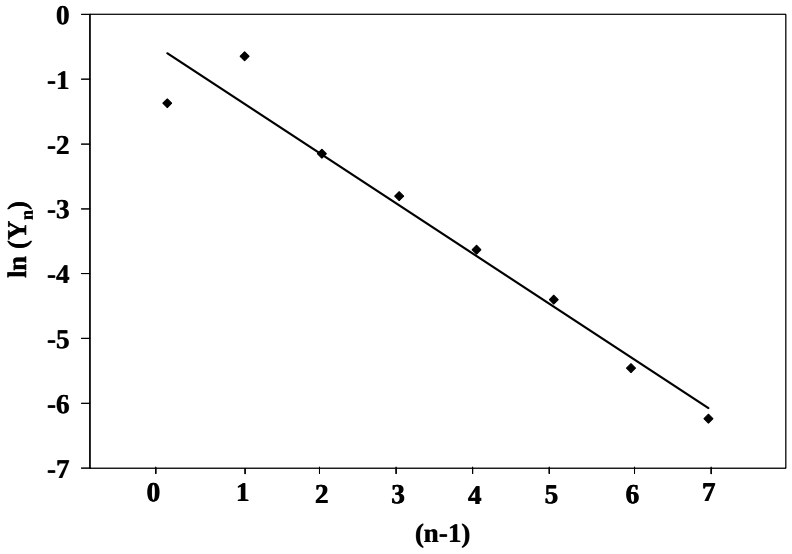

Figure 5.9. ASF plot of distributions of alcohols over the 1.5 wt % Rh-Mo-K/MWCNT catalyst

(wt. of the cat. = 2 g, P = 8.3 MPa, T = 320°C, GHSV = 3.6 m^3 (STP)/(kg of cat.)/h, H_2/CO molar ratio = 1)

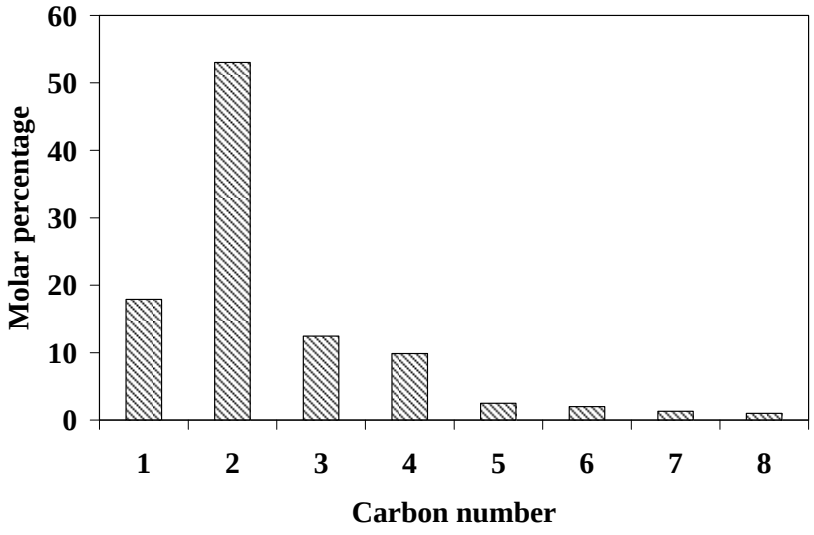

Figure 5.10. Molar percentage distribution of alcohols over the 1.5 wt % Rh-Mo-K/MWCNT catalyst

(wt. of the cat. = 2 g, P = 8.3 MPa, T = 320°C, GHSV = 3.6 m^3 (STP)/(kg of cat.)/h, H_2/CO molar ratio= 1)

The Mo-K/MWCNT catalyst promoted with 1.5 wt % Rh was used to study the temperature effects on higher alcohols synthesis in the range of 300–340°C. The reactions were performed under similar conditions at 8.27 MPa (1200 psig) and 33.6 m^3 (STP)/(kg of cat.)/h, and results are given in Table 5.4. The percentage CO conversion and hydrocarbon space time yield increased monotonically with increasing temperature. The maximum total alcohol space time yield of 0.244 g/(g of cat.)/h was obtained at 330°C. When the temperature was raised beyond 330°C, the maximum yield of alcohol was not consistent with CO conversion due to the high selectivities to hydrocarbon production and the WGS reaction. The maximum total alcohol and higher alcohol selectivities of 33 and 29%, respectively, were observed over the catalyst promoted with 1.5 wt % Rh. With increasing temperature, the methanol selectivity decreased monotonically, and the molar ratio of higher alcohols to methanol increased significantly, confirming the increased promotional ability of Rh towards selective formation of higher alcohols at higher temperatures.[37]

To investigate pressure effects, reaction pressures were varied in the range of 5.52–9.65 MPa (800–1400 psig) over 1.5 wt % Rh-promoted Mo-K/MWCNT catalysts at 320°C and 3.6 m^3 (STP)/(kg of cat.)/h. Table 5.5 shows that increasing the pressure results in a monotonic increase in CO conversion, total alcohol formation rate, hydrocarbon formation rate, and WGS reaction rate. Increasing the pressure also increases the selectivity of methanol, higher alcohols, and the molar ratio $C_{2+}OH/C_1OH$. The highest total alcohol space time yield of 0.226 g/(g of cat.)/h was obtained at 9.65 MPa.

Table 5.6 compares the activities of sulfided 1.5 wt % Rh promoted 15 wt % Mo, 9 wt % K (catalyst C) supported on MWCNTs with those given in the literature. The catalyst with highest activity from each work was selected for comparison purpose. Ir modified Rh-Mo/SiO_2 (catalyst A) was not sulfided prior to the reaction. This table indicates that the sulfided Rh-Mo-K catalysts supported on MWCNTs perform much better compared to those in the literature.

Table 5.4. Performance of 1.5 wt % Rh-Mo-K/MWCNT at different temperatures

(wt. of the cat. = 2 g, P = 8.3 MPa, GHSV = 3.6 m^3 (STP)/(kg of cat.)/h, H_2/CO molar ratio = 1)

Temperature (^oC)	CO conversion (%)	Product STY (g/(g of cat.)/h)		CO_2 produced (%)	Alcohol Selectivity (wt %)			Higher alcohols/ methanol (moles/ moles)
		Total alcohols	Total Hydrocarbons		Methanol	Ethanol	Higher alcohols	
300	34.5	0.146	0.267	27.5	9.6	10.1	14.2	0.94
310	37.6	0.177	0.298	29.6	6.9	13.2	19.4	1.72
320	40.1	0.211	0.332	34.6	5.4	16.0	24.6	2.79
330	45.1	0.244	0.348	38.2	4.6	18.7	28.6	3.65
340	48.3	0.232	0.367	41.4	4.2	17.8	27.7	4.07

Table 5.5. Performance of 1.5 wt % Rh-Mo-K/MWCNT at different pressures

(wt. of the cat. = 2 g, T = 320^{o}C, GHSV = 3.6 m^3 (STP)/(kg of cat.)/h, H_2/CO molar ratio = 1)

Pressure (psig)	CO conversion (%)	Product STY (g/(g of cat.)/h)		CO_2 produced (%)	Alcohol Selectivity (wt %)			Higher alcohols/methanol (moles/ moles)
		Total alcohols	Total Hydrocarbons		Methanol	Ethanol	Higher alcohols	
800	31.1	0.133	0.234	24.5	3.9	11.5	15.4	0.98
1000	35.7	0.165	0.271	28.6	4.7	12.9	19.7	1.83
1200	40.1	0.211	0.332	34.5	5.4	16.0	24.6	2.79
1400	44.7	0.226	0.345	37.6	6.8	16.9	25.3	3.31

Table 5.6. Comparison of the activities of sulfided Rh promoted Mo based catalysts

Sample	**A**	**B**	**C**
Catalyst	**Rh-Mo-Ir/SiO_2**	**Rh-Mo-K/Al_2O_3**	**Rh-Mo-K/MWCNT**
Temperature (°C)	240	327	330
H_2/CO molar ratio	2.0	2.0	1.0
Pressure (MPa)	1.96	4.0	8.3
CO conversion (%)	39.9	4.4	40.1
STY of alcohols (g/(g of cat./h))	0.048*	0.062*	0.244

* The units of STY is g/(ml of cat./h). (A) Matsumoto et al.[17]; (B) Li et al.[15]; (C) 1.5 wt % Rh, 15 wt % Mo 9 wt % K/MWCNT

5.5. Conclusions

Highly dispersed MWCNT-supported MoS_2 catalysts with Rh promoters were prepared from oxide precursors. XRD revealed that many kinds of K-Mo-O mixed phases exist in oxidized form of catalysts, whereas, sulfidation improved the dispersion of these active phases on the MWCNT support. From the TEM images, it was found that metal species were uniformly distributed inside and outside of the tubes, with particle sizes in the range of 3–4 nm.

DRIFT spectroscopy of absorbed CO was used to study the nature of active species in the sulfided form of catalysts and a band at 1980cm^{-1}. This indicated the formation of Rh-Mo-S phase, which was responsible for formation of higher alcohols. The catalyst with 1.5 wt % Rh loading performed better among the Rh-promoted catalysts and showed the highest total alcohol yield of 0.211 g/(g of cat.)/h, ethanol selectivity of 16%, and higher alcohols selectivity of 25% at 320°C and 8.27 MPa. The molar ratio of higher alcohols to methanol increased significantly with increases in both temperature and pressure from 300 to 340°C and 5.52 to 9.65 MPa, respectively.

5.6. Abbreviations

DRIFTS	Diffuse reflectance infrared Fourier transform spectroscopy
DTA	Differential thermal analyzer
FID	Flame ionization detection
GHSV	Gas hourly space velocity
HAS	Higher alcohol synthesis
ICP-MS	Inductively coupled plasma - mass spectroscopy
MWCNT(s)	Multi-walled carbon nanotubes
STY	Space time yield
TEM	Transmission electron microscopy
TPR	Temperature programmed reduction
XRD	X-ray diffraction

5.7. References

1. Johnston, P.; Hutchings, G. J.; Coville, N. J.; Finch, K. P.; Moss, J. R. CO hydrogenation using supported iron carbonyl complexes. *Appl. Catal., A* **1999**, *186*, 245–253.
2. Zhao, N.; Xu, R.; Wei, W.; Sun, Y. Cu/Mn/ZrO_2 catalyst for alcohol synthesis by Fischer-Tropsch modified elements. *React. Kinet. Catal. Lett.* **2002,** *75,* 297-304.
3. Feng, L.; Li, X.; Dadyburjor, D. B.; Kugler, E. L. A temperature-programmed-reduction study on alkali-promoted, carbon-sSupported molybdenum catalysts. *J. Catal.* **2000,** *190,* 1–13.
4. Stevens, R. R. *Process for producing alcohols from synthesis gas*. U.S. Patent 4,882,360, Nov. 21, 1989.
5. Quarderer, G. J.; Cochran, G.A. and, *Process for producing alcohols from synthesis gas*. U.S. Patent 4,749,724, Jun. 07, 1988.
6. Smith, K. J.; Anderson, R. B. A chain growth scheme for the higher alcohols synthesis. *J. Catal.* **1984,** *85*, 428-436.

7. Borden, G.; Rhodin, T. N.; Brucker, C.; Benbow R. and Hurych, Z. Synchrotron radiation study of chemisorptive bonding of CO on transition metals — Polarization effect on Ir(100). *Surf. Sci.* **1976,** *59*, 593-611.

8. Decanio, E. C.; Storm, D. A. Carbon monoxide adsorption by K/Co/Rh/Mo/Al_2O_3 higher alcohols catalysts. *J. Catal.* **1991,** *132*, 375-387.

9. Chuang, S. S. C.; Stevens Jr., R. W.; Khatri, R. Mechanism of C_{2+} oxygenate synthesis on Rh catalysts. *Top. Catal.* **2005,** *32*, 225-232.

10. Haider, M. A.; Gogate, M. R.; Davis, R. J. Fe-promotion of supported Rh catalysts for direct conversion of syngas to ethanol. *J. Catal.* **2009,** *261*, 9-16.

11. Burch, R.; Petch, M. I. Investigation of the synthesis of oxygenates from carbon monoxide/hydrogen mixtures on supported rhodium catalysts. *Appl. Catal., A* **1992,** *88*, 39-60.

12. Luo, H. Y.; Lin, P. Z.; Xie, S. B.; Zhou, H. W.; Xu, C. H.; Huang, S. Y.;. Lin, L. W; Liang, D. B.; Yin, P. L.; Xin, Q. The role of Mn and Li promoters in supported rhodium catalysts in the formation of acetic acid and acetaldehyde. *J. Mol. Catal. A: Chem.* **1997,** *122*, 115-123.

13. Ojeda, M.; Granados, M. L.; Rojas, S.; Terreros, P.; Garcia-Garcia, F. J.; Fierro, J. L. G. Manganese-promoted Rh/Al_2O_3 for C_2-oxygenates synthesis from syngas: Effect of manganese loading. *Appl. Catal., A* **2004,** *261*, 47-55.

14. Sudhakar, C.; Bhore, N. A.; Bischoff, K. B.; Manogue, W. H.; Mills, G. A. Molybdena enhanced Rh/Al2O3 catalysts. In *Proceedings of the 10th Meeting of the Catalysis Society of North America*, San Diego, CA, 1987.

15. Li, Z-R.; Fu, Y-L.; Jiang, M. Structures and performance of Rh–Mo–K/Al_2O_3 catalysts used for mixed alcohol synthesis from synthesis gas. *Appl. Catal., A* **1999,** *187*, 187-198.

16. Van den Berg, F. G. A.; Glezer, J. H. E.; Sachtler, W. M. H. The role of promoters in CO/H_2 reactions: Effects of MnO and MoO_2 in silica-supported rhodium catalysts. *J.Catal.* **1985,** *93*, 340-352.

17. Matsumoto, T.; Kim, W. Y.; Kishida, M.; Nagata, H.; Wakabayashi, K. Catalytic hydrogenation of carbon monoxide over silica-supported Ir-Mo-Rh catalyst. *Catal. Letters* **1994**, *24*, 391-394.

18. Serp, P.; Corrias, M.; Kalck, P. Carbon nanotubes and nanofibers in catalysis. *Appl. Catal., A* **2003**, *253*, 337-358.

19. van Steen, E.; Prinsloo, F. Comparison of preparation methods for carbon nanotubes supported iron Fischer–Tropsch catalysts. *Catal. Today* **2002**, *71*, 327-334.

20. Xiaoming, M.; Guodong, L.; Hongbin, Z. Co-Mo-K sulfide-based catalyst promoted by multiwalled carbon nanotubes for higher alcohol synthesis from syngas. *Chin. J. Catal.* **2006**, *27*, 1019–1027.

21. Pan, X.; Fan, Z.; Chen, W.; Ding, Y.; Luo, H.; Bao, X. Enhanced ethanol production inside carbon-nanotube reactors containing catalytic particles. *Nat. Mater*. **2007**, *6*, 507–511.

22. Yin, S-F.; Zhang, Q-H.; Xu, B-Q.; Zhu, W-X.; Ng, C-F.; Au, C-T. Investigation on the catalysis of CO_x-free hydrogen generation from ammonia. *J. Catal.* **2004**, *224*, 384-396.

23. Tavasoli, A.; Abbaslou, R. M. M.; Trepanier, M.; Dalai, A. K. Fischer–Tropsch synthesis over cobalt catalyst supported on carbon nanotubes in a slurry reactor. *Appl. Catal., A* **2008**, *345*, 134–142.

24. Surisetty, V. R.; Tavasoli, A.; Dalai, A. K. Synthesis of higher alcohols from syngas over alkali promoted MoS2 catalysts supported on multi-walled carbon nanotubes. *Appl. Catal. A* **2009**, *365*, 243–251.

25. Eswaramoorthi, I.; Sundaramurthy, V.; Dalai, A. K. Partial oxidation of methanol for hydrogen production over carbon nanotubes supported Cu-Zn catalysts. *Appl. Catal., A* **2006,** *313*, 22-34.

26. Eswaramoorthi, I.; Sundaramurthy, V.; Nikhil Das, Dalai, A. K.; Adjaye, J. Application of multi-walled carbon nanotubes as efficient support to NiMo hydrotreating catalyst. *Appl. Catal., A* **2008,** *339*, 187-195.

27. Jiang, M.; Bian, G.-Z.; and Fu, Y.-L. Effect of the K---Mo interaction in K---MoO_3/γ-Al_2O_3 catalysts on the properties for alcohol synthesis from syngas. *J. Catal.* **1994,** *146*, 144-154.

28. Li, D.; Yang, C.; Qi, H.; Zhang, H.; Li, W.; Sun, Y.; Zhong, B. Higher alcohol synthesis over a La promoted $Ni/K_2CO_3/MoS_2$ catalyst. *Catal. Commun.* **2004,** *5*, 605-609.

29. Qi, H. J.; Li, D. B.; Yang, C.; Li, W. H.; Sun, Y. H.; Zhong, B. Nickel and manganese co-modified K/MoS_2 catalyst: high performance for higher alcohols synthesis from CO hydrogenation. *Catal. Commun.* **2003,** *4*, 339-342.

30. Noronha, F. B.; Baldanza, M. A. S.; Schmal, M. CO and NO Adsorption on alumina–Pd–Mo catalysts: Effect of the precursor salts. *J. Catal.* **1999,** *188*, 270-280.

31. Yao, H. C. Surface interaction in the MoO_3/γ-Al_2O_3 system. *J. Catal.* **1981,** *70*, 440-444.

32. Zafeiratos, S.; Papakonstantinou, G.; Jacksic, M. M.; Neophytides, S. G. The effect of Mo oxides and TiO_2 support on the chemisorption features of linearly adsorbed CO on Pt crystallites: an infrared and photoelectron spectroscopy study. *J. Catal.* **2005,** *232*, 127-136.

33. Eswaramoorthi, I.; Dalai, A. K. DRIFT studies of adsorbed CO over sulfided K–Rh–Mo/Al_2O_3 catalysts: Detection of Rh–Mo–S phase. *Catal. Lett.* **2009,** *131*, 203-212.

34. DeCanio, E. C.; Storm, D. A. Carbon monoxide adsorption by K/Co/Rh/Mo/Al_2O_3 higher alcohols catalysts. *J. Catal.* **1991,** *132*, 375-387.

35. Storm, D. A. The production of higher alcohols from syngas using potassium promoted Co/Mo/$A1_2O_3$ and Rh/Co/Mo/$A1_2O_3$. *Top. Catal*. **1995,** *2*, 91-101.

36. Santiesteban, J. G.; Bogdan, C. E.; Herman, R. G.; Klier, K. Mechanism of C_1-C_4 alcohol synthesis over alkali/MoS_2 and alkali/Co/MoS_2 catalysts. In *Proc. 9th Intern. Congr. Catal.;* Phillips, M. J., Ternan,M., Eds.; The Chemical Institute of Canada: Ottawa, 1988; Vol. 2, p 561.

37. Liu, Z.; Li, X.; Close, M. l R.; Kugler, E. L.; Petersen, J. L.; and Dadyburjor, D. B.; Screening of alkali-promoted vapor-phase-synthesized molybdenum sulfide catalysts for the production of alcohols from synthesis gas. *Ind. Eng. Chem. Res.* **1997,** 36, 3085-3093.

CHAPTER 6

Alkali-Promoted Trimetallic Co-Rh-Mo Sulfide Catalysts for Higher Alcohols Synthesis from Synthesis gas: Comparison of MWCNT and Activated Carbon Supports

The manuscript provided in this chapter is very similar to the one published in the journal Industrial and Engineering Chemistry Research.

Citation:

Surisetty, V. R.; Dalai, A. K.; Kozinski, J. Alkali-promoted trimetallic Co-Rh-Mo sulfide catalysts for higher alcohols synthesis from synthesis gas: Comparison of MWCNT and activated carbon supports. *Ind. Eng. Chem. Res.* **2010**, *49*, 6956-6963.

Contribution of the Ph.D. Candidate

The laboratory experiments, data analysis and interpretations were performed by Venkateswara Rao Surisetty. Drs. Ajay Kumar Dalai and Janusz Kozinski provided guidance in the results and discussion while writing the submitted manuscript. The submitted manuscript was written by Venkateswara Rao Surisetty. Dr. Dalai provided editorial assistance regarding the style and content of the paper.

Contribution to Overall Study

Focusing on the sulfided alkali-modified Co-Mo/MWCNT and Rh-Mo/MWCNT bimetallic catalysts designed and developed in Chapter 4 and Chapter 5, this paper investigated the effects of alkali-modified trimetallic Co-Rh-Mo catalysts on catalytic performance of higher alcohols synthesis. The effect of supports, MWCNTs, and activated carbon (AC), as well as, the effect of reaction conditions on higher alcohols synthesis reactions were also investigated. This work revealed that hydro carbon formation and water-gas-shift reaction rate were reduced over alkali-modified trimetallic Co-Rh-Mo catalysts.

6.1. Abstract

Multi-walled carbon nanotubes (MWCNTs) and activated carbon were used as supports for the Co (4.5 and 6 wt %) promoted K (9 wt %) modified Rh-Mo catalysts (1.5 wt % Rh and 15 wt % Mo). The catalysts were extensively characterized in both oxide and sulfide phases. A drastic fall in surface area over the activated carbon-supported catalysts was observed after impregnating with metal species. Diffraction peaks were observed in the X-ray diffraction (XRD) patterns of the sulfided alkali-modified trimetallic catalysts, due to the characteristic reflections of the K-Mo-S mixed phase. H_2-temperature programmed reduction (TPR) profiles showed that the reduction behavior of metal species was improved with the addition of Co. The activated carbon-supported trimetallic catalysts showed less activity and selectivity compared to the MWCNT-supported catalyst, and metal dispersions were higher on the MWCNT-supported catalysts. The MWCNT-supported, alkali-promoted trimetallic catalyst with 4.5 wt % Co showed the highest total alcohols yield of 0.244 g/(g of cat.)/h, ethanol selectivity of 20.1%, and higher alcohols selectivity of 31.4% at 320°C and 8.28 MPa using a gas hourly space velocity (GHSV) of 3.6 m^3 (STP)/(kg of cat.)/h. A maximum total alcohol yield of 0.261 g/(g of cat.)/hand a selectivity of 42.9% were obtained on the 4.5 wt % Co-Rh-Mo-K/MWCNT catalyst, at a temperature of 330°C. The total alcohol yield increased from 0.163 to 0.256 g/(g of cat.)/hwith increased pressure from 5.52 MPa (800 psig) to 9.65 MPa (1400 psig) over the 4.5 wt % Co-Rh-Mo-K/MWCNT catalyst.

6.2. Introduction

Higher alcohols synthesis from CO hydrogenation is of interest as the alcohol mixture is an effective octane number enhancer for motor fuels.[1,2] The catalytic systems used for the higher alcohols synthesis reaction from synthesis gas are divided into two groups, based on the product distribution.[3] Alkali-doped high temperature ZnCrO-based and low temperature Cu-based catalytic systems produce mainly methanol and higher branched alcohols.[4] The second group developed from Fe, Ni, or Co modified low temperature and low pressure methanol synthesis catalysts and alkali-modified MoS_2-based catalysts yields a series of linear primary alcohols and gaseous hydrocarbons with
Anderson-Schulz-Flory (ASF) carbon number distributions.[5]

Alkali-modified MoS_2-based catalysts are commercially attractive among different higher alcohols synthesis catalysts, due to their excellent sulfur resistance and high activity for water-gas shift (WGS) reactions.[6] The promotion of Pt group metals, especially Rh in Mo-based catalysts, improved activity toward the formation of higher alcohols.[7] The Mo promotion over the Rh/Al_2O_3 catalyst increased its activity favoring the formation of oxygenates.[8] Li et al.[9] explained that a strong interaction occurred between the rhodium modifiers with the supported K-Mo-O species in the oxidic Rh-modified $Mo\text{-}K/Al_2O_3$ samples and concluded that the coexistence of cationic and metallic Rh stabilized by this interaction may be responsible for the increased selectivity toward higher alcohols ($C_{2+}OH$). Foley et al.[10] suggested that the interaction between Rh and Mo leads to the formation of electron-poor sites that are responsible for the formation of alcohols. Shen et al.[11] investigated the promotion effect of Mo in $Rh\text{-}Mo/SiO_2$ catalysts in an oxided state and suggested that Mo promotion either leads to the oxidation of Rh and consequent stabilization Rh^{1+} ions or the coverage of Rh sites by Mo oxides, depending on the interaction between Rh and Mo. Depending on the status of the rhodium species, properties of alkali promoters, nature of the support, and reaction conditions, the rhodium species are capable of catalyzing dissociation, insertion, and CO hydrogenation.[12]

The addition of 3d transition metals, such as Co and Ni to MoS_2, has a strong promotion effect on the CO hydrogenation reaction.[13,14] The promotion of Co (or Ni) on MoS_2 leads to the formation of three different phases: MoS_2, Co_9S_8 (Ni_3S_2), and a mixed Co (Ni)-Mo-S phase.[15] The formation of the Co (Ni)-Mo-S phase is related to the electron donation from Co (Ni) to Mo decreasing the Mo-S bond strength to an optimum range, thus significantly increasing the activity of the catalyst.[16] The Co-promoted alkali-modified molybdenum sulfide catalysts showed better activity and selectivity of higher alcohols compared to that of Ni.[17] The Ni promotion on alkali-modified MoS_2 catalysts favors the formation of hydrocarbon as Ni is a methanation component.[18] Fujumoto et al.[19] found that equal amounts of hydrocarbons and alcohols resulted from the CO hydrogenation reaction over the $K/Co/Mo/A1_2O_3$ and $K/Co/Mo/SiO_2$ catalysts. Li et al.[5] introduced Co as a promoter to activated carbon-supported $K\text{-}MoS_2$ catalysts and found that Co exists mainly in the form of the Co-Mo-S phase at low Co loading and partly in a Co_9S_8-like structure at high Co content. The addition of Co to alkali-modified MoS_2 catalysts enhanced the $C_1 \rightarrow C_2$

homologation step that leads to the formation of ethanol as the dominant product.[20] Wong et al.[21] investigated the incorporation of Rh into reduced K/Co/Mo/Al_2O_3 catalysts and found that the activity and selectivity of alcohols improved significantly due to the interaction of cationic Rh species with the Mo species. The alkali-promoted trimetallic Co-Rh-Mo catalyst system is attractive to reduce Rh content and to increase the activity and selectivity of the catalyst for the formation of higher alcohols, especially ethanol.

Catalyst support plays an important role for reactions involving hydrogen as a reactant or product. Supports such as activated carbon,[22] clay,[23] Al_2O_3,[24] SiO_2,[25] CeO_2,[26] ZrO_2,[27] and combinations of different metal oxides[28] have been studied in detail as supports to different catalyst systems for higher alcohols synthesis reactions from synthesis gas. Acidic metal oxide supports, such as Al_2O_3 and ZrO_2, favor the formation of hydrocarbons by suppressing the reaction rate of alcohols and their surface acidity causes deactivation by coke formation.[29,30] Concha et al.[31] compared the effects of different supports (SiO_2, Al_2O_3, activated carbon, and CeO_2) on reduced and sulfided molybdenum catalysts and found that hydrocarbon selectivity on activated carbon-supported catalysts was much less than that of others. Murchison et al.[32] found that MoS_2 supported on activated carbon showed alcohol selectivity about six times higher than that of the alumina-supported catalyst. Activated carbon has many advantages as a catalyst support because of its large surface area, limited interaction between the support, and the active material due to the inertness of the graphitic surface, resistance to acidic or basic media, and stability at high temperatures and pressures.[33] However, activated carbon supported catalysts have a microporous structure (pore size < 2 nm) that causes pore plugging due to the formation of coke and deactivation of the catalyst, which results in transport limitation in the reaction.[34] Also, activated carbons have l0-15% ash content, depending on the nature of the precursor used.[35]

Carbon, in the form of multiwalled carbon nanotubes (MWCNTs), is an alternative heterogeneous catalyst support having characteristics similar to activated carbon, like an inert graphite nature and high temperature stability.[36] MWCNTs outperform activated carbon as catalyst supports and display unique properties such as meso/macroporous structures that mitigate transport limitations, uniform, and straight pores that allow great metal dispersion, high mechanical strength, and thermal conductivity.[37,38]

The present work aims to study the effect of Co on K-promoted bimetallic Mo and Rh catalysts, the effect of supports, MWCNTs, and activated carbon (AC) on higher alcohols synthesis reactions, and the effect of reaction conditions such as temperature and pressure on catalytic performance. To study the effect of Co (0, 4.5, and 6 wt %) on K (9 wt %) promoted Mo (15 wt %) and Rh (1.5 wt %) catalysts supported on MWCNTs, we have prepared three catalysts. Two activated carbon-supported trimetallic catalysts with the same composition as the MWCNT-supported catalysts were also prepared to study the role of supports on higher alcohols synthesis.

6.3. Experimental

6.3.1. Preparation of K-promoted trimetallic catalysts

MWCNTs (M. K. Nano, surface area 178 m^2/g, pore volume 0.54 cm^3/g) and activated carbon (Aldrich, surface area 655 m^2/g, pore volume 0.93 cm3/g) were used as supports for the preparation of the catalysts. Prior to impregnation, the support was treated with 30% HNO_3 reflux at 100°C overnight, washed with distilled water several times, and dried at 120°C for 6 h. The oxide samples were prepared by the sequential pore volume impregnation method using ammonium heptamolybdate tetrahydrate (Sigma-Aldrich), potassium carbonate (Aldrich), cobalt acetate tetrahydrate (Alfa-Aesar), and rhodium chloride hydrate (Aldrich) as precursors for Mo, K, Co, and Rh, respectively. At the first step, the support was impregnated with an aqueous solution of K_2CO_3, followed by drying at 120°C for 2 h and stabilizing in an argon flow of 50 ml/min at 300°C, at a heating rate of 10°C/min for 4 h. The support was further impregnated with aqueous solutions containing the required amounts of $(NH_4)_6Mo_7O_{24}$, $Co(CH_3COO)_2$, and $RhCl_3$ followed by drying at 120°C for 2 h and stabilizing in an argon flow of 50 ml/min at 450°C, at a heating rate of 10°C/min for 12 h. The sulfide samples were obtained by heat-treating the oxide precursors in a flow of 10 mole % H_2S in H_2 gas at 450°C, at a heating rate of 2°C/min for 4 h.

6.3.2. Characterization of K-promoted trimetallic catalysts

The surface area, pore volume, and average pore diameter of oxide samples were measured by N_2 physisorption at 77 K using a Micromeritics ASAP 2000. Approximately 0.2 g of sample was used for each analysis. The moisture and other adsorbed gases present in the sample were removed before analysis by degassing the sample at 200°C for 2 h under 66.7

Pa (500 mmHg). The sample was then evacuated at 2.67 Pa (20 μm Hg) before N_2 adsorption.

The content of Mo, Co, and Rh of the oxide catalysts were determined using a Perkin-Elmer ELAN 5000 inductively coupled plasma mass spectroscopy (ICP-MS) instrument.

Powder X-ray diffraction (XRD) analysis patterns of oxide and sulfide forms of samples were recorded on a Rigaku X-ray diffraction instrument with nickel-filtered Cu KR radiation (λ = 0.1541 nm). Each sample was scanned at a rate of 0.05 °/s, with 2θ varying from 10 to 80°. To obtain the XRD patterns in sulfided form, the catalysts were first sulfided for 6 h at 450°C, at a heating rate of 2°C/min using a gaseous mixture containing 10 mole % H_2S in H_2 at a flow rate of 50 ml/min. After sulfidation, the catalysts were cooled to room temperature in a flow of He and the sample was transferred to sample holders under protection of He.

Carbon monoxide was used as a probe molecule to determine the number of accessible surface metal atoms present on the sulfided catalysts. The CO uptake (μmole/g of cat.) measured from CO chemisorption is equivalent to the number of active metal atoms that are accessible to the reactant molecules. The stoichiometric coefficient (CO to metal ratio) of 1 was used, and the extent of reduction was assumed to be 100% in metal dispersion calculations. The carbon monoxide uptake on the sulfided catalysts was measured using the Micromeritics ASAP 2000 instrument. Prior to the CO chemisorption measurement, 0.2 g of sample was sulfided in situ, using 10 mole % H_2S in H_2 at 400°C for 4 h. The sample was then evacuated at 120°C until the static pressure remained less than 6.6×10^{-4} Pa. Chemisorption was performed by passing pulses of CO over the sample to measure the total gas uptake at 35°C.

To study the reducibility of the metal oxides in the catalysts, temperature programmed reduction (TPR) profiles of the catalysts were performed. For each analysis, approximately 0.2 g of sample was used, which was first purged in a flow of argon at 170°C to remove traces of water, and then cooled to 40°C. The TPR of each sample was performed using a 3.1 mole % H_2 in He stream at a flow rate of 30 mL/min at atmospheric pressure using a CHEMBET 3000 TPD-TPR analyzer equipped with a thermal conductivity detector, heating at a linearly programmed rate of 10°C/min up to 800°C.

The oxide samples were characterized by scanning electron microscopy (SEM) using a Phillips SEM-505 scanning electron microscope operating at 300 kV in SE display mode. The outer diameter of the nanotubes was measured using Digital micrograph software (version 3.6.5, Gatan Inc.).

The morphology of the oxide samples was characterized by transmission electron microscopy (TEM) investigations, using a Philips CM20 (100 kV) transmission electron microscope equipped with a NARON energy-dispersive spectrometer with a germanium detector.

6.3.3. Higher alcohols synthesis

A single-pass tubular downflow fixedbed reactor of 450-mm length and 22-mm inside diameter made of inconel tube was used to perform higher alcohols synthesis reactions. The reactor was packed with 2 g of catalyst diluted with 12 ml of 90 mesh size silicon carbide and housed in an electric furnace controlled by a temperature controller. The reactor was pressurized with He to 3.44 MPa (500 psig) and the sulfidation, together with the reduction, was carried out for 6 h at 450°C at a heating rate of 2°C/min using a gas mixture containing 10 mole % H_2S in H_2 and a flow rate of 50 ml/min. The temperature was then lowered to the reaction temperature, and the system pressurized to the reaction conditions. The feed gas mixture CO (45 mole %), H_2 (45 mole %), and Ar (10 mole %) was passed through mass flow controllers and the higher alcohols synthesis reaction was carried out at steady-state under the reaction conditions of 300-340°C, 5.51 (800 psig) to 9.65 MPa (1400 psig), and a gas hourly space velocity (GHSV) of 3.6 m^3 (STP)/(kg of cat.)/h over a period of 24 h. The product gas was cooled to 0°C and separated into gas and liquid phases at the reaction pressure. The CO conversion and other gaseous products were monitored with a time interval of 1 h. The liquid products were collected at the end of the reaction and analyzed with a Varian 3400 gas chromatograph equipped with a capillary column and a flame ionization detector (FID). The volume and weight of liquid products were measured to check the mass balance. The gaseous products were analyzed online on a Shimadzu gas chromatograph through a sampling valve. Using Ar as an internal standard, the CO conversion was calculated and the overall mass balance of the reaction was determined. The experiments were repeated at least twice to check reproducibility and to confirm that the results obtained were within the experimental error of ± 2.5%.

6.4. Results and Discussion

6.4.1. Characterization of K-promoted trimetallic catalysts

Scanning electron microscopy was used to identify the growth of the MWCNTs. Fig. 6.1 shows the surface tophology of the grown carbon nanotubes in bundles. The outside diameter of the MWCNTs clearly shows that the nanotubes are multiwalled and have a structure with several walls of graphitic carbons in concentric circles. The nanotubes are found to be tangled. The outer diameter of the nanotubes, as measured from the micrograph ranges from 10-30 nm.

TEM images of the MWCNT-supported catalysts were recorded and, as shown in Fig. 6.2, revealed that the catalyst particles are well dispersed both inside the carbon nanotubes and on the outside of the tube walls. The carbon nanotubes are multiwalled, with inner diameters in the range of 5-12 nm and wall thickness in the range of 3 to 8 nm. The particle sizes of the metal species that are inside and outside of the tubes are in the range of 1-3 nm.

Table 6.1 shows the results for surface area, total pore volume, and average pore diameter of the stabilized catalysts. After acid treatment, the BET surface area of the MWCNTs increased from 178 to 220 m^2/g, whereas, an increase from 655 to 676 m^2/g was observed in the BET surface area of activated carbon. The MWCNT-supported bimetallic (1.5 wt % Rh and 15 wt % Mo) catalyst promoted with 9 wt % K showed a BET surface area of 77 m^2/g and a total pore volume of 0.30 cm^3/g. Increasing the amount of Co from 4.5 to 6 wt % decreased the BET surface area of the MWCNT-supported, alkali-promoted trimetallic catalysts from 68 to 59 m^2/g and the total pore volume from 0.24 to 0.20 cm^3/g. After impregnating with metal species, a drastic fall in surface area over the activated carbon-supported catalysts was observed. A BET surface area of 97 and 83 m^2/g and a total pore volume of 0.16 and 0.11 cm^3/g were observed over the activated carbon-supported, alkali-promoted trimetallic catalysts that are promoted with 4.5 and 6 wt %, respectively.

The Co, Rh, and Mo contents of the stabilized catalysts measured by ICP-MS are reported in Table 6.1, along with the targeted compositions. The measured contents of the prepared catalysts are slightly lower compared to targeted values, which may be due to the hygroscopic nature of precursors. For the activated carbon-based catalysts, the deviation is greater, indicating that metal particles are not uniformly dispersed on this support.

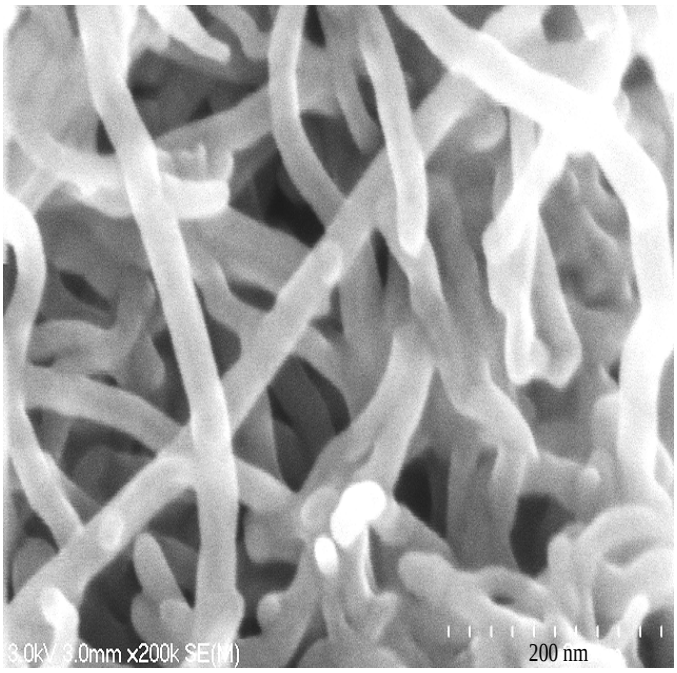

Figure 6.1. SEM image of MWCNT supported catalyst

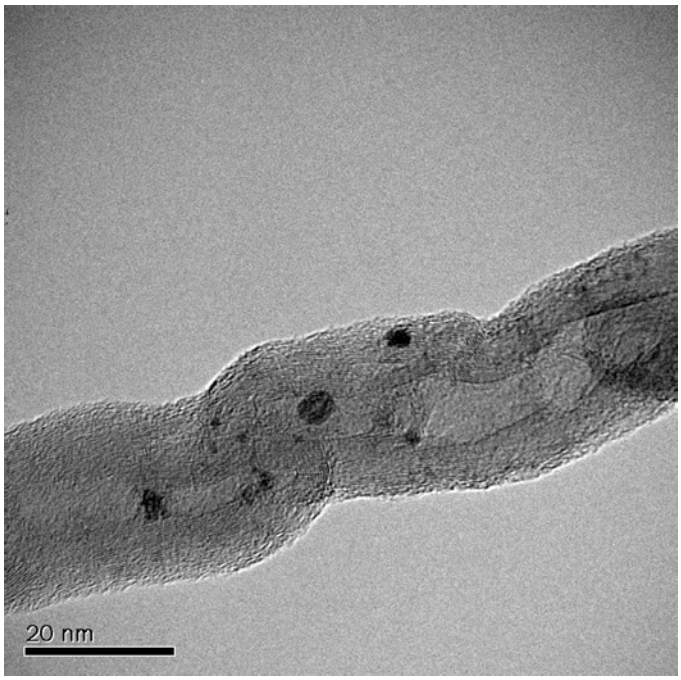

Figure 6.2. TEM image of MWCNT supported catalyst

Table 6.1. Elemental compositions, textural properties, and chemisorption measurement results

Catalyst	Targeted composition (wt %)				Measured composition (wt %)			BET surface area (m^2/g)	Total pore volume (cc/g)	Average pore diameter (nm)	CO uptake (μmole/ g of cat.)	Dispersion of metals (%)
	K	Mo	Rh	Co	Mo	Rh	Co					
Acid Treated MWCNT	--	--	--	--	--	--	--	220	0.66	10.9	--	--
Acid Treated AC	--	--	--	--	--	--	--	676	0.97	1.9	--	--
Rh-Mo-K/MWCNTs	9	15	1.5	--	14.4	1.3	--	77	0.30	17.7	135	39.5
4.5 wt % Co-Rh-Mo-K/MWCNT	9	15	1.5	4.5	14.3	1.2	4.2	68	0.24	17.9	237	47.8
6 wt % Co-Rh-Mo-K/MWCNT	9	15	1.5	6.0	14.1	1.3	5.7	59	0.20	18.3	245	44.8
4.5 wt % Co-Rh-Mo-K/AC	9	15	1.5	4.5	13.7	0.8	3.8	97	0.16	7.2	137	27.7
6 wt % Co-Rh-Mo-K/AC	9	15	1.5	6.0	13.9	0.9	5.1	83	0.11	7.9	144	26.3

The XRD patterns of the catalysts in oxidized and sulfided form were measured and shown in Figs. 6.3 and 6.4, respectively. The JCPDS chemical spectra data bank was used to detect the most probable phases present in the samples, and the results of the possible crystal phases with their corresponding reflection planes are given in Table 6.2.

The strong intensity peaks at 2θ value of 26.6° are due to the reflections of the graphite phase present in the MWCNT and activated carbon supports.[36] The characteristic reflections corresponding to the crystalline structure of MoO_3 are observed at 2θ value of 40.2°.41 In the oxidized form of the MWCNT-supported alkali-promoted bimetallic Rh-Mo catalyst, K-Mo-O mixed phases exist in several forms. The peaks at 2θ values of 19.4°, 28.5°, 29.8°, and 30.9° correspond to the characteristic reflections of the $K_2Mo_2O_7$ phase.[42] Other K-Mo-O phases, such as KMo_4O_6 (2θ = 16.0° and 37.1°) and $K_2Mo_7O_{20}$ (2θ = 23.6° and 53.8°), also exist on this catalyst.[43,44] The diffraction intensity of the peaks was greatly reduced with the incorporation of Co, which confirms that adding the third metal to the alkali-promoted bimetallic Rh-Mo catalysts improved the dispersion of the metal species on the support.

The various diffraction peaks observed in the XRD patterns of oxide samples are completely removed after sulfidation, and new diffraction peaks representing different sulfide species appeared. The reflections of MoS_2 crystallites are observed at 2θ values of 14.6°, 33.4°, 40.9°, and 58.9° in the XRD pattern of the alkali-promoted MWCNT-supported, bimetallic Rh-Mo catalyst.[45] The peak intensity of the MoS_2 crystallites decreased with the addition of Co. The peaks at 2θ values of 21.5°, 28.4°, 29.9°, and 31.5° are due to the characteristic reflections of the K-Mo-S species and are related to active sites for higher alcohols synthesis.[46] The peak at 2θ values of 52.4° is due to the different reflecting planes characteristic of bulk Co_9S_8 particles.[30] The intensity of these peaks is high on the activated support, compared to that of MWCNTs.

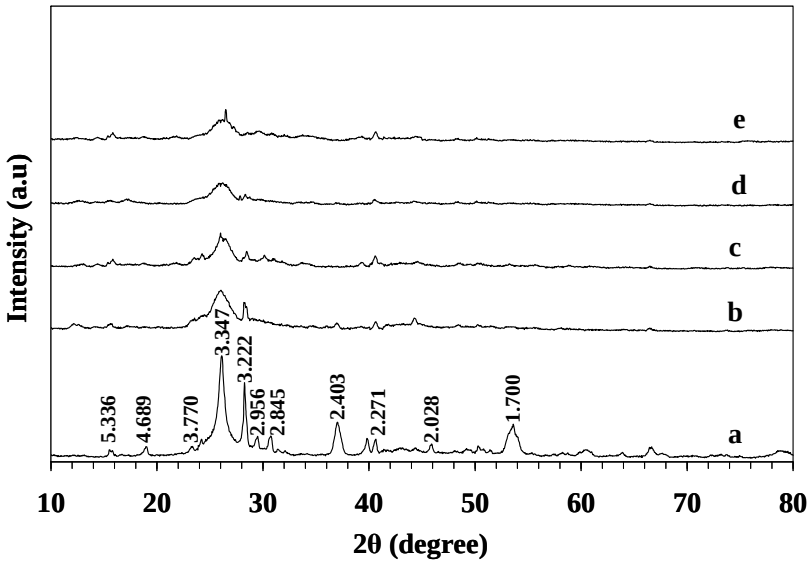

Figure 6.3. XRD patterns of catalysts in oxidized form: a. Rh-Mo-K/MWCNT; b. 4.5 wt % Co- Rh-Mo-K/MWCNT; c. 6 wt % Co-Rh-Mo-K/MWCNT; d. 4.5 wt % Co- Rh-Mo-K /AC; e. 6 wt % Co- Rh-Mo-K/AC

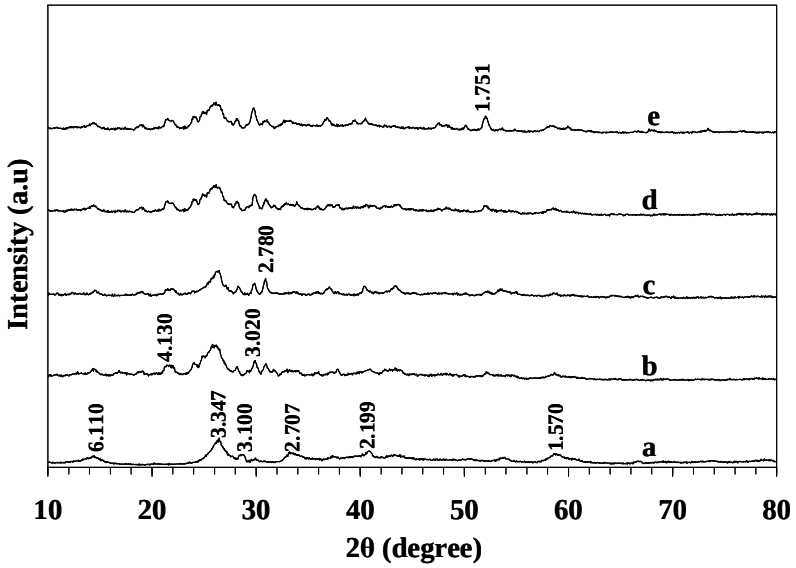

Figure 6.4. XRD patterns of catalysts in sulfided form a. Rh-Mo-K/MWCNT; b. 4.5 wt % Co- Rh-Mo-K/MWCNT; c. 6 wt % Co-Rh-Mo-K/MWCNT; d. 4.5 wt % Co- Rh-Mo-K /AC; e. 6 wt % Co- Rh-Mo-K/AC

Table 6.2. Crystal phases and reflection planes from XRD

Crystal phase	2θ	d-spacing	Reflection plane h k l
Oxidized form of catalysts:			
Graphite (C)	26.6°	3.347	1 1 1
MoO_3	40.2°	2.271	1 5 0
KMo_4O_6	16.0°	5.336	1 1 0
$K_2Mo_2O_7$	19.4°	4.689	1 1 0
$K_2Mo_7O_{20}$	23.6°	3.770	1 0 2
$K_2Mo_2O_7$	28.5°	3.222	0 0 2
$K_2Mo_2O_7$	29.8°	2.956	0 1 2
$K_2Mo_2O_7$	30.9°	2.845	2 1 0
KMo_4O_6	37.1°	2.403	4 0 0
$K_2Mo_7O_{20}$	53.8°	1.700	0 10 4
Sulfided form of catalysts:			
MoS_2	14.6°	6.110	0 0 3
MoS_2	33.4°	2.707	1 0 1
MoS_2	40.9°	2.199	0 1 5
MoS_2	58.9°	1.570	1 1 0
$K_{0.4}MoS_2$	21.5°	4.130	0 0 4
KMo_3S_3	28.7°	3.100	1 1 1
K_2MoS_4	29.9°	3.020	3 0 1
K_2MoS_4	31.5°	2.780	3 0 2
Co_9S_8	52.4	1.751	4 4 0

The results of the CO chemisorption measurements are given in Table 6.1. The CO uptake increased from 135 to 237 and 245 μmole/(g of cat.) with the incorporation of 4.5 and 6 wt % Co, respectively, to the MWCNT-supported, alkali-promoted bimetallic Rh-Mo catalyst. This confirms that MWCNT-supported alkali-promoted Co-Rh-Mo trimetallic catalysts enhanced the CO hydrogenation capability, compared to that of MWCNT-supported alkali-promoted Rh-Mo bimetallic catalyst. A metal dispersion of 48% was observed on the alkali-promoted trimetallic catalyst with 4.5 wt % Co content that was supported on the MWCNTs. When the Co content was increased to 6 wt % on the MWCNT-supported, alkali-promoted trimetallic catalyst, the metal dispersion decreased to 45%, suggesting that high Co loading (6 wt %) leads to the formation of large particles.

From XRD data, it is seen that amount of Co_9S_8 species is high at higher Co content (6 wt % Co) in Co-Mo-K/MWCNT catalysts. Higher Co loading decreases the surface area of the active Co-Mo-S phase (responsible for the formation of higher alcohols), resulting lower metal dispersion.[39] Metal dispersions of 28% and 26% were observed on the activated carbon supported alkali-promoted trimetallic catalysts containing 4.5 and 6 wt % Co, respectively. The higher dispersions on the MWCNT supported catalysts can be explained by the large pore volume and pore size of the MWCNT supports, facilitating uniform metal particle distribution and high dispersions.[40] Hence, it is expected that the catalysts supported on MWCNTs may perform better than catalysts supported on activated carbon.

The H_2-TPR studies (Fig. 6.5) of all the catalysts reveal two reduction peaks, the low temperature reduction peak is attributed to the reduction of bulk MoO_3 and the high temperature peak is due to the complete reduction of MoO_2 to lower oxidation state.[47,48] The low temperature reduction peak at 385°C, and the second peak at 760 °C were observed in the H_2-TPR profile of MWCNT-supported alkali-promoted bimetallic Rh-Mo catalyst. With the incorporation of 4.5 wt % Co, the low temperature reduction peak shifted from 385-332°C. The high temperature reduction feature for the catalyst promoted with 4.5 wt % Co was observed in the temperature range of 570-740°C, which confirms that the addition of Co to the alkali-promoted bimetallic Rh-Mo catalyst enhances the metal species to reduce at low temperatures. The temperature peak attributed to the reduction of the octahedral coordinated Mo (Mo^{6+}) species to the tetrahedral coordinated Mo (Mo^{4+}) species was further shifted to 305°C, and the reduction of the Mo^{4+} species to a lower oxidation state was observed in the temperature range of 500-700°C on the MWCNT-supported alkali-promoted trimetallic Co-Rh-Mo catalyst with 6 wt % Co.

On the activated carbon-supported catalysts, similar results were observed, but with the ratio of high to low temperature peaks being greater than on the MWCNT-supported catalysts. In addition, some weak features occurred at higher temperature positions on the activated carbon-supported catalysts, indicating that more than one kind of oxidic Mo (VI) species existed on the support. These differences are attributed to the interaction of Mo (or Co) species with the activated carbon support.

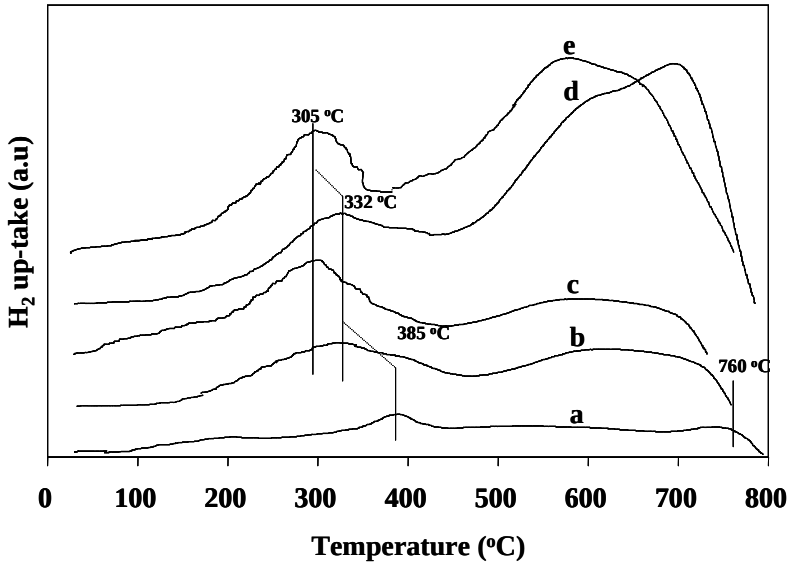

Figure 6.5. H_2 - TPR profiles a. Rh-Mo-K/MWCNT; b. 4.5 wt.% Co- Rh-Mo-K/MWCNT; c. 6 wt.% Co-Rh-Mo-K/MWCNT; d. 4.5 wt.% Co- Rh-Mo-K /AC; e. 6 wt.% Co- Rh-Mo-K/AC

6.4.2. Higher alcohols synthesis

The catalyst activity studies toward higher alcohol synthesis reaction were carried out under similar conditions at 320°C, 8.3 MPa (1200 psig), 3.6 m^3 (STP)/(kg of cat.)/h, and H_2 to CO molar ratio of 1. Fig. 6.6 gives the results of the percentage CO conversion as time-on-stream during higher alcohols synthesis reaction over the MWCNT-supported catalyst with 1.5 wt % Rh, 15 wt % Mo, and 9 wt % K, as well as the trimetallic catalysts promoted with varying loadings of Co (4.5 and 6 wt %) supported on MWCNTs and activated carbon.

As Fig. 6.6 shows, during the 24-h alcohol synthesis, CO conversion was sharply reduced in the first 12 h, and then leveled off, indicating that the catalyst was quite stable after 12 h of time-on-stream. A 40% CO conversion is observed on the alkali-modified bimetallic Rh-Mo catalyst supported on MWCNTs. The alkali-promoted trimetallic catalysts with 6 wt % Co showed the highest CO conversion, compared to the catalyst with 4.5 wt % Co, which confirms that the activity for hydrogenation reaction improved with increased Co wt % in the catalyst. The 45 and 49% CO conversions were observed on the MWCNT-supported 1.5 wt % Rh, 15 wt % Mo, and 9 wt % K catalysts promoted with 4.5 and 6 wt % Co, respectively.

The activated carbon-supported catalysts promoted with 4.5 and 6 wt % Co showed CO conversions of 31 and 35%, respectively. The catalytic activity and product selectivity data were calculated after an induction period of 15 h.

Santiesteban et al.[49] suggested that alkali-modified MoS_2-based catalysts likely follow a CO insertion mechanism for the formation of higher alcohols. The analysis of the liquid products indicates that linear alcohols are formed and no branched alcohols were observed in the GC trace corresponding to the higher alcohols. Methanol, ethanol, *n*-propanol, and *n*-butanol are the major products, together with other higher alcohols. The analysis of exit gas indicates that methane is the major component apart from CO_2 and unconverted gases, such as, CO and H_2.

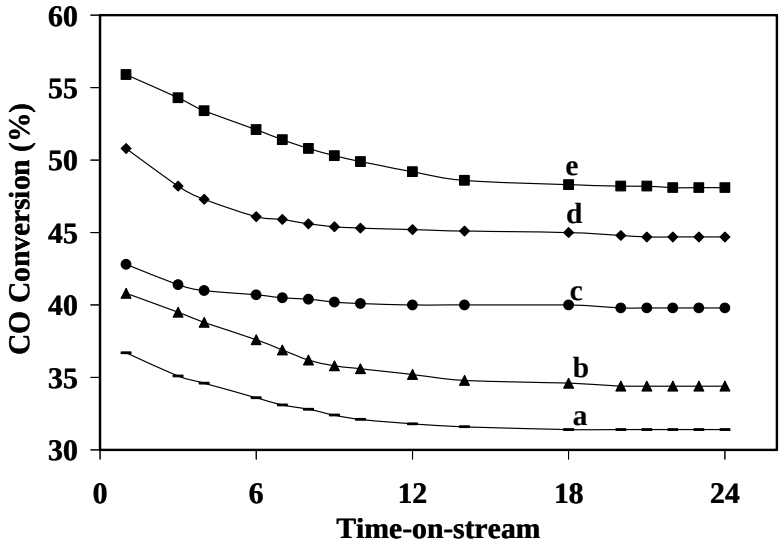

Figure 6.6. % CO Conversion with time on stream a. Rh-Mo-K/MWCNT; b. 4.5 wt % Co- Rh-Mo-K/MWCNT; c. 6 wt % Co-Rh-Mo-K/MWCNT; d. 4.5 wt % Co- Rh-Mo-K /AC; e. 6 wt % Co- Rh-Mo-K/AC

(wt. of the cat. = 2 g, P = 8.3 MPa, T = 320°C, GHSV = 3.6 m^3(STP)/(kg of cat.)/h, H_2/CO molar ratio = 1)

Table 6.3 shows the activity and selectivity results obtained from CO hydrogenation over the sulfided alkali-modified Co-Rh-Mo catalysts. The term higher alcohols represents the ethanol and alcohols with carbon numbers greater than 2 (C_{2+} alcohols). Over the cobalt-free MWCNT-supported catalyst, the total alcohols and total hydrocarbons space time yields (STY) were 0.211 and 0.332 g/(g of cat.)/h, respectively.

With the addition of 4.5 wt % Co on the MWCNT-supported 1.5 wt % Rh, 15 wt % Mo, and 9 wt % K catalyst, the total alcohols STY increased to 0.244 g/(g of cat.)/h and the total hydrocarbons STY decreased to 0.251 g/(g of cat.)/h. The methanol, ethanol, and higher alcohols selectivities increased from 5.4%, 16.0%, and 24.6% over the alkali-promoted bimetallic Rh-Mo/MWCNT catalyst to 6.7%, 20.1%, and 31.4% on the MWCNT-supported trimetallic catalyst promoted with 4.5 wt % Co.

From the CO chemisorption results, it was observed that incorporation of 4.5 wt % Co to the alkali-modified bimetallic Rh-Mo catalyst supported on MWCNTs increased the CO uptake from 135 to 237 μmole/(g of cat.) Also, Co promotion to Rh-Mo-K/MWCNT catalyst increased the metal dispersion from 39.5 to 49.8% favoring the formation of fine particles.

These results, coupled with XRD data, confirm that incorporating Co metal increased the number of active sites responsible for the formation of alcohols. The water-gas shift reaction rate decreased significantly with the addition of Co. By increasing the Co loading from 4.5 to 6 wt % on the MWCNT-supported trimetallic catalyst, the total alcohols STY decreased from 0.244 to 0.235 g/(g of cat.)/h and total hydrocarbons STY increased from 0.251 to 0.293 g/(g of cat.)/h. With increased Co content from 4.5 to 6 wt %, the CO uptake increased from 237 to 245 μmole/(g of cat.), whereas the metal dispersion decreased from 47.8 to 44.8%. These results confirmed that the methanation activity of the catalyst is increased with increased Co content from 4.5 to 6 wt %, because of the formation of large size metal sulfide (Co_9S_8) sites.

On the MWCNT-supported trimetallic catalyst promoted with 6 wt % Co, the selectivity of methanol, ethanol, and higher alcohols decreased to 5.9%, 18.5%, and 27.8%, respectively, which may be due to the formation of Co_9S_8 species at higher Co loadings decreasing the surface area of the active Co-Mo-S species and shifting the activity toward a methane formation reaction.[50]

Table 6.3. Catalytic performance of sulfided MWCNT supported catalysts

(wt. of the cat. = 2 g, P = 8.3 MPa, T = 320°C, GHSV = 3.6 m^3 (STP)/(kg of cat.)/h, H_2 to CO molar ratio = 1)

Catalyst	CO conversion (%)	Product STY (g/(g of cat.)/h)		CO_2 produced (mole%)	Alcohol selectivity (wt %)		
		Total alcohols	Total Hydro carbons		Methanol	Ethanol	Higher alcohols
Rh-Mo-K/MWCNT	40.1	0.211	0.332	34.6	5.4	16.0	24.6
4.5 wt % Co-Rh-Mo-K/MWCNT	45.2	0.244	0.251	21.7	6.7	20.1	31.4
6 wt % Co-Rh-Mo -K/MWCNT	48.9	0.235	0.293	18.9	5.9	18.5	27.8
4.5 wt % Co-Rh-Mo-K/AC	31.2	0.167	0.188	25.7	11.6	9.1	18.8
6 wt % Co-Rh-Mo-K/AC	35.3	0.155	0.231	20.2	9.8	8.3	15.9

The activity and selectivity of the activated carbon catalysts toward higher alcohols synthesis are comparatively less than that of the catalysts supported on MWCNTs. This can be explained from the textural properties of the catalysts. The activated carbon-based catalysts showed a drastic fall in surface area and exhibited relatively low pore volume and diameter compared to the MWCNT-supported catalysts. The pore size of supported catalysts can influence particle size distribution, dispersion, extent of reduction, and directly affects mass transfer diffusion rates of reactants and products. MWCNT supports have the advantage of large pore volume and pore size that facilitates uniform metal particle distribution and high dispersions.[51] The activated carbon-supported catalysts follow similar trends in STY of total alcohols and total hydrocarbons. The selectivity of methanol was higher than that of ethanol over the activated carbon-supported catalysts, confirming that the CO insertion mechanism, which promotes the chain growth probability for the formation of higher alcohols from methanol, is less effective compared to the catalysts supported on MWCNTs.

Fig. 6.7 represents the change in higher alcohols selectivity (wt %) with % CO conversion obtained over Co-promoted Rh-Mo-K sulfided catalysts supported on MWCNT. Over the MWCNT-supported catalysts, the % CO conversion and higher alcohols selectivity both increased with the addition of Co from 0 to 4.5 wt %. When Co content is increased further up to 6 wt %, then the % CO conversion increased, whereas, the higher alcohols selectivity decreased due to the formation of hydrocarbons. Similar results were obtained over the alkali promoted trimetallic catalysts supported on activated carbon (see Fig. 6.7).

The MWCNT-supported alkali-modified trimetallic catalyst promoted with 4.5 wt % Co was used to study temperature effects on higher alcohols synthesis reactions. The reactions were performed under similar conditions at 8.3 MPa (1200 psig) and 3.6 m^3 (STP)/(g of cat.)/h. As shown in Fig. 6.8, the CO conversion and hydrocarbon STY increased monotonically from 36.1 to 51.2% and 0.218 to 0.292 g/(g of cat.)/h, respectively, with increasing temperature from 300 to 340°C.

The maximum total alcohol STY of 0.261 g/(g of cat.)/h was observed at 330°C. The methanol selectivity decreased monotonically with increased temperature, whereas, the ethanol, higher alcohols, and total alcohols selectivity displayed a pronounced increase, reaching maxima of 24.5%, 37.3%, and 42.9% at 330°C (Fig. 6.9).

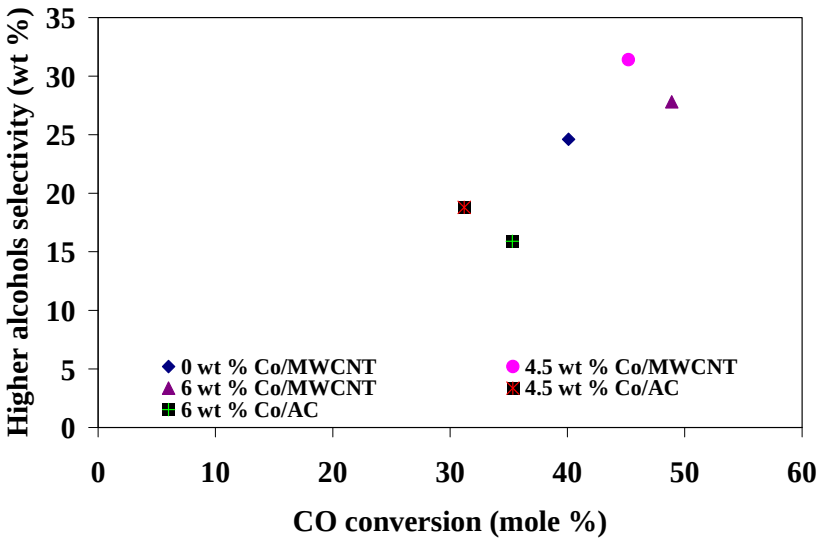

Figure 6.7. Change in higher alcohols selectivity with % CO conversion over Co-promoted Rh-Mo-K/MWCNT

(wt. of the cat. = 2 g, P = 8.3 MPa, T = 320°C, GHSV = 3.6 m^3(STP)/(kg of cat.)/h, H_2/CO molar ratio = 1)

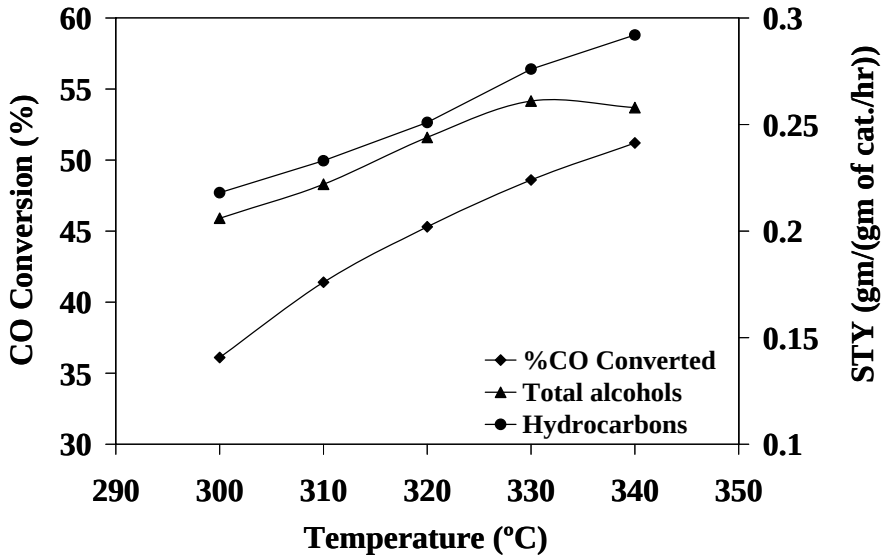

Figure 6.8. The change of % CO conversion and STY of total alcohols and hydrocarbons with temperature using 4.5 wt % Co-Rh-Mo-K/MWCNT catalyst

(wt. of the cat. = 2 g, P = 8.3 MPa, GHSV = 3.6 m^3 (STP)/(kg of cat.)/h, H_2 to CO molar ratio = 1)

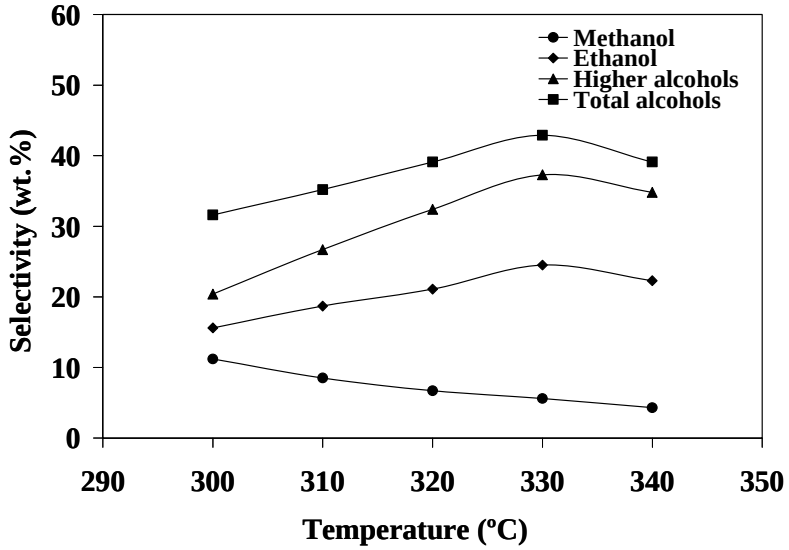

Figure 6.9. Selectivities of methanol, ethanol, higher alcohols, and total alcohols with temperature using 4.5 wt % Co-Rh-Mo-K/MWCNT catalyst

(wt. of the cat. = 2 g, P = 8.3 MPa, GHSV = 3.6 m^3 (STP)/(kg of cat.)/h, H_2 to CO molar ratio = 1)

To investigate the effects of pressure, the reaction pressures were varied in the range of 5.5 to 9.7 MPa (800 to 1400 psig) over the MWCNT-supported, alkali-modified trimetallic catalyst promoted with 4.5 wt % Co at 320°C and 3.6 m^3 (STP)/(g of cat.)/h. Fig. 6.10 shows that increased pressure monotonically increased the CO conversion, total alcohol formation rate, and hydrocarbon formation rate. The selectivity of methanol, ethanol, and higher alcohols also increased monotonically with increasing pressure, indicating that increasing pressure at a constant temperature favors the formation of higher alcohols (Fig. 6.11).

Table 6.4 compares the activities of sulfided 4.5 wt % Co, 1.5 wt % Rh, 15 wt % Mo, and 9 wt % K (catalyst D) supported on MWCNTs with those of other catalysts discussed in the literature. The catalyst with highest activity from each work was selected for comparison purposes. This table indicates that the sulfided alkali modified Co-Rh-Mo catalysts supported on MWCNTs produces 0.261 g/(g of cat./h) which is much higher than that reported in the literature.

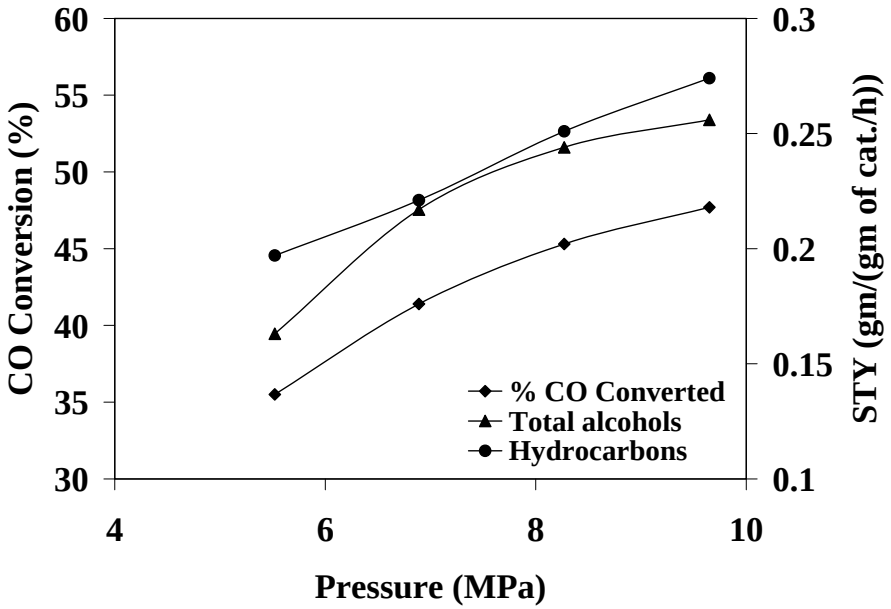

Figure 6.10. The change of % CO conversion and STY of total alcohols and hydrocarbons with pressure using 4.5 wt % Co-Rh-Mo-K/MWCNT catalyst

(wt. of the cat. = 2 g, T = 320°C, GHSV = 3.6 m^3 (STP)/(kg of cat.)/h, H_2 to CO molar ratio = 1)

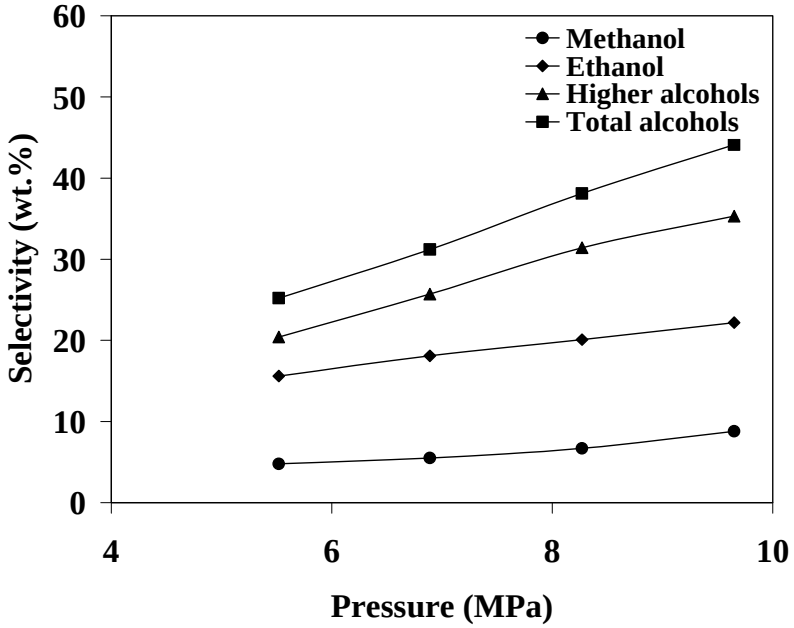

Figure 6.11. Selectivities of methanol, ethanol, higher alcohols, and total alcohols with pressure using 4.5 wt % Co-Rh-Mo-K/MWCNT catalyst

(wt. of the cat. = 2 g, T = 320 °C, GHSV = 3.6 m^3 (STP)/(kg of cat./h), H_2 to CO molar ratio = 1)

Table 6.4. Comparison of the activities of sulfided Mo-K catalysts promoted with Co and/or Rh

Sample	A	B	C	D
Catalyst	Co-Mo-K/AC	Rh-Mo-K/ Al_2O_3	Co-Mo-K/Co decorated MWCNTs	Co- Rh-Mo-K/MWCNTs
Temperature (K)	330	327	340	330
H_2/CO molar ratio	2.0	2.0	1.0	1.0
Pressure (MPa)	5.0	4.0	5.0	8.3
CO conversion (%)	14.3	4.4	12.6	48.6
STY of alcohols (g/(g of cat. /h))	0.199*	0.062**	0.154	0.261

*The units of STY is g/(ml of cat./h).; ** The units of STY is ml/(g of cat./h). (A) Li et al.[5]; (B) Li et al.[9]; (C) Ma et al.[52]; (D) Sulfided 4.5 wt.% Co, 1.5 wt.% Rh, 15 wt. % Mo, and 9 wt.% K/MWCNTs

6.5. Conclusions

The incorporation of Co to the alkali-promoted bimetallic Rh-Mo catalyst resulted in substantial changes in both structure properties and catalytic performance. The MWCNT-supported 1.5 wt % Rh, 15 wt % Mo, and 9 wt % K catalyst promoted with 4.5 wt % Co displayed the highest metal dispersion of 48%. Metal species were uniformly distributed both inside the tubes and on the outside of the tubes, with particle sizes in the range of 1-3 nm. The MWCNT-supported, alkali-promoted trimetallic catalyst with 4.5 wt % Co showed the highest total alcohols yield of 0.244 g/(g of cat.)/h, ethanol selectivity of 20.1%, and higher alcohols selectivity of 31.4% at 320°C and 8.28 MPa, using a gas hourly space velocity (GHSV) of 3.6 m^3 (STP)/(kg of cat.)/h. The activated carbon-supported trimetallic catalysts showed less activity and selectivity compared to the MWCNT-supported catalysts. The maximum total alcohol yield and selectivity of 0.261 g/(g of cat.)/h and 42.9%, respectively, were obtained on the 4.5 wt % Co-Rh-Mo-K/MWCNTs catalyst at a temperature of 330°C. The total alcohol yield increased from 0.163 to 0.256 g/(g of cat.)/h with pressure from 5.52 (800 psig) to 9.65 MPa (1400 psig) over the 4.5 wt % Co-Rh-Mo-K/MWCNT catalyst.

6.6. Abbreviations

MWCNTs	Multi-walled carbon nanotubes
AC	Activated carbon
TPR	Temperature programmed reduction
GHSV	Gas hourly space velocity
ICP-MS	Inductively coupled plasma – mass spectroscopy
XRD	X-ray diffraction
TEM	Transmission electron microscopy
SEM	Scanning electron microscopy
STY	Space time yield

6.7. References

1. Smith, K. J.; Anderson, R. B. The higher alcohol synthesis over promoted copper/zinc oxide catalysts. *Can. J. Chem. Eng.* **1983**, *61*, 40–45.
2. Sugier, A.; Freund, E. *Process of manufacturing alcohols and more particularly saturated linear primary alcohols from synthesis gas*. U.S. Patent 4,291,126, Sep 22, 1981.
3. Murchison, C. B.; Murdick, D. A. *Process for producing C2-C4hydrocarbons from carbon monoxide and hydrogen*. U.S. Patent 4,151,190, Apr 24, 1979.
4. Smith, K. J.; Herman, R. G.; Klier, K. Kinetic modelling of higher alcohol synthesis over alkali-Promoted Cu/ZnO and MoS_2 Catalysts. *Chem. Eng. Sci.* **1990**, *45*, 2639–2646.
5. Li, Z.; Fu, Y.; Bao, J.; Jiang, M.; Hu, T.; Liu, T.; Xie, Y.-N. Effect of cobalt promoter on Co-Mo-K/C catalysts used for mixed alcohol synthesis. *Appl. Catal., A* **2001**, *220*, 21–30.
6. Woo, H. C.; Park, K. Y. Mixed alcohols synthesis from carbon monoxide and dihydrogen over potassium-promoted molybdenum carbide catalysts. *Appl. Catal., A* **1991**, *75*, 267–280.
7. Te, M.; Lowenthal, E. E.; Foley, H. C. Comparative study of Rh/Al_2O_3 and $Rh-Mo/Al_2O_3$ catalysts. *Chem. Eng. Sci.* **1994**, *49*, 4851–4859.

8. Sudhakar, C.; Bhore, N. A.; Bischoff, K. B.; Manogue, W. H.; Mills, G. A. Molybdena enhanced Rh/Al_2O_3 catalysts. In *Proceedings of the 10th Meeting of the Catalysis Society of North America*, San Diego, CA, 1987.

9. Li, Z.-R.; Fu, Y.-L.; Jiang, M. Structures and performance of $Rh\text{-}Mo\text{-}K/Al_2O_3$ catalysts used for mixed alcohol synthesis from synthesis gas. *Appl. Catal., A* **1999**, *187*, 187–198.

10. Foley, H. C.; Hong, A. J.; Brinen, J. S.; Allard, L. F.; Garratt-Reed, A. J. Bimetallic catalysts comprised of dissimilar metals for the reduction of carbon monoxide with hydrogen. *Appl. Catal., A* **1990**, *61*, 351–375.

11. Shen, J. Y.; Matsuzaki, T.; Hanaoka, T.; Takeuchi, K.; Sugi, Y. The promoter function of molybdenum in $Rh/Mo/SiO_2$ catalysts for CO hydrogenation. *Catal. Lett.* **1994**, *28*, 329–339.

12. Decanio, E. C.; Storm, D. A. Carbon monoxide adsorption by $K/Co/Rh/Mo/Al_2O_3$ higher alcohols catalysts. *J. Catal.* **1991**, *132*, 375–387.

13. Gang, L.; Zhang, C. F.; Chang, Y.; Zhu, Z.; Ni, Y.; Cheng, L.; Yu, F. Synthesis of mixed alcohols from CO2 contained syngas on supported molybdenum sulfide catalysts. *Appl. Catal., A* **1997**, *150*, 243–252.

14. Qi, H.; Li, D.; Yang, C.; Ma, Y.; Li, W.; Sun, Y.; Zhong, B. Nickel and manganese co-modified K/MoS2 catalyst: high performance for higher alcohols synthesis from CO hydrogenation. *Catal. Commun.* **2003**, *4*, 339–342.

15. Sun, M.; Nelsona, A. E.; Adjaye, J. On the incorporation of nickel and cobalt into MoS_2-edge structures. *J. Catal.* **2004**, *226*, 32–40.

16. Harris, S.; Chianelli, R. R. Catalysis by transition metal sulfides: A theoretical and experimental study of the relation between the synergic systems and the binary transition metal sulfides. *J. Catal.* **1986**, *98*, 17–31.

17. Murchison, C. B.; Murdick, D. A. *Process for producing olefins from carbon monoxide and hydrogen*. U.S. Patent 4,199,522, Apr 22, 1980.

18. Tatsumi, T.; Muramatsu, A.; Fukunaga, T.; Tominaga, H. Nickel promoted molybdenum catalysts for synthesis of mixed alcohols. In *Proc. 9th Intern. Congr. Catal.*; Phillips, M. J., Ternan, M., Eds.; The Chemical Institute of Canada: Ottawa, 1988; Vol. 2, p 618.

19. Fujumoto, A.; Oba, T. Synthesis of C1-C7 alcohols from synthesis gas with supported cobalt catalysts. *Appl. Catal., A* **1985**, *13*, 289–319.

20. Santiesteban, J. G.; Bogdan, C. E.; Herman, R. G.; Klier, K. Mechanism of C_1-C_4 alcohol synthesis over alkali/MoS_2 and alkali/Co/MoS_2 catalysts. In *Proc. 9th Intern. Congr. Catal.;* Phillips, M. J., Ternan, M., Eds.; The Chemical Institute of Canada: Ottawa, 1988; Vol. 2, p 561.

21. Wong, S. F.; Stromville, N. Y.; Storm, D. A.; Montvale, N. J.; Patel, M. S. *Catalyst and method for producing lower aliphatic alcohols.* US Patents 4,983,638, Jan 8, 1991.

22. Li, X.; Feng, L.; Zhang, L.; Dadyburjor, D. B.; Kugler, E. L. Alcohol synthesis over pre-reduced activated carbon-supported molybdenum-based catalysts. *Molecules* **2003**, *8*, 13–30.

23. Iranmahboob, J.; Toghiani, H.; Hill, D. O. Dispersion of alkali on the surface of Co-MoS2/clay catalyst: a comparison of K and Cs as a promoter for synthesis of alcohol. *Appl. Catal., A* **2003**, *247*, 207–218.

24. Li, Z.; Jiang, M.; Bian, G.; Fu, Y.; Wei, S. Effect of rhodium modification on structures of sulfided Rh-Mo-K/Al2O3 catalysts studied by XAFS. *J. Synch. Radiat.* **1999**, *6*, 462–464.

25. Kohl, A.; Linsmeier, C.; Taglauer, E.; Knozinger, H. Influence of support and promotor on the catalytic activity of Rh/VO_x/SiO_2 model catalysts. *Phys. Chem. Chem. Phys.* **2001**, *3*, 4639–4643.

26. Wang, Y.; Li, J.; Mi, W. Probing study of Rh catalysts on different supports in CO hydrogenation. *React. Kinet. Catal. Lett.* **2002**, *76*, 141–150.

27. Xua, R.; Yanga, C.; Wei, W.; Li, W.-H.; Suna, Y.-H.; Hu, T.-D. Fe-modified CuMnZrO2 catalysts for higher alcohols synthesis from syngas. *J. Mol. Catal. A: Chem.* **2004**, *221*, 51–58.

28. Zurita, M. J. P.; Cifarelli, M.; Cubeiro, M. L.; Goldwasser, J. A. M.; Pietri, E.; Garcia, L.; Aboukais, A.; Lamonier, J.-F. Palladium-based catalysts for the synthesis of alcohols. *J. Mol. Catal. A: Chem.* **2003**, *206*, 339–351.

29. Ryndin, Y. A.; Hicks, R. F.; Bell, A. T. Effects of metal-support interactions on the synthesis of methanol over palladium. *J. Catal.* **1981**, *70*, 287–297.

30. Kogelbauer, A.; Goodwin, J. G.; Oukaci, R. Ruthenium promotion of Co/Al_2O_3 Fischer-Tropsch catalysts. *J. Catal.* **1996**, *160*, 125–133.
31. Concha, B. E.; Bartholomew, G. L.; Bartholomew, C. H. CO hydrogenation on supported molybdenum catalysts: Effects of support on specific activities of reduced and sulfided catalysts. *J. Catal.* **1984**, *89*, 536–541.
32. Murchison, C. B.; Conway, M. N.; Steven, R. R.; Quarderer, G. J. Mixed alcohols from syngas over molybdenum catalysts. In *Proceedings of the Ninth International Congress on Catalyst*; 1998; Vol. 2, p 626.
33. Duchet, J. C.; van Oers, E. M.; de Beer, V. H. J.; Prins, R. Carbon supported sulfide catalysts. *J. Catal.* **1983**, *80*, 386–402.
34. Zaman, M.; Khodadi, A.; Mortazavi, Y. Fischer-Tropsch synthesis over cobalt dispersed on carbon nanotubes-based supports and activated carbon. *Fuel Process. Technol.* **2009**, *90*, 1214–1219.
35. Rodriquez-Reinoso, F. The role of carbon materials in heterogeneous catalysis. *Carbon* **1998**, *36*, 159–175.
36. Eswaramoorthi, I.; Sundaramurthy, V.; Das, N.; Dalai, A. K.; Adjaye, J. Application of multi-walled carbon nanotubes as efficient support to NiMo hydrotreating catalyst. *Appl. Catal., A* **2008**, *339*, 187–195.
37. Xiaoming, M.; Guodong, L.; Hongbin, Z. Co-Mo-K sulfide-based catalyst promoted by multiwalled carbon nanotubes for higher alcohol synthesis from syngas. *Chin. J. Catal.* **2006**, *27*, 1019–1027.
38. Surisetty, V. R.; Tavasoli, A.; Dalai, A. K. Synthesis of higher alcohols from syngas over alkali promoted MoS2 catalysts supported on multi-walled carbon nanotubes. *Appl. Catal. A* **2009**, *365*, 243–251.
39. Moronta, A.; Troconis, M. E.; Gonzalez, E.; Moran, C.; Sanchez, J.; Gonzalez, A.; Quinonez, J. Dehydrogenation of ethylbenzene to styrene catalyzed by Co, Mo and CoMo catalysts supported on natural and aluminum-pillared clays: Effect of the metal reduction. *Appl. Catal., A* **2006**, *310*, 199–204.
40. van Steen, E.; Prinsloo, F. F. Comparison of preparation methods for carbon nanotubes supported iron Fischer-Tropsch catalysts. *Catal. Today* **2002**, *71*, 327–334.

41. Li, Z.; Fu, Y.; Jiang, M.; Hu, T.; Liu, T.; Xie, Y. Active carbon supported Mo-K catalysts used for alcohol synthesis. *J. Catal.* **2001**, *199*, 155–161.

42. Jiang, M.; Bian, G.-Z.; Fu, Y.-L. Effect of the K---Mo interaction in K---MoO3/γ-Al2O3 catalysts on the properties for alcohol synthesis from syngas. *J. Catal.* **1994**, *146*, 144–154.

43. Calafata, A.; Vivas, F.; Brito, J. L. Effects of phase composition and of potassium promotion on cobalt molybdate catalysts for the synthesis of alcohols from CO2 and H2. *Appl. Catal., A* **1998**, *172*, 217–224.

44. Fu, Y.-L.; Fujimoto, K.; Lin, P.; Omata, K.; Yu, Y. Effect of calcination conditions of the oxidized precursor on the structure of a sulfided K-Mo/γ-Al2O3 catalyst for mixed alcohol synthesis. *Appl. Catal., A* **1995**, *126*, 273–285.

45. Pan, X.; Fan, Z.; Chen, W.; Ding, Y.; Luo, H.; Bao, X. Enhanced ethanol production inside carbon-nanotube reactors containing catalytic particles. *Nat. Mater.* **2007**, *6*, 507–511.

46. Berge, P. J. V.; van de Loosdrecht, J.; Barradas, S.; van der Kraan, A. M. Oxidation of cobalt based Fischer-Tropsch catalysts as a deactivation mechanism. *Catal. Today* **2000**, *58*, 321–334.

47. Feng, L.; Li, X.; Dadyburjor, D. B.; Kugler, E. L. A temperature-programmed-reduction study on alkali-promoted, carbon-supported molybdenum catalysts. *J. Catal.* **2000**, *190*, 1–13.

48. Noronha, F. B.; Baldanza, M. A. S.; Schmal, M. CO and NO Adsorption on Alumina-Pd-Mo Catalysts: Effect of the Precursor Salts. *J. Catal.* **1999**, *188*, 270–280.

49. Santiesteban, J. G. Alcohol synthesis from carbon monoxide and hydrogen over MoS_2-based catalysts. Ph.D. Dissertation, Lehigh University, Bethlehem, PA, 1989.

50. Li, Z.; Fu, Y.; Bao, J.; Jiang, M.; Hu, T.; Liu, T.; Xie, Y.-N. Effect of cobalt promoter on Co-Mo-K/C catalysts used for mixed alcohol synthesis. *Appl. Catal., A* **2001**, *220*, 21–30.

51. Bhusan, B., Ed. *Springer handbook of nanotechnology*, 2nd ed., Springer: New York, 2007.

52. Ma, X.-M.; Lin, G.-D.; Zhang, H.-B. Co-decorated carbon nanotubes supported Co-Mo-K sulfide catalyst for higher alcohol synthesis. *Catal. Lett.* **2006**, *111*, 141–151.

Chapter 7

Alkali and Metal Promoters (Co and Rh) on MoS_2 Catalysts for Higher Alcohols Synthesis: Catalytic Performance and Structural Characterization Studies

The manuscript provided in this chapter is very similar to the one submitted to the journal of catalysis.

Citation:

Surisetty, V. R.; Yongfeng, H.; Dalai, A. K.; Kozinski, J. Alkali and metal promoters (Co and Rh) on MoS_2 catalysts for higher alcohols synthesis: catalytic performance and structural characterization studies. *J. Catal.* **2010**, Submitted for Review.

Contribution of the Ph.D. Candidate

The laboratory experiments, data analysis and interpretations were performed by Venkateswara Rao Surisetty. The X-ray absorption near-edge structure (XANES) analysis were done at facilities of Canadian Light Source, University of Saskatchewan, Saskatoon. Dr. Yongfeng Hu provided guidance in performing XANES characterization at Canadian Light Source. Drs. Ajay Kumar Dalai, Janusz Kozinski, and Yongfeng Hu provided guidance in the results and discussion while writing the submitted manuscript. The submitted manuscript was written by Venkateswara Rao Surisetty. Drs. Dalai, and Hu provided editorial assistance regarding the style and content of the paper.

Contribution to Overall Study

The promotion of Co and Rh to alkali-modified MoS_2 catalysts improved the higher alcohols synthesis, as revealed from Chapters 4, 5 and 6. According to the literature, alkali promotion to the active metals is essential for shifting the CO hydrogenation towards higher alcohols synthesis, but the role of alkali on the conversion of synthesis gas over MoS_2 catalysts to produce higher alcohols is not thoroughly understood. Chapter 7 emphasizes the improved performance of MoS_2 catalysts due to the addition of alkali and metal promoters on

modification of surface structure and oxidation states. This study revealed the formation of Co (Rh)-Mo-S species in the XANES spectra of bimetallic and trimetallic alkali-promoted MoS_2 catalysts, in agreement with the improved catalytic performance.

7.1. Abstract

A series of alkali and metal (Rh and Co) promoted MoS_2 catalysts were prepared for higher alcohols synthesis reaction. The effects of alkali and metal promoters on the performance and structure of molybdenum-sulfided catalysts were studied using the BET, X-ray diffraction (XRD), and X-ray absorption near edge structure (XANES) at the S K-edge and Mo L_3-edge. Catalysts promoted with K show a considerably higher conversion rate of CO to alcohols than that without K, which is consistent with the observation of higher surface area and larger pore diameters in the K-promoted catalysts. XRD patters showed that alkali-promoted catalysts were less crystalline compared to that of the catalyst not promoted with K. More oxidized S and Mo species were observed by XRD and XANES in the K-promoted catalysts, indicating the formation of more Mo oxide with the addition of K, thus increasing the active sites. The alkali-promoted trimetallic catalysts using two different supports, multi-walled carbon nanotubes (MWCNTs) and active carbon (AC), showed very different catalytic performances. The activity of the AC-supported alkali-promoted trimetallic catalyst was lower than that supported on MWCNTs. More intense features corresponding to the oxidized S and Mo species were observed in both S K-edge and Mo L_3-edge spectra of the MWCNT-supported catalysts. Finally, formation of Co (Rh)-Mo-S species was evident in the XANES spectra of bimetallic and trimetallic alkali-promoted MoS_2 catalysts, in agreement with their improved catalytic performance.

7.2. Introduction

Higher alcohols synthesis from CO hydrogenation is of interest to enhance the octane number for motor fuels, thereby reducing CO and NO_X toxic emissions.[1] Alkali-modified molybdenum-sulfided catalysts are widely used for higher alcohols synthesis from synthesis gas. Alkali promotion reduces the hydrogenation ability of alkyl species to form alkanes and increases the active sites for the formation of alcohols. These catalytic systems

displayed a high proportion of methanol to higher alcohols.[2-4] Carbon-supported catalysts hold several advantages compared to silica and alumina supports. The interaction between the support and the active material is limited due to the inertness of the graphitic surface.[5,6] Multi-walled carbon nanotubes (MWCNTs) are quite suitable as carbon-based catalytic supports. They display unique characteristics such as appropriate pore-size distribution favoring maximum metallic dispersion, highly graphitized tube-walls, and nano-sized channels.[7-9]

The addition of transition metals increases the reactivity of MoS_2, promoting the formation of MoS_x films.[10] The promotion of transition metals (Co and Rh) improved the activity and selectivity of higher alcohols by modifying the structural effects of the alkali-modified molybdenum-sulfided catalysts to obtain highly dispersed catalysts and shifted the product distribution to the formation of oxygenates.[11-13] The promotion of transition metals to MoS_2 catalysts leads to the formation of mixed metallic particles with Mo components on the support after reduction and sulfidation. This chemical interaction between the metal promoters and molybdenum gives rise to a different catalytic behaviour from that of molybdenum alone.[14,15] Sun et al.[16] investigated the modification effect of Co on the MoS_2-edge surfaces using the density functional theory under generalized gradient approximation. They explained that incorporation of Co on edge surfaces of MoS_2 caused the structural modification and increased the number of active sites for higher alcohols synthesis. One molybdenum atom of every two MoS_2 is substituted by cobalt, and the Co atoms located at edge surfaces generate partially promoted Co-Mo-S surface species. Li et al.[14] studied the local structures of the molybdenum sulfide species in the sulfided Rh-Mo-K/$A1_2O_3$ catalysts using Mo K-edge EXAFS and explained that Rh promotion reduced Mo-Mo coordination shells revealing a high dispersion of the MoS_2-like species in the catalysts by the formation of Rh-Mo-S phase. The M-Mo-S (M - Co or Rh) phase facilitates the dissociation of H_2 on the surface of the catalyst and increases the concentration of atomic hydrogen on the surface of a MoS_2 catalyst. In turn, this increases the number of unsaturated (S-free) Mo sites and the higher alcohols activity .[17]

The X-ray absorption near-edge structure (XANES) technique can be used to investigate local symmetry and electronic structure, including oxidation states of absorbing atoms even when the species formed are present as amorphous and/or highly dispersed

phases.[18] XANES of sulfur K-edge can be used to investigate variations in the sulfur species, such as sulfide, sulfite, and sulfate.[19] This technique also provides useful site-specific information for sulfur species on the catalysts and can be used to differentiate the presence of various sulfides based on the shape and the position of the XANES features.[20] Sarret et al.[21] characterized different forms of sulfur, such as, disulfide, monosulfide, thiophene, sulfoxide, sulfone, and sulfate using S K-edge of XANES. XANES of Mo *L* absorption edge holds several advantages over the Mo K-edge, such as the higher resolution in terms of both the monochromater resolution and a smaller natural width at the L-edge; and the ability of probing the bonding d orbitals at the L-edge. Mo L-edge results have been used by different groups to establish the relation between coordination and the *d*-band vacancies of the central atom.[22-24] Lede et al.[25] studied the change in the molybdenum symmetry and occupancy of the 4d level due to the incorporation of a second metal to the Mo-zeolite substrate and determined the relationships between the white line area at the Mo L_3-edge and the d-character in pure metals and in some 3d transition-metal complexes.

We have recently demonstrated that the addition of Co and Rh metal promoters to alkali-promoted MoS_2 catalysts supported on MWCNTs display improved catalytic performance towards higher alcohols formation from synthesis gas.[12,15,26] The addition of promoters may modify the chemical environment, symmetry, and location of the molybdenum in the supported catalysts. Since these factors exert a strong effect on reactivity, knowledge of the chemical and electronic structure of Mo and S species is important. The present work aims to emphasize the improved performance of molybdenum-sulfided catalysts due to the addition of alkali and metal promoters on modification of surface structure and oxidation states. In this study, five different catalysts supported on MWCNTs having the same Mo content were prepared and promoted, with or without K, Co, and Rh of same loadings. To compare the catalysts supported on MWCNTs with those on activated carbon, an alkali-modified trimetallic Co-Rh-Mo catalyst supported on activated carbon was prepared and used. These catalysts were studied using the S K-edge and Mo L_3-edge XANES to structurally characterize the S and Mo species. To differentiate the surface and bulk properties of the catalysts, both the surface sensitive total electron yield (TEY) and the bulk sensitive fluorescence yield (FLY) were recorded. Together with the X-ray diffraction (XRD)

results, these findings offer valuable information on the electronic and structural properties that can be correlated directly with the catalytic activity of various promoters over the Mo.

7.3. Experimental method

7.3.1. Preparation of catalysts

Commercially available MWCNTs and activated carbon were used as catalyst supports and the catalysts were prepared by conventional incipient wetness method, as described in our preceding papers.[4,12,15,26] Ammonium heptamolybdate tetrahydrate (AHM), potassium carbonate, cobalt acetate tetrahydrate, and rhodium chloride hydrate are used as precursors for Mo, K, Co, and Rh, respectively.

7.3.2. Catalyst studies for higher alcohols synthesis

The catalytic conversion of synthesis gas to higher alcohols were performed using the feed gas mixture CO (40 mole %), H_2 (50 mole %), and Ar (10 mole %) in a single-pass tubular downflow fixed-bed reactor under the reaction conditions of 330 °C, 9.1 (1320 psig), and 3.8 m^3 (STP)/(kg of cat./h) over a period of 24 h. The detailed description about the high pressure reaction set up used in this study was discussed in our previous papers.[4,12,15,26] Prior to the reaction, the catalyst was reduced and sulfided for 6 h at 450 °C at a heating rate of 2 °C/min using a gas mixture containing 10 mole % H_2S in H_2 and a flow rate of 50 ml/min. The product gas was cooled to 0 °C and separated into gas and liquid phases at the reaction pressure. The liquid products were collected at the end of the reaction and analyzed with a Varian 3400 gas chromatograph equipped with a capillary column and a flame ionization detector (FID). The gaseous products were analyzed online on a Shimadzu gas chromatograph through a sampling valve for every 1 h. The experiments were repeated at least twice to check reproducibility and to confirm that the results obtained were within the experimental error of ± 2.5%.

7.3.3. Catalyst characterization

The surface area, pore volume, and average pore diameter of the MoS_2 catalysts promoted with or without K, Co, and Rh-supported on MWCNT or activated carbon were measured by N_2-physisorption at 77 K using a Micromeritics ASAP 2000. Approximately 0.2 g of sample was used for each analysis. Before analysis, the moisture and other adsorbed gases present in the sample were removed by degassing the sample at 200 °C for 2 h under

66.7 Pa (500 mm Hg). The sample was then evacuated at 2.67 Pa (20 μm Hg) before N_2 adsorption.

Powder X-ray diffraction (XRD) analysis patterns of sulfide forms of samples were recorded on a Rigaku X-ray diffraction instrument with nickel filtered Cu Kα radiation (λ = 0.1541 nm). Each sample was scanned at a rate of 0.05 °/s, with 2θ varying from 10 to 80°. To obtain the XRD patterns in sulfided form, the catalysts were first sulfided for 6 h at 450 °C, at a heating rate of 2 °C/min using a gaseous mixture containing 10 mole % H_2S in H_2 at a flow rate of 50 ml/min. After sulfidation, the catalysts were cooled to room temperature in a flow of He and the sample was transferred to sample holders under protection of He.

The S K-edge and Mo L_3-edge XANES of the sulfided catalysts were obtained at the Soft X-ray Microanalysis Beamline (SXRMB) of the Canadian Light Source (CLS; Saskatoon, SK, Canada) using a Si (111) double crystal monochromator. CLS, a 2.9 GeV, third generation storage ring, presently operates with an injection current of 250 mA. The sample was dispersed on double-sided conducting carbon tapes under a dry nitrogen atmosphere, and the measurements were made in both total electron yield by recording the sample drain current and fluorescence yield using a PGT single element Si(Li) drift detector. The XANES spectra were normalized to incident photon flux and to unity at the maximum intensity of each spectrum. Linear combination fitting of Mo L_3-edge spectra was performed using Athena software. The fitting was performed using the first derivative curves, and the weights of the components were set to be between 0 and 1 and the sum was forced to 1 during the fit.

7.4. Results and Discussion

7.4.1. Catalyst studies for higher alcohols synthesis

Fig. 7.1 shows the simplified reaction scheme of higher alcohols reaction from synthesis gas over alkali-modified MoS_2-based catalysts According to this CO insertion mechanism,[13] CO hydrogenation takes place in three different steps: (a) chain initiation, (b) chain propagation, and (c) chain termination. In the first step, adsorption of CO takes place on the mixed K-Mo-S and M-Mo-S phases (M=transition metals such as Co, Ni, Fe, or Rh), while hydrogen adsorption occurs at the separated metal sulfide sites such as MoS_x and MS_x, and these surface species react to form R_1O_s (R_1-CH_3) intermediates. These species propagate

chain growth through hydrogenation, followed by insertion of molecularly adsorbed CO_s to form long chain intermediates R_{is} (R_i - C_nH_{2n+1}, n = 1, 2, 3, …) and $R_{i+1}O_s$ (R_{i+1} - $C_{2n}H_{2n+1}$, n = 1, 2, 3, …). In the final step, direct hydrogenation of these intermediate hydrocarbon species leads to the formation of alkanes and methanol, while the higher alcohols are obtained from hydrogenation of the oxygenated hydrocarbon surface species (R_1O_s and $R_{i+1}O_s$). This mechanism results in the formation of linear chain alcohols due to linear growth by C_1 intermediate insertion at the end of the chain that is bound to the surface.

(a) Chain initiation

$$CO + 0.5H_2 \rightarrow CO_s + H_s \leftrightarrow CHO_s \overset{H_s}{\leftrightarrow} CH_2O_s \overset{H_s}{\leftrightarrow} R_1O_s$$

(b) Chain propagation

$$R_iO_s \xrightarrow[-(H_2O + 2s)]{2H_s} R_{is} \xrightarrow[-s]{CO_s} R_iCO_s \xrightarrow[-2s]{2H_s} R_{i+1}O_s$$

(c) Chain termination

$$R_1O_s \overset{H_s}{\leftrightarrow} CH_3OH$$

$$R_{i+1}O_s \xrightarrow[-2s]{H_s} R_{i+1}OH$$

$$R_{is} \xrightarrow[-2s]{H_s} C_iH_{2i+2}$$

$$R_{is} \xrightarrow{-H_s} C_iH_{2i}$$

Figure 7.1. Reaction scheme for higher alcohols synthesis using CO insertion mechanism

Table 7.1 shows the activity and selectivity results obtained from the CO hydrogenation reaction carried out under similar conditions at 330 °C, 9.1 MPa (1320 psig), 3.8 m^3 (STP)/(kg of cat./h), and H_2 to CO molar ratio of 1.25 over the sulfided Mo-based catalysts promoted with or without K, Co, and/or Rh. The analysis of the liquid products indicates that linear alcohols are formed and no branched alcohols were observed in the GC trace corresponding to the higher alcohols. The term higher alcohols represents the ethanol and alcohols with a carbon number greater than 2 (C_{2+} alcohols). Methanol, ethanol, n-propanol, and n-butanol are the major liquid products, together with other higher alcohols. The analysis of exit gas indicates that methane is the major component, apart from CO_2 and unconverted gases such as CO and H_2.

The % CO conversion increased with the addition of metal promoters, Co and Rh over the sulfided Mo-K/MWCNTs catalyst. Among the alkali-promoted MWCNTs catalysts, the trimetallic Co-Rh-Mo catalyst showed the highest CO conversion of 51.2%, confirming that CO hydrogenation is improved with the addition of metal promoters to the alkali-modified MoS_2 catalysts. Improved CO hydrogenation (% CO conversion 64.8%) is observed over the MWCNT-supported trimetallic catalyst without K. Addition of alkali reduced the availability of metal sulfide sites such as MoS_2 and MS_x (M=Co or Rh), thus suppressing the adsorption of hydrogen.[27] A lower CO conversion of 35.6% was observed on the alkali-promoted trimetallic catalyst supported on activated carbon, indicating that the CO hydrogenation activity was comparatively higher on catalysts supported on MWCNTs. The poor performance of activated carbon supported catalysts can be explained due to the microporous nature of the support, resulting lower dispersions of metal species.[26]

The total alcohols and total hydrocarbons space time yields (STY) of 0.12 and 0.19 g/(g of cat./h), respectively, were observed over the sulfided Mo-K/MWCNTs catalyst. The addition of Co and Rh to the sulfided Mo-K/MWCNTs catalyst increased the total alcohols STY to 0.26 and 0.26 g/(g of cat./h), respectively, and the total hydrocarbons STY to 0.39 and 0.36 g/(g of cat./h), respectively. This may be due to the synergic interaction of the metal promoters with the molybdenum species that improves the formation of the catalytically active sites (Co (Rh)-Mo-S), leading to a decrease in the size of the molybdenum species.[26]

The alkali-promoted trimetallic Co-Rh-Mo catalyst supported on MWCNTs showed an improved total alcohol STY of 0.29 g/(g of cat.)/h, whereas the total hydrocarbon STY decreased, compared to that of alkali-promoted bimetallic catalysts. The decreased methanol selectivities and increased selectivities of ethanol and higher alcohols are observed on the bimetallic alkali-promoted catalysts supported on MWCNTs compared to that of monometallic catalyst. The highest ethanol and higher alcohols selectivities of 25.7 and 39.4% are observed on the trimetallic catalyst promoted with alkali and supported on MWCNT. The improved selectivity of higher alcohols with the addition of metal promoters can be explained from the structural modification of MoS_2, where one of the two Mo atoms is replaced by metal promoters (Co and Rh) and the metal promoter atoms located at edge surfaces generate partially promoted M-Mo-S surface species.[16] This results in an increased number of active sites, which significantly increases the selectivity towards the formation of higher alcohols.

Table 7.1. Catalytic performance of sulfided MWCNT-supported catalysts

(wt. of the cat. = 2 g, P = 9.1 MPa, T = 330 °C, GHSV = 3.8 m^3 (STP)/(kg of cat./h), H_2 to CO molar ratio = 1.25)

Catalyst	CO conversion (%)	Product STY (g/(g of cat./h))		CO_2 produced (mole %)	Alcohol Selectivity (wt %)		
		Total alcohols	Total Hydrocarbons		Methanol	Ethanol	Higher alcohols
Mo-K/MWCNTs	29.1	0.12	0.19	23.5	9.3	6.2	13.8
Co-Mo-K/MWCNTs	46.9	0.26	0.39	36.5	6.2	18.8	30.6
Rh-Mo-K /MWCNTs	47.3	0.26	0.37	39.7	6.0	19.6	30.9
Co-Rh-Mo-K /MWCNTs	51.2	0.29	0.29	28.0	6.7	25.7	39.4
Co-Rh-Mo /MWCNTs	64.8	0.05	0.83	36.2	2.2	1.1	1.8
Co-Rh-Mo K/AC	35.6	0.19	0.22	31.6	13.1	12.6	22.8

The alkali-promoted trimetallic catalyst supported on activated carbon showed a total alcohols and total hydrocarbons STY of 0.19 and 0.22 g/(g of cat./h), respectively. The alkali-promoted trimetallic catalyst supported on activated carbon showed the highest selectivity towards methanol, compared to that of ethanol and other higher alcohols. This confirms that the chain growth mechanism that promotes the formation of higher alcohols is less effective on activated carbon supported catalysts compared to the catalysts with MWCNTs support.

7.4.2. Catalyst characterization

Textural characteristics

The textural characteristics of all the catalysts are shown in Table 7.2. The surface area and pore volume of all the catalysts were decreased compared with that of the support due to the pore blocking and surface smoothing by the deposition of metals in sulfide state on the support. The BET surface area of Mo-K/MWCNTs catalyst was found to be 109 m^2/g. With the incorporation of Co and Rh to the Mo-K/MWCNTs catalyst, the surface area was decreased to 89 and 86 m^2/g, respectively. The alkali-promoted trimetallic Co-Rh-Mo/MWCNTs catalyst showed a BET surface area of 79 m^2/g, whereas the trimetallic catalyst not promoted with K showed a BET surface of 68 m^2/g. These results suggest that alkali helped to disperse the metal species on the support, favouring the formation of small particles. A drastic fall in surface area over the activated carbon-supported catalysts was observed.

Activated carbon is a microporous support and has relatively low pore volume and pore size compared to that of MWCNTs, which are mesoporous in nature. The particle size distribution, dispersion, and extent of reduction depend on the pore size of supported catalysts and directly affect mass transfer diffusion rates of reactants and products. MWCNT supports have the advantage of large pore volume and pore size that facilitate uniform metal particle distribution and high dispersions products.[28]

Table 7.2. Textural properties of sulfided catalysts

Catalyst	BET surface area (m^2/g)	Total pore volume (cc/g)	Average pore diameter (nm)
Mo-K/MWCNTs	109	0.41	14.9
Co-Mo-K/MWCNTs	89	0.36	15.7
Rh-Mo-K/MWCNTs	86	0.35	16.0
Co-Rh-Mo-K/MWCNTs	79	0.29	16.7
Co-Rh-Mo/MWCNTs	68	0.23	17.8
Co-Rh-Mo-K/AC	111	0.21	6.4

X-ray diffraction

The XRD patterns of the catalysts in sulfided form were measured and shown in Fig. 7.2. The JCPDS chemical spectra data bank was used to detect the most probable phases present in the samples, and the results of the possible crystal phases with their corresponding reflection planes are given in Table 7.3. The intense peaks at d-spacing of 3.35 are due to the reflections of the graphite phase present in the MWCNT and activated carbon supports.[29] The reflections of MoS_2 crystallites are observed at d-spacing values of 6.11, 2.71, and 1.57 (Fig. 7.2 (a)).[30] With the addition of metal promoters, Co and Rh, new peaks, such as at d-spacing of 3.02 and 1.75, can be observed, suggesting the formation of the new phases, Co (Rh)-Mo-S. These new phases are related to the electron donation from Co (Rh) to Mo. The formation of Co (Rh)-Mo-S decreases the Mo-S bond strength to an optimum range and significantly increases the activity of the catalyst towards the formation of higher alcohols.[31]

The peaks at d-spacing of 3.1, 3.02, and 2.78 are observed on all the catalysts promoted with K. These are due to the characteristic reflections of the K-Mo-S species, and are related to active sites for higher alcohols synthesis.[32] The peak at d-spacing of 1.75 is due to the different reflecting planes characteristic of bulk Co_9S_8 particles.[33] The XRD patterns of the Co-Rh-Mo trimetallic catalyst without the alkali promoter mainly revealed three peaks due to the characteristic reflections of graphite carbon, MoS_2, and Co_9S_8 species. The intensity of these crystalline peaks is found to be large compared to the alkali-promoted catalyst, suggesting that alkali reduces the crystalline nature of the catalyst particles and favours the formation of smaller particles.

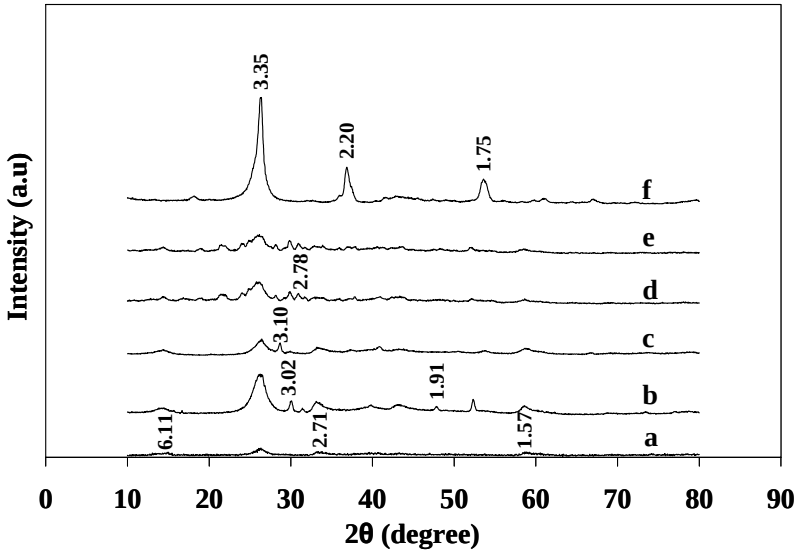

Figure 7.2. XRD patterns of catalysts in sulfide form
(a) Mo-K/MWCNTs; (b) Co-Mo-K /MWCNTs; (c) Rh-Mo-K/MWCNTs; (d) Co-Rh-Mo-K/MWCNTs; (e) Co-Rh-Mo-K/AC; (f) Co-Rh-Mo/MWCNTs

Table 7.3. Crystal phases and reflection planes from XRD

Crystal phase	2θ	d-spacing	Reflection plane h k l
Graphite (C)	26.6°	3.35	1 1 1
MoS_2	14.6°	6.11	0 0 3
MoS_2	33.4°	2.71	1 0 1
MoS_2	40.9°	2.20	0 1 5
MoS_2	58.9°	1.57	1 1 0
$K_{0.4}MoS_2$	21.5°	4.13	0 0 4
KMo_3S_3	28.7°	3.10	1 1 1
K_2MoS_4	29.9°	3.02	3 0 1
K_2MoS_4	31.5°	2.78	3 0 2
Co_9S_8	52.4	1.75	4 4 0

XANES: Overview

Fig. 7.3 shows the S K-edge and Mo L_3-edge XANES spectra of MoS_2 and three trimetallic MoS_2 catalysts. The total electron yield (TEY) is more surface sensitive, with an estimated probing depth of 100 nm at the S K-edge (Fig. 7.3(a)); while the fluorescence yield

(FLY) is more bulk sensitive, with a probing depth about 10 times deeper than that of TEY (Fig. 7.3(b)). The TEY and FLY spectra for these samples are essentially identical in peak energy positions, but quite different in relative peak intensities. These spectra can be divided into three general regions: region A, around 2471 eV, is due to the S 1s to 3p dominated transitions of S in -2 oxidation state, such as MoS_2; region B appearing at 2481 eV is associated with the presence of oxidized sulfate (SO_4^{-2}) species; and region C around 2524 eV is assigned to absorptions as a result of transitions from Mo $2p_{3/2}$ initial state to empty orbitals with mainly Mo 4d characters. Compared to the sulfide peak (A), the relative intensities of peaks B and C are higher in the TEY spectra, indicating a more oxidized surface (Fig. 7.3(a) vs Fig. 7.3(b)). It is worth noting that the sulfate peak (B) is more pronounced in the K-promoted trimetallic systems, while there is little or no sulfate observed in spectra of the MoS_2 and of the catalyst without K. This is consistent with the XRD observation that only diffraction patterns due to MoS_2 and Co_9S_8 are present in the trimetallic catalyst without the alkali promoter (Fig. 7.2). The formation of sulfate species in the K-promoted MoS_2 catalysts is due to the oxidation of sulfur in the presence of oxygen of the molybdates.[34]

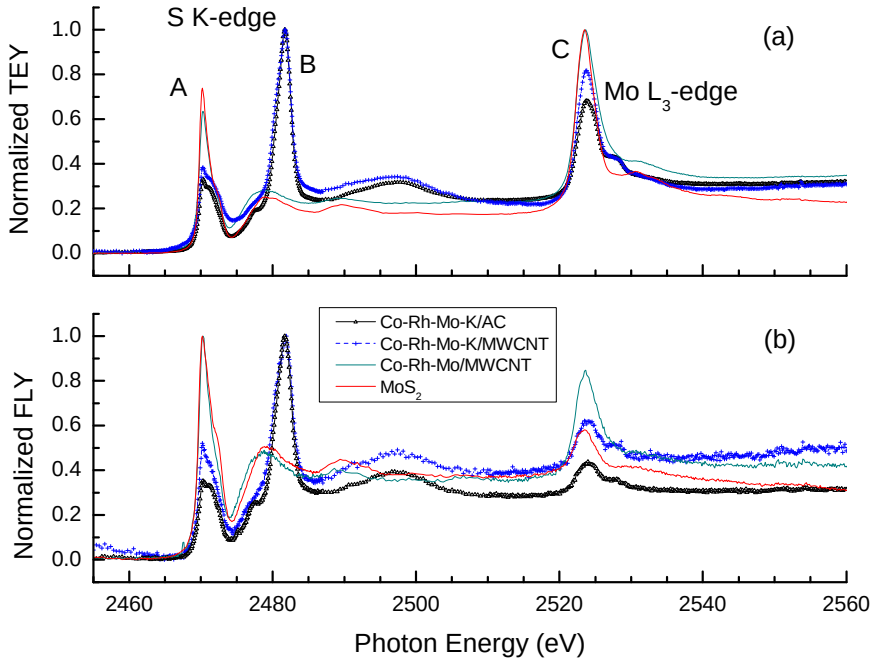

Figure 7.3. Overview of S K-edge and Mo L_3-edge XANES spectra of various catalysts

Zubavichus et al.[35] explained that the oxidation of MoS_2 takes place at surface-situated active centers located in the non-intercalated amorphous outer region of the particles. This partial oxidation of the sample is in agreement with the previous observation of S oxidation during synthesis and/or ageing by Guay et al.[36] S oxidation with Mo atom is also evident in the Mo L_3-edge results, as a shoulder peak at 2527.7 eV, due to the oxidized Mo, can be observed in the spectra of K-promoted catalysts. The alkali promotion leads to the formation of new phases, such as K-Mo-S, thus decreasing the number of available Mo sites. These results indicate that alkali promotion increased the susceptibility of MoS_2 layers to oxidation, thus improving the catalytic performance for higher alcohols yield. On the other hand, the trimetallic system without K promotion has very high (little) hydrocarbon (alcohol) conversion yield (Table 7.1). Its S K-edge spectrum is similar to that of MoS_2, confirming the importance of role of oxidation of MoS_2 in production of high alcohols. The peak intensities of sulfide and Mo of the catalyst supported on MWCNT are found to be higher than those of the activated carbon, consistent with the higher catalytic performance observed for catalysts supported on MWCNT (Table 7.1).

XANES: the S K-edge

The S K-edge XANES spectra of sulfur standards (MoS_2 and $FeSO_4$) and the MWCNT-supported alkali-promoted MoS_2 catalysts promoted with or without Co and Rh recorded in TEY are displayed in Fig. 7.4. Compared to the spectra of sulfur standards, it is clear that both sulfide and sulfate species are present in all alkali-promoted catalysts. The broadening of peak A for alkali-modified MoS_2-based catalysts, in particular the additional shoulder in peak A of the Co-Rh-Mo-K/MWCNT sample, providing further evidence of the formation of Co (Rh)-Mo-S networks in the Co and Rh-promoted catalysts. Peak B of the alkali-promoted catalysts is broader with additional intensity at the lower energy side, compared to that of $FeSO_4$. This is likely due to the formation of sulfate of a mixed nature (K-Mo-S, Co-Mo-S or Rh-Mo-S) in bimetallic and trimetallic catalysts and the chemical shift is due to stronger bonding between Fe and sulfate over the bonding between Mo (and/or Co, Rh) and sulfate. Finally, an additional shoulder around 2477 eV (peak B) can be observed in the spectra of alkali-promoted catalysts, a feature usually associated with intermediate sulfur species with an oxidation state of +4 or +2 .[37] These results indicate that the formation of new phases (K-Mo-S, Co-Mo-S, and/or Rh-Mo-S) takes place with the addition of promoters, decreasing the crystalline nature of MoS_2 species, which correlates well with the catalytic performance shown in Table 7.1.

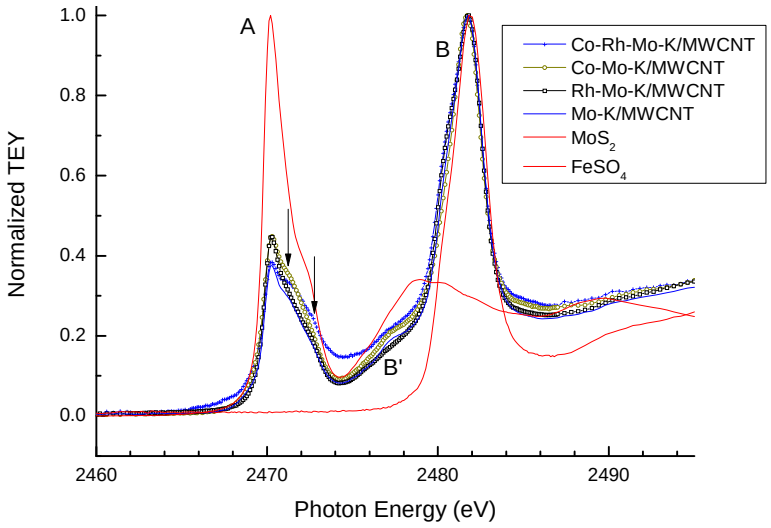

Figure 7.4. S K-edge XANES spectra of K promoted MoS_2 catalysts

XANES: Mo L_3 - edge

The Mo L_3-edge XANES of reference compounds, MoS_2 (Mo oxidation state +4) and ammonium hepta molybdate (AHM) (Mo oxidation state +6), and the MWCNT-supported alkali-promoted MoS_2 catalysts, recorded in TEY-mode spectra are given in Fig. 7.5. The Mo L_3-edge of MoS_2 was observed at 2523.6 eV with a shoulder peak at 2530.7 eV due to the tetrahedral coordination of Mo atoms.[38] The Mo L_3-edge XANES spectrum of ammonium hepta molybdate (AHM) displayed a characteristic doublet at 2525.0 and 2527.5 eV, as a result of the ligand field splitting of the d final states under octahedral symmetry.[36] The Mo L_3-edge spectra of the MWCNT-supported alkali-promoted bimetallic or trimetallic catalysts shown in Fig. 7.5 are somewhat different from those of the Mo model compounds. The main peak is at a very similar energy position (2524.0 eV) to that of MoS_2, suggesting that presence of MoS_2 in these catalysts. The broadening of the main peak and the presence of the second peak at 2527.7 eV that overlaps the doublet of the AHM spectrum, strongly suggest the oxidation of Mo in these catalysts with the addition of Co and Rh. The intensity of 2527.5 eV peak follows the order of Co-Rh-Mo-K/MWCNTs > Co-Mo-K/MWCNTs>Rh-Mo-K/MWCNTs>Mo-K/MWCNTs.

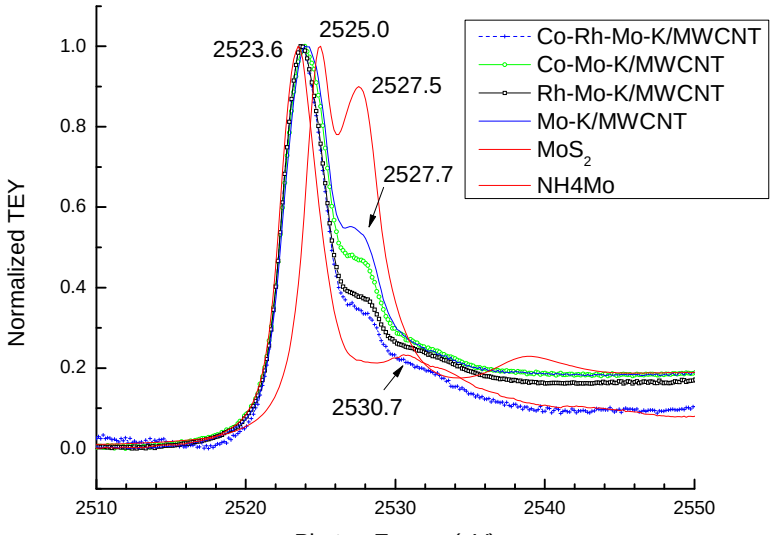

Figure 7.5. Mo L_3-edge XANES spectra of K promoted MoS_2 catalysts

Fig. 7.6 presents the linear combination fitting of the Mo L_3-edge spectra of the catalyst Mo-K/MWCNTs. Spectra of MoS_2 and AHM are used as standards in the fitting. Based on the fitting, the oxidized Mo^{+6} species is estimated to be 19.2%, 11.5%, and 0.4% for the Mo-K/MWCNTs, Co-Rh-Mo-K/MWCNTs, and Co-Rh-Mo/MWCNTs catalysts, respectively. In trimetallic catalysts without K, the Mo species mainly exist as MoS_2 state, whereas the addition of K favours the oxidation of Mo^{+4} to Mo^{+6} states. The addition of transition metal promoters (Co and Rh) to the Mo-K catalyst leads to the formation of Co-Mo-S phase, in which Mo exits mainly in +5 oxidation state, which is the active phase for the formation of higher alcohols.[39] The decreased amount of Mo^{+6} species due to the promotion of Co and Rh to the Mo-K catalyst suggests the reduction of Mo from +6 to +5 oxidation state.

The trimetallic catalyst without K showed improved activity towards the formation of hydrocarbons and very little activity for the alcohols synthesis reaction. From the results of XRD and XANES, it was observed that the intensity of the metal sulfide peaks is large (no sulfate intensity) and the BET surface area is less on the trimetallic catalyst that is not promoted with K, compared to that of alkali-promoted trimetallic catalyst. Park et al.[40] concluded that the alkali helped to improve the association of Mo oxide and Co oxide on the γ-Al_2O_3 support, favouring more active sites due to the formation of chemically combined Co-Mo-O phase. The results in the

present study also implied that the addition of K is beneficial to the dispersion of large metal sulfide agglomerates to small particles on the support by favouring the formation of chemically combined new phases (Co (Rh)-Mo-S) in sulfide state. This suggests that the promotion of alkali reduces the hydrogenation ability of alkyl species to form alkanes and increases the active sites for the formation of alcohols, as reported in the literature.[41]

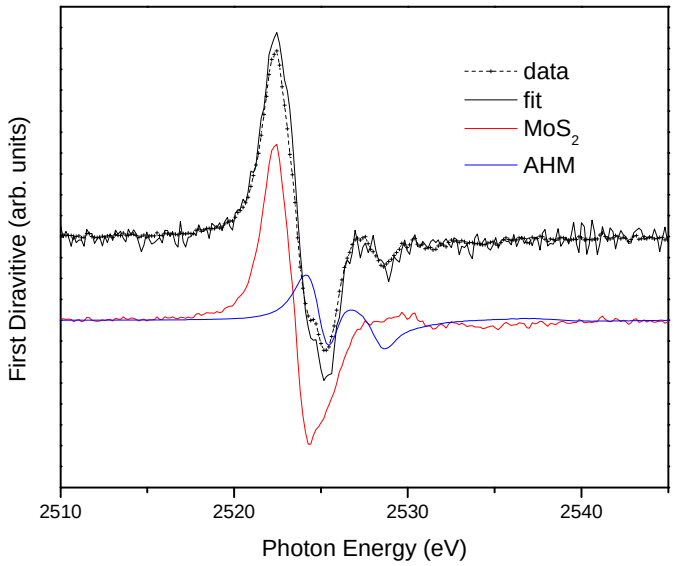

Figure 7.6. Linear combination fitting of the Mo L_3-edge spectra of the catalyst Mo-K/MWCNTs

7.5. Conclusions

The addition of Co and Rh, to the sulfided Mo-K/MWCNT catalyst improved the space time yield and selectivity of the higher alcohols. The maximum total alcohols yield of 0.29 (g/(g of cat.)/h) and higher alcohols selectivity of 39.4% were obtained over the Co-Rh-Mo-K/MWCNT catalyst at 330°C, 1320 psi (9.1 Mpa), 3.8 m^3 (STP)/(kg of cat./h) using H_2 to CO molar ratio value of 1.25. The AC-supported Co-Rh-Mo-K catalyst had a much higher hydrocarbon formation, while the MWCNT-supported alkali-promoted trimetallic catalyst showed better alcohols yield. Alkali promotion to the MoS_2 catalyst reduced the crystalline nature of the catalyst and favored the formation of alcohols. More oxidized S and Mo species were also observed by XRD and XANES in the K-promoted catalysts, indicating the formation of more Mo oxide and/or Co oxide with the addition of K, thus increasing the active sites. More intense features

corresponding to the oxidized S and Mo species were observed in both S K-edge and Mo L_3-edge spectra of the MWCNT-supported catalysts. The formation of Co (Rh)-Mo-S species was evident in the XANES spectra of the bimetallic and trimetallic alkali-promoted MoS_2 catalysts, in agreement with their improved catalytic performance.

7.6. Abbreviations

MWCNTs	Multi-walled carbon nanotubes
AC	Activated carbon
TPR	Temperature programmed reduction
GHSV	Gas hourly space velocity
ICP-MS	Inductively coupled plasma – mass spectroscopy
XRD	X-ray diffraction
TEM	Transmission electron microscopy
SEM	Scanning electron microscopy
STY	Space time yield
XANES	X-ray absorption near-edge structure

7.7. References

1. Forzatti, P.; Cristiani, C.; Ferlazzo, N.; Lietti, L.; Tronconi, E.; Villa, P. L.; Pasquon, I. Synthesis of alcohols from carbon oxides and hydrogen : VII. Preparation, activation, and catalytic behavior of a ZnMnCrK-oxide catalyst. *J. Catal.* **1988**, *111*, 120-135.
2. Christensen, J. M.; Mortensen, P. M.; Trane, R.; Jensen, P. A.; Jensen, A. D. Effects of H_2S and process conditions in the synthesis of mixed alcohols from syngas over alkali promoted cobalt-molybdenum sulfide. *Appl. Catal., A* **2009**, *366*, 29-43.
3. Woo, H. C.; Park, K. Y.; Kim, Y. G.; Namau, I.-S.; Chung, J. S.; Lee, J. S. Mixed alcohol synthesis from carbon monoxide and dihydrogen over potassium-promoted molybdenum carbide catalysts. *Appl. Catal.* 75 (1991) 267-280.
4. Surisetty, V. R.; Tavasoli, A.; Dalai, A. K. Synthesis of higher alcohols from syngas over alkali promoted MoS2 catalysts supported on multi-walled carbon nanotubes. *Appl. Catal. A* **2009**, *365*, 243–251.

5. Concha, B. E.; Bartholomew, G. L.; Bartholomew, C. H. CO hydrogenation on supported molybdenum catalysts: Effects of support on specific activities of reduced and sulfided catalysts. *J. Catal.* **1984**, *89*, 536–541.

6. Li, Z.; Fu, Y.; Jiang, M.; Hu, T.; Liu, T.; Xie, Y. Active Carbon Supported Mo-K Catalysts Used for Alcohol Synthesis. *J. Catal.* **2001**, *199*, 155–161.

7. Serp, P.; Corrias, M.; Kalck, P. Carbon nanotubes and nanofibers in catalysis. *Appl. Catal., A* 253 (2003) 337-358.

8. van Steen, E.; Prinsloo, F. F. Comparison of preparation methods for carbon nanotubes supported iron Fischer-Tropsch catalysts. *Catal. Today* **2002**, *71*, 327–334.

9. Sigurdson, S.; Sundaramurthy, V.; Dalai, A. K.; Adjaye, J. Effect of anodic alumina pore diameter variation on template-initiated synthesis of carbon nanotube catalyst supports. *J. Mol. Catal. A*: Chem. **2009**, *306*, 23-32.

10. Rodriguez, J. A. Interaction of Hydrogen and Thiophene with Ni/MoS_2 and Zn/MoS_2 Surfaces: A Molecular Orbital Study. *J. Phys. Chem. B* **1997**, *101*, 7524-7534.

11. Shen, J. Y.; Matsuzaki, T.; Hanaoka, T.; Takeuchi, K.; Sugi, Y. The Promoter Function of Molybdenum in Rh/Mo/SiO_2 Catalysts for CO Hydrogenation. *Catal. Lett.* **1994**, *28*, 329–339.

12. Surisetty, V. R.; Dalai, A. K.; Kozinski, J. Synthesis of higher alcohols from synthesis gas over Co-promoted alkali-modified MoS_2 catalysts supported on MWCNTs. *Appl. Catal., A* **2010**, in press.

13. Surisetty, V. R.; Dalai, A. K.; Kozinski, J. Intrinsic reaction kinetics of higher alcohols synthesis from synthesis gas over sulfided alkali-promoted Co-Rh-Mo trimetallic catalyst supported on MWCNTs. Energ. Fuel. **2010**, in press.

14. Li, Z-R.; Fu, Y.-L.; Jiang, M. Effect of rhodium modification on structures of sulfided Rh-Mo-K/Al_2O_3 catalysts studied by XAFS. *J. Synchrotron Rad.* **1999**, *6*, 462-464.

15. Surisetty, V. R.; Dalai, A. K.; Kozinski, J. Effect of Rh promoter on MWCNT-supported alkali-modified MoS_2 catalysts for higher alcohols synthesis from CO hydrogenation. *Appl. Catal. A*, **2010**, *381*, 282–288.

16. Sun, M.; Nelsona, A. E.; Adjaye, J. On the incorporation of nickel and cobalt into MoS_2-edge structures. *J. Catal.* **2004**, *226*, 32–40.

17. Li, S. Y.; Rodriguez, J. A.; Hrbek, J.; Huang, H.; Xu, G-Q. Reaction of hydrogen with S/Mo(110) and MoS_x films: formation of hydrogen sulfide. *Surf. Sci.* **1996**, *366*, 29-42.

18. T. Shido, K. Asdakura, Y. Noguchi, Y. Iwasawa, Structure and catalytic performance of Mo dimer oxy-carbide species in NaY supercages. *Appl. Catal., A* **2000**, *194*, 365-374.

19. Rodriguez, J. A.; Jirsak, T.; Pérez, M.; Chaturvedi, S.; Kuhn, M.; González, L.; Maiti, A. Studies on the Behavior of Mixed-Metal Oxides and Desulfurization: Reaction of H_2S and SO_2 with Cr_2O_3(0001), MgO(100), and $Cr_xMg_{1-x}O$(100). *J. Am. Chem. Soc.* **2000**, *122*, 12362-12370.

20. Huang, L.; Wang, G.; Qin, Z.; Du, M.; Dong, M.; Ge, H.; Wu, Z.; Zhao, Y.; Ma, C.; Hu, T.; Wang, J. A sulfur K-edge XANES study on the transfer of sulfur species in the reactive adsorption desulfurization of diesel oil over Ni/ZnO. *Catal. Commun.* **2010**, *11*, 592-596.

21. Sarret, G.; Connan, J.; Kasrai, M.; Berard, L. E.; Bancroft, G. M. Characterization of sulfur in asphaltenes by sulfur *K*- and *L*-edge XANES spectroscopy. *J. Synchrotron Rad. 6* (1999) 670-672.

22. George, G. N.; Cleland, Jr. W. E.; Enemark, J. H.; Smith, B. E.; Kipke, C. A.; Roberts, S. A.; Cramer, S. P. L-Edge spectroscopy of molybdenum compounds and enzymes. *J. Am. Chem. Soc.* **1990**, *112*, 2541-2548.

23. J. Evans, F.W. Mosselmans, L-edge studies on molybdenum. *J. Phys. Chem.* **1991**, *95*, 9673-9676.

24. Bare, S. R.; Mitchell, G. E.; Maj, J. J.; Vrieland, G. E.; Gland, J. L. Local site symmetry of dispersed molybdenum oxide catalysts: XANES at the Mo $L_{2,3}$-edges. *J. Phys. Chem.* **1993**, *97*, 6048-6053.

25. Lede, E. J.; Requejo, F. G.; Pawelec, B.; Fierro, J. L. G. XANES Mo *L*-Edges and XPS Study of Mo Loaded in HY Zeolite. *J. Phys. Chem. B* **2002**, *106*, 7824-7831.

26. Surisetty, V. R.; Dalai, A. K.; Kozinski, J. Alkali-promoted trimetallic Co-Rh-Mo sulfide catalysts for higher alcohols synthesis from synthesis gas: Comparison of MWCNT and activated carbon supports. *Ind. Eng. Chem. Res.* **2010**, *49*, 6845-6853.

27. K. Klier, R.G. Herman, J.G. Nunan, K.J. Smith, C.E. Bogdan, C. W. Young, J.G. Santiesteban, (D.M. Bibby, C.D. Chang, R.F. Howe, and S.Y. Yurchak, Eds.), *Methane Conversion*. Elsevier: Amsterdam, 1988, p. 109.

28. Bhusan, B., Ed. *Springer handbook of nanotechnology*, 2nd ed., Springer: New York, 2007.

29. Eswaramoorthi, I.; Sundaramurthy, V.; Dalai, A. K. Partial oxidation of methanol for hydrogen production over carbon nanotubes supported Cu-Zn catalysts. *Appl. Catal., A* **2006,** *313*, 22-34.

30. Pan, X.; Fan, Z.; Chen, W.; Ding, Y.; Luo, H.; Bao, X. Enhanced ethanol production inside carbon-nanotube reactors containing catalytic particles. *Nat. Mater.* **2007**, *6*, 507–511.

31. Li, Z-R.; Fu, Y-L.; Jiang, M. Structures and performance of Rh–Mo–K/Al_2O_3 catalysts used for mixed alcohol synthesis from synthesis gas. *Appl. Catal., A* **1999,** *187*, 187-198.

32. Berge, P. J. V.; van de Loosdrecht, J.; Barradas, S.; van der Kraan, A. M. Oxidation of cobalt based Fischer-Tropsch catalysts as a deactivation mechanism. *Catal. Today* **2000**, *58*, 321–334.

33. Kogelbauer, A.; Goodwin, J. G.; Oukaci, R. Ruthenium promotion of Co/Al_2O_3 Fischer-Tropsch catalysts. *J. Catal.* **1996**, *160*, 125–133.

34. Rodriguez, J. A.; Chaturbedi, S.; Hanson, C. J.; Albornoz, A.; Brito, J. L. Reaction of H_2 and H_2S with $CoMoO_4$ and $NiMoO_4$: TPR, XANES, Time-Resolved XRD, and Molecular-Orbital Studies. *J. Phys. Chem. B* **1999**, *103*, 770-781.

35. Zubavichus, Y. V.; Slovokhotov, Y. L.; Schilling, P. J.; Tittsworth, R. C.; Golub, A. S.; Protzenko, G. A.; Novikov, Y. N. X-ray absorption fine structure study of the atomic and electronic structure of molybdenum disulfide intercalation compounds with transition metals. *Inorg. Chim. Acta* **1998**, *280*, 211-218.

36. Guay, D.; Divigalpitiya, W. M. R.; Bdlanger, D.; Feng, X. H. Chemical Bonding in Restacked Single-Layer MoS_2 by X-ray Absorption Spectroscopy. *Chem. Mater.* **1994**, *6*, 614-619.

37. Hay, S. J.; Metson, J. B.; Hyland, M. M. Sulfur Speciation in Aluminum Smelting Anodes. *Ind. Eng. Chem. Res.* **2004**, *43*, 1690-1700.

38. Aritani, H.; Tanaka, T.; Funabiki, T.; Yoshida, S. Study of the Local Structure of Molybdenum−Magnesium Binary Oxides by Means of Mo L_3-Edge XANES and UV−Vis Spectroscopy. *J. Phys. Chem.* **1996**, *100*, 19495-19501.

39. Topsoe, H.; Clausen, B. S.; Topsoe, N. Y.; Pederson, E. Recent basic research in hydrodesulfurization catalysis. *Ind. Eng. Chem. Fundam.* **1986**, *25*, 25-36.

40. Park, J.-N.; Kim, J-H.; Lee, H.-I. A Study on the Sulfur-Resistant Catalysts for Water Gas Shift Reaction III. Modification of Mo/ γ-Al_2O_3 Catalyst with Iron Group Metals. *Bull. Korean Chem. Soc.* **2000**, *21*, 1233-1238.

41. Tatsumi, T.; Muramatsu, A.; Yokota, K.; Tominga, H. Mechanistic study on the alcohol synthesis over molybdenum catalysts : Addition of probe molecules to COH_2. *J. Catal.* **1989**, *115*, 388-398.

CHAPTER 8

Influence of Porous Characteristics of the Carbon Support on Alkali-Modified Trimetallic Co-Rh-Mo Sulfided Catalysts for Higher Alcohols Synthesis from Synthesis Gas

The manuscript provided in this chapter is very similar to the one submitted to the journal of Applied catalysis A: General.

Citation:

Surisetty, V. R.; Dalai, A. K.; Kozinski, J. Influence of porous characteristics of the carbon support on alkali-modified trimetallic Co-Rh-Mo sulfided catalysts for higher alcohols synthesis from synthesis gas. *Applied catalysis A: General* **2010**, Submitted for Review.

Contribution of the Ph.D. Candidate

Experiments were planned and performed by Venkateswara Rao Surisetty. Drs. Ajay Dalai and Janusz Kozinski provided guidance in planning the experiments. The experimental results were analyzed by Venkateswara Rao Surisetty. The submitted manuscript was written by Venkateswara Rao Surisetty, with Dr. Dalai providing discussion and editorial assistance.

Contribution to Overall Study

In Chapter 6 it was demonstrated that the performance of alkali-modified trimetallic Co-Rh-Mo catalysts was higher compared to monometallic and bimetallic catalysts. The porous characteristics of support have great influence on heterogeneous chemical reaction, which has not yet been elucidated on the catalytic performance of higher alcohols synthesis. Chapter 8 aimed to study the influence of the porous characteristics of commercially available activated carbons on the physico-chemical properties of the catalyst. It also discuss on the comparison of the performance of higher alcohols synthesis from synthesis gas using alkali promoted trimetallic Co-Rh-Mo sulfided catalysts supported on different activated carbon with that of MWCNTs support.

8.1. Abstract

Alkali-modified trimetallic Co-Rh-Mo sulfided catalysts supported on commercial activated carbons with different textural characteristics were tested for the synthesis of higher alcohols from synthesis gas and compared with a similar catalyst supported on multi-walled carbon nanotubes (MWCNTs). Addition of metals (Co, Rh, and Mo) to the microporous and mesoporous activated carbons, and the MWCNT supports increased the mean pore diameter and % mesoposity of the catalysts. The N_2 adsorption-desorption isotherms of the MWCNT support and the MWCNT-supported alkali-modified trimetallic C-Rh-Mo catalyst revealed that the mesoporous structural integrity of the catalyst was unchanged from the support after impregnation of the catalyst species. The formation of large particles took place due to the agglomeration of metal species on the microporous activated carbon supports. The metal dispersion of the sulfided catalysts on different supports is: MWCNT < AC-CGP Super < AC-Fluid Coke < AC-RX_3 Extra < AC-Darco. The total alcohols STY and selectivity of 0.296 g/(g of cat.)/h and 35.6%, respectively were found to be high on the MWCNT-supported alkali-modified trimetallic C-Rh-Mo catalyst compared to the catalysts supported on activated carbon.

8.2. Introduction

Mixture of higher alcohols is a potential gasoline blending stock to improve the octane number of the motor gasoline and reduces the emissions of NO_x, ozone, CO, and aromatic vapours. Catalytic conversion of synthesis gas derived from waste biomass to higher alcohols is an alternative approach that remains economically attractive for making fuels and chemicals.[1-3] Molybdenum sulfide catalysts have been recognized to be effective for the CO hydrogenation reactions because of their sulfur resistance and activity for water-gas shift (WGS) reaction. Addition of alkali to MoS_2 catalysts increases the formation of alcohols and suppresses the formation of hydrocarbons.[4,5]

The higher alcohols space time yield (STY) and selectivity are found to be low over the K-modified MoS_2 catalysts due to the formation of methanol, hydrocarbons and carbon dioxide. The Rh promotion to this catalyst system increased the activity towards the formation of oxygenates, due to the strong interaction between the rhodium modifiers with Mo species.[6] The incorporation of Co resulted substantial changes in the structure of K-

modified MoS_2 catalysts and enhanced the $C_1 \rightarrow C_2$ homologation step that leads to the formation of ethanol as the dominant product.[7] The formation of hydrocarbons can be greatly reduced using alkali-modified trimetallic Co-Rh-Mo catalyst. This catalyst was found to be attractive to reduce Rh content and increase the activity and selectivity of the catalyst for the formation of higher alcohols.[8,9]

Catalyst support has great influence on alcohols synthesis from CO hydrogenation. Over the unsupported catalysts, molybdenum species exists in much reduced state. The activity of the catalyst is found to be high on Mo species with lower oxidation state and the catalyst becomes more selective to hydrocarbons.[10,11] The surface acidity of acid metal oxide supports, like Al_2O_3, SiO_2 and ZrO_2 suppress the reaction rate of alcohols by favouring the formation of hydrocarbons and results the deactivation of the catalyst by coke formation.[12,13] Carbon-based materials hold several advantages as catalyst support for higher alcohols synthesis from synthesis gas. Activated carbon supports have intriguing properties such as, large surface area, inert graphitic surface, resistance to acidic or basic media, and high thermal stability. The alcohols selectivity is found to be higher on the MoS_2 catalysts that are supported on activated carbon compared to the SiO_2, Al_2O_3, and CeO_2-supported catalysts.[14-16] Carbon in the form of multi-walled carbon nanotubes (MWCNTs) display unique properties such as meso/macro porous structures that mitigate transport limitations, uniform and straight pores that allow great metal dispersion, high mechanical strength, and thermal conductivity.[17,18]

Conventional activated carbons being microporous (pore diameter < 2 nm) causes pore plugging due to the formation of coke and deactivation of the catalyst, which results in transport limitation in the reaction.[19] Most of the research on higher alcohols synthesis was done using microporous activated carbon supported catalysts that had significantly smaller surface area (350–820 m^2/g) than commercially available activated carbons (950m^2/g and higher) and long time activity of these catalysts does not meet the commercial levels. The textural properties of the support, such as average pore diameter, pore volume and surface area, could significantly influence the extent of reduction, morphology, adsorption and activity/selectivity properties of the active phase, especially in well-dispersed catalysts.[20] The effects of pore size and surface area of activated carbon support on the catalytic performance of higher alcohols synthesis from synthesis gas have not been elucidated yet.

A good understanding of the relationship between porous characteristics and performance of the support is important for designing and selecting a catalyst system with a suitable pore structure for a particular application. The goal of the present research is to study the influence of the porous characteristics of commercially available activated carbons on the physico-chemical properties of the catalyst, as well as, the performance of higher alcohols synthesis from synthesis gas using alkali-modified trimetallic Co-Rh-Mo- sulfided catalysts supported on activated carbon. The higher alcohols synthesis reaction was also performed under similar reaction conditions using the Co-Rh-Mo-K/MWCNT catalyst for comparing the MWCNT support with that of different activated carbons.

8.3. Experimental method

8.3.1. Catalyst preparation

Four catalysts listed in Table 8.1 were prepared using different activated carbons. AC-Darco, brand named activated carbon was purchased from Aldrich, Canada. Two activated carbons, brand named as AC-RX_3 extra and AC-CGP super were obtained form Norit, USA. Activated carbon named as AC-Fluid coke is obtained from Syncrude and activated in our pilot scale reactor. Commercial MWCNTs was purchased from M. K. Nano, Canada. Prior to impregnation, all the supports were treated with 30% HNO_3 reflux at 100°C overnight, washed with distilled water several times, and dried at 120°C for 6 h. The oxide samples were prepared by the incipient wetness impregnation method using ammonium heptamolybdate tetrahydrate (Sigma-Aldrich, Canada), potassium carbonate (Aldrich, Canada), cobalt acetate tetrahydrate (Alfa-Aesar, Germany), and rhodium chloride hydrate (Aldrich, Canada) as precursors for Mo, K, Co, and Rh, respectively. At the first step, the support was impregnated with an aqueous solution of K_2CO_3, followed by drying at 120°C for 2 h and stabilizing in an argon flow of 50 ml/min at 300°C, at a heating rate of 10°C/min for 4 h. The support was further impregnated with aqueous solutions containing the required amounts of $(NH_4)_6Mo_7O_{24}$, $Co(CH_3COO)_2$, and $RhCl_3$ followed by drying at 120°C for 2 h and stabilizing in an argon flow of 50 ml/min at 450°C, at a heating rate of 10°C/min for 12 h.

8.3.2. Characterization of Co-Rh-Mo-K catalysts

The surface area, pore volume, and average pore diameter of oxide samples were measured by N_2-physisorption at 77 K using a Micromeritics ASAP 2000. Approximately 0.2 g of sample was used for each analysis. The moisture and other adsorbed gases present in the sample were removed before analysis by degassing the sample at 200°C for 2 h under 66.7 Pa (500 mm Hg). The sample was then evacuated at 2.67 Pa (20 μm Hg) before N_2 adsorption.

The content of Mo, Co, and Rh of the oxide catalysts were determined using a Perkin-Elmer ELAN 5000 inductively coupled plasma mass spectroscopy (ICP-MS) instrument.

Powder X-ray diffraction (XRD) analysis patterns of oxide forms of samples were recorded on a Rigaku X-ray diffraction instrument with nickel filtered Cu Kα radiation (λ = 0.1541 nm). Each sample was scanned at a rate of 0.05°/s, with 2θ varying from 10 to 80°.

Carbon monoxide was used as a probe molecule to determine the number of accessible surface metal atoms present on the sulfided catalysts. The CO uptake (μmole/g of cat.) measured from CO chemisorption is equivalent to the number of active metal atoms that are accessible to the reactant molecules. The stoichiometric coefficient (CO to metal ratio) of 1 was used, and the extent of reduction was assumed to be 100% in metal dispersion calculations. The carbon monoxide uptake on the sulfided catalysts was measured using the Micromeritics ASAP 2000 instrument. Prior to the CO chemisorption measurement, 0.2 g of sample was sulfided in situ, using 10 mole % H_2S in H_2 at 400°C for 4 h. The sample was then evacuated at 120°C until the static pressure remained less than 6.6 x 10^{-4} Pa. Chemisorption was performed by passing pulses of CO over the sample to measure the total gas uptake at 35°C.

The morphology of the oxide samples was characterized by transmission electron microscopy (TEM) investigations, using a Philips CM20 (100 kV) transmission electron microscope equipped with a NARON energy-dispersive spectrometer with a germanium detector.

8.3.3. Catalyst activity and selectivity studies

A single-pass tubular downflow fixed-bed reactor of 450-mm length and 22-mm inside diameter made of inconel tube was used to perform higher alcohol synthesis reactions.

The reactor was packed with 2 g of catalyst diluted with 12 ml of 90 mesh size silicon carbide and housed in an electric furnace controlled by a temperature controller. The reactor was pressurized with He to 3.44 MPa (500 psig) and the sulfidation, together with the reduction, was carried out for 6 h at 450°C at a heating rate of 2°C/min using a gas mixture containing 10 mole % H_2S in H_2 and a flow rate of 50 ml/min. The temperature was then lowered to the reaction temperature, and the system pressurized to the reaction conditions. The feed gas mixture CO (30 mole %), H_2 (60 mole %), and Ar (10 mole %) was passed through mass flow controllers and the higher alcohols synthesis reaction was carried out at steady-state under the reaction conditions of 330°C, 8.27 (1200 psig) and a gas hourly space velocity (GHSV) of 3.6 m^3 (STP) /(kg of cat.)/h over a period of 24 h. The product gas was cooled to 0°C and separated into gas and liquid phases at the reaction pressure. The CO conversion and other gaseous products were monitored with a time interval of 1 h. The liquid products were collected at the end of the reaction and analyzed with a Varian 3400 gas chromatograph equipped with a capillary column and a flame ionization detector (FID). The volume and weight of liquid products were measured to check the mass balance. The gaseous products were analyzed online on a Shimadzu gas chromatograph through a sampling valve. Using Ar as an internal standard, the CO conversion was calculated and the overall mass balance of the reaction was determined. The experiments were repeated at least twice to check reproducibility and to confirm that the results obtained were within the experimental error of ± 2.5%.

8.4. Results and Discussion

8.4.1. Characterization of Co-Rh-Mo-K catalysts

The N_2 adsorption-desorption isotherm of all the supports were measured with an aim to measure the total surface area and are shown in Figs. 8.1a to 8.1e. The microporous activated carbon support, AC-Darco, exhibit a type III isotherm with a hysteresis loop of type H_2 is observed according to the IUPAC classification.[21] Type II adsorption isotherm with a hysteresis loop of type H_2 is observed on the support, AC-Rx_3 extra.[22] A horizontal plateau at relative higher pressures indicates highly microporous nature of this support with a narrow pore size distribution. On the support, AC-Fluid coke, the increment of N_2 uptake was significant at high relative pressures and showed type IV isotherm with a hysteresis loop of

type H_3 that does not exhibit any limiting adsorbtion at high relative pressures.[21] This indicates the presence of large amount of mesopores on this support.

The N_2 adsorption-desorption characteristic type IV isotherm with large condensation of adsorbate in pores at mesoporous regions ($x = p/p_s \geq 0.40$) was observed on the mesoporous support, AC-CGP super.[21] The MWCNT support showed the characteristic type IV isotherm with H_1 hysteresis loop, indicative of the existence of textural mesopores with cylindrical arrays of pore channels. The sharpness of the desorption branches suggests the narrow pore size distribution of the MWCNT support.[23] Fig. 8.2a to 8.2e displays the N_2 adsorption-desorption isotherms of all the catalysts. From these figures, it is cleat that the amount of N_2 adsorbed on the support is proportional to the available surface area. All the catalysts exhibit similar isotherms as their corresponding supports, suggesting that metal impregnation did not alter the structure of the parent support.

The results for textural characterization of supports as well as the catalysts are summarized in Table 8.1. Data are tabulated for BET surface area (S_{BET}), mesopore surface area (S_{me}), total pore volume (V_{tot}), mesoporous volume (V_{me}), average pore diameter (D), and the percentage of mesoporosity (% Me), defined as percentage ratio of mesopore due to metal loading was calculated using $BE = 1-NS_{BET}$, where NS_{BET} is the normalized surface area, and is defined as $NS_{BET} = (S_{BET})_{catalyst}/((1-y) * (S_{BET})_{support})$, in which y is the weight fraction of the total metal content of the catalyst.[24] It is observed from the table that the support, AC-Fluid coke has low surface area and pore volume among the activated carbon supports. The support, AC-CGP super display highest BET surface area, total pore volume and mesoporous volume. MWCNTs exhibit low surface area compared to that of activated carbon supports, whereas, the pore diameter is found to be quite high. The supports AC-CGP super and MWCNTs are highly mesoporous in nature with mesoporosity of 94 and 98%, respectively.

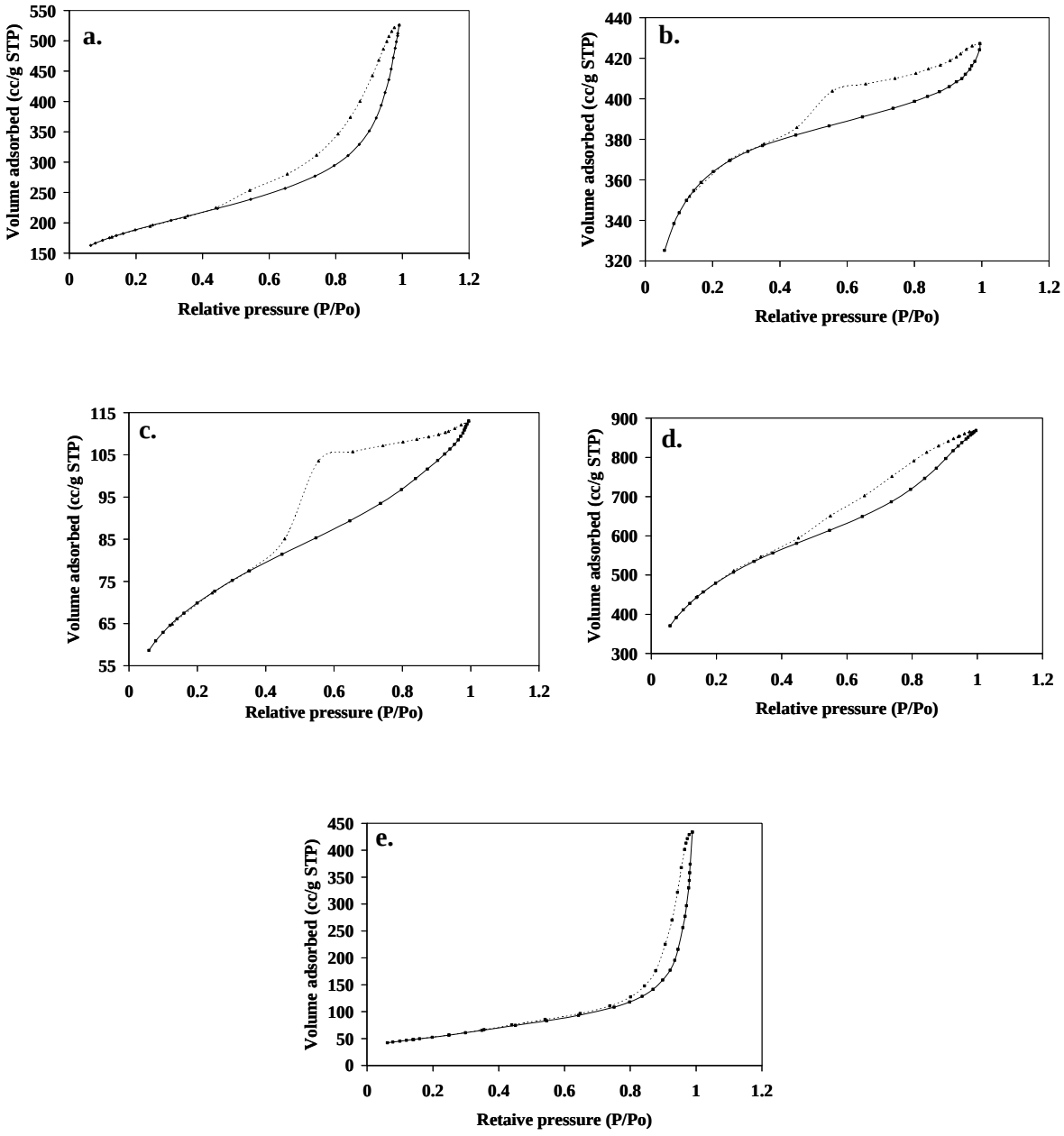

Figure 8.1. N_2 adsorption-desorption isotherms of pure supports
a. AC-Darco; b. AC-RX_3 extra; c. AC-Fluid coke; d. AC-CGP super; e. MWCNT

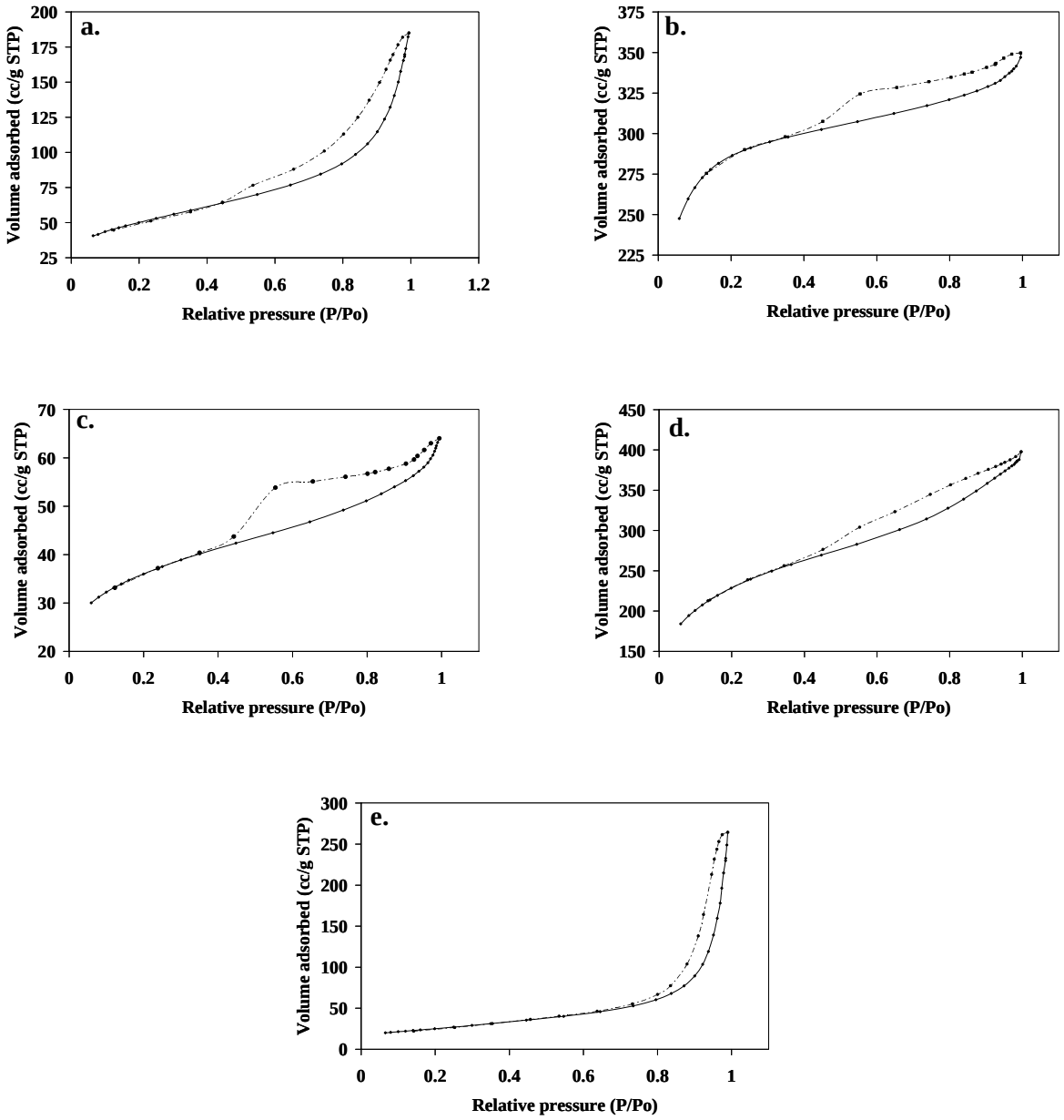

Figure 8.2. N_2 adsorption-desorption isotherms of supported catalysts a. AC-Darco; b. AC-RX_3 extra; c. AC-Fluid coke; d. AC-CGP super; e. MWCNT

Table 8.1. Textural properties of pure supports and catalysts

Catalyst Support	Pure support						Catalyst						
	S_{BET} (m^2/g)	S_{me} (m^2/g)	V_{tot} (cc/g)	V_{me} (cc/g)	D (nm)	% Me	S_{BET} (m^2/g)	S_{me} (m^2/g)	BE	V_{tot} (cc/g)	V_{me} (cc/g)	D (nm)	% Me
AC-Darco	658	197	0.93	0.35	1.95	38	97	41	0.79	0.16	0.08	7.21	50
AC-RX_3 extra	1249	483	0.66	0.31	1.58	47	292	140	0.67	0.34	0.19	4.61	56
AC-Fluid coke	245	161	0.17	0.13	2.81	76	127	87	0.26	0.10	0.08	3.03	80
AC-CGP super	1739	1534	1.33	1.25	3.07	94	816	642	0.33	0.60	0.57	3.92	95
MWCNTs	188	162	0.53	0.52	11.34	98	68	59	0.48	0.24	0.24	17.91	100

S_{BET} - BET surface area; S_{me} - Mesopore surface area; V_{tot} - Total pore volume; V_{me} - Mesoporous volume; D - Average pore diameter; % Me - Percentage of mesoporosity; and BE - Blocking extent of the pores of the support due to metal loading

The textural properties of the stabilized catalysts display some changes to that of pure supports. The mean pore diameter and % mesoposity were shifted towards higher values after the impregnation of alkali and metals on the supports. These results suggest that the addition of metals most likely block the micropores of the support.[25] The BET surface area and pore volume decrease were observed after the incorporation of metals, suggesting the partial pore blocking of the support by the metals. The blocking extent of the metal species was found to be high on the microporous activated carbon supported catalysts. The large surface area of the AC-CGP super supported catalyst indicates negligible blocking of pores with the impregnated metals. The decreased mesopore volume and surface area of AC-CGP super-supported catalyst indicated that the metal species block the mesopore pores of this support. In spite of the pore blockage, the mesoporous structural integrity of the MWCNT-supported alkali-promoted trimetallic C-Rh-Mo catalyst was unchanged from the support as seen from the N_2 adsorption- desorption isotherms of MWCNT support and the catalyst (Fig. 8.2e). These results suggest that MWCNTs have unique characteristics, such as uniform pore-size distribution, nano-sized channels, and mesoporous nature make them a promising support for various catalytic applications.[9]

Fig. 8.3 shows the XRD patterns of the alkali-promoted trimetallic Co-Rh-Mo catalysts supported on various activated carbons and that of the MWCNTs in oxide form. The JCPDS chemical spectra data bank was used to detect the most probable phases present in the samples. The variation in peak intensity of the catalysts was observed, confirming the role of the support on the dispersion of catalyst species. The strong intensity peak at 2θ value of 26.6° for the catalyst supported on MWCNTs is due to the reflections of the graphite phase. It is of interest to note that the graphite nature of the support was observed on micro porous activated carbons, AC-Darco and AC-RX_3 extra, whereas, the XRD patterns of the catalysts supported on mesoporous activated carbons, AC-Fluid Coke and AC-CGP super showed no graphite phase. The characteristic reflections corresponding to the crystalline structure of MoO_3 are observed at 2θ value of 40.7° on all the catalysts.[4] The peak at 2θ value of 28.4° corresponds to the characteristic reflections of the $K_2Mo_2O_7$ phase.[26] Other K-Mo-O phases, such as KMo_4O_6 (2θ = 15.9, and 37.1°) also exist on these catalysts.[27,28]

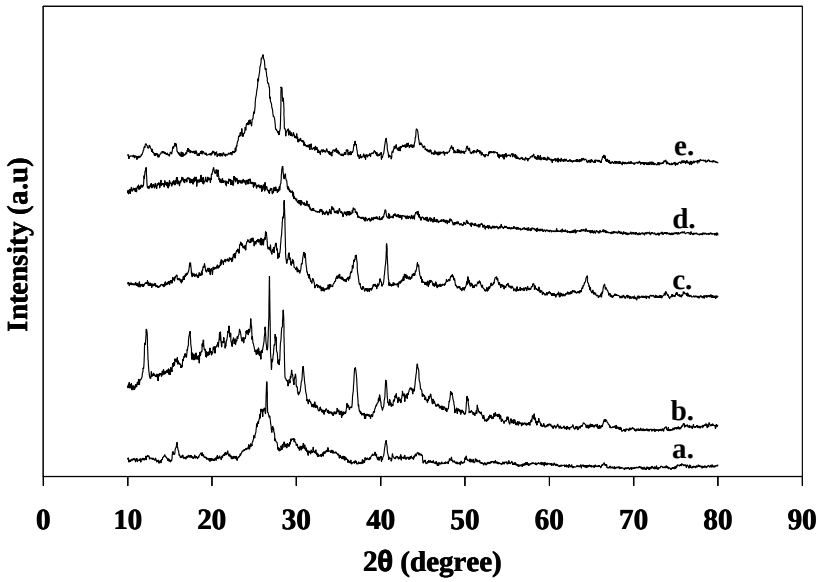

Figure 8.3. XRD patterns of catalysts in oxidized form a. AC-Darco; b. AC-RX_3 extra; c. AC-Fluid coke; d. AC-CGP super; e. MWCNT

TEM images of the AC-Darco, AC-RX_3 extra, AC-Fluid coke, AC-CGP super and MWCNT-supported catalysts were recorded and are as shown in Figure 8.4. These micrographs reveal the morphology differences of alkali-promoted trimetallic Co-Rh-Mo catalysts supported on different supports and the development of a considerable amount of agglomerates, especially on the surface of the microporous activated carbon supported catalysts. The metal species are well dispersed on the mesoporous activated carbon support, AC-CGP super with particle size in the range of 3-6 nm (Fig. 8.4d). The TEM image of MWCNT-supported catalyst revealed that the catalyst particles are well dispersed both inside and outside the carbon nanotubes. The particle sizes of the metal species that are inside and outside of the tubes are in the range of 1 to 3 nm (Fig. 8.4e).

The results of the CO chemisorption of the sulfided catalysts are given in Table 8.2. The CO uptake values of 137 and 140 μmole/(g of cat.) were observed on the alkali promoted trimetallic catalysts supported on microporous activated carbon supports, AC-Darco and AC-RX_3 extra, respectively. Even though the surface area of the AC-RX_3 extra support is almost double, the pore volume and pore diameter are comparatively less than that of AC-Darco and hence about equal amounts of CO chemisorption was observed on these two supports.

From the TEM images, it is observed that the formation of large particles takes place due to the agglomeration of metal species on the microporous activated carbon supports. This result in lower dispersions on these supports compared to that on mesoporous activated carbons. Due to the mesoporous nature of activated carbon supports, AC-Fluid coke and AC-CGP super, most of the metal deposition takes place inside the pores, resulting higher CO uptake values on these supports. The amounts of adsorbed CO on the surface of MWCNT-supported catalyst is found to be higher compared to all activated carbon supported catalysts, indicating the presence of large number of active sites on the catalyst. The metal dispersion of catalysts on different supports is in the following order: MWCNTs < AC-CGP super < AC-Fluid coke < AC-RX_3 extra < AC-Darco. The large pore volume and pore size of the MWCNT support facilitates uniform metal particle distribution and high metal dispersions.[29] These results suggest that the catalyst supported on MWCNTs may perform better than catalysts supported on microporous, as well as, mesoporous activated carbons.

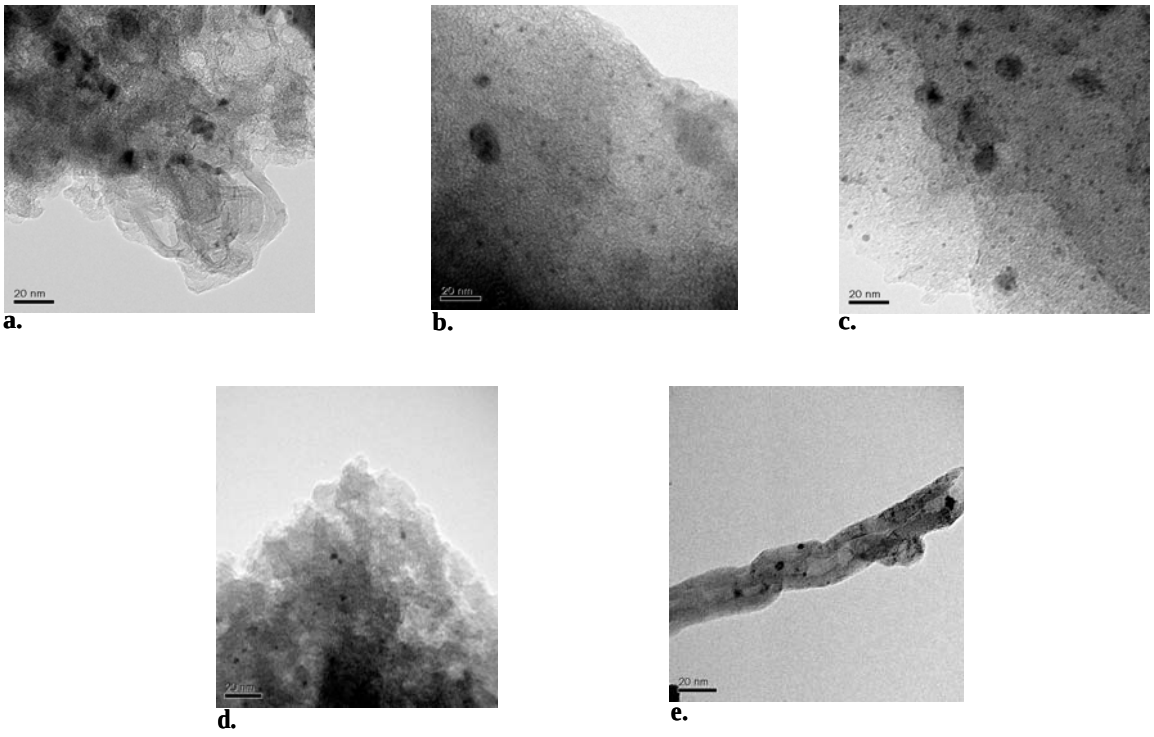

Figure 8.4. TEM image of supported catalysts a. AC-Darco; b. AC-RX_3 extra; c. AC-Fluid coke; d. AC-CGP super; e. MWCNT

Table 8.2. CO chemisorption measurement results

Catalyst support	CO uptake (µmole/g of cat.)	Total number of metal atoms present in the sample (µmole/g of cat.)	Dispersion of metals (%)
AC-Darco	137	495	27.7
AC-RX_3 extra	140	495	28.3
AC-Fluid coke	161	495	32.6
AC-CGP super	195	495	39.4
MWCNT	237	495	47.9

8.4.2. Catalyst activity and selectivity studies

The catalyst activity studies towards higher alcohol synthesis reaction were carried out under similar conditions at 330°C, 8.3 MPa (1200 psig), 3.6 m^3 (STP)/(kg of cat.)/h, and H_2 to CO molar ratio of 2. Fig. 8.5 gives the results of the percentage CO conversion as time-on-stream during 24 h of higher alcohol synthesis over the different activated carbon and MWCNT-supported alkali modified trimetallic Co-Rh-Mo catalysts. It is observed that the CO hydrogenation activity of the supported catalysts followed the same order as that of CO chemisorption according to their pore structures. The stability of MWCNT-supported catalyst was much better than the catalysts supported on activated carbons. The uniform pore size distribution of the MWCNT support facilitates the large dispersion of metal particles on the support, which results in higher activity compared to that on activated carbon supported catalysts.[5] The catalyst supported on AC-CGP Super showed the high initial activity at the start-of-run, but dropped sharply as the reaction progressed within 24 h period. Similar stability results were observed on the AC-Fluid Coke supported catalyst. It can be deduced that the partially blocked mesopores by metal species raised the mass diffusion restriction of synthesis gas as well as products, thus decreasing the CO hydrogenation activity with time-on-stream.[30]

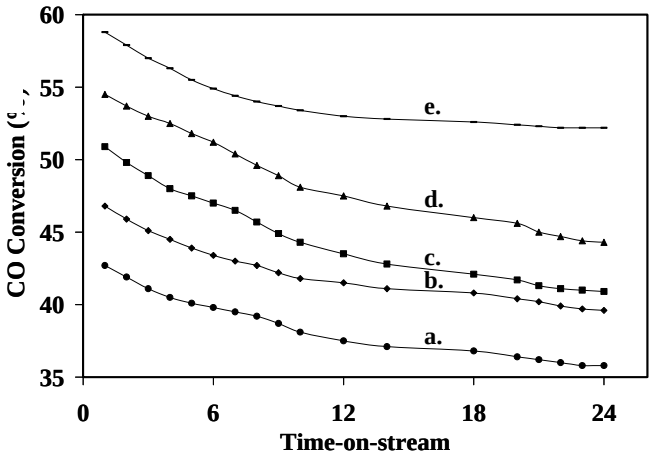

Figure 8.5. CO Conversion (%) with time-on-stream a. AC-Darco; b. AC-RX_3 extra; c. AC-Fluid coke; d. AC-CGP super; e. MWCNT

(wt. of the cat. = 2 g, P = 8.3 MPa, T = 330°C, GHSV = 3.6 m^3 (STP)/(kg of cat.)/h, H_2/CO molar ratio = 2)

The analysis of the liquid products indicates that linear alcohols are formed and no branched alcohols were observed in the GC trace corresponding to the higher alcohols. Methanol, ethanol, n-propanol, and n-butanol are the major products, together with other higher alcohols. The analysis of exit gas indicates that methane is the major component apart from CO_2 and unconverted gases, such as, CO and H_2. Table 8.3 shows the activity and selectivity results obtained from CO hydrogenation over the sulfided alkali-promoted trimetallic Co–Rh–Mo catalysts after an induction period of 15 h. The term higher alcohols represents the ethanol and alcohols with carbon number greater than 2 (C_{2+} alcohols). Over the catalysts supported on microporous activated carbons, AC-Darco and AC-RX_3 extra, the total alcohols space time yields (STY) of 0.141 and 0.154 g/(g of cat./h), respectively, were observed. Catalysts prepared on mesoporous activated carbon, AC-Fluid coke and AC-CGP super had substantially higher STY of alcohols of 0.187 and 0.202 g/(g of cat./h), respectively than microporous activated carbon supported catalysts. The support AC-CGP super has the advantage of high surface area, large pore diameter and pore volume compared to the other activated carbon supports. This results in high dispersion of active metal species on the surface as seen from the XRD profiles and CO chemisorption results, favouring the formation of alcohols. The STY of total hydrocarbons follow the similar trend as that of the total alcohols STY, whereas, the water-gas-shift reaction rate is almost constant on all activated carbon supported catalysts. It is also noted that the selectivity of methanol, ethanol and higher alcohols are almost constant on all the activated carbon-supported catalysts.

Table 8.3. Catalytic performance of sulfided MWCNT-supported catalysts

(wt. of the cat. = 2 g, P = 8.3 MPa, T = 330°C, GHSV = 3.6 m^3 (STP)/(kg of cat.)/h, H_2/CO molar ratio = 2)

Catalyst support	CO conversion (%)	Product STY (g/(g of cat.)/h)		CO_2 produced (mole %)	Alcohol Selectivity (wt %)		
		Total alcohols	Total hydro carbons		Methanol	Ethanol	Higher alcohols
AC-Darco	35.6	0.141	0.204	28.2	13.2	8	11.7
AC-RX_3 extra	39.6	0.154	0.217	27.3	13.7	8.3	12.1
AC-Fluid coke	41.8	0.187	0.253	26.3	14.3	8.7	12.7
AC-CGP super	44.5	0.202	0.275	25.0	14.4	9	13.1
MWCNT	52.4	0.296	0.345	18.4	17.8	11.7	16.8

MWCNT-supported catalysts outperformed the catalysts supported on activated carbon. The total alcohols and total hydrocarbons STY of 0.296 and 0.345 g/(g of cat./h) were observed on this catalyst, whereas, the carbon dioxide formation rate is less compared to that of the activated carbon supported catalysts. These results explain that the pore size of the support has direct influence on the synthesis of mixed alcohols from synthesis gas. Support pore size can influence particle size distribution, dispersion, extent of reduction and plays an important role to diffuse the reactant molecules to the catalytically active centers that are located inside the pores.[31] The micro-porous structure of activated carbon-supported catalysts causes pore plugging due to the formation of coke and deactivation of the catalyst, which results in transport limitation in the reaction.[32] It is also worth to note that all these activated carbons are associated with 5-10% ash content as indicated by the manufacturer, whereas, the MWCNTs are highly purified and has almost negligible ash content.

8.5. Conclusions

Addition of alkali (K) and metals (Co, Rh, and Mo) to the microporous and mesoporous activated carbons as well as MWCNT supports increased the mean pore diameter and % mesoposity of the catalysts. The extent of blocking of the metal species was found to be high on the microporous activated carbon supported catalysts. From the N_2 adsorption-desorption isotherms of MWCNT support and the MWCNT-supported alkali-promoted trimetallic C-Rh-Mo catalyst, it was found that the mesoporous structural integrity of the catalyst was unchanged from the support after the impregnation of catalyst species. The TEM images revealed that the formation of large particles takes place due to the agglomeration of metal species on the microporous activated carbon supports. The metal dispersion of catalysts on different supports is in the following order: MWCNTs < AC-CGP Super < AC-Fluid Coke < AC-RX3 Extra < AC-Darco. The total alcohols STY and selectivity of 0.296 g/(g of cat.)/h and 35.6%, respectively were observed on the MWCNT-supported alkali-promoted trimetallic C-Rh-Mo catalyst. These results confirmed the fact that the pore size of the support has direct influence on the synthesis of mixed alcohols from synthesis gas.

8.6. Abbreviations

AC	Activated carbon
BE	Blocking extent
GHSV	Gas hourly space velocity
ICP-MS	Inductively coupled plasma – mass spectroscopy
MWCNTs	Multi-walled carbon nanotubes
SEM	Scanning electron microscopy
STY	Space time yield
TEM	Transmission electron microscopy
TPR	Temperature programmed reduction
XRD	X-ray diffraction

8.7. References

1. Campos-Martin, J. M.; Fierro, J. L. G; Guerrero-Ruiz, A; Herman, R. G.; Klier, K. Promoter effect of cesium on C–C bond formation during alcohol synthesis from CO/H_2 over $Cu/ZnO/Cr_2O_3$ catalysts. *J. Catal.* **1996**, *163*, 418–428.
2. Majocchi L, Lietti L, Beretta A, Forzatti P, Micheli E, Tagliabue L. Synthesis of short chain alcohols over a Cs-promoted $Cu/ZnO/Cr_2O_3$ catalyst. *Appl. Catal., A* **1998**, *166*, 393–405.
3. Rostrup-Nielsen, J. R. Making fuels from biomass. *Science* **2005**, *308*, 1421–1422.
4. Li, Z.-R.; Fu, Y.-L.; Jiang, M.; Hu, T.-D.; Liu, T.; Xie Y.-N. Active carbon supported Mo–K catalysts used for alcohol synthesis. *J. Catal.* **2001**, *199*, 155–161.
5. Surisetty, V. R.; Tavasoli, A.; Dalai, A. K. Synthesis of higher alcohols from syngas over alkali promoted MoS_2 catalysts supported on multi-walled carbon nanotubes. *Appl. Catal., A* **2009**, *365*, 243–251.
6. Surisetty, V. R.; Dalai A. K.; Kozinski J. Effect of Rh promoter on MWCNT-supported alkali-modified MoS_2 catalysts for higher alcohols synthesis from CO hydrogenation. *Appl. Catal., A* **2010**, *381*, 282–288.
7. Surisetty, V. R.; Dalai, A. K.; Kozinski, J. Intrinsic reaction kinetics of higher alcohols synthesis from synthesis gas over sulfided alkali-promoted Co-Rh-Mo trimetallic catalyst supported on MWCNTs. *Energ. Fuel.* **2010**, in press.

8. Wong, S. F.; Stromville, N. Y.; Storm, D. A.; Montvale NJ, Patel, M. S. Catalyst and method for producing lower aliphatic alcohols. US Patent 4,983,638, Jan,08, 1991.

9. Surisetty, V. R.; Dalai, A. K.; Kozinski J. Alkali-promoted trimetallic Co-Rh-Mo sulfide catalysts for higher alcohols synthesis from synthesis gas: Comparison of MWCNT and activated carbon supports. *Ind. Eng. Chem. Res.* **2010**, *49*, 6953-6963.

10. Tatsumi, T.; Muramatsu, A.; Tominaga, H.; Importance of sequence of impregnation in the activity development of alkali-promoted mo catalysts for alcohol synthesis from CO---H_2. *J. Catal.* **1986**; *101*, 553–556.

11. Saito, M.; Anderson, R. B. The activity of several molybdenum compounds for the ethanation of CO. *J. Catal.* **1980,** *63*, 438–446.

12. Ryndin, Y. A.; Hicks, R. F.; Bell, A. T. Effects of metal-support interactions on the synthesis of methanol over palladium. *J. Catal.* **1981**, *70*, 287–297.

13. Kogelbauer, A.; Goodwin, J. G.; Oukaci, R. Ruthenium promotion of Co/Al_2O_3 Fischer–Tropsch catalysts. *J. Catal.* **1996**, *160*, 125–133.

14. Duchet, J. C.; van Oers, E. M.; de Beer, V. H. J.; Prins, R. Carbon-supported sulfide catalysts. *J. Catal.* **1983**, *80*, 386–402.

15. Rodriquez-Reinoso, F. The role of carbon materials in heterogeneous catalysis. *Carbon* **1998**, *36*, 159–175.

16. Concha, B. E.; Bartholomew, G. L. Bartholomew CH. CO hydrogenation on supported molybdenum catalysts: Effects of support on specific activities of reduced and sulfided catalysts. *J. Catal.* **1984**, *89*, 536–541.

17. Li, W. Z.; Liang, C.H.; Qiu, J. S.; Zhou, W. J.; Han, H. M.; Wei, Z. B.; et al. Carbon nanotubes as support for cathode catalyst of a direct methanol fuel cell. *Carbon* **2002**, *40*, 791–794.

18. Moodley, P.; Loos, J.; Niemantsverdriet, J. W.; Thune, P. C. Is there a correlation between catalyst particle size and CNT diameter? *Carbon* **2009**, *47*, 2002–2013.

19. Zaman, M.; Khodadi, A.; Mortazavi, Y. Fischer–Tropsch synthesis over cobalt dispersed on carbon nanotubes-based supports and activated carbon. *Fuel Process. Technol.* **2009**, *90*, 1214–1219.

20. Reuel, R. C.; Bartholomew, C. H. Effects of support and dispersion on the CO hydrogenation activity/selectivity properties of cobalt. *J. Catal.* **1984**, *85*, 78–88.

21. Rouquerol, J.; Avnir, D; Fairbridge, C. W.; Everett, D. H.;, Haynes, J. H.; Pernicone, N.; et al. Recommendations for the characterization of porous solids. *Pure Appl. Chem.* **1994**, *66*, 1739–1758.

22. Azevedo, D. C. S.; Araujo, J. C. S.; Bastos-Neto, M.; Torres, A. E. B.; Jaguaribe, E. F.; Cavalcante, C. L. Microporous activated carbon prepared from coconut shells using chemical activation with zinc chloride. *Micropor. Mesopor. Mat.* **2007**, *100*, 361–364.

23. Huang, Z.-D.; Bensch, W.; Kienle, L.; Fuentes, S.; Alonso, G.; Ornelas, C. SBA-15 as support for MoS_2 and Co-MoS_2 catalysts derived from thiomolybdate complexes in the reaction of HDS of DBT. *Catal. Lett.* **2008**, *122*, 57–67.

24. Vradman, L.; Landau, M. V.; Herskowitz, M.; Ezersky, V.; Talianker, M.; Nikitenko, S.; et al. High loading of short WS_2 slabs inside SBA-15: promotion with nickel and performance in hydrodesulfurization and hydrogenation. *J. Catal.* **2003**, *213*, 163–175.

25. Kumaran, G. M.; Garg, S.; Soni, K.; Kumar, M.; Sharma, L. D.; Dhar, G. M.; et al. Effect of Al-SBA-15 support on catalytic functionalities of hydrotreating catalysts: I. Effect of variation of Si/Al ratio on catalytic functionalities. *Appl. Catal., A* **2006**, *305*, 123–129.

26. Jiang, M.; Bian, G.-Z.; Fu, Y.-L. Effect of the K---Mo interaction in K---MoO_3/γ-Al_2O_3 catalysts on the properties for alcohol synthesis from syngas. *J. Catal.* **1994**, *146*, 144–154.

27. Calafata, A.; Vivas, F.; Brito, J. L. Effects of phase composition and of potassium promotion on cobalt molybdate catalysts for the synthesis of alcohols from CO_2 and H_2, *Appl. Catal., A* **1998**, *172*, 217–224.

28. Fu, Y.-L.; Fujimoto, K.; Lin, P.; Omata, K.; Yu, Y. Effect of calcination conditions of the oxidized precursor on the structure of a sulfided K-Mo/γ-Al_2O_3 catalyst for mixed alcohol synthesis. *Appl. Catal., A* **1995**, *126*, 273–285.

29. van Steen, E.; Prinsloo, F. F. Comparison of preparation methods for carbon nanotubes supported iron Fischer–Tropsch catalysts. *Catal. Today* **2002**, *71*, 327–334.

30. Li, Y.; Wang, T.; Wu, C.; Lv, Y.; Tsubaki, N. Gasoline-range hydrocarbon synthesis over cobalt-based Fischer–Tropsch catalysts supported on SiO_2/HZSM-5. *Energ. Fuel.* **2008**, *22*, 1897–1901.

31. Tost, A.; Widmann, D.; Behm, RJ. Stable active oxygen on mesoporous Au/TiO_2 supported catalysts and its correlation with the CO oxidation activity. *J. Catal.* **2009**, *266*, 299–307.

32. Zaman, M.; Khodadi, A.; Mortazavi, Y. Fischer–Tropsch synthesis over cobalt dispersed on carbon nanotubes-based supports and activated carbon. *Fuel Process. Technol.* **2009**, *90*, 1214–1219.

CHAPTER 9

Higher Alcohols Synthesis from Synthesis Gas over Sulfided Alkali-Promoted Co-Rh-Mo Trimetallic Catalyst: Experimental and Modeling Studies

The manuscript provided in this chapter is very similar to the one submitted to the journal Industrial and Engineering Chemistry Research.

Citation:

Surisetty, V. R.; Dalai, A. K.; Kozinski, J. Higher alcohols synthesis from synthesis gas over sulfided alkali-promoted Co-Rh-Mo trimetallic catalyst: Experimental and Modeling Studies. *Ind. Eng. Chem. Res.* **2010**, Submitted for Review.

Contribution of the Ph.D. Candidate

Experiments were planned and performed by Venkateswara Rao Surisetty. Drs. Ajay Kumar Dalai and Janusz Kozinski provided guidance in planning the experiment. The submitted manuscript was written by Venkateswara Rao Surisetty, while Drs. Dalai and Kozinski provided comments and suggestions regarding the style and content of the paper.

Contribution to Overall Study

This paper investigated the interaction effects of experimental conditions, reaction temperature, pressure, gas hourly space velocity (GHSV) at a constant H_2 to CO molar ratio. It is also intended to optimize the operating conditions to obtain maximum ethanol yield and selectivity. The sulfided K (9 wt %)-promoted trimetallic Co (4.5 wt %)-Rh (1.5 wt %)-Mo (15 wt %) supported on MWCNTs was used for this study as this catalyst display improved catalytic properties for higher alcohols yield and selectivity (from Chapters 6, 7 and 8).

9.1. Abstract

The effects of operating conditions on the higher alcohols synthesis reaction from synthesis gas were studied in a single-pass tubular down-flow fixed-bed reactor, using sulfided K-promoted trimetallic Co-Rh-Mo catalyst supported on multi-walled carbon nanotubes (MWCNTs). The interaction effects between the temperature (275– 350°C), pressure (800–1400 psig), and gas hourly space velocity (2.4–4.8 m^3 (STP)/(kg of cat.)/h for % CO conversion, product space time yield (STY), and alcohol selectivities were analyzed as quadratic models using Design-Expert software. The statistical tests, test of significance, and R^2-value statistics proved that the models could adequately represent the experimental data. The % CO conversion increased monotonically with increasing reaction temperature (from 275 to 350°C) and pressure (from 800 to 1400 psig), while decreasing monotonically with increasing GHSV (from 2.4 to 4.2 m^3 (STP)/(kg of cat.)/h). To maximize the ethanol STY and selectivity, the optimum operating conditions were determined as 330°C, 1320 psig, and 3.8 m^3 (STP) /(kg of cat.)/h by the models. The optimum ethanol STY and selectivity of 0.153 (g/(g of cat.)/h) and 27.1 wt %, respectively, were in good agreement with the experimental values. The effects of H_2 to CO molar ratio on higher alcohols synthesis from synthesis gas were also studied at optimum operating conditions. Ethanol STY and selectivity reached a maximum value at H_2 to CO molar ratio around 1.25. A Student's *t* test confirmed that the data were reproducible, with small (<±5) experimental errors.

9.2. Introduction

Mixed alcohols are used as blend stocks for motor gasoline.[1] The addition of oxygenates, such as alcohols and ethers, into gasoline gives rise to the reduction of greenhouse gases and toxic exhaust emissions.[2] Since ether compounds are banned as gasoline octane improvers in North America, there is an increased demand for mixed alcohols.[3] The direct catalytic synthesis of higher alcohols from synthesis gas is one alternative for the production of fuels and chemicals.[4] Although much work has been done on the catalytic conversion of synthesis gas to higher alcohols, it is still necessary to further increase the alcohol yield, as well as higher alcohols, especially ethanol selectivity, to commercial levels. Molybdenum sulfide catalysts are of special interest for higher alcohols

synthesis because of their resistance to sulfur poisoning and high activity for water-gas-shift (WGS) reactions.[5,6] These catalysts are modified with alkali to increase the active sites for alcohol formation and to suppress the hydrogenation ability of surface alkyl species to form alkanes.[7] The alcohol products from these catalyst systems are linear alcohols and the mechanism for formation of higher alcohols is classical insertion of CO into the corresponding precursor alcohol.[8] The product distribution over these catalysts follows an Anderson–Schulz–Flory (ASF) polymerisation process and, hence, the control of product selectivity is of major interest.[9] The higher alcohols activity over these catalysts is low, due to the formation of hydrocarbons and CO_2.[10]

The promoters, the supports, and the reaction conditions influence the activity and selectivity for higher alcohols formation over Mo catalysts.[11] Both activity and selectivity to higher alcohols, especially ethanol, are greatly increased by the addition of Co to alkali-modified MoS_2-based catalysts, due to the enhanced $C_1 \rightarrow C_2$ homologation step.[12,13] Rh incorporation to alkali-modified MoS_2-based catalysts improves the interaction between Rh and Mo and leads to the formation of electron-poor sites that are responsible for the formation of alcohols.[14] The alkali-promoted trimetallic Co-Rh-Mo catalyst system is attractive for reducing Rh content and increasing catalyst activity and selectivity for the formation of higher alcohols.[15] Catalysts supported on multi-walled carbon nanotubes (MWCNTs) outperform others for higher alcohol synthesis.[16,17] MWCNTs display unique properties such as meso/macro porous structures that mitigate transport limitations, uniform and straight pores that allow great metal dispersion, high mechanical strength, and thermal conductivity.[18,19]

The operating conditions such as reaction temperatures, total pressures, gas hourly space velocity (GHSV), and H_2 to CO molar feed ratios have direct effect on the activity and selectivity of the higher alcohols synthesis from catalytic conversion of synthesis gas. The typical operating temperature and pressure are in the range of 250 to 350°C and 5 to 10 MPa, respectively.[20] The effects of operating conditions as independent variables on the % CO conversion, space time yield (STY) of alcohols, hydrocarbons and CO_2 have been studied,[21-23] but their interaction effects have not been investigated and no model has been developed to correlate STY and selectivity of alcohols with operating conditions in CO hydrogenation reactions. Our own research[24] has demonstrated that sulfided K (9 wt %)-modified

trimetallic Co (4.5 wt %)-Rh (1.5 wt %)-Mo (15 wt %) supported on MWCNTs display improved catalytic properties in CO hydrogenation, with a total alcohols yield of 0.244 g/(g of cat.)/h, ethanol selectivity of 20.1%, and higher alcohols selectivity of 31.4% at 320°C, 8.28 MPa, and 3.6 m^3 (STP)/(kg of cat.)/h. The intent of the present study is to develop models that correlate the interaction effects of temperature (T), pressure (P), and GHSV with that of % CO conversion, space time yield (STY) of alcohols, hydrocarbons and CO_2, as well as selectivity of alcohols in CO hydrogenation reactions using the H_2 to CO molar ratio of 1, using higher alcohols synthesis from synthesis gas over the sulfided K-promoted Co-Rh-Mo MWCNT-supported catalyst. The study aims to optimize the operating conditions to obtain maximum ethanol selectivity. It is also intended to study the effect of H_2 to CO molar ratio on higher alcohols synthesis using optimum conditions of T, P and GHSV.

9.3. Experimental

9.3.1. Catalyst preparation

MWCNTs (M.K. Nano, surface area-178 m^2/g, pore volume-0.54 cc/g) were used as supports for the preparation of the catalysts. Prior to impregnation, the supports were treated with 30% HNO_3 reflux at 100°C overnight, washed with distilled water several times, and dried at 120°C for 6 h. The oxide sample was prepared by the incipient wetness impregnation method using ammonium heptamolybdate tetrahydrate (Sigma-Aldrich), potassium carbonate (Aldrich), cobalt acetate tetrahydrate (Alfa-Aesar), and rhodium chloride hydrate (Aldrich) as precursors for Mo, K, Co, and Rh, respectively. At the first step, the support was impregnated with an aqueous solution of K_2CO_3, followed by drying at 120°C for 2 h, and stabilizing in an argon flow of 50 ml/min at 300°C, at a heating rate of 10°C/min for 4 h. The support was further impregnated with aqueous solutions containing the required amounts of $(NH_4)_6Mo_7O_{24}$, $Co(CH_3COO)_2$, and $RhCl_3$ followed by drying at 120°C for 2 h, and stabilizing in an argon flow of 50 ml/min at 450°C, at a heating rate of 10°C/min for 12 h.

9.3.2. Catalytic studies

The higher alcohols synthesis reaction from synthesis gas was studied using a single-pass tubular downflow fixed-bed reactor of 450-mm length and 22-mm inside diameter made of inconel tube. The reactor was packed with 2 g of catalyst diluted with 12 ml of 90 mesh size silicon carbide and housed in an electric furnace controlled by a temperature controller. The reactor was pressurized with He to 500 psig (3.44 MPa) and sulfidation, together with reduction, were carried out for 6 h at 450°C at a heating rate of 2 °C/min using a gas mixture containing 10 mole % H_2S in H_2 and a flow rate of 50 ml/min. The temperature was then lowered to the reaction temperature, and the system pressurized to the reaction conditions. The feed gas mixture (desired molar ratio of CO and H_2 mixed with 10 mole % Ar) was passed through mass flow controllers and the higher alcohols synthesis was carried out at steady-state under the reaction conditions over a period of 24 h. The product gas was cooled to 0°C and separated into gas and liquid phases at the reaction pressure. The CO conversion and other gaseous products were monitored with a time interval of 1 h. The liquid products were collected at the end of the reaction and analyzed with a Varian 3400 gas chromatograph equipped with a capillary column and a flame ionization detector. The volume and weight of liquid products were measured to check the mass balance. The gaseous products were analyzed online on a Shimadzu gas chromatograph through a sampling valve. Using Ar as an internal standard, the CO conversion was calculated and the overall mass balance of the reaction was determined.

9.3.3. Experimental Design

The parameters T, P, and GHSV were varied in the ranges of 275 to 350°C, 800 to 1400 psig (5.52–9.65 Mpa), and 2.4 to 4.2 m^3 (STP)/(kg of cat.)/h, respectively. To analyze the interaction effects between the operating parameters for higher alcohols synthesis and to optimize the effective parameters, the Taguchi orthogonal array design method was used to develop the experimental plan. This statistical design approach minimizes the overall variance of the estimated parameters and reduces the number of trials required without restricting the confidence region for the estimated parameter.[25] An orthogonal array selector determines the number of trials necessary and the factor levels for each parameter in each trial.[26] The experiments were designed using Design-Expert software version 6.0.1, and were performed using a feed gas mixture of 45 mole % CO, 45 mole % H_2, and 10 mole % Ar.

Specific experimental conditions were repeated several times to observe the reproducibility of the results. A separate set of experiments were performed to study the effect of the H_2 to CO molar ratio on higher alcohols synthesis at the optimum conditions of T, P, and GHSV.

The perturbation plots were used in conjunction with the 3-D surface responses, as interpreting the 3-D surface response alone can be difficult.[27] Perturbation plots were used to show the effect of each individual variable as the others were held constant. This plot is a powerful method of comparing the relative influences of factors, and can be used to look at one-dimensional paths through a multifactor surface.

9.4. Results and Discussion

Analysis of the liquid products indicates that the alcohols likely followed the CO insertion mechanism; forming linear alcohols.[8] Methanol, ethanol, n-propanol, and n-butanol are the major products, together with other higher alcohols. The term higher alcohols represent alcohols with a carbon number greater than 1, whereas, total alcohols represent methanol and higher alcohols combined. The analysis of exit gas indicates that methane is the major hydrocarbon component apart from CO_2, unconverted CO, and H_2.

To evaluate the model with the experimental data, two tests were necessary from a statistical point of view; the test of significance of factors or interactions and the coefficient of determination.[28] The significance of factors of the mathematical model are tested using the probability value (*p*-value) and can be simplified by eliminating the insignificant factors to ease the interpretation.[29] The factor or interaction is insignificant at a 95% confidence level, when a *p*-value is greater than 0.05.[29] The coefficient of determination, R^2 value is the relative predictive power of a model to test the goodness of fit and applies to matching observed data to the proposed equation. The R^2 value varies between 0 and 1, depending on the fitness of the model; with a value approaching one meaning good fit and zero meaning no fit. R^2 value may be improved by incorporating more factors or interactions, while the predictive power of the model cannot be improved.[30] Adjusted R^2 value (also called $\overline{R}^2$ value) is a modification of R^2, which improves its value only if the newly added factors or interactions are significant.[31] Predicted R^2 value is another quantity that predicts the responses for new observations.[32]

9.4.1. Effects of the temperature, pressure, a nd gas hourly space velocity on % CO conversion

The model (response surface) that represents the interaction effects of the T (275 to 350°C), P (800 to 1400 psig), and GHSV (2.4 to 4.2 m^3 (STP)/(kg of cat.)/h) using H_2 to CO molar ratio equal to 1 on % CO conversion was derived from the regression analysis of experimental data after discarding the insignificant factors and is given as:

$$\%\ CO\ conversion = -334.788 + 2.145 * T + 0.019 * P - 20.052 * GHSV - 2.79 * 10^{-3} * T^2 + 2.101 * GHSV^2 \quad (9.1)$$

where T is in ºC, P is in psi and GHSV is in m^3 (STP)/(kg of cat./h).

Tables 9.1 and 9.2 show results of the test of significance of factors or interactions and the coefficient of determination statistics, respectively, for the % CO conversion before and after discarding insignificant terms. *A*, *B*, and *C* are coded factors of T, P, and GHSV, respectively, given by the following equations:

$$A = -1 + (T - 275) / 37.5 \quad (9.2)$$

$$B = -1 + (P - 800) / 300 \quad (9.3)$$

$$C = -1 + (GHSV - 2.4) / 1 \quad (9.4)$$

Table 9.1. Results of test of significance of factors or interactions for the model representing % CO conversion

Factor or interaction	*p*-value of % CO conversion	
	All factors included	Insignificant factors excluded
A	<0.0001	<0.0001
B	0.0002	<0.0001
C	<0.0001	<0.0001
A^2	0.0006	<0.0001
B^2	0.2946	--
C^2	0.0298	0.0232
AB	0.3724	--
BC	0.1841	--
AC	0.4312	--
Model	<0.0001	<0.0001

Table 9.2. Coefficient of determination statistics for the model representing % CO conversion

Coefficient of determination	All factors included	Insignificant factors excluded
R^2	0.997	0.995
Adjusted R^2	0.994	0.993
Predicted R^2	0.965	0.985

Figs. 9.1a and 9.1b are three-dimensional (3-D) plots of the effects of T, P, and GHSV on % CO conversion. The plots show that inlet % CO conversion increased monotonically with increasing reaction temperature and pressure from 275 to 350 °C and 800 to 1400 psig, respectively. This confirms that the hydrogentaion of CO over the MWCNTs-supported alkali-promoted trimetallic Co-Rh-Mo catalyst was greatly improved at high temperature and pressure. With increased GHSV from 2.4 to 4.2 m^3 (STP)/(kg of cat.)/h, it was observed that the % CO conversion decreased monotonically.

Short contact time between the reactants at high GHSV resulted in the low CO conversion. Fig. 9.1c is the perturbation plot showing that the effects of the variables T, P, and GHSV are significant on % CO conversion. Fig. 9.1d compares the experimental values to the predicted % CO conversion, and clearly shows that the model for % CO conversion is valid within the experimental ranges.

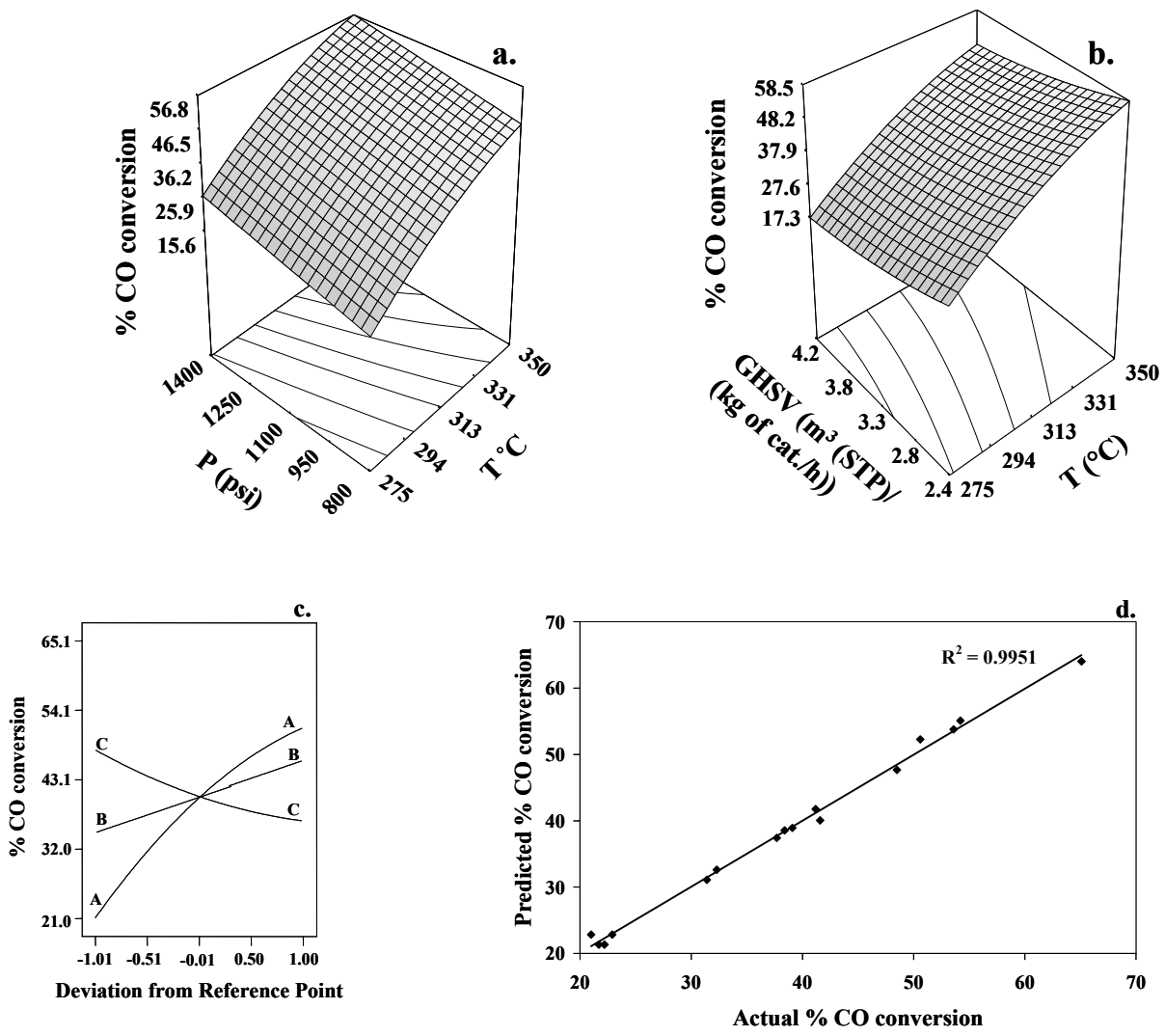

Figure 9.1. The effects of the temperature, pressure, and gas hourly space velocity on % CO conversion over Co-Rh-Mo-K/MWCNT catalyst

a and b. 3-D surface responses; c. Perturbation plot; d. Quality of fit

9.4.2. Effects of the temperature, pressure, and gas hourly space velocity onSTY of alcohols, hydrocarbons, and CO_2

The regression analysis of the experimental data generated the following equations that represent the effects of T (275 to 350°C), P (800 to 1400 psig), and GHSV (2.4 to 4.2 m^3 (STP)/(kg of cat.)/h) using H_2 to CO molar ratio equal to 1 on STY of methanol, ethanol, higher alcohols, total alcohols, hydrocarbons, and CO_2 after eliminating insignificant factors:

$$Methanol\ STY = 0.347 - 1.821 * 10^{-3} * T - 4.091 * 10^{-6} * P + 1.875 * 10^{-3} * GHSV - 5.313 * 10^{-8} * P^2 - 6.944 * 10^{-3} * GHSV^2 + 6.455 * 10^{-7} * T * P + 1.924 * 10^{-4} * T * GHSV \quad (9.5)$$

$$(Ethanol\ STY)^{0.5} = -6.743 + 0.0379 * T + 6.184 * 10^{-4} * P + 0.214 * GHSV - 5.682 * 10^{-5} * T^2 - 2.297 * 10^{-7} * P^2 - 0.029 * GHSV^2 \quad (9.6)$$

$$(Higher\ alcohols\ STY)^{0.5} = -8.0276 + 0.046 * T + 7.147 * 10^{-4} * P + 0.198 * GHSV - 6.851 * 10^{-5} * T^2 - 2.704 * 10^{-7} * P^2 - 0.0266 * GHSV^2 \quad (9.7)$$

$$(Total\ alcohols\ STY)^{0.5} = -5.441 + 0.030 * T + 7.768 * 10^{-4} * P + 0.206 * GHSV - 4.592 * 10^{-5} * T^2 - 2.762 * 10^{-7} * P^2 - 0.0268 * GHSV^2 \quad (9.8)$$

$$Total\ hydrocarbons\ STY = 2.152 - 0.015 * T + 9.863 * 10^{-5} * P - 0.0278 * GHSV + 2.93 * 10^{-5} * T^2 \quad (9.9)$$

$$CO_2\ STY = 3.877 - 0.0281 * T + 1.264 * 10^{-4} * P - 0.0264 * GHSV + 5.21 * 10^{-5} * T^2 \quad (9.10)$$

where T is in ºC, P is in psig and GHSV is in m^3 (STP)/(kg of cat.)/h.

Table 9.3 shows the results of the test of significance of factors or interactions in terms of *A*, *B*, and *C* for the STY of methanol, ethanol, higher alcohols, total alcohols, hydrocarbons, and CO_2 after power transformation (applying a mathematical power function to all the response data) and discarding insignificant terms. The *p*-value of each model is less than 0.05 and that for all the models is less than 0.0001, indicating that the models are significant. Table 9.4 shows the statistics for coefficient of determination of all the models, representing the STY of different products. The predicted R^2 values of all models are in reasonable agreement with the adjusted R^2 values, suggesting that these models can be used to navigate the design space.

Table 9.3. Results of test of significance of factors or interactions for the models representing different products STY

Factor or interaction	*p*-value of model after insignificant factors excluded					
	Methanol STY	(Ethanol STY)$^{0.5}$	(Higher alcohols STY)$^{0.5}$	(Total alcohols STY)$^{0.5}$	Hydrocarbons STY	CO_2 STY
A	<0.0001	<0.0001	<0.0001	<0.0001	<0.0001	<0.0001
B	<0.0001	<0.0001	0.0194	<0.0001	0.0005	0.0085
C	<0.0001	0.0009	0.0014	<0.0001	0.0017	0.0407
A^2	--	<0.0001	<0.0001	<0.0001	0.0020	0.0036
B^2	0.0111	0.0182	0.0084	0.0029	--	--
C^2	0.0048	0.0099	0.0153	0.0063	--	--
AB	0.0060	--	--	--	--	--
BC	--	--	--	--	--	--
AC	0.0107	--	0.0264	--	--	--
Model	<0.0001	<0.0001	<0.0001	<0.0001	<0.0001	<0.0001

Table 9.4. Coefficient of determination statistics for the models representing different products STY

Coefficient of determination	*p*-value of model after insignificant factors excluded					
	Methanol STY	(Ethanol STY)$^{0.5}$	(Higher alcohols STY)$^{0.5}$	(Total alcohols STY)$^{0.5}$	Hydrocarbons STY	CO_2 STY
R^2	0.993	0.987	0.992	0.987	0.971	0.954
Adjusted R^2	0.987	0.978	0.986	0.978	0.960	0.937
Predicted R^2	0.969	0.950	0.968	0.954	0.943	0.912

Figs. 9.2a and 9.2b (3-D response surface) and Fig. 9.2c (perturbation plot) depict the effects of T, P, and GHSV on STY of methanol using H_2 to CO molar ratio equal to 1. The methanol STY decreased monotonically with increasing temperature, suggesting that conversion of methanol to higher alcohols takes place at high temperatures. The formation of methanol increased monotonically with increasing pressure and GHSV. The effect of pressure on methanol STY can be explained by Le-Chatelier's principle. As the pressure increases, the equilibrium counters this change by shifting the reaction to the right hand side, resulting in the increased formation of methanol. At high GHSVs, the consumption of methanol to higher alcohols is low, which explains the high methanol yields. Table 9.5 shows the R^2 value of 0.993 obtained from the fitness of the experimental methanol STY values with that of the predicted values, confirms that the model fits well within the experimental conditions.

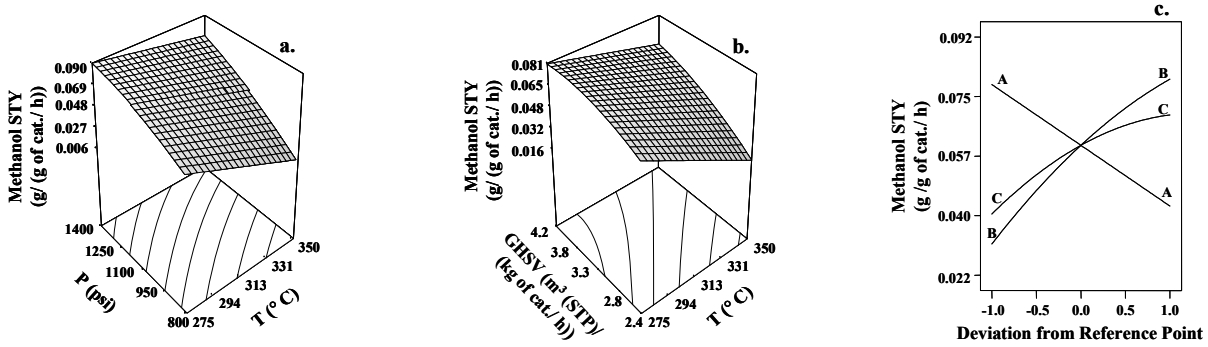

Figure 9.2. The effects of the temperature, pressure, and gas hourly space velocity on methanol STY over Co-Rh-Mo-K/MWCNT catalyst
a and b. 3-D surface responses; c. Perturbation plot

The effects of T, P, and GHSV reactions on the STY of ethanol at H_2 to CO molar ratio of 1 are represented as 3-D plots in Figs. 9.3a and 9.3b and the perturbation plot in Fig. 9.3c. Compared to P and GHSV, temperature had great effect on ethanol STY, with the rate of ethanol formation reaching a maximum value and then decreasing at higher temperatures. Depending on the temperature, the ethanol formation increased upto certain pressures and then remained constant. With respect to GHSV, a maxima in the ethanol STY was also observed. The model fits the experimental results with an R^2 value of 0.981 as seen from Table 9.5. Higher alcohols STY exhibit similar trends of operating conditions dependency as

that of ethanol STY, with the maximum amount of higher alcohols formation observed with respect to temperature and GHSV (figure not given). With increased pressure, the higher alcohols STY increased to a certain value and then remained constant at higher pressures. The fit of the model is good with an R^2 value of 0.980 (Table 9.5).

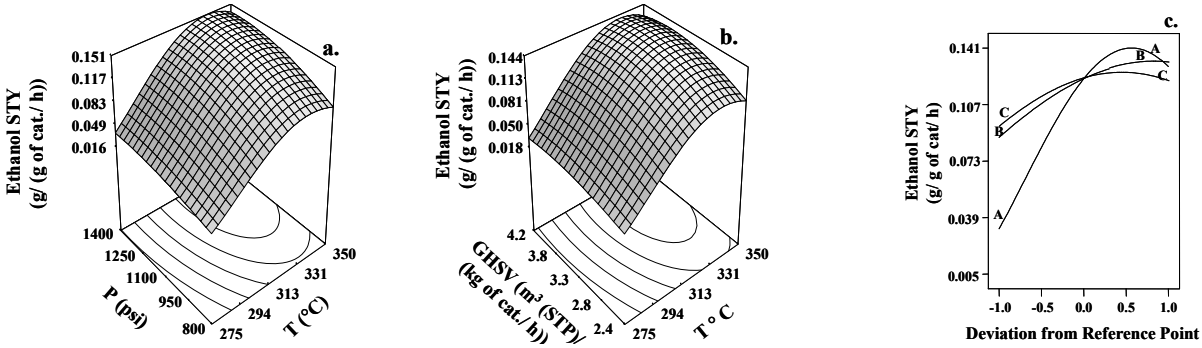

Figure 9.3. The effects of the temperature, pressure, and gas hourly space velocity on ethanol STY over Co-Rh-Mo-K/MWCNT catalyst a and b. 3-D surface responses; c. Perturbation plot

Table 9.5. Coefficients of determination statistics for the models representing product STY

Model	Quality of fit (R^2 Value)
Methanol STY	0.993
(Ethanol STY)$^{0.5}$	0.981
(Higher alcohols STY)$^{0.5}$	0.980
(Total alcohols STY)$^{0.5}$	0.982
Hydrocarbons STY	0.971
CO_2 STY	0.954
(Methanol selectivity)$^{0.5}$	0.987
(Ethanol selectivity)$^{0.5}$	0.975
Higher alcohols selectivity	0.943
Total alcohols selectivity	0.860

The dependence of total alcohol formation on the T, P, and GHSV reactions at H_2 to CO molar ratio of 1 are presented as 3-D plots in Fig. 9.4a and 9.4b and the perturbation plot in Fig. 9.4c. Table 9.5 displays the quality of the model's fit with an R^2 value of 0.982. The total alcohols STY exhibits the maximum with respect to reaction temperature. Increased

pressure favors the formation of total alcohols, whereas, the STY of total alcohols increased to a certain value and then remained constant with increasing GHSV. Fig. 9.4c shows that GHSV had a small effect on total alcohols STY, compared to that of T and P. Park et al.[22] studied the effect of temperature as independent variables on mixed alcohols (total alcohols) synthesis from syngas over K-MoS_2 catalyst and found that the mixed alcohols formation attained a maximum value at 320°C. Studies by Li et al.[21] on the temperature effects on total alcohols STY with and without Co promotion to Mo-K/C catalysts, disclosed that Co promotion causes a shift to the higher temperature side for the total alcohol STY, which shifts the maximum value of total alcohols STY to the higher temperature side.

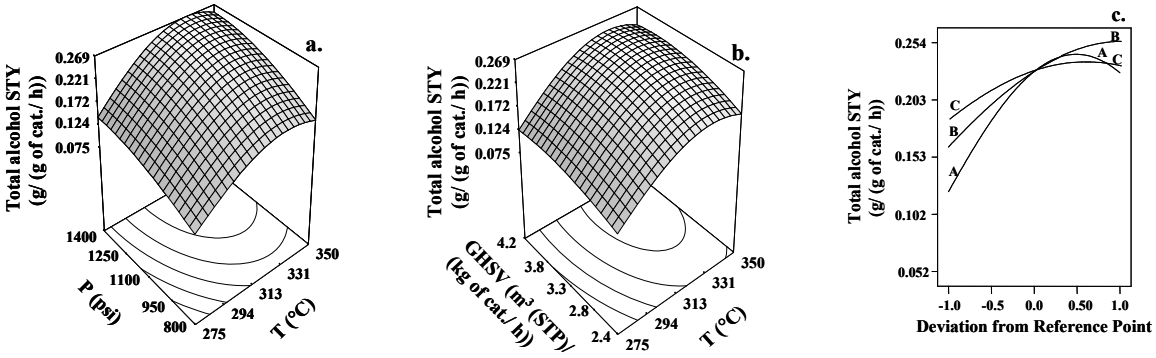

Figure 9.4. The effects of the temperature, pressure, and gas hourly space velocity on total alcohol STY over Co-Rh-Mo-K/MWCNT catalyst
a and b. 3-D surface responses; c. Perturbation plot

Figs. 9.5a, 9.5b, and 9.5c exhibit the dependency of operating conditions (T, P, and GHSV) on hydrocarbons STY at H_2 to CO molar ratio of 1. As observed, the formation of hydrocarbons exponentially increases at high reaction temperatures. These results combined with total alcohols STY suggest that the produced alcohols are consumed to form hydrocarbons with synthesis gas at higher temperatures. Hydrocarbon STY increased slightly with increasing pressure, whereas, the hydrocarbon formation decreased with GHSV. Table 9.5 shows that the model fits well with the experimental results. The CO_2 formation model follows a similar trend as that of the hydrocarbon formation (figure not given). Compared to that of hydrocarbons, higher STY of CO_2 were observed at all experimental conditions. Table 9.5 shows that the CO_2 model fits with R^2 value of 0.954.

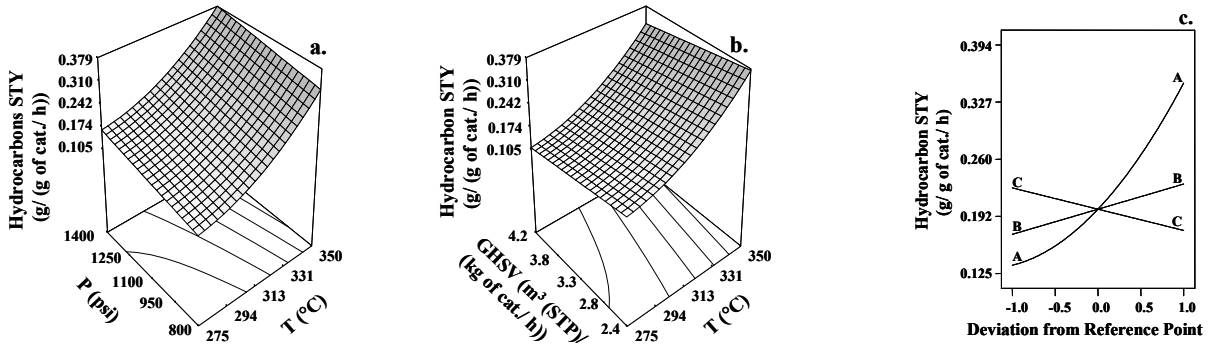

Figure 9.5. The effects of the temperature, pressure, and gas hourly space velocity on hydrocarbon STY over Co-Rh-Mo-K/MWCNT catalyst a and b. 3-D surface responses; c. Perturbation plot

9.4.3. Effects of the temperat ure, pressure, and gas hourly space velocity on selectivity of alcohols

The interaction effects of the temperature (275 to 350°C), pressure (800 to 1400 psig), and GHSV (2.4 to 4.2 m^3 (STP)/(kg of cat.)/h) using H_2 to CO molar ratio equal to 1 on selectivities of methanol, ethanol, higher alcohols, and total alcohols were derived from the regression analysis of experimental data after discarding insignificant factors. The model equations are:

$$(Methanol\ selectivity)^{0.5} = 42.541 - 0.21 * T - 7.674 * 10^{-3} * P + 0.497 * GHSV + 2.342 * 10^{-4} * T^2 + 2.819 * 10^{-5} * T * P \quad (9.11)$$

$$(Ethanol\ selectivity)^{0.5} = -90.028 + 0.521 * T + 7.116 * 10^{-3} * P + 2.802 * GHSV - 7.985 * 10^{-4} * T^2 - 2.555 * 10^{-6} * P^2 - 0.372 * GHSV^2 \quad (9.12)$$

$$Higher\ alcohols\ selectivity = -766.748 + 4.728 * T + 0.013 * P + 3.283 * GHSV - 7.26 * 10^{-3} * T^2 \quad (9.13)$$

$$Total\ alcohols\ selectivity = -468.918 + 2.976 * T + 0.02 * P + 5.408 * GHSV - 4.78 * 10^{-3} * T^2 \quad (9.14)$$

where T is in ºC, P is in psig and GHSV is in m^3 (STP)/(kg of cat.)/h.

Table 9.6 shows the results of the test of significance of factors or interactions for the selectivities of methanol, ethanol, higher alcohols, and total alcohols after power transformation and discarding insignificant terms. These models were significant, with the *p*-value less than 0.0001. Table 9.7 gives the statistics for coefficient of determination for all

models representing the selctivity of alcohols. The predicted R^2 and adjusted R^2 values were comparable.

Table 9.6. Results of test of significance of factors or interactions for the models representing alcohols selectivities

Factor or interaction	*p*-value of model after insignificant factors excluded			
	(Methanol selectivity)$^{0.5}$	(Ethanol selectivity)$^{0.5}$	Higher alcohols selectivity	Total alcohols selectivity
A	<0.0001	<0.0001	<0.0001	0.0494
B	<0.0001	<0.0001	0.0005	0.0001
C	0.0003	0.0009	0.0029	0.0008
A^2	0.0028	<0.0001	<0.0001	0.0030
B^2	--	0.0164	--	--
C^2	--	0.0206	--	--
AB	0.0183	--	--	--
BC	--	--	--	--
AC	--	--	--	--
Model	<0.0001	<0.0001	<0.0001	<0.0001

Table 9.7. Coefficient of determination statistics for the models representing alcohols selectivities

Coefficient of determination	*p*-value of model after insignificant factors excluded			
	(Methanol selectivity)$^{0.5}$	(Ethanol selectivity)$^{0.5}$	Higher alcohols selectivity	Total alcohols selectivity
R^2	0.986	0.976	0.943	0.860
Adjusted R^2	0.978	0.959	0.923	0.809
Predicted R^2	0.960	0.905	0.876	0.741

The influence of the operating conditions T (275 to 350°C), P (800 to 1400 psig), and GHSV (2.4 to 4.2 m^3 (STP)/(kg of cat.)/h) on selectivities of methanol, ethanol, higher alcohols, and total alcohols using H_2 to CO molar ratio of 1 are investigated. There was good agreement between the simulated results and the experimental observations (Table 9.7). The methanol selectivity decreased monotonically with increasing temperature, but increased with increasing pressure and GHSV.

The ethanol (Fig. 9.6), higher alcohols, and total alcohols selectivities displayed a pronounced increase with increasing temperature and reached a maximum value, suggesting that the significant activity for the dehydration of alcohols takes place at higher temperatures. With increasing pressure, ethanol selectivity increased to a certain value and remained constant, whereas, a maximum was obtained with increased GHSV (Fig. 9.6). The higher alcohols and total alcohols selectivity monotonically increased with increasing pressure and GHSV (figures are shown). This discrepency between the ethanol and higher alcohols selectivities at higher pressures and GHSVs is due to the increasing ability of chain growth from ethanol to higer alcohols.

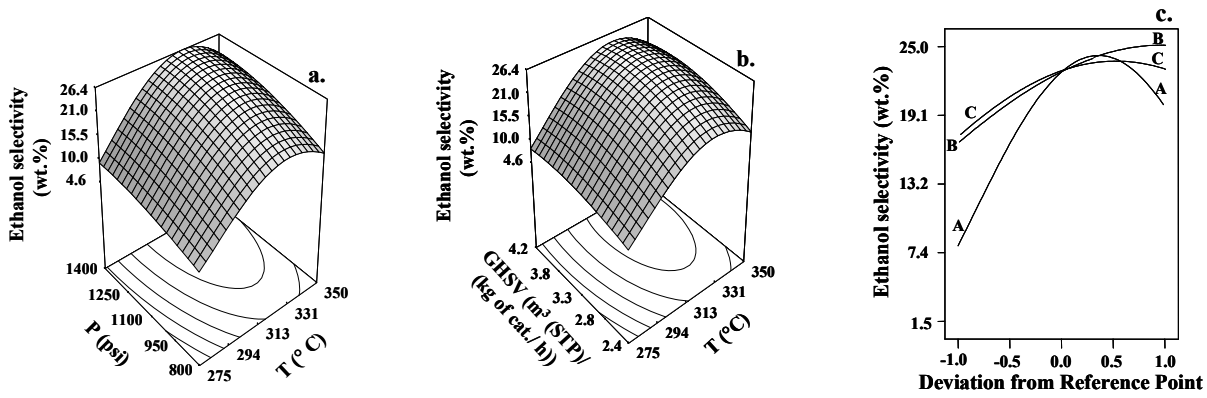

Figure 9.6. The effects of the temperature, pressure, and gas hourly space velocity on ethanol selectivity over Co-Rh-Mo-K/MWCNT catalyst
a and b. 3-D surface responses; c. Perturbation plot

9.4.4. Optimization of operating conditions

The optimum operating conditions using H_2 to CO molar ratio of 1 were defined according to the following constraints: (1) Ethanol STY to be maximum; and (2) ethanol selectivity to be maximum. The solution for the model was obtained as follows: T = 330°C, P = 1320 psig (9.1 Mpa), GHSV = 3.8 m^3 (STP)/(kg of cat.)/h. The experiments were performed at these operating conditions, with both the ethanol STY and selectivity presented together with the model predictions. The difference of ethanol STY was around 3% and that of the selectivity was less than 5%.

9.4.5. Effects of H_2 to CO molar ratio on higher alcohols synthesis from synthesis gas

In this study, the H_2 to CO molar ratio (Θ) was varied from 0.5 to 2.0 and the experiments were carried out using the optimum operating conditions of T, P, and GHSV. Fig. 9.7 depicts the influence of Θ on the % CO conversion, hydrocarbons STY, and CO_2 STY. The results show that increasing the Θ from 0.5 to 2.0 led to increased % CO conversion from 33.0 to 54.2%, suggesting that the catalyst activity is improved with Θ. The hydrocarbons formation rate increased monotonically from 0.141 to 0.354 g/(g of cat.)/h, whereas the CO_2 STY decreased monotonically from 0.541 to 0.239 g/(g of cat.)/h with increasing Θ from 0.5 to 2.0. The responses of methanol, ethanol, higher alcohols, and total alcohols formation (Fig. 9.8) show that the rate of methanol formation increased with increasing Θ, while the ethanol and higher alcohols STY revealed their maximum at Θ value between 1 to 1.5. Fig. 9.8 also shows that the total alcohols formation increased to specific Θ and remained constant.

These results can be explained from the CO insertion mechanism of higher alcohols synthesis reaction[8]. The partial pressure of CO was high at low values of Θ, which resulted in enhanced CO insertion and C-C chain growth favoring the formation of compounds with a carbon number greater than 1. With increasing Θ value, the partial pressure of H_2 increased, resulting in the formation of C_1 products, such as methanol and methane. (Note: the distribution of hydrocarbons is not discussed in our results). Because of a decreased amount of higher alcohols and hydrocarbons with a carbon number greater than 1, the water gas shift reaction rate was low due to small water formation.

From Figs. 9.7 and 9.8 the following simulated equations were obtained for the % CO conversion and products STY as a function of Θ:

$$\%\ CO\ conversion = -11.4 * \Theta^2 + 42.18 * \Theta + 15.1;\ R^2 = 0.991 \quad \text{.....(9.15)}$$

$$Hydrocarbons\ STY = -0.093 * \Theta^2 + 0.374 * \Theta - 0.022;\ R^2 = 0.999 \quad \text{.....(9.16)}$$

$$CO_2\ STY = 0.145 * \Theta^2 - 0.554 * \Theta + 0.774;\ R^2 = 0.977 \quad \text{.....(9.17)}$$

$$Methanol\ STY = 0.005 * \Theta^2 + 0.08 * \Theta - 0.004;\ R^2 = 0.961 \quad \text{.....(9.18)}$$

$$Ethanol\ STY = -0.065 * \Theta^2 + 0.172 * \Theta + 0.028;\ R^2 = 0.747 \quad \text{.....(9.19)}$$

$$Higher\ alcohols\ STY = -0.1 * \Theta^2 + 0.256 * \Theta + 0.037;\ R^2 = 0.751 \quad \text{.....(9.20)}$$

$$Total\ alcohols\ STY = -0.097 * \Theta^2 + 0.34 * \Theta + 0.031;\ R^2 = 0.995 \quad \text{.....(9.21)}$$

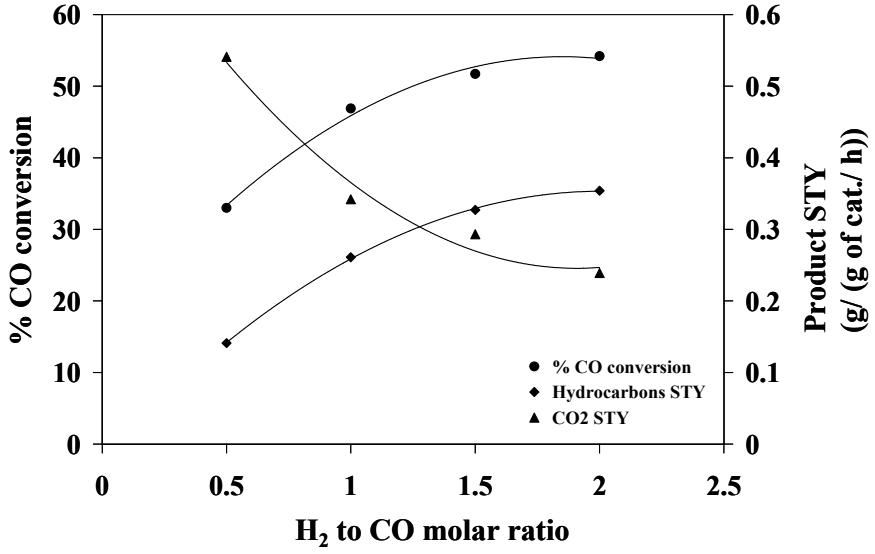

Figure 9.7. The effect of the H_2 to CO molar ratio on % CO conversion, hydrocarbons, and CO_2 STY over Co-Rh-Mo-K/MWCNTs catalyst at 330°C, 1320 psig, and 3.8 m^3 (STP)/(kg of cat.)/h

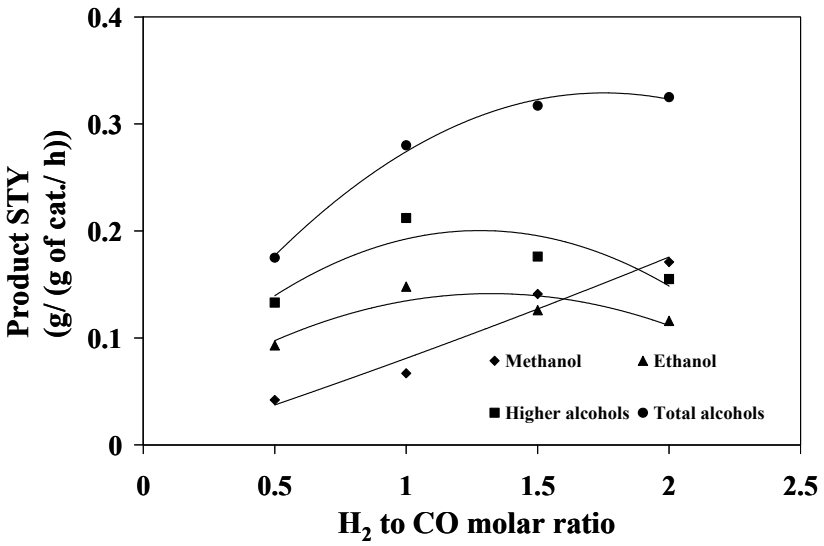

Figure 9.8. The effect of the H_2 to CO molar ratio on methanol, ethanol, higher alcohols, and total alcohols STY over Co-Rh-Mo-K/MWCNT catalyst at 330°C, 1320 psig, and 3.8 m^3 (STP)/(kg of cat.)/h

The selectivities of methanol, ethanol, and higher alcohols exhibit similar trends as that of their STYs (Fig. 9.9). Methanol selectivity monotonically increased from 4.9 to 18.6 wt %, with increased Θ from 0.5 to 2.0. A maxima was observed in the selectivity of ethanol and higher alcohols at around Θ value of 1.25, whereas the total alcohols selectivity showed a maximum at Θ value of approximately 1.5.

The following simulated equations were obtained for the selectivities of methanol, ethanol, higher alcohols, and total alcohols as a function of Θ:

$$\textit{Methanol selectivity} = 0.7 * \Theta^2 + 7.91 * \Theta + 0.375;\ R^2 = 0.974 \quad (9.22)$$

$$\textit{Ethanol selectivity} = -25.0 * \Theta^2 + 58.84 * \Theta - 7.2;\ R^2 = 0.931 \quad (9.23)$$

$$\textit{Higher alcohols selectivity} = -23.6 * \Theta^2 + 0.256 * \Theta + 0.037;\ R^2 = 0.751 \quad (9.24)$$

$$\textit{Total alcohols selectivity} = -22.9 * \Theta^2 + 66.75 * \Theta - 6.82;\ R^2 = 0.991 \quad (9.25)$$

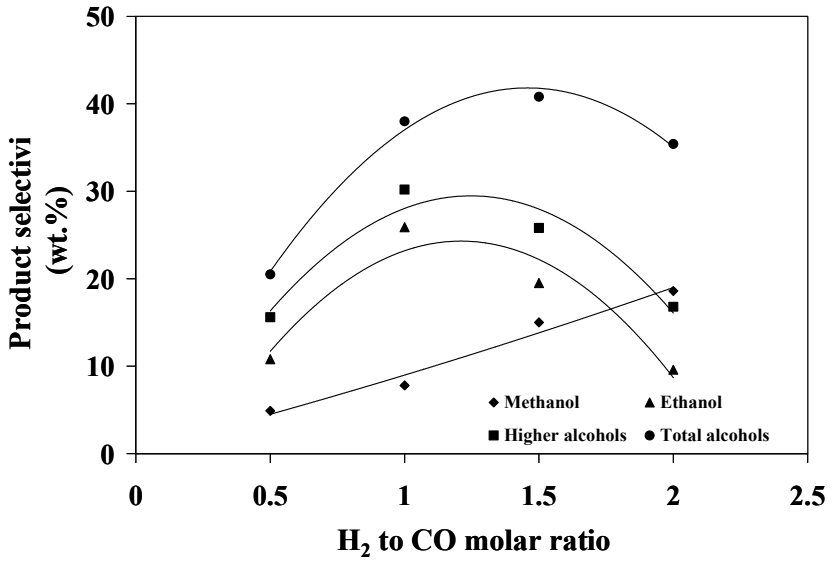

Figure 9.9. The effect of the H_2 to CO molar ratio on methanol, ethanol, higher alcohols, and total alcohols selectivity over Co-Rh-Mo-K/MWCNT catalyst at 330°C, 1320 psig, and 3.8 m^3 (STP)/(kg of cat.)/h

9.4.6. Reproducibility study

Reproducibility of the experimental data was tested at optimum operating T, P, and GHSV using Θ values of 1, 1.5, and 2, and the results representing ethanol STY and selectivity are reported in Table 9.8. Some experimental conditions were repeated to determine the *t*- and *p*- values.

To determine the effect of packing on the experimental results, the reactor was reloaded with a fresh batch of catalyst and the experiments and repetitions were carried out. The *unequal sample sizes equal variance* Student's *t* test method was used to determine reproducibility of the results. The results indicated that the calculated *p*-value associated with the *t* test was not small (> 0.05), providing evidence that the means are not different. This proves that the data are reproducible with small (<±5)experimental errors.

Table 9.8. The results of reproducibility studies

(T= 330°C, P = 1320 psig (9.1 Mpa), and GHSV = 3.8 m^3 (STP)/(kg of cat./h))

H_2/CO (moles/moles)	**1**	**1.5**	**2**
Repetitions #	4*	3*	3*
Ethanol STY (g/(g of cat.)/h)	0.148, 0.150, 0.151, 0.154	0.126, 0.128, 0.124	0.116, 0.114, 0.115
Ethanol selectivity (wt %)	25.8, 26.1, 26.6, 25.7	19.5, 20.1, 19.1	9.6, 9.1, 9.6
Repetitions #	2**	2**	2**
Ethanol STY (g/(g of cat.)/h)	0.151, 0.152	0.122, 0.127	0.113, 0.119
Ethanol selectivity (wt %)	26.5, 26.7	18.8, 19.7	9.5, 10.2
t - value			
Ethanol STY (g/(g of cat.)/h)	0.39	0.29	0.42
Ethanol selectivity (wt %)	1.78	0.63	1.23
p - value			
Ethanol STY (g/(g of cat.)/h)	0.358	0.287	0.351
Ethanol selectivity (wt %)	0.075	0.287	0.153

*experiments were repeated using same catalyst; **experiments were repeated using freshly loaded catalyst every time

9.5. Conclus ions

A MWCNT-supported K-promoted trimetallic sulfided Co-Rh-Mo catalyst was used to study the effects of operating conditions on the higher alcohols synthesis reaction from synthesis gas. Quadratic models were developed using the Taguchi orthogonal array design method for % CO conversion, products STY, and alcohol selectivities as functions of T, P and GHSV using an H_2 to CO molar ratio of 1. The statistical tests, test of significance, and R^2 -value statistics proved that the models could adequately represent the experimental data. The % CO conversion increased monotonically with increasing reaction temperature (from 275 to 350°C) and pressure (from 800 to 1400 psig), while decreasing monotonically with increasing GHSV (from 2.4 to 4.2 m^3 (STP)/(kg of cat.)/h). The ethanol STY and selectivity reached a maximum value with respect to temperature and GHSV, while increasing to a constant value with increasing pressure.

The ethanol STY and selectivity obtained at optimum T, P, and GHSV were in good agreement with model predictions. The effects of H_2 to CO molar ratio on higher alcohols synthesis from synthesis gas was studied at optimum T, P, and GHSV. Our results show an increase in % CO conversion with increasing the H_2 to CO molar ratio from 0.5 to 2.0. Methanol and hydrocarbons (methane) formation rates also increased with the H_2 to CO molar ratio, whereas ethanol STY reached a maximum value at H_2 to CO molar ratio around 1.25. A Student's *t* test confirmed that the data are reproducible with small (<±5)experimental errors.

9.6. Abbreviations

GHSV	Gas hourly space velocity
MWCNTs	Multi-walled carbon nanotubes
P	Pressure
STY	Space time yield
T	Temperature
WGS	Water-gas shift reaction

9.7. References

1. Tien-Thao, N.; Zahedi-Niaki, M. H.; Alamdari, H.; Kaliaguine, S. Conversion of syngas to higher alcohols over nanosized LaCo0.7Cu0.3O3 perovskite precursors. *Appl. Catal. A* **2007**, *326*, 152–163.
2. Tien-Thao, N.; Alamdari, H.; Zahedi-Niaki, M. H.; Kaliaguine, S. $LaCo_{1-x}Cu_xO_{3-\delta}$ perovskite catalysts for higher alcohol synthesis. *Appl. Catal. A* **2006**, *311*, 204–212.
3. Xiang, M.; Li, D.; Li, W.; Zhong, B.; Sun, Y. Synthesis of higher alcohols from syngas over K/Co/β-Mo_2C catalysts. *Catal. Commun.* **2007**, *8*, 503–507.
4. Smith, K. J.; Young, C-W.; Herman, R. G.; Klier, K. Development of a kinetic model for alcohol synthesis over a cesium-promoted Cu/ZnO catalyst. *Ind. Eng. Chem. Res.* **1991**, *30*, 61-71.
5. Woo, H. C.; Park, K. Y. Mixed alcohols synthesis from carbon monoxide and dihydrogen over potassium-promoted molybdenum carbide catalysts. *Appl. Catal. A* **1991**, *75*, 267–280.
6. Smith, K. J.; Herman, R. G.; Klier, K. Kinetic modelling of higher alcohol synthesis over alkali-Promoted Cu/ZnO and MoS_2 Catalysts. *Chem. Eng. Sci.* **1990**, *45*, 2639–2646.
7. Gandia, L. M.; Montes, M. Effect of thermal treatments on the properties of nickel and cobalt activated-charcoal-supported catalysts. *J. Catal.* **1994**, *145*, 276–288.
8. Surisetty, V. R.; Dalai, A. K.; Kozinski, J. Intrinsic reaction kinetics of higher alcohols synthesis from synthesis gas over sulfided alkali-promoted Co-Rh-Mo trimetallic catalyst supported on MWCNTs. Energ. Fuel. **2010**, in press.
9. Smith, K. J.; Anderson, R. B. A chain growth scheme for the higher alcohols synthesis. *J. Catal.* **1984,** *85*, 428–436.
10. Jiang, M.; Bian, G.-Z.; Fu, Y.-L. Effect of the K-Mo interaction in K-MoO_3/γ-Al_2O_3 catalysts on the properties for alcohol synthesis from syngas. *J. Catal.* **1994**, *146*, 144–154.
11. Li, X. G.; Feng, L. J.; Liu, Z. Y.; Zhong, B.; Dadyburjor, D. B.; Kugler, E. L. Higher alcohols from synthesis gas using carbon-supported doped molybdenum-based catalysts. *Ind. Eng. Chem. Res.* **1998**, *37*, 3853– 3863.
12. Fujumoto, A.; Oba, T. Synthesis of C_1-C_7 alcohols from synthesis gas with supported cobalt catalysts. *Appl. Catal. A* **1985,** *13*, 289–319.

13. Surisetty, V. R.; Dalai, A. K.; Kozinski, J. Synthesis of higher alcohols from synthesis gas over Co-promoted alkali modified-MoS_2 catalysts supported on MWCNTs. *Appl. Catal., A* **2010**, in press.

14. Surisetty, V. R.; Dalai, A. K.; Kozinski, J. Effect of Rh promoter on MWCNT-supported alkali-modified MoS_2 catalysts for higher alcohols synthesis from CO hydrogenation. *Appl. Catal. A,* **2010**, *381*, 282-288.

15. Wong, S. F.; Stromville, N. Y.; Storm, D. A.; Montvale, N. J.; Patel, M. S. Catalyst and method for producing lower aliphatic alcohols. US Patents 4,983,638, Jan 8, 1991.

16. Xiaoming, M. A.; Guodong, L.; Hongbin, Z. Co-Mo-K sulfide-based catalyst promoted by multiwalled carbon nanotubes for higher alcohol synthesis from syngas. *Chinese J. Catal.* **2006,** *27*, 1019–1027.

17. Surisetty, V. R.; Tavasoli, A.; Dalai, A. K. Synthesis of higher alcohols from syngas over alkali promoted MoS_2 catalysts supported on multi-walled carbon nanotubes. . *Appl. Catal. A* **2009**, *365*, 243-251.

18. Kennedy, L. J.; Vijaya, J. J.; Sekaran, G.; Joseph, J.; Rani, J. D.; Pragasam, J. Bulk preparation and characterization of mesoporous carbon nanotubes by catalytic decomposition of cyclohexane on sol–gel prepared Ni–Mo–Mg oxide catalyst. *Materials Letters* **2006**, *60*, 3735–3740.

19. Sigurdson, S.; Sundaramurthy, V.; Dalai, A. K.; Adjaye, J. Effect of anodic alumina pore diameter variation on template-initiated synthesis of carbon nanotube catalyst supports. *J. Mol. Catal. A: Chem.* **2009**, *306*, 23–32.

20. Xiaoding, X.; Doesburg, E. B. M.; Scholten, J. J. F. Synthesis of higher alcohols from syngas - recently patented catalysts and tentative ideas on the mechanism. *Catal. Today* **1987**, *2*, 125–170.

21. Li, X.; Feng, L.; Liu, Z.; Zhong, B.; Dadyburjor, D. B.; Kugler, E. L. Higher alcohols from synthesis gas using carbon-supported doped molybdenum-based catalysts. *Ind. Eng. Chem. Res.* **1998**, *37*, 3853–3863.

22. Park, T. Y.; Nam, I-S.; Kim, Y. G. Kinetic analysis of mixed alcohol synthesis from syngas over K/MoS_2 catalyst. *Ind. Eng. Chem. Res.* **1997**, *36*, 5246–5257.

23. Christensen, J. M.; Mortensen, P. M.; Trane, R.; Jensen, P.A.; Jensen, A. D. Effects of H_2S and process conditions in the synthesis of mixed alcohols from syngas over alkali promoted cobalt-molybdenum sulfide. *Appl. Catal. A* **2009**, *366*, 29–43.

24. Surisetty, V. R.; Dalai, A. K.; Kozinski, J. Alkali-promoted trimetallic Co-Rh-Mo sulfide catalysts for higher alcohols synthesis from synthesis gas: Comparison of MWCNT and activated carbon supports. *Ind. Eng. Chem. Res.*, **2010**, *49*, 6956-6963.

25. Taguchi, G. *System of experimental design. Quality Resources*, Kraus and Americans Supplier Institute (eds): USA, 1991.

26. Bolboaca, S. D.; Jantschi, L. Design of experiments: Useful orthogonal arrays for number of experiments from 4 to 16. *Entropy* **2007**, *9*, 198-232.

27. Anderson, Mark J.; Whitcomb, Patrick J. *RSM Simplified: Optimizing Processes Using Response Surface Methods for Design of Experiments*, Productivity Press: New York, NY, 2005.

28. Azargohar, R.; Dalai, A. K. Steam and KOH activation of biochar: Experimental and modeling studies. *Microporous Mesoporous Mater.* **2008**, *110*, 413–421.

29. Lazic, Z. R. *Design of Experiments in Chemical Engineering*, 1st ed.; Wiley-VCH Verlag GmbH: Weinheim, Germany, 2004.

30. Steel, R. G. D.; Torrie, J. H. *Principles and Procedures of Statistics*, McGraw-Hill: New York, USA, 1960.

31. Montgomery, D. C. *Design and Analysis of Experiments*, 4th ed.; John Wiley and Sons: New York, USA, 1997.

32. Hogg, R.V.; Ledolter J. *Applied Statistics for Engineers and Physical Scientists*, Macmillan: New York, USA, 1992.

CHAPTER 10

Intrinsic Reaction Kinetics of Higher Alcohols Synthesis from Synthesis Gas over Sulfided Alkali-Promoted Co-Rh-Mo Trimetallic Catalyst Supported on Multi-Walled Carbon Nanotubes

The manuscript provided in this chapter is very similar to the one accepted for publication in the journal Energy and Fuels.

Citation:

Surisetty, V. R.; Dalai, A. K.; Kozinski, J. Intrinsic reaction kinetics of higher alcohols synthesis from synthesis gas over sulfided alkali-promoted Co-Rh-Mo trimetallic catalyst supported on MWCNTs. *Energ. Fuel.* **2010**, in press.

Contribution of the Ph.D. Candidate

The experiments were planned and conducted by Venkateswara Rao Surisetty. Drs. Ajay Kumar Dalai and Janusz Kozinski provided guidance in planning the experiment. The MATLAB program was developed by Venkateswara Rao Surisetty. Data analysis and interpretations were performed by Venkateswara Rao Surisetty. Drs. Ajay Kumar Dalai and Janusz Kozinski provided guidance in the results and discussion while writing the submitted manuscript. The submitted manuscript was written by Venkateswara Rao Surisetty. Dr. Dalai provided editorial assistance regarding the style and content of the paper.

Contribution to Overall Study

This chapter aims to investigate the intrinsic kinetic data for higher alcohols synthesis from synthesis gas. The highly performed K (9 wt %)-promoted trimetallic Co (4.5 wt %)-Rh (1.5 wt %)-Mo (15 wt %) sulfided catalyst supported on MWCNTs was used for this study as mentioned in Chapter 9. Prior to kinetic studies, experiments were performed to study the effects of mass transfer diffusions. Power Law model was used to fit the data. The results of the activation energies for methanol, ethanol, higher alcohols, and hydrocarbons obtained over the alkali-promoted trimetallic Co-Rh-Mo catalyst supported on MWCNTs were compared with those of values from available literature.

10.1. Abstract

A statistically designed set of experiments was run in a continuous downflow fixed-bed reactor to evaluate the intrinsic kinetics of the formation of methanol, higher alcohols, total hydrocarbon, and carbon dioxide from synthesis gas under a range of experimental conditions. To eliminate mass transfer resistance, a multi-walled carbon nanotube (MWCNT)-supported K-promoted trimetallic sulfided Co-Rh-Mo catalyst was used in the particle size range of 147-210 μm. To predict the reaction rate for higher alcohols synthesis, the power law model was used for the reaction between CO and H_2 on the catalyst surface. The operating conditions such as, reactor temperature (T), pressure (P), gas hourly space velocity (GHSV), and H_2 to CO molar ratio were varied in the ranges of 275-350°C, 800-1400 psig (5.52-9.65 MPa), 2.4-4.2 m^3 (STP)/(kg of cat.)/h, and 0.5 to 2.0, respectively. The data of this study are well fitted by the power law model. The activation energies of ethanol and higher alcohols obtained over Co-Rh-Mo-K/MWCNT were low compared to those values reported in the literature.

10.2. Introduction

Higher alcohols are used as gasoline additives to improve the octane number of the fuel and reduce the emissions of NO_x, ozone, CO, and aromatic vapors.[1] The catalytic conversion of synthesis gas to higher alcohols is a promising process for the production of fuels and chemicals.[2] Sulfur poisoning of metallic catalysts, because of the presence of H_2S in synthesis gas, can be avoided using molybdenum sulfide catalysts.[3] In our previous work, it was observed that the addition of potassium to MoS_2 increased the formation of alcohols by suppressing the hydrocarbon reaction rate.[4] The Rh promotion to K-MoS_2 catalysts improved the activity and selectivity of higher alcohols synthesis because of the synergistic effect of Rh and Mo, leading to the formation of a Rh-Mo mixed phase.[5] The incorporation of Co to the alkali-promoted bimetallic Rh-Mo catalyst resulted in substantial changes in structural properties and enhanced the formation of higher alcohols.[6] In comparison to acidic metal oxide supports and activated carbon-supported catalysts, increased activity and selectivity of higher alcohols from CO hydrogenation were observed on multi-walled carbon nanotube (MWCNT) supports.[6-8] In our previous work,[6] the alkali-promoted trimetallic catalyst with K loading of 9 wt %, Co loading of 4.5 wt %, Rh loading of 1.5 wt %, and Mo loading of 15 wt % supported on

MWCNTs showed the highest yield and selectivity toward higher alcohols compared to that of a similar catalyst supported on activated carbon.

The K-promoted MoS_2-based catalysts likely follow a CO insertion mechanism for the formation of higher alcohols from CO hydrogenation.[9] In this mechanism, adsorption of CO and hydrogen takes place at different sites to form intermediate surface species. These surface species propagate chain growth through hydrogenation, followed by insertion of molecularly adsorbed CO species to form different long-chain intermediates. The direct hydrogenation of these intermediate hydrocarbon species leads to the formation of hydrocarbon, methanol, and higher alcohols. The rate expressions for higher alcohols synthesis are generally represented using either the Langmuir–Hinshelwood or power law models.[10,11] Kulawska et al.[12] explained that the Langmuir–Hinshelwood kinetic model for alcohols synthesis did not consider the effect of partial pressure of CO for the investigated range of operating conditions over a Cs-doped Cu-Zn composite catalyst, and the results obtained from the model were not properly fitted to their experimental values.

The heterogeneous catalytic reaction is associated with external and internal diffusional resistances. The diffusion of the reactants or products between the bulk fluid and the external surface of the catalyst is known as external resistance, and diffusion of the reactants from the external surface (pore mouth) to the interior of the particles and diffusion of the products from the interior of the particles to the external surface is referred as internal resistance.[13] Reaction rates in the absence of these internal and external diffusion resistances are termed as intrinsic kinetics.[14]

The objective of the present work is to investigate the intrinsic kinetic data for higher alcohols synthesis from synthesis gas over a sulfided K-promoted Co-Rh-Mo/MWCNT catalyst designed using a Taguchi orthogonal array experimental plan. This statistical design approach minimizes the overall variance of the estimated parameters and reduces the number of trials required without restricting the confidence region for the estimated parameter.[15] An orthogonal array selector determines the necessary number of trials and the factor levels for each parameter in each trial.[16] The first part of this work deals with the effects of mass-transfer diffusions followed by intrinsic kinetic calculations of higher alcohols reactions from synthesis gas.

10.3. Experimental

10.3.1. Catalyst preparation

A MWCNT (M.K. Nano; surface area,178 m^2/g, pore volume, 0.54 cc/g) was used as a support for the preparation of the catalysts. Prior to impregnation, the support was treated with 30% HNO_3 reflux at 100°C overnight, washed with distilled water several times, and dried at 120°C for 6 h. The oxide sample was prepared by the incipient wetness impregnation method using ammonium heptamolybdate tetrahydrate (Sigma-Aldrich), potassium carbonate (Aldrich), cobalt acetate tetrahydrate (Alfa Aesar), and rhodium chloride hydrate (Aldrich) as precursors for Mo, K, Co, and Rh, respectively. At the first step, the support was impregnated with an aqueous solution of K_2CO_3, followed by drying at 120°C for 2 h, and stabilizing in an argon flow of 50 ml/min at 300°C, at a heating rate of 10°C/min for 4 h. The support was further impregnated with aqueous solutions containing the required amounts of $(NH_4)_6Mo_7O_{24}$, $Co(CH_3COO)_2$, and $RhCl_3$, followed by drying at 120°C for 2 h and stabilizing in an argon flow of 50 ml/min at 450°C, at a heating rate of 10°C/min for 12 h. After stabilization, the catalysts are palletized and then ground to different particle sizes.

10.3.2. Catalyst characterization

The contents of Mo, Co, and Rh of different particle size pellet samples were determined using a Perkin-Elmer ELAN 5000 inductively coupled plasma mass spectroscopy (ICP-MS) instrument.

10.3.3. Catalytic studies

The higher alcohols synthesis was tested in the experimental unit (Fig. 10.1), which had a single-pass tubular downflow fixed-bed reactor of 450-mm length and 22-mm inside diameter, made of inconel tube. The reactor was packed with 2 g of catalyst diluted with 12 ml of 90 mesh size silicon carbide and housed in an electric furnace controlled by a temperature controller. The reactor was pressurized with He to 500 psig (3.44 MPa) and the sulfidation, together with the reduction, was carried out for 6 h at 450°C at a heating rate of 2°C/min using a gas mixture containing 10 mole % H_2S in H_2 and a flow rate of 50 ml/min. The temperature was then lowered to the reaction temperature, and the system pressurized to the reaction conditions. The feed gas mixture (desired molar ratio of CO and H_2 mixed with 10 mole % Ar) was passed through mass flow controllers and the higher alcohols synthesis

was carried out at steady-state under the reaction conditions over a period of 24 h, after an initial induction period of 15 h. The product gas was cooled to 0°C and separated into gas and liquid phases at the reaction pressure. The CO conversion and other gaseous products were monitored with a time interval of 1 h. After an induction period on 15 h, the liquids were removed from the condensers. The variation in gas concentration is found to be little after an induction period, and hence, constant values of liquid concentrations are assumed during that reaction time. The liquid products were collected at the end of the reaction and analyzed with a Varian 3400 gas chromatograph equipped with a capillary column and a flame ionization detector. The volume and weight of liquid products were measured to check the mass balance. The gaseous products were analyzed online on a Shimadzu gas chromatograph through a sampling valve. Using Ar as an internal standard, the CO conversion was calculated and the overall mass balance of the reaction was determined.

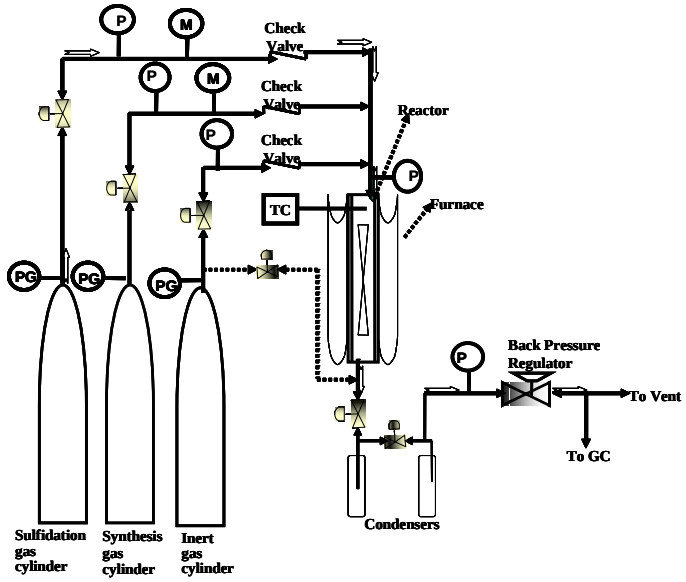

Figure 10.1. Experimental set-up for higher alcohols synthesis from synthesis gas

10.3.4. Experimental design for intrinsic kinetics

Four parameters, such as reactor temperature (T), pressure (P), gas hourly space velocity (GHSV), and H_2 to CO molar ratio were varied using four different levels in the ranges of 275-350°C, 800-1400 psig (5.52-9.65 MPa), 2.4-4.2 m^3 standard temperature and pressure (STP)/(kg of cat.)/h, and 0.5-2.0, respectively. A Taguchi orthogonal array method

was used to develop the experimental plan to analyze the intrinsic kinetics for higher alcohols synthesis from synthesis gas, and the set of experiments are shown as set 1 in Table 10.1. Design-Expert software, version 6.0.1 was used to design the set of experiments performed in this study. The experiments were performed randomly, and the center-point experiment was repeated after every four runs during the activity tests to verify the catalyst stability. Additional experiments were designed using a H_2 to CO molar ratio of 1.25 and performed at the conditions as listed as set 2 in Table 10.1. Each run was performed over a period of 24 h using 2 g of catalyst. The catalytic activity and product selectivity data were calculated after an induction period of 15 h. The catalyst was kept under a constant inert gas (He) flow of 50 ml/min between the runs, when it was necessary to shut down the reactor.

Table 10.1. Design of experiments for the kinetic analysis

Run	T (ºC)	P (psi)	GHSV (m^3 (STP)/(kg of cat.)/h)	H_2/CO (moles/moles)
Set -1				
14	350	1000	3.6	0.5
13	350	800	4.2	1.0
1	275	800	2.4	0.5
11	325	1200	2.4	1.0
15	350	1200	3.0	2.0
2	275	1000	3.0	1.0
12	325	1400	3.0	0.5
5	300	800	3.0	1.5
8	300	1400	3.6	1.0
4	275	1400	4.2	2.0
9	325	800	3.6	2.0
6	300	100	2.4	2.0
3	275	1200	3.6	1.5
10	325	1000	4.2	1.5
7	300	1200	4.2	0.5
16	350	1400	2.4	1.5
CP	315	1100	3.3	1.25
Set - 2				
1	320	1200	3.6	1.25
3	320	1400	4.0	1.25
5	330	1300	4.0	1.25
4	330	1200	3.8	1.25
6	330	1400	3.6	1.25
7	340	1200	4.0	1.25
8	340	1300	3.6	1.25
2	320	1300	3.8	1.25
9	320	1400	3.8	1.25

10.4. Results and Discussion

10.4.1. External mass-transfer diffusion

The external mass-transfer diffusion can be eliminated by decreasing the mass-transfer boundary layer thickness, which is the distance from a solid object to the region where the concentration of the diffusing species reaches 99% of the bulk concentration. This can be eliminated by increasing the velocity past the particle or using very small particles.[13] To determine the effect of external mass transfer on the performance of the K-promoted Co-Rh-Mo/MWCNTs catalyst for CO hydrogenation, sample pellets of different particle size ranges of 707-841, 420-500, 210-297, and 147-210 μm with average particle sizes of 0.774, 0.460, 0.254, and 0.179 mm, respectively, were prepared.

To confirm the homogeneous distribution of active sites through the pellet and from pellet to pellet, the samples were collected from different catalyst pellets and the metal contents of these samples were analyzed using ICP-MS. The results were given in Table 10.2 along with the targeted compositions. From this table, it is clear that the measured contents of the prepared catalysts are slightly lower compared to targeted values, which may be due to the hygroscopic nature of precursors. The metal contents of different sample pellets are found to be comparable, confirming the uniform distribution of active sites through the catalyst.

Table 10.2. ICP-MS results

Particle size range (μm)	Targeted composition (wt %)				Measured composition (wt %)		
	K	Mo	Rh	Co	Mo	Rh	Co
707-841	9	15	1.5	4.5	14.0	1.4	4.3
420-500	9	15	1.5	4.5	14.1	1.3	4.1
210-297	9	15	1.5	4.5	14.0	1.1	4.1
147-210	9	15	1.5	4.5	14.3	1.2	4.2

The effect of the particle size on external mass-transfer diffusion was studied by performing the experiments at an inlet pressure of 1320 psig (9.1 MPa), flow rate of 120 ml/min, and reaction temperatures in the range of 275-350ºC. For each experiment, 2 g of catalyst was used and the reaction was carried out using a feed gas mixture of CO (40 mole %), H_2 (50 mole %), and Ar (10 mole %). Figs. 10.2 and 10.3 shows the % CO conversions and total alcohols space time yield (STY) of the catalysts with different particle sizes at different temperatures, respectively. The % CO conversion and total alcohol STY increased linearly at all reaction temperatures with decreasing catalyst average particle size from 0.774 to 0.254 mm, but no significant change was observed in the reaction with further decreasing particle size to 0.179 mm. These results suggested that the catalyst particle size has a great influence on the higher alcohols synthesis from synthesis gas and that the mass transfer across the boundary layer limited the rate of reaction, using the catalyst with a particle size greater than 0.254 mm. Use of the catalyst with an average particle size less than 0.254 mm ensured that the film resistance to external mass transfer was negligible for the kinetic parameter estimation experiments, and hence, the catalyst with a particle size in the range of 147-210 μm was selected.

The Frössling correlation[17] is used in flow around spherical particles to obtain the relation between the particle size (d_p) of the catalyst, mass-transfer coefficient (k_c), and boundary layer thickness (δ). The required parameters and constants for the estimation of Frössling correlation are calculated and are shown in Appendix D.1. The mass-transfer correlation is given as follows:

$$Sh = 2 + 0.6(\mathrm{Re})^{1/2}(Sc)^{1/3} \quad \text{.....(10.1)}$$

$$Sh = \frac{k_c d_p}{D_e} \quad \text{.....(10.2)}$$

$$\mathrm{Re} = \frac{\rho u d_p}{\mu} \quad \text{.....(10.3)}$$

$$Sc = \frac{\mu}{\rho D_e} \quad \text{.....(10.4)}$$

where k_c is the average mass transfer coefficient of a reactant from the bulk flow to catalyst surface (m/s), d_p is the average diameter of the catalyst particle (m), D_e is the effective diffusivity for a binary gas mixture (m^2/s), u is the free stream velocity of fluid (m/s), ρ is the gas density (kg/m^3), and μ is the gas dynamic viscosity (kg/(m-s)).

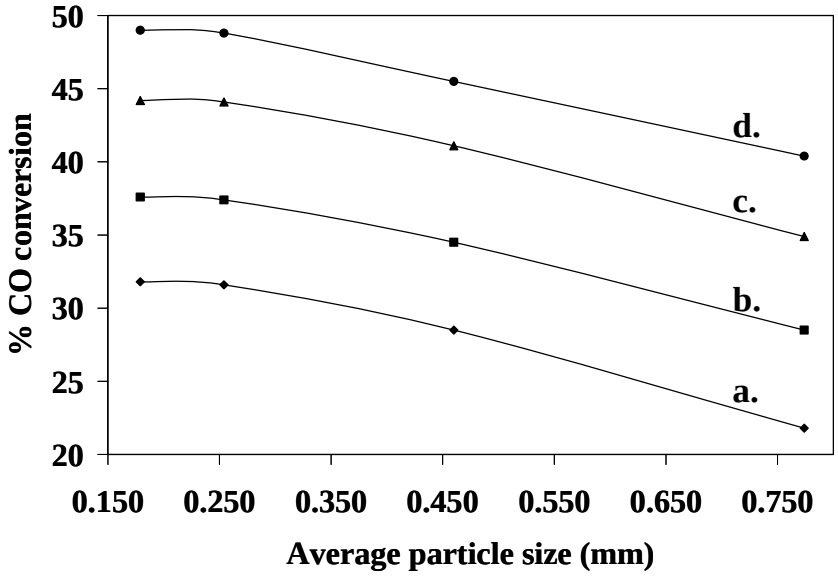

Figure 10.2. Effect of particle size on % CO conversion
a. 275ºC; b. 300ºC; c. 325ºC; d. 350ºC

(wt. of the cat. = 2 g, P = 9.1 MPa, GHSV = 3.6 m^3 (STP)/(kg of cat.)/h, H_2 to CO molar ratio = 1.25)

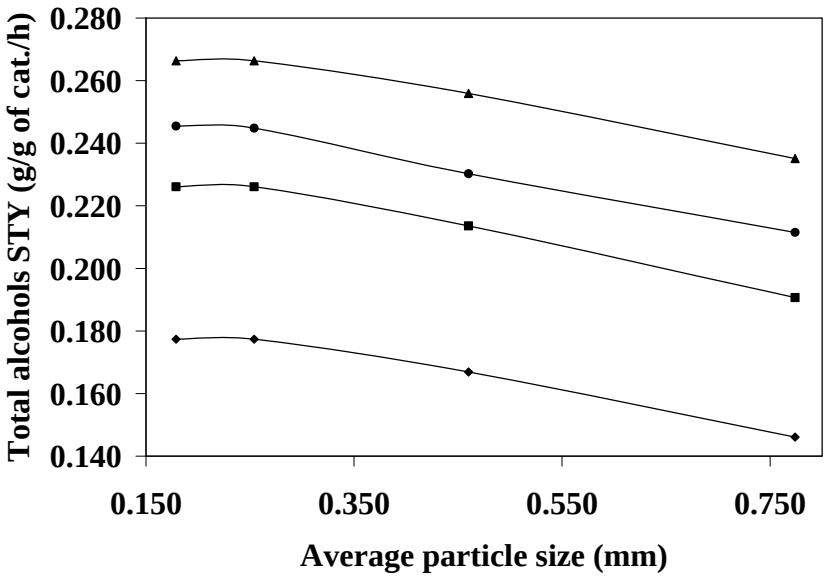

Figure 10.3. Effect of particle size on total alcohols STY
a. 275ºC; b. 300ºC; c. 325ºC; d. 350ºC

(wt. of the cat. = 2 g, P = 9.1 MPa, GHSV = 3.6 m^3 (STP)/(kg of cat.)/h, H_2 to CO molar ratio = 1.25)

Table 10.3 shows results of the mass-transfer coefficient of carbon monoxide from the bulk flow to the surface of the catalyst particle (k_c) and the boundary layer thickness (δ) calculated using the Frössling correlation. From these results, it is observed that decreasing d_p of catalyst particles from 0.774 to 0.179 mm, increased k_c value about 3 times more and decreased δ about 3 times less than that of the initial value. It is also noted that the temperature has a negligible effect on the external mass-transfer diffusion.

Table 10.3. Effect of particle size on the external mass transfer diffusion

Particle size range (μm)	d_p (mm)	k_c (m/s)	δ (mm)
T = 275ºC			
707-841	0.774	$3.62 * 10^{-4}$	0.142
420-500	0.460	$5.21 * 10^{-4}$	0.099
210-297	0.254	$8.06 * 10^{-4}$	0.064
147-210	0.179	$1.05 * 10^{-4}$	0.049
T = 300ºC			
707-841	0.774	$3.65 * 10^{-4}$	0.144
420-500	0.460	$5.25 * 10^{-4}$	0.100
210-297	0.254	$8.13 * 10^{-4}$	0.065
147-210	0.179	$1.06 * 10^{-4}$	0.049
T = 325ºC			
707-841	0.774	$3.69 * 10^{-4}$	0.146
420-500	0.460	$5.32 * 10^{-4}$	0.101
210-297	0.254	$8.24 * 10^{-4}$	0.065
147-210	0.179	$1.08 * 10^{-4}$	0.050
T = 350ºC			
707-841	0.774	$3.72 * 10^{-4}$	0.147
420-500	0.460	$5.37 * 10^{-4}$	0.102
210-297	0.254	$8.34 * 10^{-4}$	0.066
147-210	0.179	$1.09 * 10^{-4}$	0.050

(wt. of the cat. = 2 g, P = 9.1 MPa, Flow rate = 120 ml/min, H_2/CO molar ratio = 1.25)

The effect of the feed gas flow rate on external mass-transfer diffusion was studied by performing the experiments at an inlet temperature of 325ºC, pressure of 1320 psig (9.1 MPa), and H_2 to CO molar ratio of 1.25 using 2 g of catalyst with average particle size of 0.179 mm. The variation in % CO conversion with flow rate is given in Fig. 10.4. It is expected that, in the case of existing external mass-transfer resistance, the boundary layer thickness becomes reduced with an increased flow rate and results in the enhanced CO conversion at higher flow rates. From Fig. 10.4, it is observed that the % CO conversion decreased monotonically from 52 to 42% with an increased flow rate from 80 to 120 ml/min, which resulted because of the short contact time between the reactants at high flow rates. k_c and δ values were calculated for different flow rates, and the results are given in Table 10.4. It is clear from this table that the flow rate has a negligible effect on external mass-transfer diffusion under the investigated operating conditions using the sample pellets of average particle diameter of 0.179 mm.

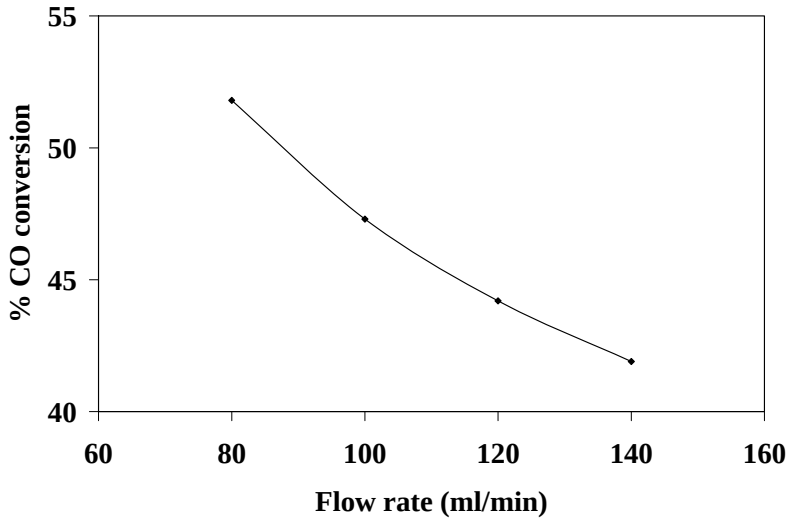

Figure 10.4. Effect of flow rate on % CO conversion

(wt. of the cat. = 2 g, T = 325°C, P = 9.1 MPa, H_2 to CO molar ratio = 1.25, Average particle size = 0.179 mm ml/min)

Table 10.4. Effect of flow rate on the external mass transfer diffusion

Flow rate (ml/min)	k_c (m/s)	δ (mm)
80	$9.94 * 10^{-4}$	0.054
100	$1.04 * 10^{-3}$	0.052
120	$1.08 * 10^{-3}$	0.050
140	$1.12 * 10^{-3}$	0.048

(wt. of the cat. = 2 g, T = 325°C, P = 9.1 MPa (1320 psig), H_2/CO molar ratio = 1.25, average particle size = 0.179 mm)

10.4.2. Internal mass-transfer diffusion

The Weisz–Prater criterion (C_{WP}) is used to estimate the internal mass-transfer resistance in heterogeneous catalytic reactions.[18] If C_{WP} « 1, there is no internal diffusion limitation, and if C_{WP} » 1, internal diffusion limits the reaction severely.[13] This criterion is given as follows:

$$C_{WP} = \frac{-(r_A^{'})_{obs} * \rho_C * R^2}{D_e * C_{A_s}} \quad \text{.....(10.5)}$$

where $(r_A^{'})_{obs}$ is the reaction rate per unit mass of catalyst, ρ_c is the catalyst density, R is the particle radius, C_{A_s} is the surface concentration of reactant A, and D_e is the effective diffusivity. The calculation of Weisz–Prater criterion is shown in Appendix D.2

The value of C_{WP} is calculated for the catalysts with average particle diameter of 0.179 mm at 300°C. The C_{WP} value of this parameter is obtained as 0.007, which is far less than 1. This confirms that internal diffusion limitation is negligible on the catalyst with the average particle diameter of 0.179 mm.

10.4.3. Intrinsic kinetics

The analysis of liquid products indicates that the alcohols likely followed the CO insertion mechanism, forming linear alcohols. Methanol, ethanol, n-propanol, and n-butanol are the major products together with other higher alcohols. Very little water (<1% by weight) was found in the liquid product, and hence, the concentration of water was neglected. The

analysis of exit gas indicates that methane is the major hydrocarbon component apart from CO_2 as well as unconverted CO and H_2.

Reaction scheme

The reaction scheme suggested by Santiesteban et al.[9] for the production of alcohols from synthesis gas over MoS_2 catalysts was used to determine the intrinsic reaction kinetics. It is difficult to obtain a statistically valid model for such an extremely complex reaction scheme; hence, the simplified reaction scheme was assumed. The liquid and gas streams were simplified into a selected number of components, namely, CO, H_2, CO_2, methanol, and ethanol, as well as pseudo-components, *Hyd* that represents methane and higher hydrocarbons, and HA_{C3+} that represents higher alcohols (alcohols with carbon number greater than 2). All the reactions were assumed to be stoichiometric, and the simplified reaction scheme is as shown below[11]

$$CO + 2H_2 \leftrightarrow CH_3OH \quad (10.6)$$

$$2CH_3OH \rightarrow C_2H_5OH + H_2O \quad (10.7)$$

$$(N_{HA} - 2)CH_3OH + C_2H_5OH \rightarrow HA_{C3+} + (N_{HA} - 2)H_2O \quad (10.8)$$

$$N_{HC}CO + (2N_{HC} + 1)H_2 \rightarrow Hyd + N_{HC}H_2O \quad (10.9)$$

$$CO + H_2O \leftrightarrow CO_2 + H_2 \quad (10.10)$$

where N_{HA} and N_{HC} stand for the average carbon atom number of the pseudo-components HA_{C3+} and *Hyd*, respectively.

In this reaction scheme, the formation of methanol and hydrocarbons are obtained directly from CO and H_2. It is assumed that hydrocarbon products are composed exclusively of methane. Methanol formation and the water-gas shift (WGS) reaction are assumed to be in thermodynamic equilibrium, and other reactions are assumed to be irreversible.[19] The formation of ethanol and higher alcohols were assumed to follow stepwise chain growth alcohols by taking methanol as the recurrent C_1 reactant; that is, one mole of ethanol is produced from two moles of methanol and one mole of propanol is obtained from one mole of methanol and one mole of ethanol, etc. The present reaction scheme is similar to the lumped kinetic model, which accounts for the global formation of higher oxygenates suggested by Tronconi et al.[20]

Rate expressions

The power law model was used for the reaction between CO and H_2 on the catalyst surface, because this model is simple and widely used to predict the reaction rate for the higher alcohols synthesis reaction.[10,21] A reversible kinetic expression was used for the methanol synthesis and the WGS reaction. Ideal gas behaviour was assumed with WGS reaction, whereas the non-ideal behavior of methanol was considered.[11] Ethanol, higher alcohols, and hydrocarbon formations were represented using irreversible kinetic expressions. The rate equations for all of the components are represented as follows:

$$r_{CH_3OH} = k_{CH_3OH}(P_{CO}^{a}P_{H_2}^{b} - P_{CH_3OH}^{c} / K_{CH_3OH}) \quad \text{.....(10.11)}$$

$$K_{CH_3OH} = \exp(-\Delta G_{CH_3OH}^{o} / R / T) / K_{\gamma,CH_3OH} \quad \text{.....(10.11.1)}$$

$$\Delta G_{CH_3OH}^{o} = -24306 + 58.57T \ (cal/mol) \quad \text{.....(10.11.2)}$$

$$K_{\gamma,CH_3OH} = 1 - P(6.713*10^{-5})*\exp(1.7308*10^{3}/T) \quad \text{.....(10.11.3)}$$

$$R = 1.987 \ (cal/mol/K) \quad \text{.....(10.11.4)}$$

$$r_{C_2H_5OH} = k_{C_2H_5OH}P_{CH_3OH}^{d} \quad \text{.....(10.12)}$$

$$r_{HA} = k_{HA}P_{CH_3OH}^{e}P_{C_2H_5OH}^{f} \quad \text{.....(10.13)}$$

$$r_{HC} = k_{HC}P_{CO}^{g}P_{H_2}^{h} \quad \text{.....(10.14)}$$

$$r_{CO_2} = k_{CO_2}(P_{CO}^{i}P_{H_2O}^{j} - P_{CO_2}^{k}P_{H_2}^{l} / K_{WS}) \quad \text{.....(10.15)}$$

$$K_{WS} = \exp(-\Delta G_{WS}^{o} / R / T) \quad \text{.....(10.15.1)}$$

$$\Delta G_{WS}^{o} = -8514 + 7.71T \ (cal/mol) \quad \text{.....(10.15.2)}$$

$$r_{CO} = k_{CH_3OH}(P_{CO}^{a}P_{H_2}^{b} - P_{CH_3OH}^{c} / K_{CH_3OH}) - N_{HC}k_4P_{CO}^{g}P_{H_2}^{h} - k_{CO_2}(P^{i}{}_{CO}P^{j}{}_{H_2O} - P^{k}{}_{CO_2}P^{l}{}_{H_2} / K_{WS}) \quad \text{.....(10.16)}$$

$$r_{H_2} = -2k_{CH_3OH}(P^{a}{}_{CO}P_{H_2}^{b} - P_{CH_3OH}^{c} / K_{CH_3OH}) - (2N_{HC}+1)k_4P_{CO}^{g}P_{H_2}^{h} + k_5(P^{i}{}_{CO}P_{H_2O}^{j} - P_{CO_2}^{k}P_{H_2}^{l} / K_{WS}) \quad \text{.....(10.17)}$$

$$r_{H_2O} = k_{C_2H_5OH}P_{CH_3OH}^{d} + (N_{HA}-2)k_{HA}P_{CH_3OH}^{e}P_{C_2H_5OH}^{f} + N_{HC}k_4P_{CO}^{g}P_{H_2}^{h} - k_{CO_2}(P_{CO}^{i}P_{H_2O}^{j} - P_{CO_2}^{k}P_{H_2}^{l} / K_{WS}) \quad \text{.....(10.18)}$$

Reactor model

The plug-flow reactor was used in the kinetic study of the higher alcohols synthesis reaction over the alkali-promoted trimetallic Co-Rh-Mo catalyst supported on MWCNTs. As discussed in the previous section, the catalyst particle size in the range of 147-210 μm was selected to eliminate the external and internal mass-transfer resistances and the reactor was regarded as isothermal. The following differential mole balance equations were used:

$$\frac{dY_{CH_3OH}}{d(W_C/F)} = r_{CH_3OH} - 2r_{C_2H_5OH} - (N_{HA}-2)r_{HA} \quad \text{.....(10.19)}$$

$$\frac{dY_{C_2H_5OH}}{d(W_C/F)} = r_{C_2H_5OH} - r_{HA} \quad \text{.....(10.20)}$$

$$\frac{dY_{HA}}{d(W_C/F)} = r_{HA} \quad \text{.....(10.21)}$$

$$\frac{dY_{HC}}{d(W_C/F)} = r_{HC} \quad \text{.....(10.22)}$$

$$\frac{dY_{CO_2}}{d(W_C/F)} = r_{CO_2} \quad \text{.....(10.23)}$$

$$\frac{dY_{CO}}{d(W_C/F)} = r_{CO} \quad \text{.....(10.24)}$$

$$\frac{dY_{H_2}}{d(W_C/F)} = r_{H_2} \quad \text{.....(10.25)}$$

$$\frac{dY_{H_2O}}{d(W_C/F)} = r_{H_2O} \quad \text{.....(10.26)}$$

$$Y_i = \frac{F_i}{F^0} \quad \text{.....(10.27)}$$

where F_i (mole/h) is the mole flow rate of the *i*th species,

F^0 (mole/h) is the total inlet mole flow rate, in correspondence with the reactor entrance (mole/h)

Y_i - The mole fraction of the *i*th species in the product stream.

Y_i^0 - The mole fraction of the *i*th species in the feed stream.

Initial conditions: $Y_i = Y_i^0$ for each species.

W_C/F^0: catalyst load (kg)/total mole flow rate (mole/h)) = $22.4*10^{-3}$ (m^3 (STP)/mole)/GHSV

Units of GHSV: m^3 (STP)/(kg of cat./h).

The differential equations are solved by using ode45 routines in MATLAB, and, simultaneously, the sum of the squares function was minimized by using *fminsearch*. The kinetic parameters were estimated by fitting the experimental data in the sum of the squares function and minimizing the errors. The residual error values obtained at 275, 300, 325, and 350ºC are 0.0954, 0.0335, 0.0874, and 0.0395, respectively. Arrhenius plots are drawn for obtaining activation energies and frequency factors from the kinetic parameters, and the values shown in Table 10.5. Figs. 10.5 to 10.9 show the fit between observed values and the predicted model values of methanol, ethanol, higher alcohols, hydrocarbons, and carbon dioxide, respectively. The R^2 values by the models show a good fit with the experimental results.

Table 10.5. Optimum estimated values of kinetic parameters

Parameter	Value
$k^0_{CH_3OH}$	$1.502 * 10^{-4}$
$k^0_{C_2H_5OH}$	$3.511 * 10^{-2}$
k^0_{HA}	$1.837 * 10^{3}$
k^0_{HC}	$3.270 * 10^{4}$
k_{CO_2}	$2.928 * 10^{2}$
E_{CH_3OH}	35
$E_{C_2H_5OH}$	57
E_{HA}	94
E_{HC}	112
E_{CO_2}	103
a	0.871
b	1.898
c	0.765
d	1.237
e	0.356
f	1.023
g	0.124
h	1.132
i	1.118
j	0.012
k	1.232
l	0.234

k_i^0 units depend on the kinetic expression obtained for the corresponding r_i which is expressed as mole/(kg of cat.)/h; units of E_i are in kJ/mole.

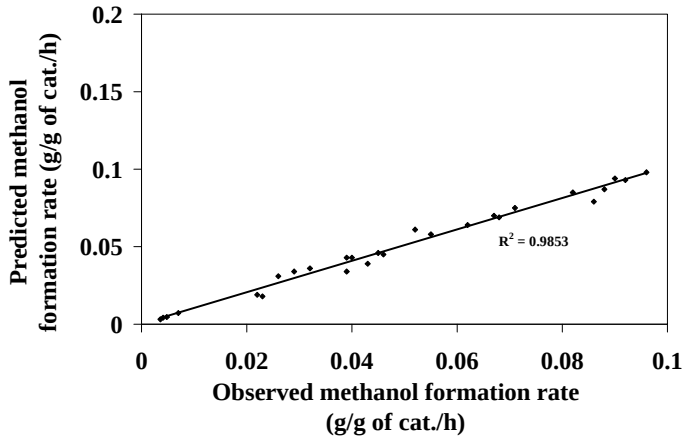

Figure 10.5. Comparison plots for observed methanol formation rate

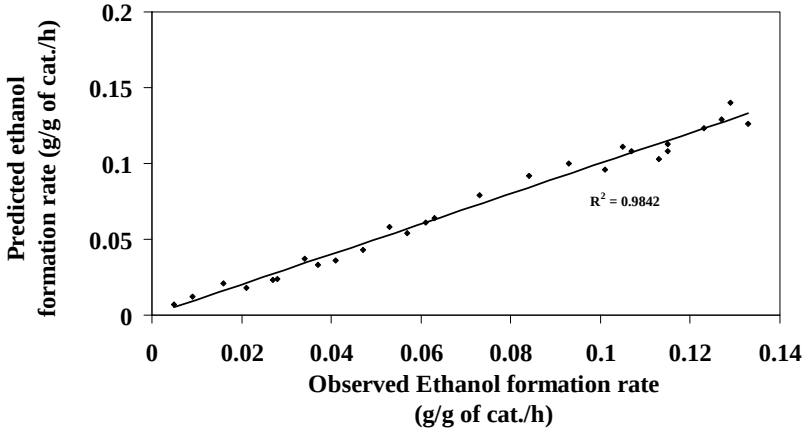

Figure 10.6. Comparison plots for observed ethanol formation rate

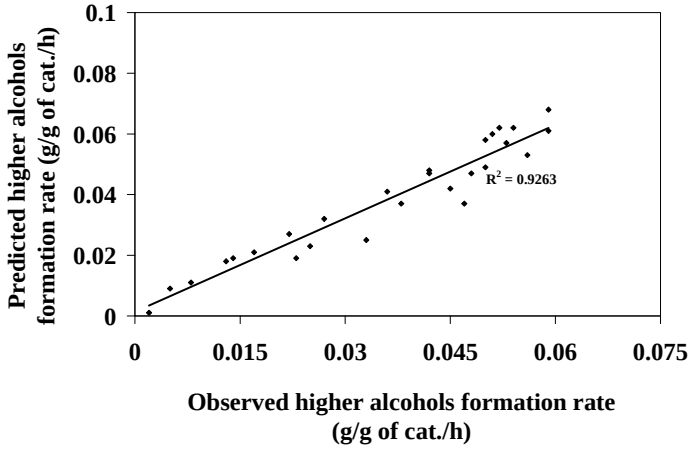

Figure 10.7. Comparison plots for observed higher alcohols formation rate

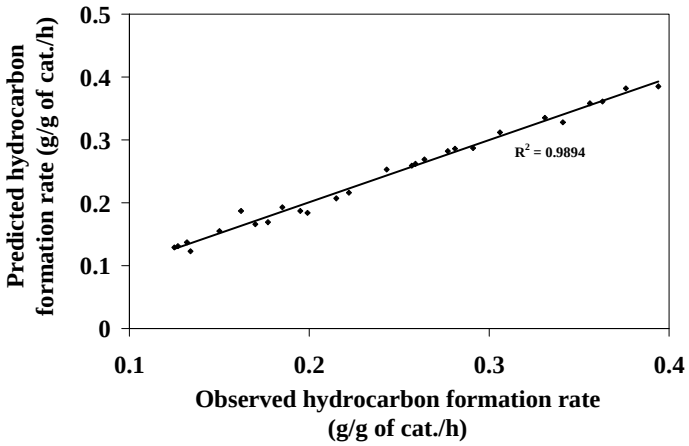

Figure 10.8. Comparison plots for observed hydrocarbons formation rate

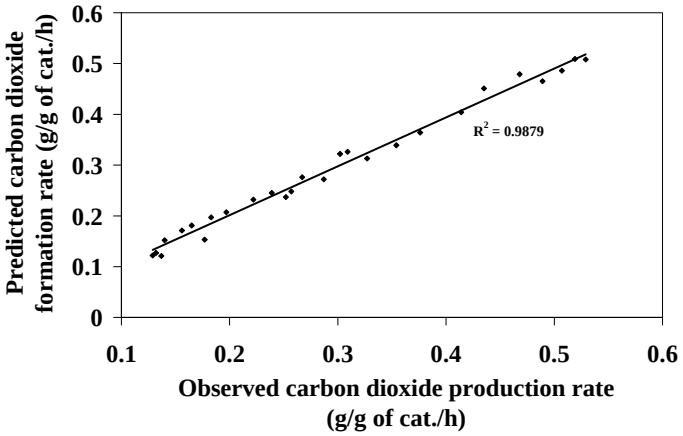

Figure 10.9. Comparison plots for observed carbon dioxide formation rate

It is observed that the CO conversion, hydrocarbon formation rate, and the WGS reaction rate increased monotonically with an increased temperature, whereas, methanol formation decreased monotonically with an increased temperature from 275 to 350ºC. A maxima is observed in ethanol and higher alcohols formation at 330ºC. As shown in Table 10.5, the activation energy of hydrocarbons and carbon dioxide were higher than that of the alcohols. This is because the hydrocarbon formation rate and the water gas shift reaction rate both increased at higher temperatures. The activation energy of alcohols is observed in the following order: methanol < ethanol < higher alcohols. This explains that an increasing temperature favors the conversion of lower molecular-weight alcohols to higher alcohols. Christensen et al.[21] explained

that an increased temperature favors the high CO surface coverage on the catalyst which favors the improved rate of the CO insertion step and yields chain growth. This is an uncommon behavior for such chain growth reactions.

Table 10.6 compares the activation energies for methanol, ethanol, higher alcohols, and hydrocarbons obtained over the alkali-promoted trimetallic Co-Rh-Mo catalyst supported on MWCNTs to those of values from available literature. The increase in activation energy with the alcohol carbon number was in agreement with the literature.[21] The activation energies of ethanol and higher alcohols obtained over the Co-Rh-Mo-K/MWCNT catalyst were low compared to those values reported in the literature. Low activation energies of alcohols might be possible because of the structural modification of Mo species with the promotion of K, Co, and Rh, which favor the formation of small particles uniformly dispersed inside and outside the straight pores of the MWCNTs support.[6] This study reveals on the better performance of Co-Rh-Mo-K/MWCNT as compared to those studied so far available in the open literature.

Table 10.6. Comparison of the activation energies of alcohols over sulfided Mo-based catalysts

Reference	Christensen et al.[21]	Gunturu et al.	Santiesteban et al.[9]	Present work
Catalyst	Sulfided Co-Mo-K/C*	Co-Mo-K/C	Cs/MoS_2	Co-Rh-Mo-K/MWCNTs
Conditions	P = 100 bar, H_2/CO = 1.01	P = 40–70 bar, H_2/CO = 0.5-2.0	P = 82.7 bar, H_2/CO = 0.96	P = 55.2–96.5 bar, H_2/CO = 0.5 -2.0
Methanol	49	117.7****	68	35
Ethanol	76	38.3	94.9	57
Higher alcohols	109**	97.9**	98.5**	94
Hydro carbons	118***	106.5	--	112

*260 ppmv of H_2S in the synthesis gas feed; **Activation energy of propanol only; ***Activation energy of methane only; ****Langmuir–Hinshelwood model was used for methanol rate expression.

10.5. Conclusions

A MWCNT-supported K-promoted trimetallic sulfided Co-Rh-Mo catalyst was used to study the intrinsic kinetics of the higher alcohols synthesis reaction from synthesis gas. The catalyst particle size in the range of 147-210 μm was selected to eliminate the external mass-transfer resistance. The Weisz–Prater criterion confirmed that internal diffusion limitation is negligible in the catalyst. Methane, carbon dioxide, methanol, ethanol, n-propanol, and n-butanol are the major products. The reaction scheme suggested by Santiesteban, et al. for the production of alcohols from synthesis gas over MoS_2 catalysts was used to determine the intrinsic reaction kinetics. A Taguchi orthogonal array method was used to develop the experimental plan by varying the reactor temperature (T), pressure (P), gas hourly space velocity (GHSV), and H_2 to CO molar ratio in the ranges of 275-350°C, 800-1400 psig (5.52-9.65 MPa), 2.4-4.2 m^3 (STP)/ (kg of cat.)/ h, and 0.5 to 2.0, respectively. The data of this study are well-fitted by the power law model. The activation energies of ethanol and higher alcohols obtained over Co-Rh-Mo-K/MWCNTs were low compared to those values reported in the literature.

10.6. Abbreviations

MWCNTs	Multi-walled carbon nanotubes
GHSV	Gas hourly space velocity
STY	Space time yield
WGS	Water-gas shift

10.7. Symbols

C_{As}	Surface concentration of reactant A
C_{WP}	Weisz-Prater criterion
d_p	Particle size of the catalyst
D_e	Effective diffusivity for a binary gas mixture
E_A	Activation energy of component A
F_i	Molar flow rate of the i^{th} species
F^0	Total inlet molar flow rate in correspondence with the reactor entrance
k_A	Frequency factor of component A
k_c	Mass transfer coefficient

K	Equilibrium constant
P	Pressure
r_A	Rate of reaction of component A
$(r_A')_{obs}$	Reaction rate per unit mass of catalyst
R	Particle radius
Re	Reynolds number
Sc	Schmidt number
Sh	Sherwood number
T	Temperature
u	Free stream velocity of fluid
W_C	Catalyst load
Y_i	Mole fraction of the i^{th} species in the product stream
Y_i^0	Mole fraction of the i^{th} species in the feed stream
δ	Boundary layer thickness
ρ	Gas density
ρ_c	Catalyst density
μ	Gas dynamic viscosity
ΔG^o	Gibbs free energy

10.8. References

1. Chianelli, R.R.; Lyons, J.E.; Mills, G.A. Catalysts for liquid transportation fuels from petroleum, coal, residual oil, and biomass. *Catal. Today* **1994**, *22*, 361–396.
2. Xiang, M.; Li, D.; Li, W.; Zhong, B.; Sun, Y. Synthesis of higher alcohols from syngas over K/Co/b-Mo_2C catalysts. *Catal. Commun.* **2007**, *8*, 503–507.
3. Li, Z.-R.; Fu, Y.-L.; Jiang, M.; Hu, T.-D.; Liu, T.; Xie, Y.-N. Active carbon supported Mo–K catalysts used for alcohol synthesis. *J. Catal.* **2001**, *199*, 155-161.
4. Surisetty, V. R.; Tavasoli, A.; Dalai, A. K. Synthesis of higher alcohols from syngas over alkali-promoted MoS_2 catalysts supported on multi-walled carbon nanotubes. *Appl. Catal. A* **2009**, *365*, 243-251.

5. Surisetty, V. R.; Dalai, A. K.; Kozinski, J. Effect of Rh promoter on MWCNT-supported alkali-modified MoS_2 catalysts for higher alcohols synthesis from CO hydrogenation. *Appl. Catal. A,* **2010**, *381*, 282-288.

6. Surisetty, V. R.; Dalai, A. K.; Kozinski, J. Alkali-promoted trimetallic Co-Rh-Mo sulfide catalysts for higher alcohols synthesis from synthesis gas: Comparison of MWCNT and activated carbon supports. *Ind. Eng. Chem. Res.*, **2010**, *49*, 4956-4963.

7. Concha, B. E.; Bartholomew, G. L.; Bartholomew, C. H.; CO hydrogenation on supported molybdenum catalysts: Effects of support on specific activities of reduced and sulfided catalysts. *J. Catal*. **1984**, *89*, 536–541.

8. Xiaoming, M. A.; Guodong, L.; Hongbin, Z. Co-Mo-K sulfide-based catalyst promoted by multi-walled carbon nanotubes for higher alcohol synthesis from syngas. *Chinese J. Catal*. **2006,** *27*, 1019–1027.

9. Santiesteban, J. G.; Bogdan, C. E.; Herman, R. G.; Klier, K.; Mechanism of C_1-C_4 alcohol synthesis over Alkali/MoS_2 and Alkali/Co/MoS_2 catalysts. In *Catalysis: Theory to Practice, C_1 Chemistry;* Phillips, M. J., Ternan, M., Eds.; 9th International Congress on Catalysis: Calgary, 1988; Vol. 2, p 561.

10. Gunturu, A. K.; Kugler, E. L.; Cropley, J. B.; Dadyburjor, D. B. A kinetic model for the synthesis of high-molecular-weight alcohols over a sulfided Co-K-Mo/C catalyst. *Ind. Eng. Chem. Res.* **1998,** *37*, 2107–2115.

11. Beretta, A.; Micheli, E.; Tagliabue, L.; Tronconi, E. Development of a process for higher alcohol production via synthesis gas. *Ind. Eng. Chem. Res.* **1998,** *37*, 3896–3908.

12. Kulawska, M.; Skrzypek, J. Kinetics of the synthesis of higher aliphatic alcohols from syngas over a modified methanol synthesis catalyst. *Chem. Eng. Process.* **2001**, *40*, 33–40.

13. Fogler, H. S. *Elements of Chemical Reaction Engineering*, Prentice Hall PTR, USA, 3rd ed., 1999.

14. Butt, J. B. *Reaction Kinetics and Reactor Design*, USA, 2nd ed., 2000.

15. Taguchi, G. *System of Experimental Design. Quality Resources*, Kraus and Americans Supplier Institute (eds): USA, 1991.

16. Bolboaca, S. D.; Jantschi, L. Design of experiments: Useful orthogonal arrays for number of experiments from 4 to 16. *Entropy* **2007**, *9*, 198–232.

17. Frössling N. The evaporation of falling drops. *Gerlands Beitr. Geophys.* **1938**, *52*, 170–216.

18. Weisz, P. B.; Prater, C. D. Interpretation of measurements in experimental catalysis. *Adv. Catal.* **1954**, *6*, 143–196.

19. Tronconi, E.; Forzatti, P.; Pasquon, I.I. An investigation of the thermodynamic constraints in higher alcohol synthesis over Cs-promoted ZnCr-oxide catalyst. *J. Catal.* **1990**, *124*, 376–390.

20. Tronconi, E.; Ferlazzo, N.; Pasquon, I. Synthesis of alcohols from carbon oxides and hydrogen. *Ind. Eng. Chem. Res.* **1987**, *26*, 2122–2129.

21. Christensen, J. M.; Mortensen, P. M.; Trane, R.; Jensen, P. A.; Jensen, A. D. Effects of H_2S and process conditions in the synthesis of mixed alcohols from syngas over alkali-promoted cobalt-molybdenum sulfide. *Appl. Catal. A*, **2009**, *366*, 29–43.

CHAPTER 11

Deactivation Studies of Alkali-Modified Trimetallic Co-Rh-Mo Sulfided Catalysts for Higher Alcohols Synthesis from Synthesis Gas

The manuscript provided in this chapter is very similar to the one submitted in the journal of Industrial and Engineering Chemistry Research.

Citation:

Surisetty, V. R.; Dalai, A. K.; Kozinski, J. Long-term deactivation studies of alkali-modifieded trimetallic Co-Rh-Mo sulfide catalysts for higher alcohols synthesis from synthesis gas. *Green Chem.* **2010**, Submitted for Review.

Contribution of the Ph.D. Candidate

Experiments were designed and performed by Venkateswara Rao Surisetty. Drs. Ajay Kumar Dalai and Janusz Kozinski provided guidance in planning the experiment. Data analysis and interpretations were performed by Venkateswara Rao Surisetty. Drs. Ajay Kumar Dalai and Janusz Kozinski provided guidance in the results and discussion while writing the submitted manuscript. The submitted manuscript was written by Venkateswara Rao Surisetty. Dr. Dalai provided editorial assistance regarding the style and content of the paper.

Contribution to Overall Study

Chapters 6, 7 and 8, it was shown that the sulfided K (9 wt %)-promoted trimetallic Co (4.5 wt %)-Rh (1.5 wt %)-Mo (15 wt %) catalyst supported on MWCNTs outperformed other catalysts for higher alcohols reactions in terms of activity and selectivity. In Chapter 9, the optimum operating conditions for obtaining maximum ethanol space time yield and selectivity were determined as 330°C, 1320 psig, and 3.8 m^3 (STP)/kg of cat.)/h. As the final step of this Ph.D. research, Chapter 11 aimed to understand the decay of catalyst activity during continuous higher alcohols synthesis for 720 h in a fixed-bed micro reactor under

optimum operating conditions. Two different supports, MWCNTs and activated carbon were used as support to understand the role of support on catalyst stability.

11.1. Abstract

Multi-walled carbon nanotubes (MWCNTs) and activated carbon-supported K (9 wt %)-promoted trimetallic Co (4.5 wt %)-Rh (1.5 wt %)-Mo (15 wt %) catalysts were used to study the long term deactivation for continuous 720 h of higher alcohols synthesis. The fresh catalysts were extensively characterized in both oxide and sulfide phases, together with the spent catalysts. The catalysts were tested for the synthesis of higher alcohols from synthesis gas under similar conditions of 330°C, 9.1 MPa (1320 psig), and 3.8 m^3 (STP)/(kg of cat.)/h using H_2 to CO molar ratio of 1.25. The alkali-modified trimetallic Co-Rh-Mo catalyst supported on MWCNTs has shown two different deactivation steps: loss of sulfur from the catalyst surface and sintering of the catalyst species located on the outer surfaces of the carbon nanotubes. After regeneration, the total activity recovery (about 10%) is close to the total activity loss during the first deactivation step over this catalyst. Deactivation of the catalyst supported on activated carbon was high compared to the MWCNT-supported catalyst. Characterizations of the spent catalyst supported on activated carbon revealed that deactivation occurs due to the large sintering rate of the catalyst species (especially, metal sulfides), which causes low metal dispersions and high pore blockage of the support. The total hydrocarbon formation decreased rapidly during the first deactivation step and then slowly leveled off. The initial decrease in total hydrocarbons STY might be explained from the loss of sulfur from unstable metal sulfide crystallites on the surface of the catalyst to the products and sintering of the catalyst species is responsible for the later steps. The sulfided catalyst supported on MWCNTs showed excellent reaction stability for the synthesis of higher alcohols from synthesis gas, whereas a slight reduction in total alcohols formation was observed on the activated carbon-supported catalyst.

11.2. Introduction

Catalytic conversion of synthesis gas to produce higher alcohols is one of the most promising processes for reducing greenhouse effects and utilizing natural source of carbon.[1, 2] A higher alcohol mixture can replace tetraethyl lead (TEL) and methyl tertiary butyl ether

(MTBE) as an octane booster in gasoline.[3] Alkali-modified MoS_2-based catalysts are of special interest among different higher alcohols synthesis (HAS) catalysts, due to their excellent sulfur resistance and high activity for water-gas shift (WGS) reactions, which saves the cost of ultra-desulfurization for feed gas and water separation.[4, 5] In this catalytic system, potassium is a key promoter that shifts the product distribution towards higher alcohols. The products obtained over these catalysts yield a series of linear primary alcohols and gaseous hydrocarbons with Anderson-Schulz-Flory (ASF) carbon number distributions.[6, 7]

The activity and selectivity of higher alcohols over these catalysts were greatly improved by the promotion of Rh, due to the synergistic effect of Rh and Mo, leading to the formation of an Rh-Mo mixed phase.[8] Vit *et al.*[9] defined the magnitude of the synergetic effect (SE) as the ratio of the rate constants over the promoted catalyst and the sum of the individual rate constants over Mo and metal catalysts. Lamber *et al.*[10] observed the formation of bimetallic Rh-Mo particles and concluded that these particles were responsible for the improvement in the catalytic behaviour in the CO hydrogenation. The interaction of rhodium with molybdenum in sulfide state changes the status of the rhodium species by favoring the formation of electron-poor sites (Rh-Mo-S) on the catalytic sites.[11] The electron-poor sites decrease the heat of CO chemisorption and increase the concentration of surface molecular CO, thus favouring the formation of higher alcohols.[12] The hydrocarbon products are formed via CO dissociation and hydrogenation of surface carbon over the electron-rich metallic sulfide species.[13]

The high rates of higher alcohols were observed compared to the rate of methanol formation over the alkali-promoted Co-Rh-Mo trimetallic catalyst due to the increased availability of electron-poor sites on the catalyst system.[14] The Co incorporation to the K-Rh-MoS_2 catalyst supported on multi-walled carbon nanotubes (MWCNTs) resulted in substantial changes in both structure properties, thus improving the catalytic performance towards higher alcohols formation from synthesis gas.[15] According to the literature[11, 16], the catalytic species mainly exists in the form of K-Mo-S, Co-Mo-S, Rh-Mo-S, MoS_2 and Co_9S_8 over the alkali, Co, and Rh-promoted MoS_2 bimetallic catalysts. Sun *et al.*[17] explained that one molybdenum atom of every two is substituted by transition metal promoters (Co or Rh) and the promoter atoms located at edge surfaces generate partially promoted Co (Rh)-Mo-S surface species. Thus, the presence of metal promoters reduces the formation of metallic sulfide species that are responsible for the

formation of hydrocarbons. The formation of the metallic sulfide species (MoS_2 and Co_9S_8) was greatly reduced using the alkali-promoted trimetallic Co-Rh-Mo catalysts for higher alcohols synthesis from CO hydrogenation.[15]

Catalyst deactivation is an industrial problem related to the use of heterogeneous catalysts that results in loss of catalytic activity and/or selectivity over time.[18] The stability of catalyst impacts greatly on the research, development, design, and operation of commercial processes as well as the costs for catalyst replacement and process shut down.[19] The coke or carbon formation rate in a given reaction depends on the reaction conditions, such as temperature and reactant composition, and on catalyst structure, including metal type, metal crystallite size, promoter, and catalyst support.[20] For coke-insensitive reactions, such as higher alcohols synthesis, methanol synthesis, or Fischer–Tropsch synthesis on metals, carbon/coke formation is avoided in regions of temperature in which the precursor gasification rate exceeds the deposition rate.[19] It is also known that supported metals such as Co, Fe, and Ni are active to coke formation at temperatures above 350-400ºC from CO and hydrocarbons. The filamentous carbon formation can be reduced by adding noble metals such as Pt, Ru, and Rh to base metals.[21] Bitter *et al.*[22] demonstrated that catalyst deactivation occurs rapidly on larger metal crystallites compared to those containing small crystallites. The coke formation rate is higher on acidic metal oxide supports, such as Al_2O_3, SiO_2, and ZrO_2 because of their surface acidity.[23]

The deactivation of alkali-modified MoS_2 catalysts in a synthesis gas atmosphere is mainly due to the loss of sulfur (sulfur leaching) and coke deposition.[24] Marafi *et al.*[25] compared the deactivation behaviour of Mo/Al_2O_3 and transition metal (Ni) -promoted Mo/Al_2O_3 for hydrotreating reaction and found that transition metal promotion to Mo/Al_2O_3 reduced the tendency of coke formation. The presence of a Co (Rh)-Mo-S phase on the transition metal-promoted MoS_2 catalysts has the ability for better hydrogenation of CO, reducing the deposition of coke.[26] Courty *et al.*[27] mention that the catalyst deactivation can be reduced using 50–100 ppmv H_2S in the synthesis gas feed. Christensen *et al.*[28] concluded that the pre-sulfided alkali-promoted Co-Mo catalyst supported on activated carbon stabilizes rapidly in the presence of H_2S in the synthesis gas feed, but the presence of H_2S lowers the alcohol selectivity by enhancing hydrocarbon formation. The sintering of MoS_2 crystallites during the reaction is another possibility for catalyst deactivation, resulting in surface area decrease that leads to collapse of the internal porous structure.[29]

The advantages of activated carbon-supported catalysts are a large support surface area, limited interaction between the support and the active material, resistance to acidic or basic media, and stability at high temperatures and pressures.[30] However, the micro-porous structure (pore size < 2 nm) of activated carbon-supported catalysts results in transport limitation in the reaction and causes pore plugging due to coke formation.[31] Multi-walled carbon nanotubes (MWCNTs) display unique properties and outperform as catalyst supports due to the meso/macro porous structures that mitigate transport limitations, uniform and straight pores that allow great metal dispersion, nano-sized channel confinement that prevents metal sintering, high mechanical strength, and thermal conductivity.[32,33]

Our previous research demonstrated that the MWCNT-supported alkali-modified trimetallic Co-Rh-Mo catalyst outperformed similar catalysts supported on activated carbon in terms of activity and selectivity towards higher alcohols synthesis studied under the same experimental conditions.[15] The large-sized and straight pores facilitate uniform metal particle distribution to attain high dispersions and achieve improved performance over catalysts supported on MWCNTs. Key to the development of a commercially attractive higher alcohols production scheme from synthesis gas is to discover a highly efficient catalyst that must be highly active and stable with suitable reaction conditions during the production period. However, few publications have focused on the deactivation behavior of alkali-promoted MoS_2 catalysts. To understand the decay of catalyst activity towards CO hydrogenation and higher alcohols synthesis, it is important to study in detail the contribution of each deactivating feature on total catalyst deactivation. The present work investigates the stability of sulfided alkali-modified Co-Rh-Mo catalysts supported on MWCNTs and activated carbon during continuous higher alcohols synthesis for 720 h in a fixed-bed micro reactor.

11.3. Experimental

11.3.1. Preparation of catalysts

Both commercial catalyst supports, MWCNTs (M.K. Nano, surface area-178 m^2/g and pore volume-0.54 cc/g) and activated carbon (Aldrich, surface area-655 m^2/g and pore volume-0.93 cc/g), were treated with 30% HNO_3 reflux at 100°C overnight and washed with distilled water several times, followed by drying at 120°C for 6 h. The support, MWCNTs has a surface area of 220 m^2/g and pore volume of 0.66 cc/g,

whereas, the activated carbon support exhibits a surface area of 676 m^2/g and pore volume of 0.97 cc/g. Ammonium heptamolybdate tetrahydrate (AHM), potassium carbonate, cobalt acetate tetrahydrate, and rhodium chloride hydrate were used as precursors for Mo, K, Co, and Rh, respectively. The catalysts were prepared by conventional incipient wetness method, as described in our preceding papers.[4,8,and15]

11.3.2. Characterization of fresh and spent catalysts

The morphology of both the fresh and spent catalysts was characterized by transmission electron microscopy (TEM) investigations, using a Philips CM20 (100 kV) transmission electron microscope equipped with a NARON energy-dispersive spectrometer with a germanium detector.

The content of Mo, Co, and Rh of the oxide catalysts were determined using a Perkin-Elmer ELAN 5000 inductively coupled plasma mass spectroscopy (ICP-MS) instrument.

The surface area, pore volume, and average pore diameter of fresh catalysts in oxide and sulfide forms, as well as the spent catalysts were measured by N_2-physisorption at 77 K using a Micromeritics ASAP 2000. Approximately 0.2 g of sample was used for each analysis. The moisture and other adsorbed gases present in the sample were removed before analysis by degassing the sample at 200°C for 2 h under 66.7 Pa (500 mm Hg). The sample was then evacuated at 2.67 Pa (20 μm Hg) before N_2 adsorption.

The carbon monoxide uptake on the fresh and used catalysts was measured using the Micromeritics ASAP 2000 instrument. Prior to the CO chemisorption measurement, 0.2 g of sample was sulfided in situ, using 10 mole % H_2S in H_2 at 400 °C for 4 h. The sample was then evacuated at 120°C until the static pressure remained less than 6.6×10^{-4} Pa. Chemisorption was performed by passing pulses of CO over the sample to measure the total gas uptake at 35°C. The CO uptake (μmole/g of cat.) measured from CO chemisorption is equivalent to the number of active metal atoms that are accessible to the reactant molecules. The stoichiometric coefficient (CO to metal ratio) of 1 was used, and the extent of reduction was assumed to be 100% in metal dispersion calculations.

Powder X-ray diffraction (XRD) analysis patterns of oxide and sulfide forms of both the fresh and spent catalysts were recorded on a Rigaku X-ray diffraction instrument with nickel filtered Cu Kα radiation (λ = 0.1541 nm). Each sample was scanned at a rate of 0.05

°/s, with 2θ varying from 10 to 80°. To obtain the XRD patterns in sulfided form, the catalysts were first sulfided for 6 h at 450°C, at a heating rate of 2°C/min using a gaseous mixture containing 10 mole % H_2S in H_2 at a flow rate of 50 ml/min. After sulfidation, the catalysts were cooled to room temperature in a flow of He and the sample was transferred to sample holders under protection of He.

To study the reducibility of the fresh and spent catalysts, temperature programmed reduction (TPR) profiles of the catalysts were performed. For each analysis, approximately 0.2 g of sample was used, which was first purged in 50 cm^3 (STP)/min flow of He at 170°C to remove traces of water, and then cooled to 40°C. The TPR of each sample was performed using a 10 mole % H_2 in Ar stream at a flow rate of 50 cm^3 (STP)/min and a heating ramp rate of 10°C/min from 40°C to 650°C. Hydrogen consumption was monitored by a thermal conductivity detector (TCD) attached to a Micromeritics AutoChem II chemisorption analyzer. During the analysis the effluent gas was passed through a cold trap placed before the TCD in order to remove water from the exit stream of the reactor.

The amount of carbon deposition after 720 h of continuous higher alcohols synthesis was analyzed by performing thermogravimetric analysis (TGA) of fresh and spent catalyst using a Perkin-Elmer thermogravimetric (TG) differential thermal analyzer (DTA) under air flow of 40 ml/min. The samples were heated in a platinum sample holder from room temperature to 600°C with a heating rate of 5°C/min.

11.3.3. Catalytic durability studies

The catalytic durability studies for conversion of synthesis gas to higher alcohols were performed using the feed gas mixture CO (40 mole %), H_2 (50 mole %), and Ar (10 mole %) in a single-pass tubular downflow fixed-bed reactor under the reaction conditions of 330°C, 9.1 MPa (1320 psig), and 3.8 m^3 (STP) /(kg of cat.)/h over a period of 720 h. The detailed description about the high pressure reaction set up used in this study is as discussed in our previous papers.[4,8,and15] Prior to the reaction, the catalyst was reduced and sulfided, for 6 h at 450°C at a heating rate of 2°C/min using a gas mixture containing 10 mole % H_2S in H_2 at a flow rate of 50 ml/min. The product gas was separated into gas and liquid phases inside the condensers at 0°C and reaction pressure. The liquid products were collected from the cold traps every 12 h during the first 2 days and then obtained after every 24 h. The sulfur content of the liquid product obtained at different time intervals was

measured using the combustion-fluorescence technique of the ASTM 5463 method. The instrumental error for S analysis was approximately ±3%, based on analyzing standard solutions of known composition. The liquid products were analyzed with a Varian 3400 gas chromatograph equipped with a capillary column and a flame ionization detector (FID). The gaseous products were analyzed online on a Shimadzu gas chromatograph through a sampling valve for every 1 h. The results obtained were within the experimental error of ± 2.5%.

After 720 h of the higher alcohols synthesis, the flow of synthesis gas was switched off, and the catalyst was re-sulfided and reduced in a flow rate of 50 ml/min of 10 mole % H_2S in H_2 at 450°C for 6 h. The higher alcohols synthesis was again carried out under the same conditions, as discussed above for 24 h. The temperature of the reactor was lowered to room temperature and the catalytic bed was treated by helium flow for 3 h at room temperature to washout the H_2S and synthesis gas present inside the reactor. The catalyst was then passivated with pulses of dry air to stop further oxidation. The spent catalyst was removed from the reactor and characterized extensively.

11.4. Results and Discussion

11.4.1. Characterization of fresh and spent catalysts

TEM images of the fresh and spent alkali-modified trimetallic Co-Rh-Mo catalysts supported on MWCNTs were recorded and shown as Figs. 11.1a and 11.1b, respectively. The tubular morphology of the grapheme layers make MWCNTs a different support compared to activated carbon. The TEM image of the fresh MWCNT-supported catalyst (Fig.11.1a) revealed that the metal species are well dispersed both inside the carbon nanotubes and on the outside of the tube walls in the particle size range of 1 to 5 nm. Fig. 11.1b shows that sintering occurs on the particles located on the outer surface of the MWCNTs, whereas the size of the particles inside the tubes is almost similar to that of the fresh catalyst. The π-electron density creates a deviation in the concave inner and convex outer surface of the graphite layers, leading to an electron-deficient interior and an electron-enriched exterior surface.[34] This results in a strong interaction of metal species with the support on the particles located on the inner surface of the MWCNTs, compared to their outer layers. The little or no mobility of the particles inside the tubes prevents the occurrence of sintering.[35]

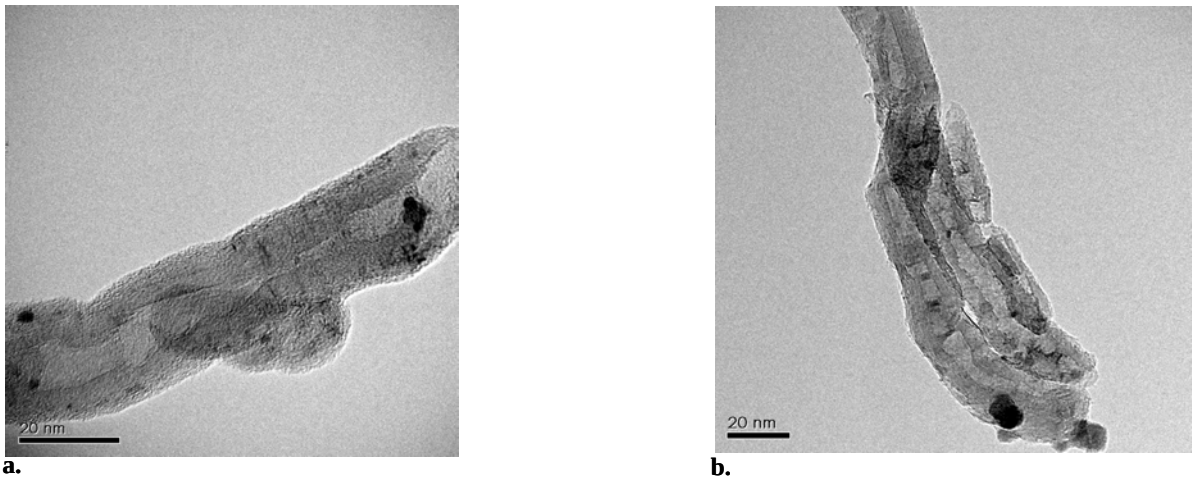

a. b.

Figure 11.1. TEM image of MWCNT-supported catalyst
a. Fresh catalyst; b. Spent catalyst

Figs. 11.2a and11.2b show the TEM images of fresh and spent Co-Rh-Mo-K catalysts supported on activated carbon. Some of the metal species are inside the pores and a considerable amount of agglomerates are formed on the surface of the microporous activated carbon support (Fig. 11.2a). The TEM image of the spent catalyst (Fig. 11.2b) shows the formation of large agglomerates, resulting from the large sintering rate of metal species on the catalyst. Iranmahboob *et al.*[36] explained that agglomeration of cobalt and sulfur takes place after exposure to synthesis gas on the catalyst surface, leading to the formation of square-like planes of cubic crystallites (Co_9S_8). These results confirm that the agglomeration of catalytic species is high on the activated carbon support compared to that of MWCNTs.

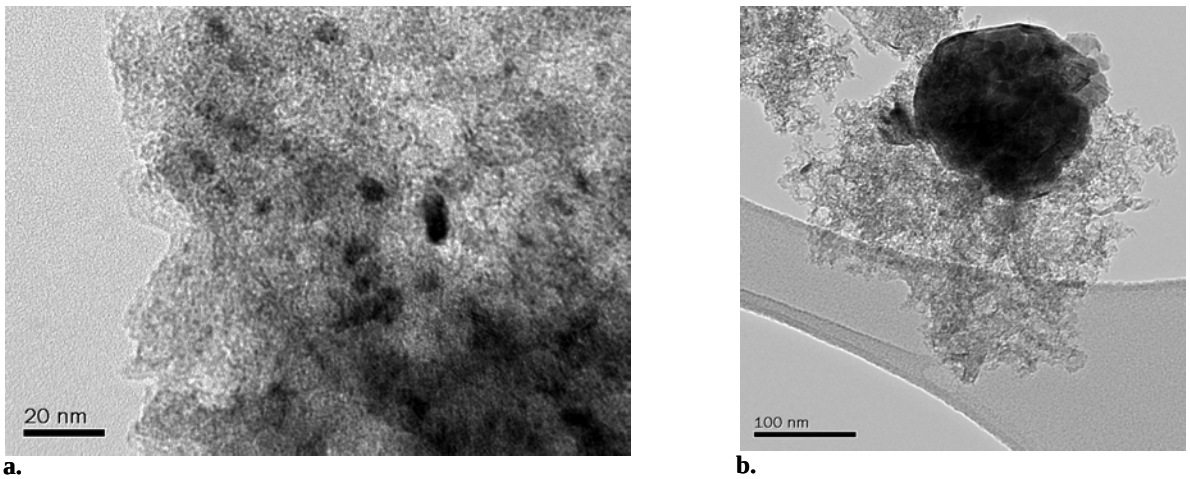

a. b.

Figure 11.2. TEM image of activated carbon-supported catalyst
a. Fresh catalyst; b. Spent catalyst

Table 11.1 presents the Co, Rh, and Mo contents of the fresh and spent catalysts measured by ICP-MS, along with the targeted compositions. Due to the hygroscopic nature of precursors, the measured contents of the catalysts are slightly low compared to targeted values. Deviation in the targeted and measured metal contents is high over the activated carbon-based catalysts compared to the MWCNT-supported catalysts, indicating that the concentration of metal particles is not uniform on this support. ICP analyses revealed that the metal content of the spent catalysts was close to that of the fresh catalysts.

Results of the textural characteristics such as surface area, total pore volume, and average pore diameter obtained over the fresh, sulfided, and spent catalysts are given in Table 11.1. The MWCNT-supported alkali-promoted trimetallic Co-Rh-Mo catalyst showed a BET surface area of 68 m^2/g and a total pore volume of 0.24 cm^3/g. Upon sulfidation of this catalyst, the BET surface area and pore volume increased to 79 m^2/g and 0.29 cm^3/g, respectively,. After 720 h of higher alcohols synthesis, both the catalyst BET surface area and pore volume decreased to 71 m^2/g and 0.26 cm^3/g, respectively. After impregnating the metal species, a drastic fall in surface area was observed over the activated carbon-supported catalyst. The activated carbon-supported alkali-promoted trimetallic catalyst showed a BET surface area and pore volume of 97 m^2/g and 0.16 cm^3/g, respectively. These results suggest that pore blocking of the activated carbon by the metal species is high compared to that of MWCNTs, due to the microporous nature of the activated carbon support.

Similar to the MWCNT-supported catalyst, sulfidation of the activated carbon-supported Co-Rh-Mo-K catalyst improved both the BET surface area and pore volume. Sulfidation causes reduction in particle size of the metal species that decreases the blocking extent of the support, resulting in improved BET surface area and pore volume. After 720 h over the spent activated carbon-supported catalyst, a BET surface area of 85 m^2/g and pore volume of 0.10 cm^3/g were observed. From these results, it is clear that sintering of the metal species and pore blockage due to coke deposition during higher alcohols synthesis is high on the activated carbon-supported catalyst, causing a large decrease in both BET surface area and pore volume, compared to that of the MWCNT-supported catalyst.

Table 11.1 also gives the results of the CO chemisorption measurements. The CO uptake on the fresh alkali-modified Co-Rh-Mo trimetallic catalysts supported on MWCNTs and activated carbon was 237 and 137 μmole/(g of cat.), respectively.

The MWCNT- supported catalyst outperformed the activated carbon-supported catalyst, confirming that the support plays an important role on CO hydrogenation capability. Metal dispersions observed on the alkali-modified trimetallic catalysts supported on MWCNTs and activated carbon were 48% and 28%, respectively. MWCNTs have the advantage of well-defined hollow interiors and uniform straight pores with a large pore size, providing uniform distribution of metal species to obtain high dispersion on the support.[37]

The CO uptake value and metal dispersion for the spent catalyst supported on MWCNTs are slightly lower (7% and 6%, respectively) than that of the fresh catalyst. The spent catalyst supported on activated carbon was found to be 43% less in both CO uptake value and dispersion of metal species compared to that of the fresh catalyst. As mentioned earlier, sintering of metal species and pore blockage due to coke deposition might be responsible for low metal dispersions of the spent catalyst supported on activated carbon.

Figs. 11.3 and 11.4 show the XRD patterns of the MWCNTs and activated carbon-supported alkali-modified trimetallic Co-Rh-Mo catalysts measured in oxidized and sulfided form, together with the spent catalysts after 720 h of higher alcohols synthesis. The JCPDS chemical spectra data bank was used to detect the most probable phases present in the samples.

The results of the possible crystal phases with their corresponding reflection planes are given in Table 11.2. The reflections of the graphite phase are observed at d spacing of 3.347 in both the MWCNTs and activated carbon supports.[38] The characteristic reflections corresponding to the crystalline structure of MoO_3 are observed at 2θ value of 40.2° in the XRD patterns of the oxidized form of catalysts supported on MWCNTs and activated carbon.[39] Peaks corresponding to the characteristic reflections of different K-Mo-O phases, such as KMo_4O_6 (d-spacing of 5.366 and 2.403), $K_2Mo_7O_{20}$ (d-spacing of 3.770), and $K_2Mo_2O_7$ (d-spacing of 3.222) are also observed.[40-42] The formation of MoS_2 crystallites are observed at d-spacing of 6.110, 2.707, 2.199, and 1.570 in the XRD pattern of the sulfided catalysts (Figs. 11.3b and 11.4b).[43] The characteristic reflections of the K-Mo-S species are observed at d-spacing of 3.100, 3.020, and 2.780.[44] The peak corresponding to the characteristic of bulk Co_9S_8 particles is observed at d-spacing of 1.751.[45] XRD patterns of the spent catalysts supported on MWCNTs and activated carbon are shown in Figs. 11.3c and 11.4c, respectively.

Table 11.1. Elemental compositions, textural properties, and chemisorption measurement results

Catalyst	Targeted composition (wt %)				Measured composition (wt %)			BET surface area (m^2/g)	Total pore volume (cc/g)	Average pore diameter (nm)	CO uptake (μmole/g of cat.)	Dispersion of metals (%)
	K	Mo	Rh	Co	Mo	Rh	Co					
Fresh catalyst supported on MWCNT	9	15	1.5	4.5	14.3	1.2	4.2	68	0.24	17.9	--	--
Sulfided catalyst supported on MWCNT	9	15	1.5	4.5	--	--	--	79	0.29	16.7	237	47.8
Spent catalyst supported on MWCNT	9	15	1.5	4.5	14.1	1.3	4.0	71	0.26	17.4	221	44.7
Fresh catalyst supported on AC	9	15	1.5	4.5	13.7	0.8	3.8	97	0.16	7.2	--	--
Sulfided catalyst supported on AC	9	15	1.5	4.5	--	--	--	111	0.21	6.4	137	27.7
Spent catalyst supported on AC	9	15	1.5	4.5	13.8	0.6	3.4	85	0.10	8.1	78	15.8

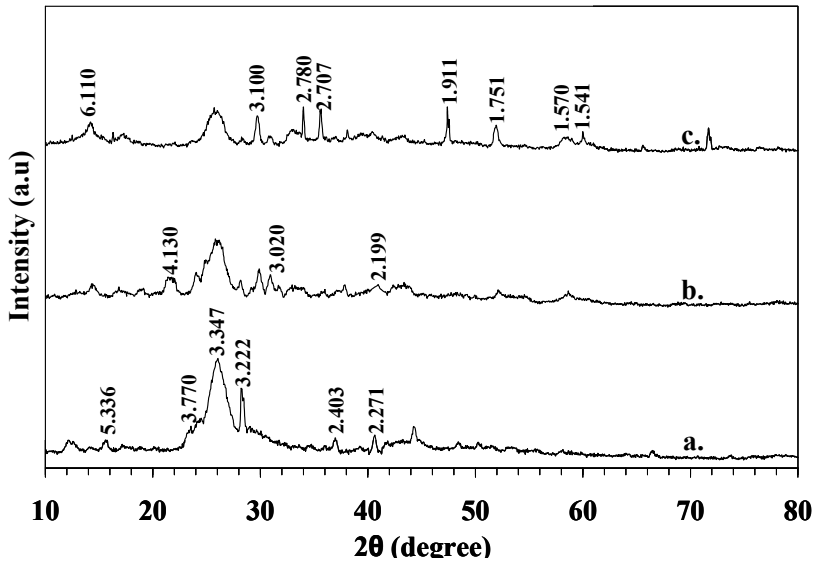

Figure 11.3. XRD patterns of MWCNT-supported catalyst
a. Fresh catalyst; b. Sulfided catalyst; c. Spent catalyst

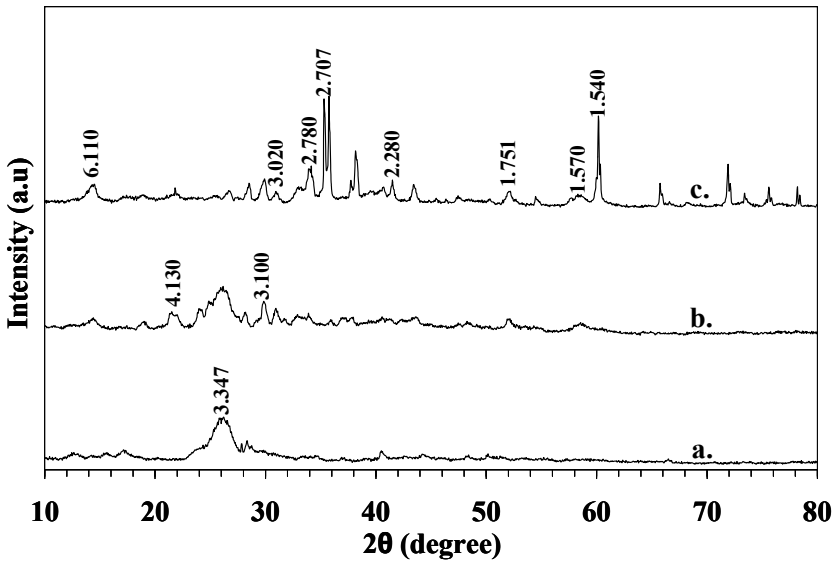

Figure 11.4. XRD patterns of activated carbon-supported catalyst
a. Fresh catalyst; b. Sulfided catalyst; c. Spent catalyst

Table 11.2. Crystal phases and reflection planes from XRD

Crystal phase	2θ	d-spacing	Reflection plane h k l
Graphite (C)	26.6°	3.347	1 1 1
MoO_3	40.7°	2.271	1 5 0
KMo_4O_6	15.8°	5.336	1 1 0
$K_2Mo_7O_{20}$	23.6°	3.770	1 0 2
$K_2Mo_2O_7$	28.5°	3.222	0 0 2
KMo_4O_6	37.1°	2.403	4 0 0
MoS_2	14.6°	6.110	0 0 3
MoS_2	33.4°	2.707	1 0 1
MoS_2	40.9°	2.199	0 1 5
MoS_2	58.9°	1.570	1 1 0
MoS_2	60.0°	1.541	0 0 3
$K_{0.4}MoS_2$	21.5°	4.130	0 0 4
KMo_3S_3	28.7°	3.100	1 1 1
K_2MoS_4	29.9°	3.020	3 0 1
K_2MoS_4	31.1°	2.780	3 0 2
Co_9S_8	47.9°	1.911	5 1 1
Co_9S_8	52.4	1.751	4 4 0

There is no significant change in the intensity of the peaks corresponding to the K-Mo-S mixed phases, but increased peak intensities of the MoS_2 and Co_9S_8 phases were observed. These results confirm that sintering of metal sulfide crystallites such as MoS_2 and Co_9S_8 takes place upon exposure to the synthesis gas, leading to the agglomeration of these species on the support. Compared to the MWCNT-supported spent catalyst (Fig. 11.3c) , a significant increase in peak intensity for the MoS_2 and Co_9S_8 species is noted in the spent catalyst supported on activated carbon (Fig. 11.4c) ,indicating that particle size increased with time on stream for 720 h. This may be due to the sintering of metallic particles during the reaction, as a result of the poor interaction between metal particles and the support.

The activation of the fresh and spent alkali-modified trimetallic Co-Rh-Mo catalysts supported on MWCNTs and activated carbon in a hydrogen atmosphere was proven by TPR experiments and shown in Figs. 11.5 and 11.6, respectively. The H_2-TPR studies of the fresh catalyst supported on MWCNTs (Fig. 11.5a) reveal the main reduction peak at 328°C, due to the complete reduction of bulk MoO_3 species to lower oxidation state.[46] A shoulder peak in the temperature range 250-300°C is due to the reduction of bulk CoO_3-related species.[47] A small peak attributed to the reduction of Rh species is noted in the temperature range 97°C.[11] Over the spent catalyst supported on MWCNTs (Fig. 11.5b), the reduction of Mo species took place in two different steps; first the reduction of octahedral coordinated Mo (Mo^{+6}) species to tetrahedral coordinated Mo (Mo^{+4}) species occurs at 326°C, followed by the reduction of Mo^{+4} species to a lower oxidation state at 601°C.[48] The peak corresponding to the reduction of Co species shifted to a lower temperature of 197°C, indicating that the easier reduction of the cobalt occurred in the spent catalyst compared to the fresh.

The easier reduction of Co species can be explained by the formation larger particles on the outer surface of the nanotubes, which is evident from TEM image of the spent catalyst supported on MWCNTs (Fig. 11.1b). No peaks corresponding to the reduction of Rh species were present, indicating that Rh exists in completely reduced form over the spent catalyst. These results coupled with and the XRD pattern (Fig. 11.3c) confirm that the sintering of Co species is high after exposure of synthesis gas on the catalyst surface, whereas the Mo and Rh species are quite stable with little or no sintering over the alkali-promoted trimetallic Co-Rh-Mo catalyst supported on MWCNTs.

Two main reduction peaks are observed in the TPR studies of the fresh activated carbon-supported alkali-modified trimetallic Co-Rh-Mo catalyst (Fig. 11.6a), with the low temperature reduction peak appearing around 321°C and the high temperature peak around 640°C. No peak is observed representing the reduction of Co species, but the small peak at 94°C represents the reduction of Rh species. The peak representing the reduction of Mo^{+6} to Mo^{+4} oxidation state shifted to higher temperatures over the spent catalyst supported on activated carbon (Fig. 11.6b). These results indicate that the interaction of Mo species occurred with the activated carbon support after the catalyst was exposed to synthesis gas. Compared to the fresh catalyst, an extra peak was observed at 216°C representing the presence of Co species over the spent catalyst supported on activated carbon. As seen from the TEM image (Fig. 11.2b) and XRD patterns (Fig. 11.4c) of the spent catalyst, agglomeration of metal species were found to be high on the surface of activated carbon, due to the sintering of active phases.

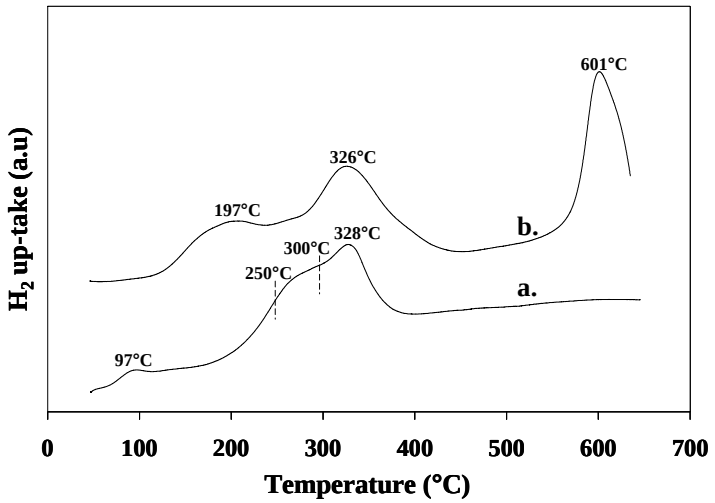

Figure 11.5. H_2 - TPR profiles of MWCNT-supported catalyst
a. Fresh catalyst; b. Spent catalyst

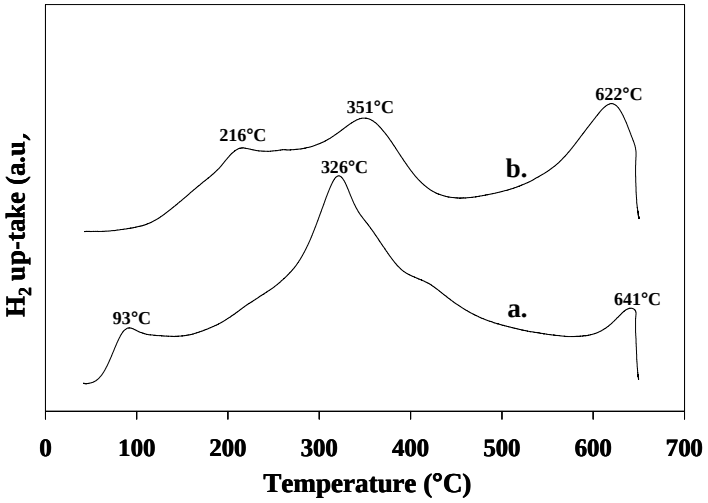

Figure 11.6. H_2 - TPR profiles of activated carbon-supported catalyst
a. Fresh catalyst; b. Spent catalyst

The thermo-gravimetric (TG) profiles of the temperature-programmed oxidation (TPO) in air of the fresh and spent catalysts supported on MWCNTs are shown in Fig. 11.7. The slight weight loss over the catalysts occurring at around 100°C was probably resulted from the evaporation of moisture. The weight loss over the MWCNT-supported spent catalyst (Fig. 11.7b) in the range of 100 to 400°C might be due to the oxidization of S species. However, the carbon deposits were oxidized at around 450–600°C (Fig. 11.7a and

11.7b). The TG profiles of the fresh and spent catalysts supported on activated carbon revealed that activated carbon support is more susceptible to coke formation and deactivation (Figs 11.8a and 11.8b). These result confirmed that coke deposition is high on the activated carbon-supported catalyst compared to that of the catalyst supported on MWCNTs.

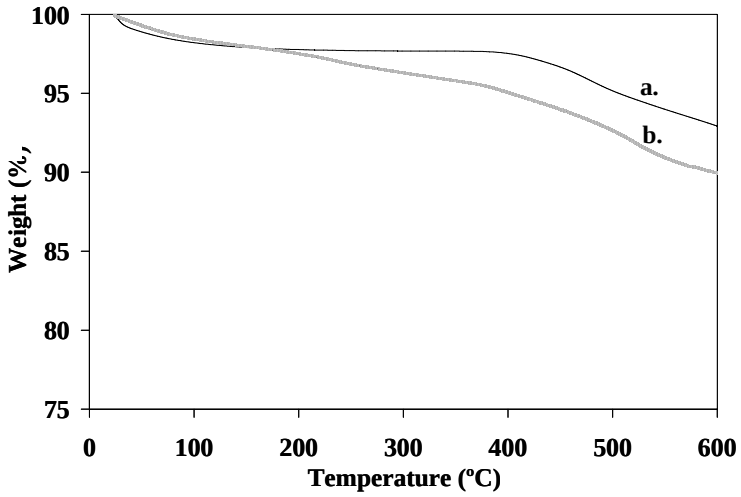

Figure 11.7. TG profiles of MWCNT-supported catalyst
a. Fresh catalyst; b. Spent catalyst

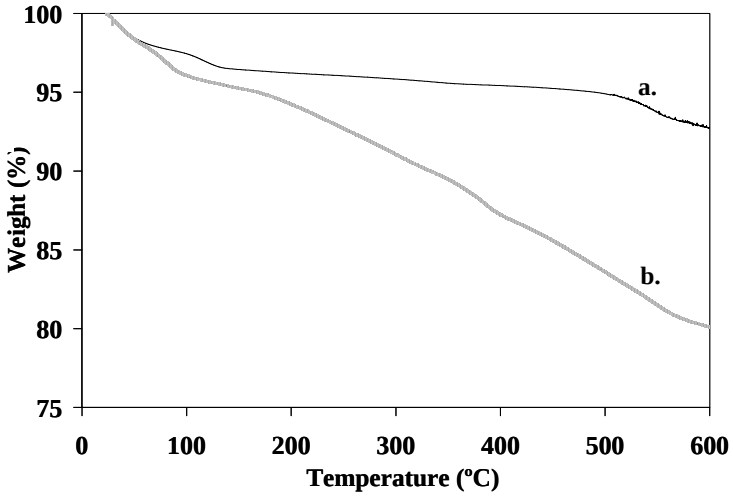

Figure 11.8. TG profiles of activated carbon-supported catalyst
a. Fresh catalyst; b. Spent catalyst

11.4.2. Catalytic durability studies

The sulfided alkali-promoted trimetallic Co-Rh-Mo catalysts supported on MWCNTs and activated carbon were tested for the synthesis of higher alcohols from synthesis gas under similar conditions of 330°C, 9.1 MPa (1320 psig), and 3.8 m^3 (STP)/(kg of cat.)/h.

The profiles of % CO conversion as functions of time on stream for 720 h, with a synthesis gas feed containing 40 mole % CO, 50 mole % H_2, and 10 mole % Ar obtained over alkali-modified trimetallic Co-Rh-Mo catalysts supported on MWCNTs and activated carbon are shown in Figs. 11.9a and 11.9b, respectively. Over the MWCNT-supported catalyst, two different deactivation steps are observed; the % CO conversion dropped by 10% (from 58% to 52%) during the first 12 h and remained almost constant with % CO conversion dropping by only 1.9% for the remaining time-on-stream of higher alcohols synthesis. Three different deactivation steps are distinguishable over the activated carbon-supported catalyst (1) during the first 36 h, the % CO conversion dropped by 21% (from 43% to 34%); (2) during 36 to 350 h, the % CO conversion dropped by 9% (from 34% to 31%); and (3) during 350 to 720, the % CO conversion dropped by 3% and almost reached a plateau region.

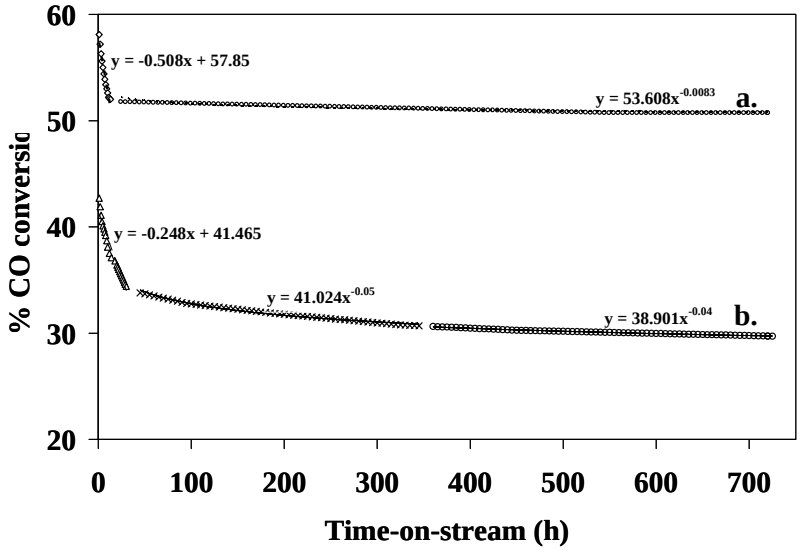

Figure 11.9. % CO Conversion with time-on-stream a. MWCNT-supported catalyst; b. activated carbon-supported catalyst

(wt. of the cat. = 2 g, P = 9.1 MPa, T = 330°C, GHSV = 3.8 m^3(STP)/h/(kg of cat.)/h, H_2 to CO molar ratio = 1.25)

The loss of activity over the MWCNT-supported catalyst for the two deactivation steps can be simulated with the following linear correlation:

$$X_{CO} = -0.508 * T + 57.85,\ T < 12 \text{ h} \quad \text{.....(11.1)}$$

$$X_{CO} = 53.608 * T^{-0.01},\ 12 \text{ h} < T < 720 \text{ h} \quad \text{.....(11.2)}$$

where, X_{CO} represents the % CO conversion (mole %), and T represents time-on-stream (h).

During the first 12 h, the deactivation curve is steeply sloped, which can be explained from two different factors: first, when the catalyst surface comes into contact with the synthesis gas, the catalyst bed temperature increases about 10ºC, due to the exothermic nature of the CO hydrogenation reaction, causing the initial higher CO conversions and reaching steady state after the temperature reaches the set point. The second factor that contributes to the reduction of % CO conversion is the significant loss of sulfur from the catalyst surface. The sulfur concentration of the alcohol samples collected after a 12 h reaction period was high (75 ppm) and the concentration of sulfur present in the samples decreased with time-on-stream. The samples obtained after a 48 h reaction period were sulfur free. Ratnasamy et al.[49] explained that the loss of sulfur from sulfided Mo-based catalysts occurs due to the formation of unstable negative charge sulfur ions located at the edge of MoS_2 crystallites. The transition metal promoters incorporate cations such as, Co^{2+} or Rh^{+2} at the edges of the MoS_2 sheet and increased the structural stability to the MoS_2, suppressing the excessive formation of anion vacancies at crystallite edges. From the XRD patterns of the alkali-modified trimetallic Co-Rh-Mo catalysts, sulfide phases such as MoS_2 and Co_9S_8 were observed. The loss of sulfur from the metallic sulfide sites resulted in reduced hydrogen adsorption, which decreased the CO conversion during the initial reaction period. The second step catalyst deactivation can be attributed to the sintering of the catalyst species located on the outer surfaces of the carbon nanotubes, as observed from the TEM image of the spent catalyst (Fig. 11.1b).

Over the activated carbon-supported catalyst, the % CO conversion significantly decreased during the first 350 h of continuous higher alcohols synthesis. As seen from Fig. 11.9b, different profiles of three step catalyst deactivations were observed over this catalyst. The deactivation of the catalyst is high for the first step, then moderates for the second step, and slowly levels off for the final step. The following linear correlations are simulated to represent the loss of activity over the activated carbon-supported catalyst for these three deactivation steps:

$$X_{CO} = -0.248 * T + 57.85,\ T < 30\ \text{h} \quad (11.3)$$

$$X_{CO} = 41.024 * T^{-0.05},\ 30\ \text{h} < T < 350\ \text{h} \quad (11.4)$$

$$X_{CO} = 38.901 * T^{-0.04},\ 350\ \text{h} < T < 720\ \text{h} \quad (11.5)$$

The initial deactivation is high in the activated carbon-supported catalyst, due to the excessive loss of sulfur from the catalyst surface to the liquid product. The sulfur concentration observed in the liquid product after 12 h time-on-stream of higher alcohols reaction over this catalyst was 223 ppm and dropped to 42 ppm after 36 h. These results suggest that the presence of unstable sulfur ions are high on the metal sulfide crystallites supported on activated carbon compared to that of MWCNTs. The power law expressions (eqs. 11.4 and 11.5) were used to explain the second and the third deactivation steps, which occurred mainly due to the sintering of metal species[35]. It is clear from these equations that the rate of sintering during the second deactivation step was significantly higher than during the third step. The deactivation of the catalyst supported on activated carbon was high compared to the MWCNT-supported catalyst. Characterization of the spent catalyst supported on activated carbon revealed that deactivation occurs due to the large sintering rate of catalyst species (especially metal sulfides) that causes low metal dispersions and high pore blockage of the support.

Figs. 11.10a and 11.10b present the total alcohols STY changes with time on stream of continuous higher alcohols synthesis for a period of 720 h obtained over alkali-modified trimetallic Co-Rh-Mo catalysts supported on MWCNTs and activated carbon, respectively., The total alcohols STY increased from 0.256 g/(g of cat.)/h after a 12 h reaction period to 0.281 g/(g of cat.)/h after 24 h over the MWCNT-supported catalyst and remained almost constant over the remaining reaction time (Fig. 11.10a). The improved formation of total alcohols after the induction period of 12 h can be explained from the gradual spreading of the alkali promoter across the catalytic surface.[28] Using X-ray photoelectron spectroscopy, Iranmahboob et al.[36] observed the surface enrichment of the alkali promoter on K-Co-MoS_2/Clay catalysts after exposure to synthesis gas. The STY of total alcohols over the activated carbon-supported catalyst, increased from 0.194 to 0.209 g/(g of cat.)/h for samples collected from 12 to 36 h of time-on-stream, and decreased slowly to 0.193 g/(g of cat.)/h before it leveled off (Fig. 11.10b). As observed from the TEM image (Fig 11.1b), the decreased yield of total alcohols after 36 h might be due to the limited accessibility of active phases to the reactants due to pore blockage of the activated carbon support.

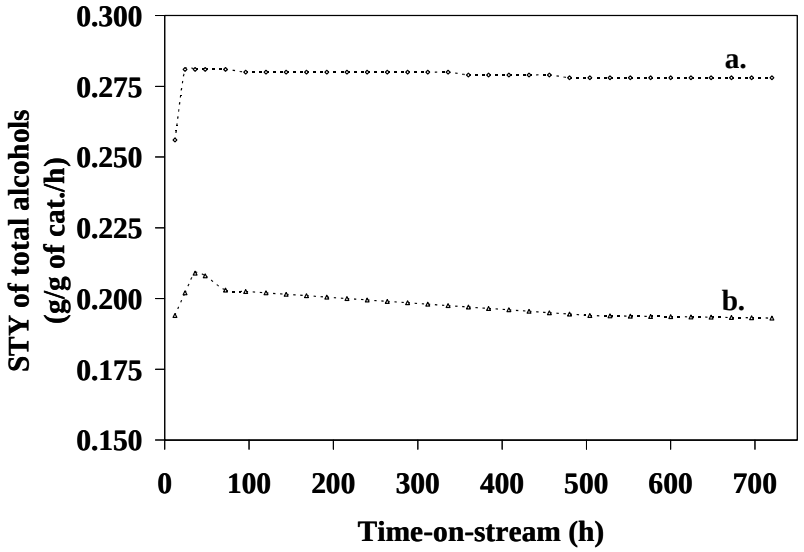

Figure 11.10. Total alcohols STY with time-on-stream
a. MWCNT-supported catalyst; b. activated carbon-supported catalyst

(wt. of the cat. = 2 g, P = 9.1 MPa, T = 330°C, GHSV = 3.8 m^3(STP)/h/(kg of cat.)/h, H_2/CO molar ratio = 1.25)

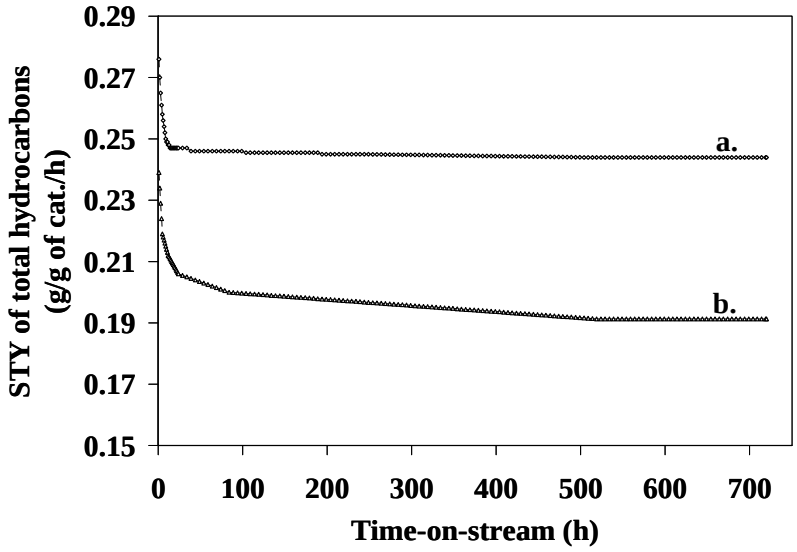

Figure 11.11. Total hydrocarbons STY with time-on-stream
a. MWCNT-supported catalyst; b. activated carbon-supported catalyst

(wt. of the cat. = 2 g, P = 9.1 MPa, T = 330°C, GHSV = 3.8 m^3(STP)/h/(kg of cat.)/h, H_2/CO molar ratio = 1.25)

The change in total hydrocarbon STY with time-on-stream for a continuous reaction time of 720 h over the alkali-modified trimetallic catalysts supported on MWCNTs and activated carbon are given in Figs. 11.11a and 11.11b, respectively. Fig. 11.11a shows that during the first 12 h reaction time, the total hydrocarbon STY decreased from 0.276 to 0.249 g/(g of cat.)/h and remained almost steady state in the next 710 h over the catalyst supported on MWCNTs. A rapid decrease in the STY of total hydrocarbons from 0.239 to 0.206 g/(g of cat.)/h occurred during the first 30 h of time-on-stream and then slowly leveled off to a constant value of 0.191 g/(g of cat.)/h (Fig. 11.11b). The initial decrease in total hydrocarbons STY might be explained from the loss of sulfur from unstable metal sulfide crystallites on the surface of the catalyst to the products and the sintering of catalyst species is responsible for the later steps. Metal sulfide sites favour the adsorption of hydrogen adsorption, which leads to the formation of hydrocarbons.[50]

The CO_2 produced in the reactor during 720 h of continuous operation over the MWCNTs and activated carbon-supported catalysts are reported in Figs. 11.12a and 11.12b, respectively. The water-gas-shift (WGS) reaction rate was almost constant during the entire reaction period over the MWCNT-supported catalyst, whereas over the catalyst supported on activated carbon a drastic fall was noticed in the WGS reaction for first 30 h and then slowly leveled off to a constant value due to pore blockage of the support due to the sintering of catalyst species.

Regeneration of the spent catalyst at 450°C increased the % CO conversion from 51 to 56% and over the catalysts supported on MWCNTs and activated carbon it increased from 29 to 36%, respectively. The total activity recovery over the MWCNTs and activated carbon-supported catalysts after regeneration is close to the total activity loss during the first deactivation step (about 10% and 19%, respectively). The addition of Co (Rh) to MoS_2 catalysts leads to the formation of active phase Co (Rh)-Mo-S that has a dual promotion effect of enhancing the activity by increasing S-vacancies and reducing the deposition of coke due to the improved hydrogenation rate of the coke ingredients.[51] The catalyst deactivation that occurred after the first step is due to the sintering of metal sulfide species on the support, which is an irreversible process.[49] Baghalha et al.[26] observed the loss of the Co-Mo-S active phase during hydrodesulfurization of a naphtha stream that caused about 19% of permanent catalyst activity deactivation during the first deactivation step. Our results demonstrate that the permanent loss of the active phase was negligible over the alkali-promoted trimetallic catalyst for higher alcohols synthesis and the

recoverable activity loss can be assigned to the loss of unstable sulfur ions from the edges of metal sulfide crystallites. This study revealed that MWCNT is a novel catalyst support to decrease sintering, metal support interaction and coke formation during catalytic process.

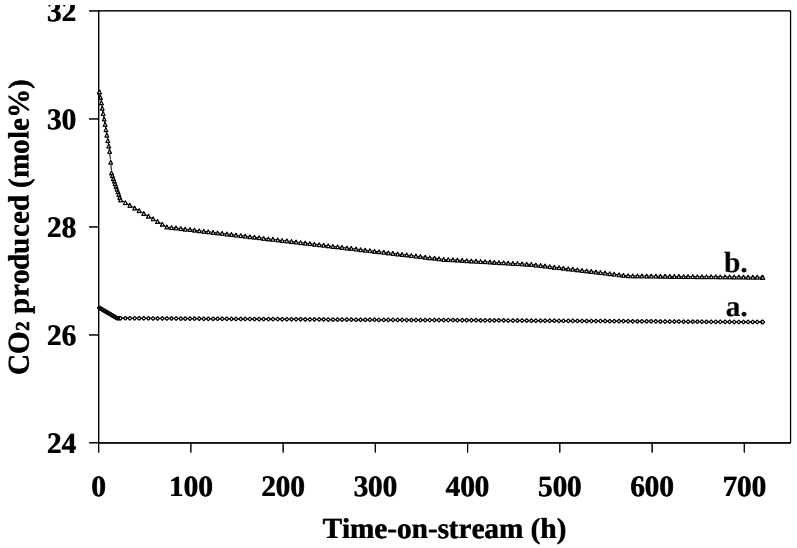

Figure 11.12. Water-gas-shift reaction rate with time-on-stream a. MWCNT-supported catalyst; b. activated carbon-supported catalyst

(wt. of the cat. = 2 g, P = 9.1 MPa, T = 330°C, GHSV = 3.8 m^3(STP)/h/(kg of cat.)/h, H_2/CO molar ratio = 1.25)

11.5. Conclusions

The alkali-promoted trimetallic Co-Rh-Mo catalyst supported on MWCNTs has shown two different deactivation steps during 720 h of continuous reaction: loss of sulfur from the catalyst surface and sintering of the catalyst species located on the outer surfaces of the carbon nanotubes. After regeneration, the total activity recovery (about 10%) is close to the total activity loss during the first deactivation step over this catalyst. Deactivation of the catalyst supported on activated carbon was high compared to the MWCNT-supported catalyst. Characterization of the spent catalyst supported on activated carbon revealed that deactivation occurs due to the large sintering rate of catalyst species (especially metal sulfides) that causes low metal dispersions and high pore blockage of the support. The total hydrocarbons formation decreased rapidly during the first deactivation step and slowly leveled off. The initial decrease in total hydrocarbons STY might be explained from the loss of sulfur from unstable metal sulfide crystallites on the surface of the catalyst to the products and sintering of the catalyst species is responsible for the later

steps. The sulfided catalyst supported on MWCNTs showed excellent reaction stability for the synthesis of higher alcohols from synthesis gas, whereas slight reduction in total alcohols formation was observed on the activated carbon-supported catalyst. This study revealed that MWCNTs is a novel catalyst support to decrease sintering, metal support interaction and coke formation during catalytic process.

11.6. Abbreviations

GHSV	Gas hourly space velocity
ICP-MS	Inductively coupled plasma – mass spectroscopy
MWCNTs	Multi-walled carbon nanotubes
STY	Space time yield
TEM	Transmission electron microscopy
TPR	Temperature programmed reduction
WGS	Water-gas-shift
XRD	X-ray diffraction

11.7. References

1. Ma, L.; Wainwright, M. S. Development of skeletal copper–chromia catalysts I. Structure and activity promotion of chromia on skeletal copper catalysts for methanol synthesis. *Appl. Catal., A* **1999**, *187*, 89–98.
2. Smith, K. J.; Anderson, R. B. The higher alcohol synthesis over promoted copper/zinc oxide catalysts. *Can. J. Chem. Engg.* **1983,** *61*, 40–45.
3. Breman, B.B.; Beenackers , A. A. C. M.; Schuurman, H. A.; Oesterholt, E. Kinetics of the gas-slurry methanol-higher alcohol synthesis from $CO/CO_2/H_2$ over a Cs-$Cu/ZnO/A1_2O_3$ catalyst, including simultaneous formation of methyl esters and hydrocarbons. *Catalysis Today* **1995**, *24*, 5-14.
4. Surisetty, V. R.; Tavasoli, A.; Dalai, A. K. Synthesis of higher alcohols from syngas over alkali promoted MoS_2 catalysts supported on multi-walled carbon nanotubes. *Appl. Catal. A* **2009**, *365*, 243-51.

5. Woo, H. C.; Park, K.Y.; Kim, Y. G.; Namau, I-S.; ShikChung, J.; Lee, J. S. Mixed alcohol synthesis from carbon monoxide and dihydrogen over potassium-promoted molybdenum carbide catalysts. *Appl. Catal.* 75 (1991) 267-280.

6. Tatsumi, T.; Muramatsu, A.; Yokota, K.; Tominga, H. Mechanistic study on the alcohol synthesis over molybdenum catalysts : Addition of probe molecules to CO---H_2. *J. Catal.* **1989**, *115*, 388-398.

7. Liu, Z.; Li, X.; Close, M. R.; Kugler, E. L.; Petersen, J. L.; Dadyburjor, D. B. Screening of alkali-promoted vapor-phase-synthesized molybdenum sulfide catalysts for the production of alcohols from synthesis gas. *Ind. Eng. Chem. Res.* **1997**, *36*, 3085–3093.

8. Surisetty, V. R.; Dalai, A. K.; Kozinski, J. Effect of Rh promoter on MWCNT-supported alkali-modified MoS2 catalysts for higher alcohols synthesis from CO hydrogenation. *Appl. Catal., A* **2010**, *381*, 282–288.

9. Vit, Z.; Cinibulk, J.; Gulkova, D. Promotion of Mo/Al2O3 sulfide catalyst by noble metals in simultaneous hydrodesulfurization of thiophene and hydrodenitrogenation of pyridine: a comparative study. *Appl. Catal., A* **2004**, *272*, 99–107.

10. Lamber, R.; Jaeger, N. I. Formation of bimetallic Rh-Mo crystallites supported on SiO_2 by decomposition of a heteronuclear cluster precursor. *Catal. Letters* **1991**, *11*, 1–10.

11. Li, Z-R.; Fu, Y-L.; Jiang M. Structures and performance of Rh–Mo–K/Al_2O_3 catalysts used for mixed alcohol synthesis from synthesis gas. *Appl. Catal., A* **1999**, *187*, 187–198.

12. Sudhakar, C.; Bhore, N. A.; Bischoff, K. B.; Manogue, W. H.; Mills, G. A. In: Proc. 10^{th} Meeting of the Catalysis Society of North America, San Diego, CA, 1987.

13. van Den Berg, F. G. A.; Glezer, J. H. E.; Sachtler, W. M. H. The role of promoters in CO/H_2 reactions: Effects of MnO and MoO_2 in silica-supported rhodium catalysts. *J. Catal.* **1985**, *93*, 340-352.

14. Storm, D. A. The production of higher alcohols from syngas using potassium promoted Co/Mo/$A1_2O_3$ and Rh/Co/Mo/$A1_2O_3$. *Top. Catal.* **1995**, *2*, 91-101.

15. Surisetty, V. R.; Dalai, A. K.; Kozinski, J. Alkali-promoted trimetallic Co-Rh-Mo sulfide catalysts for higher alcohols synthesis from synthesis gas: Comparison of

MWCNT and activated carbon supports. *Ind. Eng. Chem. Res.* **2010**, *49*, 6956-6963.

16. Li, Z.; Fu, Y.; Bao, J.; Jiang, M.; Hu, T.; Liu, T.; Xie, Y-N. Effect of cobalt promoter on Co–Mo–K/C catalysts used for mixed alcohol synthesis. *Appl. Catal., A* **2001,** *220*, 21–30.
17. Sun, M.; Nelsona, A. E.; Adjaye, J. On the incorporation of nickel and cobalt into MoS_2-edge structures. *J. Catal.* **2004**, *226*, 32–40.
18. Petrov, L.; Kumbilieva, K. Kinteic studies of catalyst deactivation in heterogeneous catalysis (Review). *J. Univ. Chem. Technol. Metallurgy* **2006**, *41*, 5–14.
19. Bartholomew, C. H. Catalyst deactivation and regeneration. *Chem. Inform.* **2007**, *38*, 1522-2667.
20. Bartholomew, C. H. Carbon deposition in steam reforming and methanation. *Catal. Rev. Sci. Eng.* **1982**, *24*, 67–112.
21. Besenbacher, F.; Chorkendorff, I.; Clausen, B. S.; Hammer, B.; Molenbroek, A. M.; Norscov, J. K.; Stensgaard, I. Design of a surface alloy catalyst for steam reforming. *Science* **1998**, *279*, 1913–1915.
22. Bitter, J. H.; Seshan, K.; Lercher, J. A. Deactivation and coke accumulation during CO_2/CH_4 reforming over Pt catalysts. *J. Catal.* **1999**, *183*, 336–343.
23. Kogelbauer, A.; Goodwin, J. G.; Oukaci, R. Ruthenium promotion of Co/Al_2O_3 Fischer–Tropsch catalysts *J. Catal.* **1996**, *160*, 125–133.
24. Bian, G-Z.; Fu, Y-L.; Yamada, M. Reaction stability and structure studies of sulfided $K\text{-}MoO_3/\gamma\text{-}Al_2O_3$ catalyst for the synthesis of mixed alcohols. *Appl. Catal., A* **1996**, *144*, 79–91.
25. Marafi, A.; Hauser, A.; Stanislaus, A. Deactivation patterns of Mo/Al_2O_3, $Ni\text{-}Mo/Al_2O_3$ and $Ni\text{-}MoP/Al_2O_3$ catalysts in atmospheric residue hydrodesulphurization. *Catal. Today* **2007**, *125*, 192–202.
26. Baghalha, M.; Hoseini, S. M. Long-term deactivation of a commercial $CoMo/\gamma\text{-}Al_2O_3$ catalyst in hydrodesulfurization of a naphtha stream. *Ind. Eng. Chem. Res.* **2009**, *48*, 3331-3340.

27. Courty, P.; Chaumette, P.; Rimbault, C.; Travers, P. Production of methanol-higher alcohol mixtures from natural gas via syngas chemistry. *Oil Gas Sci. Technol.* **1990**, *45*, 561–578.

28. Christensen, J. M.; Mortensen, P. M.; Trane, R.; Jensen, P. A.; Jensen A. D. Effects of H_2S and process conditions in the synthesis of mixed alcohols from syngas over alkali promoted cobalt-molybdenum sulfide. *Appl. Catal., A* **2009**, *366*, 29–43.

29. Pedraza, F.; Fuentes, S.; Vrinat, M.; Lacroix, M. Deactivation of MoS_2 catalysts during the HDS of thiophene. *Catal. Letters* **1999**, *62*, 121–126.

30. Duchet, J. C.; van Oers, E. M.; de Beer, V. H. J.; Prins, R. Carbon-supported sulfide catalysts. *J. Catal.* **1983**, *80*, 386–402.

31. Kaluza, L.; Zdrazil, M. Carbon-supported Mo catalysts prepared by a new impregnation method using a MoO_3/water slurry: saturated loading, hydrodesulfurization activity and promotion by Co. *Carbon* **2001**, *39*, 2023–2034.

32. Xiaoming, M.; Guodong, L.; Hongbin, Z. Co-Mo-K sulfide-based catalyst promoted by multiwalled carbon nanotubes for higher alcohol synthesis from syngas. *Chinese J. Catal.* **2006**, *27*, 1019–1027.

33. Kennedy, L. J.; Vijaya, J. J.; Sekaran, G.; Joseph, J.; Rani, J. D.; Pragasam, J. Bulk preparation and characterization of mesoporous carbon nanotubes by catalytic decomposition of cyclohexane on sol–gel prepared Ni–Mo–Mg oxide catalyst. *Materials Letters* **2006**, *60*, 3735–3740.

34. Chen, W.; Fan, Z.; Pan, X.; Bao, X. Effect of confinement in carbon nanotubes on the activity of Fischer-Tropsch iron Catalyst, *J.Am.Chem.Soc*, **2008**, *130*, 9414–9419.

35. Tavasoli, A.; Tre´panier, M.; Dalai, A. K.; Abatzoglou, N. Effects of confinement in carbon nanotubes on the activity, selectivity, and lifetime of Fischer-Tropsch Co/carbon nanotube catalysts. *J. Chem. Eng. Data* **2010**, in press.

36. Iranmahboob, J.; Toghiani, H.; Hill, D. O. Dispersion of alkali on the surface of Co-MoS_2/clay catalyst: a comparison of K and Cs as a promoter for synthesis of alcohol. *Appl.Catal. A* **2003**, *247*, 207–218.

37. van Steen, E.; Prinsloo, F. F. Comparison of preparation methods for carbon nanotubes supported iron Fischer–Tropsch catalysts. *Catal. Today* **2002**, *71*, 327–334.

38. Eswaramoorthi, I.; Sundaramurthy, V.; Das, N.; Dalai, A. K.; Adjaye, J. Application of multi-walled carbon nanotubes as efficient support to NiMo hydrotreating catalyst. *Appl. Catal. A* **2008**, *339*, 187–195.

39. Li, Z.; Fu, Y.; Jiang, M.; Hu, T.; Liu, T.; Xie, Y. Active carbon supported Mo–K catalysts used for alcohol synthesis. *J. Catal.* **2001**, *199*, 155–161.

40. Jiang, M.; Bian, G-Z.; Fu, Y-L. Effect of the K---Mo interaction in K---MoO_3/γ-Al_2O_3 catalysts on the properties for alcohol synthesis from syngas. *J. Catal.* **1994**, *146*, 144–154.

41. Calafata, A.; Vivas, F.; Brito, J. L.; Effects of phase composition and of potassium promotion on cobalt molybdate catalysts for the synthesis of alcohols from CO_2 and H_2, *Appl. Catal., A* **1998**, *172*, 217–224.

42. Fu, Y-L.; Fujimoto, K.; Lin, P.; Omata, K.; Yu, Y. Effect of calcination conditions of the oxidized precursor on the structure of a sulfided K-Mo/γ-Al_2O_3 catalyst for mixed alcohol synthesis. *Appl. Catal. A* **1995**, *126*, 273–285.

43. Pan, X.; Fan, Z.; Chen, W.; Ding, Y.; Luo, H.; Bao, X. Enhanced ethanol production inside carbon-nanotube reactors containing catalytic particles. *Nature Materials* **2007,** *6*, 507–511.

44. Berge, P. J. V.; van de Loosdrecht, J.; Barradas, S.; van der Kraan, A. M. Oxidation of cobalt based Fischer–Tropsch catalysts as a deactivation mechanism. *Catal. Today* **2000**, *58*, 321–334.

45. Kogelbauer, A.; Goodwin, J. G.; Oukaci, R. Ruthenium promotion of Co/Al_2O_3 Fischer–Tropsch catalysts *J. Catal.* **1996**, *160*, 125–133.

46. Feng, L.; Li, X.; Dadyburjor, D. B.; Kugler, E. L. A temperature-programmed-reduction study on alkali-promoted, carbon-supported molybdenum catalysts. *J. Catal.* **2000**, *190*, 1–13.

47. Travert, A.; Dujardin, C.; Mauge, F.; Veilly, E.; Cristol, S.; Paul, J.-F.; Payen, E. CO adsorption on CoMo and NiMo sulfide catalysts: A combined IR and DFT study. *J. Phys. Chem. B* **2006**, *110*, 1261–1270.

48. Noronha, F. B.; Baldanza, M. A. S.; Schmal, M. CO and NO adsorption on alumina–Pd–Mo catalysts: Effect of the precursor salts. *J. Catal.* **1999**,*188*, 270–280.

49. Ratnasamy, P.; Sivasanker, S. Structural chemistry of Co-Mo-alumnina catalysts. *Cat. rev.* **1980**, *22*, 401–429.

50. Santiesteban, J. G.; Bogdan, C. E.; Herman, R. G.; Klier, K. Mechanism of C_1-C_4 alcohol synthesis over alkali/MoS_2 and alkali/Co/MoS_2 catalysts. In *Proc. 9th Intern. Congr. Catal.;* Phillips, M. J., Ternan, M., Eds.; The Chemical Institute of Canada: Ottawa, 1988; Vol. 2, p 561.

51. Vogelaar, B. M.; Steiner, P.; van der Zijden, P. F.; van Langeveld, A. D.; Eijsbouts, S.; Moulijn, J. A. Catalyst deactivation during thiophene HDS: The role of structural sulfur. *Appl. Catal., A.* **2007**, *318*, 28–36.

CHAPTER 12

Conclusions and Recommendations

12.1. Overall project discussion and conclusions

This compilation of research studies involves the development of a novel alkali-promoted trimetallic catalyst supported on multi-walled carbon nanotubes (MWCNTs), a new generation catalyst support for higher alcohols synthesis from CO hydrogenation. This was achieved in various phases of research on the optimization of different catalytic species, such as active metal (Mo), alkali (K) promoter, and structural (Co and Rh) promoters. This work also included the screening of different supports like alumina, activated carbon, and MWCNTs; studies of catalyst structural properties and the influence of textural properties of supports; the optimization of operating conditions; kinetic model development; and long-term catalyst stability studies towards higher alcohols synthesis.

Chapter 2 demonstrates the interaction effects of various promoters, Co, Rh, and Ni with that of Mo, as well as, the influence of alumina and activated carbon supports for the synthesis of higher alcohols from synthesis gas. The Ni-promoted alkali-modified MoS_2 catalyst showed activity towards the formation of hydrocarbons. The addition of Co to the Ni-Mo-K/Al_2O_3 catalyst improved the activity towards the formation of alcohols and hydrocarbons. The activity of Rh-promoted catalysts for higher alcohol synthesis was much higher than that obtained over the rhodium-free catalysts. The total alcohols space-time yield and higher alcohols selectivities were significantly higher over the activated carbon-supported catalysts compared to those supported on alumina.

Contents of the active metal (Mo) and alkali (K) to produce higher alcohols from synthesis gas were optimized in Chapter 3 using commercial MWCNT as support. The support was pre-treated with HNO_3 acid at 100°C before alkali and metal impregnation. This resulted in opening the nanotube caps, improved the surface area of the support, and provided functional groups on the surface. The TEM images of the stabilized catalysts revealed that most of the catalyst species were uniformly distributed inside the tubes. K loading to the Mo/MWCNT catalyst increased the K–Mo–O interactions, decreased the Mo particle sizes,

and increased the percentage dispersion. The Mo content of 15 wt % Mo and K content of 9 wt % were optimum towards alcohols synthesis.

Studies on the effect of different loadings of Co metal promoter on alkali-modified molybdenum-based catalysts supported on MWCNTs for higher alcohols synthesis are discussed in Chapter 4. The addition of Co improved the metal dispersion and reducibility of the catalyst, which improved the activity and selectivity of the higher alcohols reaction. The highest total alcohol space-time yield was observed on the catalyst promoted with 6 wt % Co, whereas the catalyst with 4.5 wt % Co exhibited maximum selectivities towards ethyl alcohol and higher alcohols.

The work discussed in Chapter 5 aimed to optimize the content of Rh metal promoter on alkali-modified molybdenum-based catalysts supported on MWCNTs towards the activity and selectivity of higher alcohols. The addition of Rh promoters to alkali-modified MoS_2 catalysts increased the reaction rate towards the formation of higher alcohols, with ethanol as a dominant product, by accelerating the CO insertion mechanism during the C_1 to C_2 homologation step. The catalyst with 1.5 wt % Rh loading on 15 wt % Mo and 9 wt % K performed better among the investigated range of Rh metal content and showed the highest total alcohol yield and higher alcohols selectivity.

Chapter 6 describes the alkali-modified trimetallic Co-Rh-Mo catalysts that are supported on MWCNTs and activated carbon for higher alcohols synthesis using two different loadings of Co (4.5 and 6 wt %) and the optimum contents of K (9 wt %), Mo (15 wt %), and Rh (1.5 wt %). The alkali-modified trimetallic catalyst resulted in substantial changes in both structural properties and catalytic performance. The MWCNT-supported 1.5 wt % Rh, 15 wt % Mo, and 9 wt % K catalyst promoted with 4.5 wt % Co outperformed in terms of total alcohols yield and higher alcohols selectivity by substantially decreasing hydrocarbon formation and the water-gas shift reaction, compared to alkali-modified monometallic and bimetallic catalysts. The activated carbon-supported alkali-modified trimetallic catalysts showed less activity and selectivity compared to the MWCNT-supported catalysts.

In Chapter 7 the chemical and electronic structures of Mo and S species were examined. This work aimed to emphasize the improved performance of molybdenum-sulfided catalysts for higher alcohols synthesis due to the addition of alkali and metal

promoters on modification of surface structure and oxidation states. Alkali promotion to the MoS_2 catalyst reduced the crystalline nature of the catalyst and favored the formation of alcohols. More oxidized S and Mo species were observed by XRD and XANES in the K-promoted catalysts, indicating the formation of more Mo oxide and/or Co oxide with the addition of K, thus increasing the active sites. The formation of Co (Rh)-Mo-S species was evident in the XANES spectra of the bimetallic and trimetallic alkali-promoted MoS_2 catalysts, which was in agreement with their improved catalytic performance.

In Chapter 8 the influence of porous characteristics of the support on the catalytic performance of higher alcohols synthesis using different types of commercially available microporous and mesoporous structured activated carbons were explained. For this study, the alkali-modified trimetallic Co-Rh-Mo catalyst was used and the results compared with the catalyst supported on MWCNTs. The extent of blocking of the metal species was high on the microporous activated carbon-supported catalysts. The formation of large particles on the microporous activated carbon supports due to the agglomeration of metal species is revealed from the TEM images. The catalyst activity and selectivity studies revealed that the pore size of the support has a direct influence on the synthesis of mixed alcohols from synthesis gas.

Chapter 9 focused on the investigation of the interaction effects of experimental conditions, reaction temperature (T), pressure (P), gas hourly space velocity (GHSV) at a constant H_2 to CO molar ratio, and the optimization of the operating conditions to obtain maximum ethanol yield and selectivity using the sulfided K (9 wt %)-modified trimetallic Co (4.5 wt %)-Rh (1.5 wt %)-Mo (15 wt %) supported on MWCNTs. Quadratic models were developed using the Taguchi orthogonal array design method for % CO conversion, products STY, and alcohol selectivities as functions of T, P, and GHSV using an H_2 to CO molar ratio of 1. The ethanol STY and selectivity reached a maximum value with respect to temperature and GHSV, while increasing to a constant value with increasing pressure. Ethanol STY reached a maximum value at H_2 to CO molar ratio around 1.25, which was obtained at optimum conditions of 330°C, 1320 psi, and 3.8 m^3 (STP)/(kg of cat.)/h.

As Chapter 10 describes, a statistically representative intrinsic kinetic model was developed using the MWCNT-supported K-modifeed trimetallic sulfided Co-Rh-Mo catalyst for the higher alcohols synthesis reaction from synthesis gas. The catalyst particle size in the range of 147-210 μm was selected to eliminate the external mass transfer resistance. The Weisz–Prater

criterion confirmed that internal diffusion limitation is negligible in the catalyst. The data of this study are well fitted by the power law model. The activation energy of ethanol and higher alcohols obtained over the Co-Rh-Mo-K/MWCNT catalyst were low compared to those values reported in the literature.

Chapter 11 describes the study of the long-term deactivation behaviour of alkali-modifieded trimetallic Co-Rh-Mo catalysts supported on MWCNTs and activated carbon for 720 h of continuous higher alcohols synthesis reaction. The sulfided catalyst supported on MWCNTs showed excellent reaction stability for the synthesis of higher alcohols from synthesis gas, whereas a slight reduction in total alcohols formation was observed on the activated carbon-supported catalyst. This study revealed that MWCNTs are an innovative catalyst support to decreasing the sintering, metal support interaction, and coke formation during the catalytic process.

12.2. Recommendations

This research provides valuable insight in the development of a highly efficient Co and Rh-promoted alkali-modified MoS_2 catalyst supported on MWCNTs that is highly active, selective, and stable during the production period of higher alcohols from synthesis gas. However, specific recommendations should be considered for the advancement of this research in the future.

(1) Catalyst preparation methods

The activity and selectivity of products depends on the selection of precursors and the method of catalyst preparation. In this work, the MoS_2-based catalysts were prepared by either sequential pore volume impregnation or incipient wetness methods using ammonium heptamolybdate tetrahydrate as the precursor, followed by sulfidation of the catalyst. MoS_2 can also be prepared by other precursors such as the reduction of a thiomolybdate stabilized in aqueous solution by polyvinyl pyrrolidone or the reaction between ammonium heptamolybdate tetrahydrate with ammonium sulfide, and by using alternative preparation methods like sol gel technique and microemulsion methods.

(2) Catalyst pre-treatment process

The thermal treatment of stabilization has major effects on the nature of active sites, such as metal-support interaction, the growth of particle size, and the reduction

behaviour of the catalyst. In the present work, stabilization temperatures were determined based on thermogravimetric analysis, but the stabilization time at final stabilization temperatures and temperature ramp during the pre-treatment were selected based on experience without specific investigation. In future studies, the influence of these two important variables should be investigated.

(3) Catalyst reduction and sulfidation process

The catalyst reduction and sulfidation process are significant effects on the catalyst performance. Four parameters, including reduction and sulfidation temperature, time, temperature ramp rate, and gas composition during the activation process are to be investigated before using the alkali-modified trimetallic Co-Rh-Mo catalyst supported on MWCNTs in industry.

(4) Catalyst palletizing

MWCNT support is used in the form of powder while preparing the catalysts. To use the catalysts for industrial scale reactors, it is important to palletize the catalyst and to study their effect as well as various binders on higher alcohols synthesis.

(5) In-situ catalyst characterization

Some characterizations of the sulfided forms of the catalysts, such as X-ray diffraction and X-ray absorption near edge structure were performed after sulfidation inside the reactor. Because the nature and structure of catalysts may change during sulfidation and reaction, a comprehensive in situ catalyst characterization plan should be made to gain a clear understanding of the catalysts during the activation and higher alcohols synthesis.

(6) Extended x-ray absorption fine structure

Co, Rh, Mo, and K extended X-ray absorption fine structure study is needed to identify the different metal species present on the catalyst surface and to study the surface structure such as bond lengths, coordination numbers, and slab lengths of the different catalytic species. This information will be helpful in understanding the relationship between surface structure and catalyst activity.

(7) Catalyst activity studies using industrial synthesis gas

In this research, synthesis gas composed of pure CO and H_2 were mixed in desired composition and used for higher alcohols synthesis. The synthesis gas obtained from biomass or coal gasification is associated with H_2S, CO_2, N_2, and H_2O. The presence of these

undesirable compounds may change the activity and selectivity of the reaction products and cause deactivation to the catalyst. Hence, it is important to perform catalyst activity studies using industrial synthesis gas before using the catalyst on an industrial scale.

(8) Evaluation of the higher alcohols reaction in a pilot plant reactor

Before using the catalyst in industry, a detailed pilot plant study under optimum operating conditions may be performed to evaluate heat transfer and mass transfer resistances associated with the higher alcohols synthesis reaction.

APPENDIX A

Research Outcome

A.1. Publications from Results of the Thesis

1. Surisetty, V. R.; Dalai, A. K.; Kozinski, J. Intrinsic reaction kinetics of higher alcohols synthesis from synthesis gas over sulfided alkali-promoted Co-Rh-Mo trimetallic catalyst supported on MWCNTs. *Energ. Fuel.* **2010**, 24, 4130–4137.
2. Surisetty, V. R.; Dalai, A. K.; Kozinski, J. Synthesis of higher alcohols from synthesis gas over Co-promoted alkali modified-MoS_2 catalysts supported on MWCNTs. *Appl. Catal., A* **2010**, *385*, 153-162.
3. Surisetty, V. R.; Dalai, A. K.; Kozinski, J. Effect of Rh promoter on MWCNT-supported alkali-modified MoS_2 catalysts for higher alcohols synthesis from CO hydrogenation. *Appl. Catal., A* **2010**, *381*, 282–288.
4. Surisetty, V. R.; Dalai, A. K.; Kozinski, J. Alkali-promoted trimetallic Co-Rh-Mo sulfide catalysts for higher alcohols synthesis from synthesis gas: Comparison of MWCNT and activated carbon supports. *Ind. Eng. Chem. Res.* **2010**, *49*, 6956-6963.
5. Surisetty, V. R.; Tavasoli, A.; Dalai, A. K. Synthesis of higher alcohols from syngas over alkali promoted MoS_2 catalysts supported on multi-walled carbon nanotubes. *Appl. Catal., A* **2009**, *365*, 243–251.
6. Surisetty, V. R.; Eswaramoorthi, I.; Dalai, A. K. Comparative study of higher alcohols synthesis over alumina and activated carbon supported alkali modified MoS_2 catalysts promoted with group VIII metals. *Fuel* **2010**, Submitted for Review.
7. Surisetty, V. R.; Yongfeng, H.; Dalai, A. K.; Kozinski, J. Alkali and metal promoters (Co and Rh) on MoS_2 catalysts for higher alcohols synthesis: catalytic performance and structural characterization studies. *Appl. Catal., A* **2010**, Submitted for Review.
8. Surisetty, V. R.; Dalai, A. K.; Kozinski, J. Influence of porous characteristics of the carbon support on alkali-modified trimetallic Co-Rh-Mo sulfided catalysts for

higher alcohols synthesis from synthesis gas. *Appl. Catal., A* **2010**, Submitted for Review.

9. Surisetty, V. R.; Dalai, A. K.; Kozinski, J. Higher alcohols synthesis from synthesis gas over sulfided alkali-promoted Co-Rh-Mo trimetallic catalyst: Experimental and Modeling Studies. *Ind. Eng. Chem. Res.* **2010**, Submitted for Review.
10. Surisetty, V. R.; Dalai, A. K.; Kozinski, J. Long-term deactivation studies of alkali-promoted trimetallic Co-Rh-Mo sulfide catalysts for higher alcohols synthesis from synthesis gas. *Energ. Fuel.* **2010**, Submitted for Review.

A.2. Refereed Conference Presentations

1. Surisetty, V. R.; Hu, Y.; Dalai, A. K.; Kozinski, J. Structural characterization and catalytic performance of alkali and metal promoters (Co and Rh) on MoS2 catalysts for higher alcohols synthesis reaction. CLS 13th Annual Users' Meeting, Saskatoon, Saskatchewan, Canada, June 17-18, 2010.
2. Surisetty, V. R.; Dalai, A. K. Higher alcohols synthesis using alkali promoted trimetallic C-Rh-Mo Sulfide catalysts supported on MWCNT and activated carbon. 21st Canadian Symposium on Catalysis, Banff, Albert, Canada, May 9-12, 2010.
3. Surisetty, V. R.; Dalai, A. K.; Kozinski, J. Applications of CNTs as Support on Co-promoted alkali-modified MoS_2 catalysts for Synthesis of Higher Alcohols from Synthesis gas. Agricultural Biorefinery Innovation Network (ABIN) Conference, London, Ontario, Canada, March 14-16, 2010.
4. Surisetty, V. R.; Dalai, A. K. Higher alcohol synthesis from syngas over Rh promoted alkali modified molybdenum sulfide catalysts. AIChE Annual Meeting, 2009, Nashville, Tennesse, USA, November 8-13, 2009.
5. Surisetty, V. R.; Dalai, A. K. Effect of Co and Rh on K-MoS_2/MWCNT catalysts for higher alcohols synthesis from synthesis gas. 8th World Congress of Chemical Engineering (WCCE8), Montreal, Quebec, Canada, August 23-27, 2009.
6. Surisetty, V. R.; Tavasoli, A.; Dalai, A. K. Synthesis of higher alcohols from syngas over alkali promoted MoS_2 catalysts supported on multi walled carbon nano tubes.

58th Canadian Chemical Engineering Conference (CSChE2008), Ottawa, Ontario, Canada, October 19-22, 2008.

7. Surisetty, V. R.; Dalai, A. K.; Kozinski, J. Effect of textural properties of carbon supports on alkali-promoted trimetallic Co-Rh-Mo sulfide catalysts for higher alcohols synthesis from synthesis gas. 60th Canadian Chemical Engineering Conference (CSChE2010), Saskatoon, Saskatchewan, Canada, October 24-27, 2010.
8. Surisetty, V. R.; Hu, Y.; Dalai, A. K.; Kozinski, J. XANES characterization and catalytic performance of alkali and metal (Co and Rh)-promoted MoS_2 catalysts for higher alcohols synthesis. 60th Canadian Chemical Engineering Conference (CSChE2010), Saskatoon, Saskatchewan, Canada, October 24-27, 2010.
9. Surisetty, V. R.; Dalai, A. K.; Kozinski, J. An intrinsic kinetic model for higher alcohols synthesis from synthesis gas using sulfided alkali-promoted Co-Rh-Mo trimetallic catalyst supported on MWCNTs. CHEMCON, 2010, Annamalinagar, Tamil Nadu, India, December 27-29, 2010.

A.3. Patent (submitted)

1. Surisetty, V. R.; Dalai, A. K. Higher alcohols synthesis using alkali-modified Co-Rh-Mo trimetallic catalyst supported on multi-walled carbon nanotubes (submitted to Patent and Industry Liaison Office, University of Saskatchewan, Canada)

APPENDIX B

Experimental Calibrations

This section gives the details about the calibration of different instruments of the experimental reactor set-up used for higher alcohols synthesis.

B.1. Reactor temperature calibration

The reactor was packed with catalyst and the temperature was calibrated by pressurizing the reactor using He gas at 1400 psig. Temperature of the furnace was varied from 150 to 350^{o}C and the corresponding reactor temperature was measured using a single thermocouple inserted just below the catalyst bed. The thermocouple was then moved every 2 cm from the bottom of the catalyst bed to measure the temperature along the reactor bed. Temperature profiles along the reactor bed are shown in Fig. B.1 and the calibration curve for the temperature controller is presented in Fig. B.2.

B.2. Mass flow controller calibration

The mass flow controller was calibrated for the flow of gaseous mixtures, 10 mole % H_2S in hydrogen and synthesis gas in 10 mole % Ar at the experimental operating conditions using a bubble flow meter connected to the exit of the back pressure regulator. All the flow rates were measured at atmospheric conditions and the calibration curves are given in Figs. B3 and B4. The following equation was used to calculate the flow rates at operating conditions.

$$V_o = \frac{P_s * T_o}{P_o * T_s} * V_s \quad \text{.....(B1)}$$

Where V is the flow rate in ml/hr, T is temperature; P is pressure, the subscripts‘s’ and ‘o’ represent standard and operating conditions, respectively.

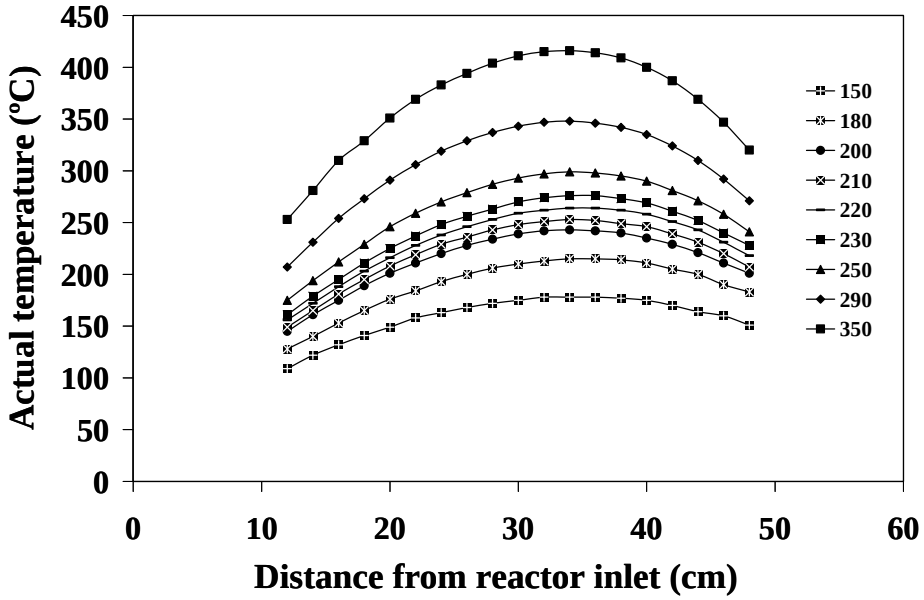

Figure B.1. Temperature profiles along the reactor bed

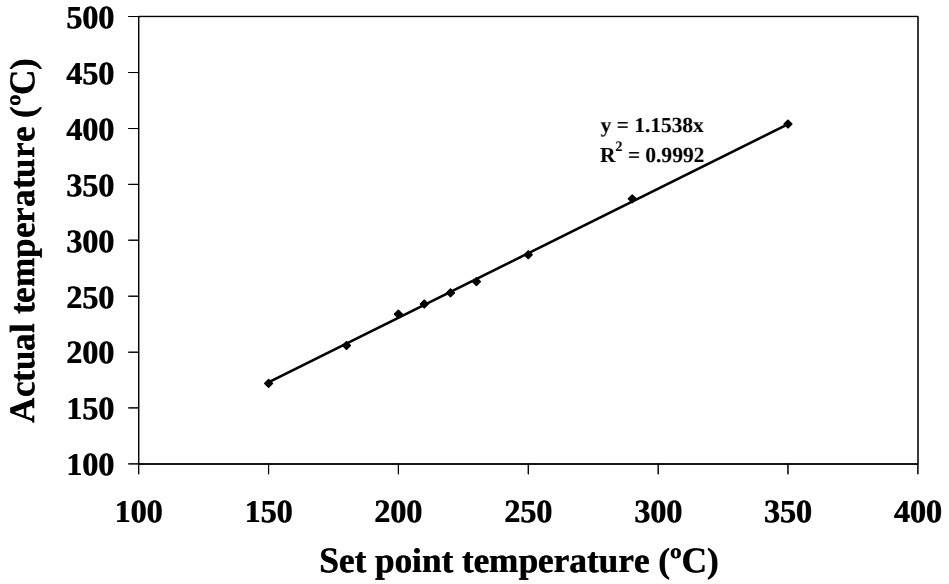

Figure B.2. Calibration of temperature controller

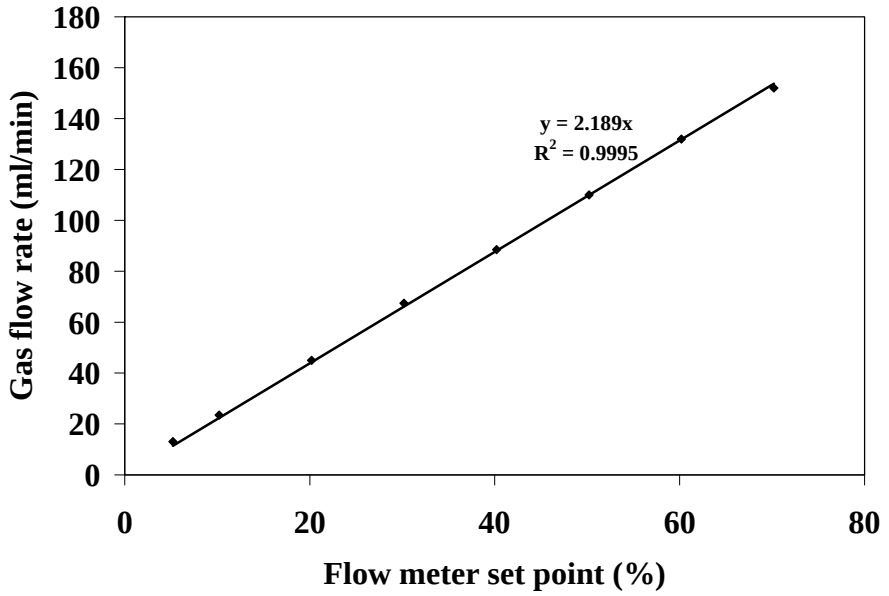

Figure B.3. Calibration of mass flow controller measuring 10 mole % H_2S in H_2 gas

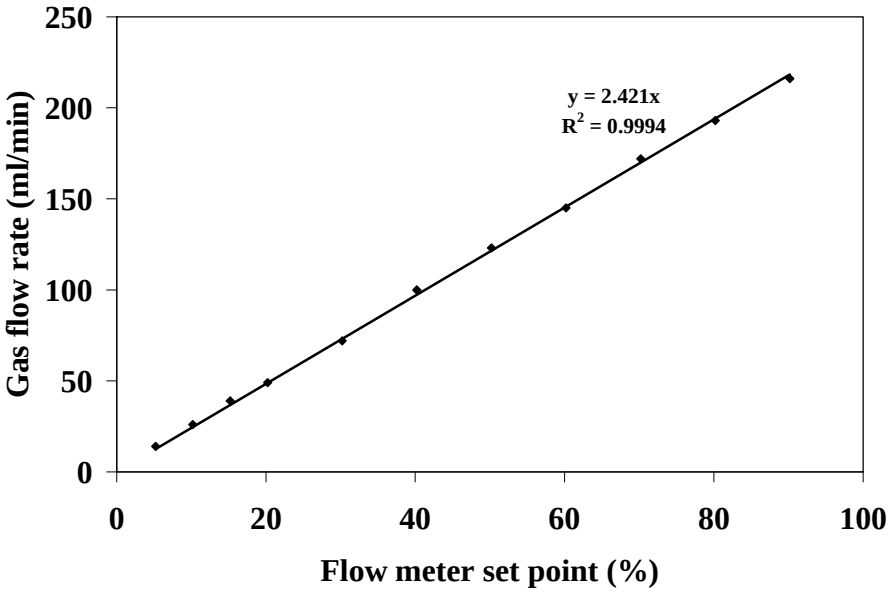

Figure B.4. Calibration of mass flow controller measuring 10 mole % Ar in synthesis gas

APPENDIX C

Material Balance Data

Catalyst	**15 wt % Mo 6 wt % K/AC**
Catalyst Mass (g)	2
Process Pressure (psi)	1200
Process Temp (deg C)	320
Inlet moles of gas	7.71
Inlet H_2 Flowrate (l/min STP)	0.072
Inlet CO Flowrate (l/min STP)	0.036
Inlet Ar Flowrate (l/min STP)	0.012
Inlet Gas Flowrate (l/min STP)	0.12
H2/CO Molar Ratio	2.00
Outlet Gas Flowrate (l/min)	0.1160
Product Gas Moles (g mole)	7.46
Product Gas Volume (l)	167.0
Product Gas Temperature (^oC)	0.0
Barometric Pressure(psi)	760.0
Product Gas Molar density(g mole/l)	0.045
Mass of Liquid Collected	2.025
Length of Run (min)	1440.0

Outlet Gas compsition

Component	Volume %
H_2	59.676
CO	25.808
Argon	11.090
CO_2	1.787
Methane	1.516
Propane	0.028
Propylene	0.001
n-Butane	0.002
Ethylene	0.007
Ethane	0.085
TOTAL	100

Liquid composition

Mass % Water	0.9
Mass % Methanol	64.77
Mass % Ethanol	27.37
Mass % n-propanol	5.91
Mass % n-butanol	0.84
Volume % n-pentanol	0.09
TOTAL	100

	Inlet (g/min)	Outlet (g/min)	Difference	% Difference
OVERALL	0.074	0.075	0.0003	0.4
Carbon	0.020	0.020	0.0001	0.5
Hydrogen	0.007	0.007	0.0003	3.6
Oxygen	0.026	0.026	0.0001	0.5
Argon	0.022	0.022	0.0000	0.1

Appendix D

Mass-Transfer Calculations

D.1. External mass-transfer limitation

Sample calculation of mass transfer coefficient and boundary layer thickness were done using Frössling correlation[1].

The particle size is in the range of 707-841 μm.

The average particle size (d_p) = 0.0774 cm.

Calculation of free stream velocity of gas (u):

$$u = \frac{Q}{A_c} = \frac{120 \frac{ml}{\min} * \frac{1}{10^6} \frac{m^3}{ml} * \frac{1}{60} \frac{\min}{s}}{\pi * \frac{(22 * 10^{-3})^2}{4} m^2} = 5.26 * 10^{-3} m/s \quad \text{.....(D1)}$$

Calculation of density of gas (ρ):

The feed gas mixture is assumed to behave as an ideal gas at reaction conditions.

The density of individual gases is obtained online at (http://www.globalspec.com/calculators/gas-density).

The density of CO at 1320 psig and 300ºC = 54.08 kg/m^3

The density of H_2 at 1320 psig and 300ºC = 3.86 kg/m^3

The density of Ar at 1320 psig and 300ºC = 77.16 kg/m^3

The average density of feed gas mixture (CO (40 mole%), H_2 (50 mole%), and Ar (10 mole%)) at 1320 psi and 300ºC = (40* 54.08 + 50 * 3.86 + 10 * 77.16)/100 kg/m^3 = 31.28 kg/m^3

Calculation of dynamic viscosity:

The dynamic viscosity of individual gases is obtained online at (http://www.lmnoeng.com/Flow/GasViscosity.htm)

The dynamic viscosity of CO at 1320 psig and 300ºC = 2.84 * 10^{-5} kg/(m-s)

The dynamic viscosity of H_2 at 1320 psig and 300ºC = 1.35 * 10^{-5} kg/(m-s)

The dynamic viscosity of Ar at 1320 psig and 300ºC = 4.8 * 10^{-5} kg/(m-s)

The average dynamic viscosity of feed gas mixture at 1320 psig and 300ºC = (40* $2.84 * 10^{-5}$ + 50 * $1.35 * 10^{-5}$ + 10 * $4.8 * 10^{-5}$)/100 kg/(m-s) = $2.291*10^{-5}$ kg/(m-s)

Calculation of effective diffusivity:

The effective diffusivity for binary gas mixtures is calculated based on the modern kinetic theory and the Lennard-Jones expression for intermolecular forces.[2]

$$D_{AB} = \frac{0.001858 * T^{1.5} * [(M_1 + M_2)/M_1 M_2]^{0.5}}{P * \sigma_{12}^2 * \Omega_D} \quad \text{.....(D2)}$$

D_{AB} is the diffusivity for a binary gas mixtures; T is the temperature (K); M_i is the molecular weight of species i; P is the pressure (atm); Ω_D is the collision integral; σ is the constant of Lennard-Jones potential function.

$$\Omega_D = \frac{k * T}{\varepsilon 12} \quad \text{.....(D3)}$$

where ε is the Lennard-Jones potential function and k is the Boltzmann constant

T = 573.15 K, M_1 = 28, M_2 = 2, P = 92.81 atm

Values of σ_1 and σ_2 were obtained from Table 1.3 of Satterfield, 1970[2] (species 1-CO and species 2-H_2).

$$\sigma_{12} = \frac{\sigma_1 + \sigma_2}{2} = \frac{3.806A^o + 2.899A^o}{2} = 3.353A^o \quad \text{.....(D4)}$$

$$\frac{\varepsilon_{12}}{kT} = \left(\frac{\varepsilon_1}{k}\right)^{0.5} * \left(\frac{\varepsilon_2}{k}\right)^{0.5} * \left(\frac{1}{T}\right) = (29.790)^{0.5} * (99.699)^{0.5} * \left(\frac{1}{573.15}\right) = 0.095 \quad \text{.....(D5)}$$

$$\frac{kT}{\varepsilon_{12}} = 10.526$$

$\Omega_D = 4.21$ (from Satterfield, 1970[3])

$$D_{AB} = \frac{0.001858 * (573.15)^{1.5} * [(28+2)/(28*2)]^{0.5}}{92.81 * (3.353)^2 * 4.21} = 0.0042 \frac{cm^2}{s}$$

$$D_e = D_{AB} * \frac{\theta}{\tau} = 0.0042 * \frac{0.5}{4} = 5.25 * 10^{-4} \frac{cm^2}{s} \quad \text{.....(D6)}$$

Where θ is porosity of catalyst and τ is tortuosity factor.

In the absence of other information a value of θ=0.5 and a value of τ = 4 are recommended for estimation purposes.[4]

Calculation of Reynolds number:

$$\mathrm{Re} = \frac{\rho u d_p}{\mu} = \frac{31.28\frac{kg}{m^3} * 5.26 * 10^{-3}\frac{m}{s} * 7.74 * 10^{-4} m}{2.291 * 10^{-5}\ \mathrm{kg/(m-s)}} = 5.56 \quad \text{(D7)}$$

Calculation of Scmidt number:

$$Sc = \frac{\mu}{\rho D_e} = \frac{2.291 * 10^{-5}\ \mathrm{kg/(m-s)}}{31.28\frac{kg}{m^3} * 5.25 * 10^{-8}\frac{m^2}{s}} = 13.95 \quad \text{(D8)}$$

Calculation of Sherwood number:

$$Sh = 2 + 0.6(\mathrm{Re})^{1/2}(Sc)^{1/3} = 2 + 0.6 * (5.56)^{1/2} * (13.95)^{1/3} = 5.41 \quad \text{(D9)}$$

Calculation of mass transfer coefficient:

$$Sh = \frac{k_c d_p}{D_e} \quad \text{(D10)}$$

where k_c is the mass transfer coefficient

$$k_c = \frac{5.41 * 5.25 * 10^{-8}\frac{m^2}{s}}{7.74 * 10^{-4} m} = 3.67 * 10^{-4}\frac{m}{s}$$

Calculation of boundary layer thickness:

$$k_c = \frac{D_e}{\delta} \quad \text{(D11)}$$

where δ is the boundary layer thickness

$$\delta = \frac{5.25 * 10^{-8}\frac{m^2}{s}}{3.67 * 10^{-4}\frac{m}{s}} = 1.431 * 10^{-4} m = 0.143 mm \quad \text{(D12)}$$

D.2. Internal mass-transfer limitation

Weisz-Prater criterion (C_{WP}) is used for estimation of internal mass transfer resistance.[5]

The particle size is in the range of 147-210 μm.

The average particle size (dp) = 0.0179 cm.

$$C_{WP} = \frac{-(r_A^{'})_{obs} * \rho_C * r^2}{D_e * C_{A_s}} \quad \text{.....(D13)}$$

where $(r_A^{'})_{obs}$ is the reaction rate per unit mass of catalyst; ρ_c is the catalyst density; r is the particle radius; C_{A_s} is the surface concentration of reactant A; D_e is the effective diffusivity.

If C_{WP} « 1, there is no internal diffusion limitation and if C_{WP} » 1, internal diffusion limits the reaction severely.[5]

r = 8.95 * 10^{-5} m; $\rho_c = 3248 \frac{kg}{m^3}$; $-(r_A^{'})_{obs} = 1.161*10^{-5} \frac{kgmole}{kgofcat.*\sec}$; $D_e = 5.37*10^{-8} \frac{m^2}{\sec}$

Calculation of surface concentration of reactant:

$$C_{A_s} = \frac{P_A}{RT} = \frac{92.81atm*0.4}{0.0821\frac{m^3atm}{Kkgmole}*598K} = 0.756\frac{kgmole}{m^3} \quad \text{.....(D14)}$$

$$C_{WP} = \frac{1.161*10^{-5}\frac{kgmole}{kgofcat.*\sec}*3248\frac{kg}{m^3}*(8.95*10^{-5})^2 m^2}{5.37*10^{-8}\frac{m^2}{\sec}*0.756\frac{kgmole}{m^3}} = 0.007 < 1.0$$

D.3. References

1. Frössling, N. The evaporation of falling drops. *Gerlands Beitr. Geophys.* **1938**, *52*, 170–216.
2. Hirschfelder, J.; Curtis, C.; Bird. R. *Molecular Theory of Gases and Liquids*. John Wiley and Sons: New York, USA, 1954.
3. Satterfield C N. *Mass Transfer in Heterogeneous Catalysis*. MIT Press: Cambridge, England, 1970.
4. Satterfield, C. N. *Heterogeneous Catalysis in Industrial Practice*, 2nd ed., McGraw-Hill: New York, USA, 1991, p. 471-539.
5. Fogler, H. S. *Elements of Chemical Reaction Engineering*, 3rd ed., Prentice Hall PTR: New Jersey, USA, 1999, p.581-809.